Journal of the Serbian Chemical Society

*e*version
electronic

Available on line at

СХД
1897

www.shd.org.rs/JSCS/

The full search of JSCS
is available through

DOAJ DIRECTORY OF
OPEN ACCESS
JOURNALS

www.doaj.org

CONTENTS

Available online at www.shd.org.rs/JSCS/

AUTHORS' REVIEW

The study of linear solvation energy relationship for the reactivity of carboxylic acids with diazodiphenylmethane in protic and aprotic solvents

GORDANA S. UŠĆUMLIĆ*[#] and JASMINA B. NIKOLIĆ[#]

Department of Organic Chemistry, Faculty of Technology and Metallurgy, University of Belgrade, Karnegijeva 4, P.O. Box 3505, 11120 Belgrade, Serbia

Abstract: Solvent effects on the reactivity of cycloalkenecarboxylic, cycloalkeneacetic, 2-substituted cyclohex-1-enecarboxylic, 2-substituted benzoic, 2-substituted cyclohex-1-eneacetic, 2-substituted phenylacetic, 2-phenylcyclohex-1-enecarboxylic, 2-phenylbenzoic and 2-phenylacrylic acids with diazodiphenylmethane (DDM) were investigated. In order to explain the kinetic results through solvent effects, the second-order rate constants for the reaction of the examined acids with DDM were correlated using the Kamlet–Taft solvatochromic equation. The correlations of the kinetic data were realized by means of multiple linear regression analysis and the solvent effects on the reaction rates were analyzed in terms of the contributions of the initial and the transition state. The signs of the equation coefficients support the proposed mechanism. Solvation models for all the investigated acids are suggested. The quantitative relationship between the molecular structure and the chemical reactivity is also discussed.

Keywords: carboxylic acids; linear solvation energy relationship; diazodiphenylmethane; aprotic solvents; protic solvents.

CONTENTS

1. INTRODUCTION
2. HYDROXYLIC SOLVENT EFFECTS ON THE KINETICS OF THE REACTION OF CARBOXYLIC ACIDS WITH DIAZODIPHENYLMETHANE
3. THE KAMLET–TAFT METHOD FOR THE EXAMINATION OF SOLVENT EFFECTS ON THE REACTIVITY OF CARBOXYLIC ACIDS WITH DIAZODIPHENYLMETHANE
    3.1. Cycloalkenecarboxylic and cycloalkeneacetic acids
    3.2. 2-Substituted cyclohex-1-enecarboxylic and 2-substituted benzoic acids
    3.3. 2-Substituted cyclohex-1-eneacetic and 2-substituted phenylacetic acids
    3.4. 2-Phenylcyclohex-1-enecarboxylic, 2-phenylbenzoic and 2-phenylacrylic acids
4. CONCLUDING REMARKS

Available online at www.shd.org.rs/JSCS/

1. INTRODUCTION

The effect of different solvents on the rates of chemical changes was one of the earliest kinetic problems to be studied.[1–3] The development of correlation analysis in the area of solvent effects has proved to be a slow and difficult process and only within the last 20 years has there been any considerable progress. Application of the techniques of multiple regression has proved to be strikingly successful and has greatly increased the understanding of the role of the solvent. Over the years, two main methods for the examination of the solvent effects on the reaction rates have been developed. First, the rate constants, either as $\log k$ or as $\Delta G^{\#}$ may be correlated with a physical parameter characteristic of the solvent, for example dielectric constant, solubility parameter, viscosity, *etc.*, or with an empirical solvent parameter, such as *Y*, *Z*, *etc.*[4–6] This type of analysis has been extended to multiple linear correlations with a number of solvent parameters, notably by Shorter *et al.*[7] on the reaction of diazodiphenylmethane (DDM) and benzoic acid and more generally by Koppel and Palm[8] and by Kamlet and Taft and their co-workers.[9–11] In the second method, the solvent effect on $\log k$ or $\Delta G^{\#}$ is dissected into contributions of the reactants (initial state) and the transition state, followed, where possible, by a comparison of solvent effects on the transition state with solvent effects on solutes that might function as suitable models for the transition state. This method has been applied not only to a number of standard organic reactions but also to organometallic and inorganic reactions.

Two groups of workers set out general equations for the correlations of solvent effects through multiple regression analysis. Koppel and Palm[8] used the four-parameter Eq. (1):

$$\log k = \log k_0 + gf(\varepsilon) + pf(n) + eE + bB \qquad (1)$$

in which $f(\varepsilon)$ is a dielectric constant function, usually $Q = (\varepsilon - 1)/(2\varepsilon + 1)$, $f(n)$ is a refractive index function, $(n^2 - 1)/(n^2 + 2)$, and E and B are measures of the electrophilic and nucleophilic solvation ability of the solvent, respectively. Koppel and Palm[8] and later Shorter *et al.*[7] quite successfully applied Eq. (1) to a variety of reaction types.

The Kamlet and Taft group of workers[11] used the alternative Eq. (2):

$$\log k = A_0 + s\pi^* + a\alpha + b\beta \qquad (2)$$

in which π^* is a measure of solvent dipolarity/polarizability, β represents the scale of the solvent hydrogen bond acceptor basicity, α represents the scale of the solvent hydrogen bond donor acidity and A_0 is the regression value of the solute property in the reference solvent, cyclohexane. The regression coefficients *s*, *a* and *b* measure the relative susceptibilities of the solvent-dependent solute property ($\log k$ or as $\Delta G^{\#}$) to the corresponding solvent parameters. Both Eq. (1) and Eq.(2) are general enough to be applied to almost any type of reaction. However,

Available online at www.shd.org.rs/JSCS/

as will be shown, there are considerable advantages to be gained by the use of Eq. (2).[12]

This review demonstrates how the linear solvation energy relationship (LSER) method can be used to explain and present the multiple interacting effects of the solvent on the reactivity of carboxylic acids in their reaction with DDM. The solvent effects on the reaction rates were analyzed in terms of the contributions of the initial and the transition state. The quantitative relationship between the molecular structure and the chemical reactivity is discussed.

2. HYDROXYLIC SOLVENT EFFECTS ON THE KINETICS OF THE REACTION OF CARBOXYLIC ACIDS WITH DIAZODIPHENYLMETHANE

The reactivity of carboxylic acids with diazodiphenylmethane (DDM) is closely related to the molecular structure of the acid and the solvent present. The main advantage that makes this esterification convenient for examining the influence of the solvent and structure on the reactivity of the carboxylic acid is that a catalyst is not necessary for this reaction. It may vary in rate, but it occurs without any additional support and it follows second-order kinetics in protic and aprotic solvents.[13,14] The mechanism of this reaction has been thoroughly examined[15–17] and it was established that the rate-determining step involves a proton transfer from the carboxylic acid to DDM, whereby a diphenemethane-diazonium–carboxylate ion pair is formed, which rapidly reacts to give esters in the subsequent product-determining step (or ethers in the case of hydroxylic solvents):

$$Ph_2CN_2 + RCOOH \rightarrow Ph_2CHN_2^+ \, {}^-O_2CR$$
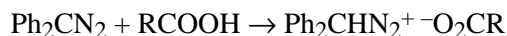
In previous studies, the reactivity of 2-substitutedcyclohex-1-enecarboxylic acids,[18–20] 2-substitutedbenzoic acids,[13,14,18–20] 2-substitutedcyclohex-1-ene-acetic acids,[21–23] 2-substitutedphenylacetic acids,[21–23] cycloalkanecarboxylic acids,[24–26] cycloalkenecarboxylic acids,[25,27,28] cycloalkeneacetic acids,[21,28,29] 2-(4-substitutedphenyl)cyclohex-1-enecarboxylic acids,[30–35] 2-(4-substituted phenyl)benzoic acids[35–38] and 2-(4-substitutedphenyl)acrylic acids[35,39,40] with DDM in various alcohols were investigated. The rate data for these acids were correlated with the simple and extended Hammett equations. The results showed that linear free energy relationships (LFER) are applicable to the kinetic data for the investigated acid systems. In recent papers,[23,25,28] hydroxylic solvent effects were examined on the reaction of the same carboxylic acids with DDM by means of the linear solvation energy relationship (LSER) concept, developed by Kamlet and Taft.[9]

The correlation equations obtained by stepwise regression for all the examined acids showed that the best approach, which helps the understanding of the hydroxylic solvent effects in the reaction, lies in the separate correlations of the

Available online at www.shd.org.rs/JSCS/

kinetic data with the hydrogen bond donating (HBD) and hydrogen bond accepting (HBA) ability of a solvent (Eqs. (3a–3p)). The correlations are as follows:

Cyclopent-1-enecarboxylic acid:

$$\log k = -1.93 + (1.03 \pm 0.23)\pi^* + (1.43 \pm 0.53)\alpha \qquad (3a)$$
$$R = 0.977, s = 0.08, n = 7;$$

$$\log k = -0.31 + (0.63 \pm 0.31)\pi^* - (1.06 \pm 0.36)\beta \qquad (3b)$$
$$R = 0.981, s = 0.072, n = 7.$$

Cyclohex-1-enecarboxylic acid:

$$\log k = -1.92 + (1.05 \pm 0.23)\pi^* + (1.30 \pm 0.52)\alpha \qquad (3c)$$
$$R = 0.977, s = 0.077, n = 7;$$

$$\log k = -0.06 + (0.79 \pm 0.38)\pi^* - (0.83 \pm 0.46)\beta \qquad (3d)$$
$$R = 0.970, s = 0.089, n = 7.$$

Cyclohept-1-enecarboxylic acid:

$$\log k = -1.91 + (1.06 \pm 0.22)\pi^* + (1.16 \pm 0.51)\alpha \qquad (3e)$$
$$R = 0.977, s = 0.070, n = 7;$$

$$\log k = -0.35 + (0.98 \pm 0.48)\pi^* - (0.66 \pm 0.44)\beta \qquad (3f)$$
$$R = 0.960, s = 0.090, n = 7.$$

Cyclopent-1-eneacetic acid:

$$\log k = -3.56 + (0.80 \pm 0.33)\pi^* + (3.74 \pm 0.75)\alpha \qquad (3g)$$
$$R = 0.980, s = 0.110, n = 7;$$

$$\log k = 1.91 - (2.47 \pm 0.31)\beta \qquad (3h)$$
$$R = 0.963, s = 0.133, n = 7.$$

Cyclohex-1-eneacetic acid:

$$\log k = -3.33 + (0.75 \pm 0.41)\pi^* + (3.91 \pm 0.94)\alpha \qquad (3i)$$
$$R = 0.960, s = 0.140, n = 7;$$

$$\log k = 1.66 - (2.26 \pm 0.36)\beta \qquad (3j)$$
$$R = 0.940, s = 0.150, n = 7.$$

Cyclohept-1-eneacetic acid:

$$\log k = -3.12 + (0.67 \pm 0.42)\pi^* + (3.13 \pm 0.96)\alpha \qquad (3k)$$
$$R = 0.950, s = 0.140, n = 7;$$

$$\log k = 1.44 - (2.06 \pm 0.35)\beta \qquad (3l)$$
$$R = 0.930, s = 0.150, n = 7.$$

Benzoic acid:

$$\log k = -2.87 + (0.83 \pm 0.36)\pi^* + (3.02 \pm 0.73)\alpha \qquad (3m)$$
$$R = 0.975, s = 0.103, n = 7;$$

$$\log k = 1.69 - (2.07 \pm 0.29)\beta \qquad (3n)$$
$$R = 0.954, s = 0.124, n = 7.$$

Phenylacetic acid:

$$\log k = -2.48 + (0.85 \pm 0.31)\pi^* + (2.59 \pm 0.71)\alpha \qquad (3o)$$
$$R = 0.972, \; s = 0.105, \; n = 7;$$
$$\log k = 1.70 - (1.99 \pm 0.27)\beta \qquad (3p)$$
$$R = 0.950, \; s = 0.120, \; n = 7.$$

As the solvent effects on the examined reaction could not be clearly presented when all the solvent properties were taken together, an attempt was made to separate them into those that stabilize the transition state and those that influence the ground state before the reaction starts. Taking into consideration the reaction mechanism (Fig. 1), it can be noticed that, because of the charge separation in the transition state, a solvent of high polarity can stabilize this state, making the reaction faster; the electrophilic ability of a solvent can have a similar effect, affecting the carboxylic anion which also exists in the transition state. On the contrary, the nucleophilic solvating ability can be prominent in the ground state, stabilizing the carboxylic proton and, hence, retarding the reaction.
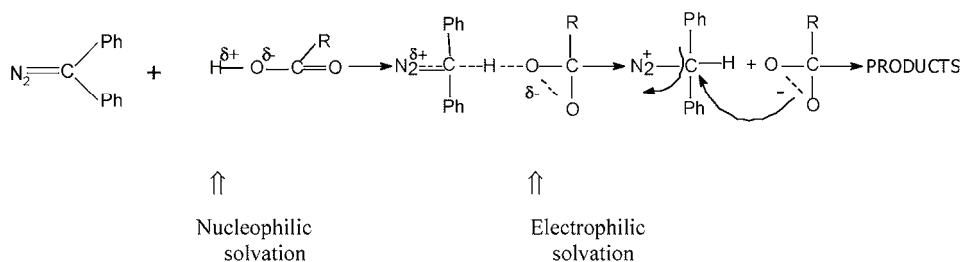

Fig. 1. The effects of the solvent on the mechanism of the reaction of carboxylic acids with DDM.

Multiple linear regression analysis (MLRA) is very useful in separating and quantifying such interactions on the examined reactivity. The first comprehensive application of multiple linear regression analysis to kinetic phenomena was that of Koppel and Palm[8] who listed regression constants for the simple Koppel–Palm equation for various processes. Aslan *et al.*[14] showed that correlation analysis of the second-order rate constants for the reaction of benzoic acid with DDM in hydroxylic solvents did not give satisfactory results with the Koppel–Palm mode.[8] They came to the conclusion that the possibility of Koppel–Palm analysis of data related to protic solvents depends on the fitting of the data in a regression with the main lines being determined by a much larger number of aprotic solvents.

These results point to a rather complex influence of hydroxylic solvents on the rate constants of the reaction between carboxylic acids and DDM. In these amphiprotic solvents, the complications can be caused by self-association type-AB hydrogen bonding, and multiple type-A and type-B interactions. In type-A hyd-

rogen bonding, the solute acts as a HBA base and the solvent as a HBD acid. In type-B hydrogen bonding, the roles are reversed. Type-AB represents hydrogen bonding in which the solute acts as both a HBD acid and a HBA base, associating with at least two molecules of amphiprotic solvent in a probably cyclic complex. The obtained satisfactory results of the correlations of the kinetic data of examined acids by Kamlet–Taft equations with separate HBD and HBA abilities of the solvent, presented in this review, indicate that the selected model was correct. This means that this model gives a detailed interpretation of the solvating effects of the carboxylic group in different hydroxylic solvents. In these circumstances where both the solvent and solute are hydrogen bond donors, it has been proven to be quite difficult to untangle solvent dipolarity/polarizability, type-B hydrogen bonding and variable self-association effects from the usual multiple type-A hydrogen bonding interactions.

3. THE KAMLET–TAFT METHOD FOR THE EXAMINATION OF SOLVENT EFFECTS ON THE REACTIVITY OF CARBOXYLIC ACIDS WITH DIAZODIPHENYLMETHANE

Kamlet *et al.*[9] established that the effect of a solvent on the reaction rate should be given in terms of the following properties: *i*) the behavior of the solvent as a dielectric, facilitating the separation of opposite charges in the transition state, *ii*) the ability of the solvent to donate a proton in a solvent-to-solute hydrogen bond and thus stabilize the carboxylate anion in the transition state and *iii*) the ability of the solvent to donate an electron pair and therefore stabilize the initial carboxylic acid, by way of a hydrogen bond between the carboxylic proton and the solvent electron pair. The parameter π^* is an appropriate measure of the first property, while the second and the third properties are governed by the effects of the solvent acidity and basicity, quantitatively expressed by the parameters α and β, respectively. The solvent parameters (π^*, α and β) for hydrogen bond donor and non-hydrogen bond donor solvents (Eq. (2)) taken from the literature[11] are given in Table I. The linear dependence (LSER) on the solvent parameters were used to correlate and predict a wide variety of solvent effects, as well as to provide an analysis in the terms of knowledge and the theoretical concepts of molecular structural effects.[9]

To the best of our knowledge, the influence of aprotic solvents on the reactivity of carboxylic acids with DDM using the Kamlet–Taft treatment has not hitherto been systematically presented, except for benzoic acid.[9]

In recent papers,[41–44] the effects of a set of 12 aprotic and 3 protic solvents on the reaction of various carboxylic acids with DDM was examined by means of the linear solvation energy relationship (LSER) concept developed by Kamlet and Taft[9] (Eq. (2)). The correlation equations obtained by stepwise regression for all the examined acids showed that the total solvatochromic equation can be used in its complete form, without the separation of effects supporting the transition

state (solvent polarity and hydrogen bond donating ability) and the ground state (hydrogen bond accepting ability).

TABLE I. Solvent parameters[11]

Solvent	π^*	α	β
Methyl acetate	0.60	0.00	0.42
Cyclohexanone	0.76	0.00	0.53
Diethyl ketone	0.72	0.00	0.45
Carbon tetrachloride	0.28	0.00	0.00
Chloroform	0.58	0.44	0.00
Ethyl acetate	0.55	0.00	0.45
Cyclopentanone	0.76	0.00	0.52
Dioxane	0.55	0.00	0.37
Acetonitrile	0.85	0.19	0.31
Acetone	0.72	0.08	0.48
Methanol	0.60	0.93	0.62
Ethanol	0.54	0.83	0.77
Ethylene glycol	0.92	0.90	0.52
Dimethyl sulfoxide	1.00	0.00	0.76
Tetrahydrofuran	0.58	0.00	0.55

The present review demonstrates how the linear solvation energy relationship method can be used to unravel, quantify, correlate and rationalize the multiple interacting effects of the selected solvent set on the reactivity parameters of carboxylic acids in their reaction with DDM.

3.1. Cycloalkenecarboxylic and cycloalkeneacetic acids

The values of the second-order rate constants for the reaction of cycloalkene-carboxylic, cycloalkeneacetic, benzoic and phenylacetic acids with DDM in 12 aprotic solvents and 3 protic solvents are given in Tables II and III.

The obtained results show that the rate constants increase with increasing solvent polarity. This is in accordance with the supposed mechanism of the re-action.[15–17,45,46]

The exceptionally high value of the reaction rate constant in chloroform could be explained by the low polarity of this solvent ($\pi^* = 0.58$) and the complete lack of proton acceptor effects, because of which the carboxylic acid dissolved in it exists in the form of dimers.[45] The dimer can appear in two forms, *i.e.*, a cyclic (I) and an open (II) form, which is a very reactive form because it can easily loose a proton and convert into a resonance-stabilized anion (III) (Fig. 2). As the carboxylic anion is the reacting form in this system, it continuously converts into products and this is the probable reason why the open chain dimer, which stabilizes the anion, is the dominant form.

In aprotic solvents of higher polarity, where the proton-acceptor effect exists, solvation of a dissolved acid does not allow the formation of any kind of

TABLE II. Second-order rate constants, dm^3 mol^{-1} min^{-1}, for the reaction of cycloalkene-carboxylic acids and benzoic acid with diazodiphenylmethane at 30 °C in various solvents

Solvent	Cyclopent-1-ene-carboxylic acid	Cyclohex-1-ene-carboxylic acid	Cyclohept-1-ene-carboxylic acid	Benzoic acid
Methyl acetate	0.044	0.032	0.031	0.260
Cyclohexanone	0.028	0.020	0.019	0.220
Diethyl ketone	0.073	0.053	0.051	0.265
Carbon tetrachloride	0.399	0.329	0.286	0.638
Chloroform	5.373	4.335	3.378	12.30
Ethyl acetate	0.038	0.025	0.016	0.180
Cyclopentanone	0.036	0.025	0.025	0.293
Dioxane	0.088	0.065	0.062	0.058
Acetonitrile	0.430	0.318	0.199	3.730
Acetone	0.059	0.048	0.039	0.350
Methanol	1.106	0.818	0.654	2.470
Ethanol	0.534	0.417	0.332	0.995
Ethylene glycol	2.452	1.962	1.570	4.020
Dimethyl sulfoxide	0.012	0.008	0.007	0.141
Tetrahydrofuran	0.027	0.019	0.016	0.105

TABLE III. Second-order rate constants, dm^3 mol^{-1} min^{-1}, for the reaction of cycloalkene-acetic acids and phenylacetic acid with diazodiphenylmethane at 30 °C in various solvents

Solvent	Cyclopent-1-ene-acetic acid	Cyclohex-1-ene-acetic acid	Cyclohept-1-ene-acetic acid	Phenylacetic acid
Methyl acetate	0.181	0.144	0.098	0.132
Cyclohexanone	0.187	0.149	0.102	0.153
Diethyl ketone	0.268	0.214	0.148	0.279
Carbon tetrachloride	2.161	1.759	1.299	6.628
Chloroform	46.06	37.84	29.02	613.0
Ethyl acetate	0.036	0.028	0.017	0.210
Cyclopentanone	0.139	0.110	0.074	0.117
Dioxane	0.319	0.255	0.177	0.169
Acetonitrile	1.535	1.294	0.972	8.919
Acetone	0.246	0.194	0.146	0.233
Methanol	2.237	1.652	1.299	2.539
Ethanol	0.828	0.659	0.614	1.139
Ethylene glycol	4.080	3.020	2.237	5.049
Dimethyl sulfoxide	0.031	0.024	0.016	0.014
Tetrahydrofuran	0.071	0.056	0.039	0.057

dimer or, therefore, of the anion (III). Taking this into consideration, there still remains the question of why the reaction of carboxylic acids and DDM in other non-polar solvent, carbon tetrachloride for example ($\pi^* = 0.28$) does not proceed as fast as in chloroform. The answer could be found in the fact that the structure of chloroform includes a hydrogen atom bonded to a carbon surrounded by three

electronegative chlorine molecules – therefore it has a proton-donating effect, which accelerates the reaction ($\alpha = 0.44$).
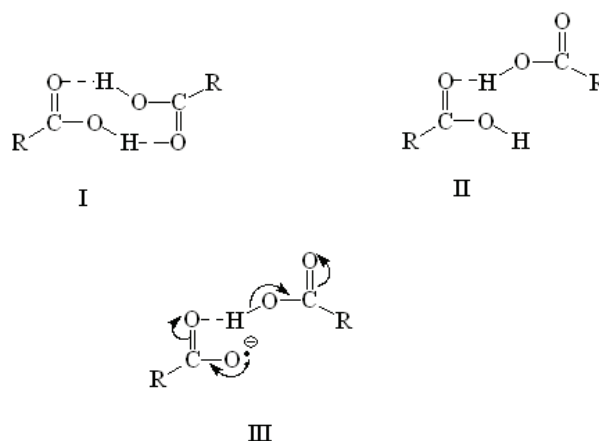

Fig. 2. Different forms of dimers of carboxylic acids that exist in non-polar aprotic solvents.

It is interesting to compare the differences in the rate constants for examined acids because strain effects due to the endocyclic double bond are responsible for prominent changes in the acid reactivity. The presence of a double bond in a five-membered ring leads to a "tension" in the system, which is in a six-membered ring, for example, relieved by folding of the molecule into the "half-chair" conformation – in a five-membered one, there is no similar effect. It was found that the cyclopentene acids have higher rate constants than the corresponding cyclohexene acids (Tables II and III). Cyclohept-1-enecarboxylic and cyclohept--1-eneacetic acids have slightly lower rate constants than the other two mentioned acid systems, which is probably due to the fact that even the slight strain present in the cyclohexene acid systems is absent from the larger seven-membered rings.

The rate constants for cycloalkeneacetic acids (Table III) in all the employed solvents were higher than those for cycloalkenecarboxylic acids in the corresponding alcohols. This is in accordance with the fact that the resonance interaction between the double bond and the carbonyl group in the cycloalkenecarboxylic acids causes a decrease in the acid strength.

In order to explain the obtained kinetic results through the solvent polarity and basicity or acidity, the rate constants were correlated with the solvatochromic parameters π^*, α and β[11] using the total solvatochromic equation, Eq. (2). The correlations of the kinetic data were realized by means of multiple linear regression analysis. It was found that the rate constants in fifteen solvents showed satisfactory correlation with the π^*, α and β solvent parameters. The obtained correlation results are as follows:

Cyclopent-1-enecarboxylic acid:

$$\log k = -0.46 + (0.42 \pm 0.18)\pi^* + (2.04 \pm 0.08)\alpha - (2.47 \pm 0.19)\beta \quad (4a)$$
$$R = 0.992, \, s = 0.13, \, n = 15.$$

Cyclohex-1-enecarboxylic acid:

$$\log k = -0.57 + (0.41 \pm 0.19)\pi^* + (2.09 \pm 0.08)\alpha - (2.54 \pm 0.16)\beta \quad (4b)$$
$$R = 0.992, \, s = 0.11, \, n = 15.$$

Cyclohept-1-enecarboxylic acid:

$$\log k = -0.63 + (0.36 \pm 0.22)\pi^* + (2.03 \pm 0.09)\alpha - (2.47 \pm 0.18)\beta \quad (4c)$$
$$R = 0.989, \, s = 0.13, \, n = 15.$$

Cyclopent-1-eneacetic acid:

$$\log k = 0.18 + (0.76 \pm 0.41)\pi^* + (1.88 \pm 0.18)\alpha - (3.22 \pm 0.34)\beta \quad (4d)$$
$$R = 0.968, \, s = 0.24, \, n = 15.$$

Cyclohex-1-eneacetic acid:

$$\log k = 0.09 + (0.77 \pm 0.42)\pi^* + (1.86 \pm 0.18)\alpha - (3.25 \pm 0.35)\beta \quad (4e)$$
$$R = 0.966, \, s = 0.25, \, n = 15.$$

Cyclohept-1-eneacetic acid:

$$\log k = -0.02 + (0.70 \pm 0.47)\pi^* + (1.95 \pm 0.20)\alpha - (3.25 \pm 0.39)\beta \quad (4f)$$
$$R = 0.961, \, s = 0.27, \, n = 15.$$

Similar results were obtained by correlating the literature kinetic data for benzoic acid[29,47] determined at 37 °C and the kinetic data determined previously for phenylacetic acid[44] (Table III). The obtained correlation results are given below:

Benzoic acid:

$$\log k = -0.58 + (1.43 \pm 0.44)\pi^* + (1.57 \pm 0.19)\alpha - (2.23 \pm 0.39)\beta \quad (5a)$$
$$R = 0.940, \, s = 0.26, \, n = 15.$$

Phenylacetic acid:

$$\log k = 0.82 + (0.92 \pm 0.57)\pi^* + (2.27 \pm 0.25)\alpha - (4.71 \pm 0.47)\beta \quad (5b)$$
$$R = 0.967, \, s = 0.33, \, n = 15.$$

From all the equations above, it can be concluded that the solvent effects influence the carboxylic acid–DDM reaction by two opposing effects. The opposite signs of the electrophilic and the nucleophilic parameters are in accordance with the described mechanism (Fig. 1). The positive signs of the s and α coefficients prove that classical solvation and HBD effects dominate the transition state and increase the reaction rate, and the negative sign of the β coefficient indicate that HBA effects stabilize the initial state before commencement of the reaction and are responsible for a decrease in the reaction rate. The degree of success of above correlations is shown in Fig. 3 by means of a plot of log k cal-
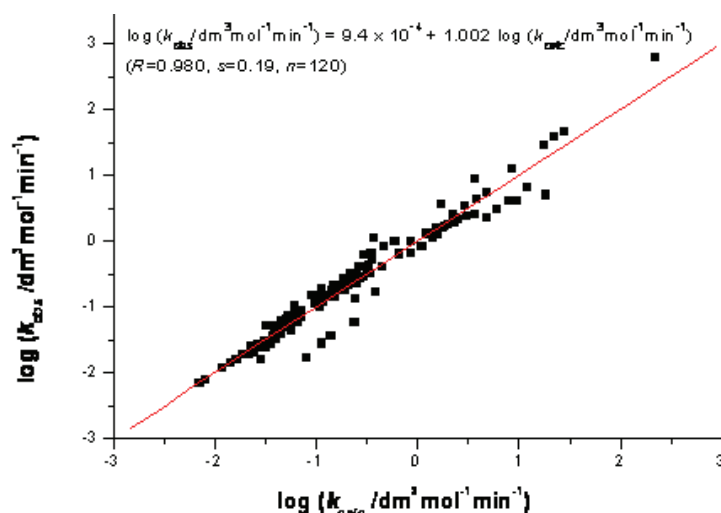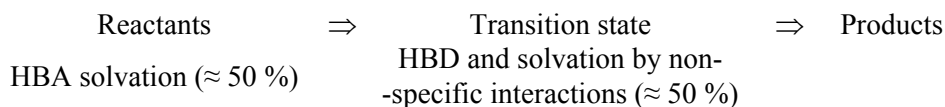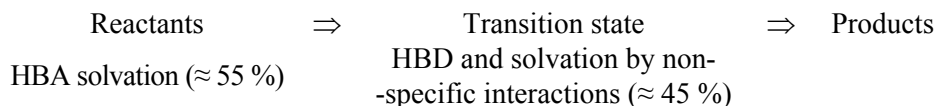
Fig. 3. The plot of *log k* observed (Tables II and III) against *log k* calculated from
Eq. (2) for cycloalkenecarboxylic, cycloalkeneacetic, benzoic
and phenylacetic acids in different solvents.

culated *vs*. log *k* obtained experimentally for cycloalkenecarboxylic, cycloalkeneacetic, benzoic and phenylacetic acid in different solvents. From the values of regression coefficients, the contribution of each parameter to the reactivity, on a percentage basis, were calculated and are listed in Table IV. The percentage contribution of solvatochromic parameters for the reaction of the examined acids with DDM, show that most of the solvatochromism is due to solvent basicity and acidity rather than to the solvent dipolarity/polarizability. Considering these results, the solvation models of the reactants and the transition states, separately for cycloalkenecarboxylic and cycloalkeneacetic acids can be represented as:

Cycloalkenecarboxylic acids:

Reactants	$\Rightarrow$	Transition state	$\Rightarrow$	Products
HBA solvation ($\approx 50\ \%$)		HBD and solvation by non-specific interactions ($\approx 50\ \%$)		

Cycloalkeneacetic acids:

Reactants	$\Rightarrow$	Transition state	$\Rightarrow$	Products
HBA solvation ($\approx 55\ \%$)		HBD and solvation by non-specific interactions ($\approx 45\ \%$)		

The suggested solvation models indicate that the cycloalkeneacetic acid system is more sensitive to HBA interactions of the solvent than the cycloalkenecarboxylic acid system (Table IV) and less sensitive to the HBD ability of the solvent. This is in accordance with the fact that the resonance interaction between

Available online at www.shd.org.rs/JSCS/

the double bond and the carbonyl group in the case of cycloalkenecarboxylic acids destabilizes the carboxylic anion and causes a stronger solvation of the transition state in this system than in the case of cycloalkeneacetic acid system.

Table IV. The percentage contributions of the Kamlet–Taft solvatochromic parameters to the reactivity of various acids

Acid	P_{π^*} / %	P_{α} / %	P_{β} / %
Cyclopent-1-enecarboxylic	9	41	50
Cyclohex-1-enecarboxylic	8	42	50
Cyclohept-1-enecarboxylic	7	42	51
Benzoic	27	30	43
Cyclopent-1-eneacetic	13	32	55
Cyclohex-1-eneacetic	13	32	55
Cyclohept-1-eneacetic	12	33	55
Phenylacetic	12	29	59

3.2. 2-Substituted cyclohex-1-enecarboxylic and 2-substituted benzoic acids

The obtained second-order rate constants for the examined 2-substituted cyclohex-1-enecarboxylic and benzoic acids in 11 aprotic solvents (excluding chloroform), and 3 protic solvents, are given in Tables V and VI, respectively.

TABLE V. Reaction rate constants, dm^3 mol^{-1} min^{-1}, for the reaction of 2-substituted cyclohex-1-enecarboxylic acids with diazodiphenylmethane at 30 °C in various solvents

Solvent	2-Methylcyclohex-1-ene-carboxylic acid	2-Ethylcyclohex-1-ene-carboxylic acid	2-Chlorocyclohex-1-ene-carboxylic acid	2-Bromocyclohex-1-ene-carboxylic acid	2-Iodocyclohex-1-ene-carboxylic acid
Methyl acetate	0.093	0.095	0.563	0.614	0.642
Cyclohexanone	0.044	0.099	0.531	0.583	0.603
Diethyl ketone	0.064	0.110	0.583	0.634	0.653
Carbon tetrachloride	0.359	0.256	0.795	1.006	1.036
Ethyl acetate	0.058	0.082	0.501	0.574	0.606
Cyclopentanone	0.053	0.108	0.569	0.614	0.658
Dioxane	0.077	0.046	0.554	0.646	0.684
Acetone	0.106	0.116	0.680	0.831	0.891
Methanol	0.567	0.583	2.244	2.321	2.614
Ethanol	0.264	0.278	1.130	1.279	1.470
Dimethyl sulfoxide	0.013	0.060	0.198	0.210	0.230
Tetrahydrofuran	0.027	0.055	0.179	0.191	0.204
Acetonitrile	0.420	0.347	1.580	1.623	1.782
Ethylene glycol	1.631	1.649	5.222	5.169	5.738

The obtained results show that the rate constants increased with increasing solvent polarity. Comparison of the values of the reaction constants in protic and aprotic solvents indicates that the examined reaction is slower in aprotic solvents, which is in accordance with the proposed reaction mechanism.[15–17,45,46]

TABLE VI. Reaction rate constants, dm^3 mol^{-1} min^{-1}, for the reaction of 2-substituted benzoic acids with diazodiphenylmethane at 30 °C in various solvents

Solvent	2-Methylben-zoic acid	2-Ethylben-zoic acid	2-Chloroben-zoic acid	2-Bromoben-zoic acid	2-Iodobenzoic acid
Methyl acetate	0.124	0.130	1.543	1.620	1.720
Cyclohexanone	0.129	0.138	1.393	1.510	1.580
Diethyl ketone	0.157	0.160	1.510	1.690	1.760
Carbon tetrachloride	0.389	0.496	1.200	1.380	1.412
Ethyl acetate	0.094	0.106	1.479	1.480	1.590
Cyclopentanone	0.145	0.154	1.530	1.620	1.780
Dioxane	0.035	0.048	0.750	0.758	0.813
Acetone	0.152	0.170	2.087	2.440	2.680
Methanol	1.860	2.526	12.71	13.75	15.22
Ethanol	0.933	0.986	4.388	5.627	5.960
Dimethyl sulfoxide	0.079	0.072	0.512	0.522	0.586
Tetrahydrofuran	0.060	0.062	0.454	0.464	0.482
Acetonitrile	1.590	1.654	5.852	6.023	6.759
Ethylene glycol	2.590	2.680	10.69	11.08	11.84

The correlations of the kinetic data were realized by means of multiple linear regression analysis. It was found that the rate constants in the applied set of fourteen solvents showed satisfactory correlation with the π^*, α and β solvent parameters together in the same equation. The obtained correlation results are given in Table VII.

From the values of the regression coefficients, the contributions of each parameter to the reactivity, on a percentage basis, were calculated and are listed in Table VIII.

From these results, it can be noticed that the non-specific interactions (π^*) are less pronounced than the specific (α and β) in both carboxylic acid systems. However, the specific interactions have more influence on the cyclohexene system than on the benzoic system. This probably means that the carboxyl group of the cyclohexene acids is more susceptible to proton-donor and proton-acceptor solvent effects than the carboxyl group of the benzoic acids.

In order to obtain a complete view of the solvent interactions with the molecules of the examined carboxylic acids, the solvent effects were expressed quantitatively for every acid, referring separately to the reactants and the transition state and the results are given in Table IX.

Higher reaction rates and more pronounced effects of HBD solvation and non-specific interactions (polarity/polarizability) can be noticed for the halogen--substituted acids in both systems. As the negative inductive effect of the halogen at C-2 stabilizes the carboxylic anion, it supports the transition state, thus accelerating the reaction.

UŠĆUMLIĆ and NIKOLIĆ

TABLE VII. The results of the correlations of the kinetic data for 2-substituted cyclohex-1--enecarboxylic and 2-substituted benzoic acids with Eq. (2)

Acid	s^a	a^a	b^a	R^b	s^c	F^d	n^e
Cyclohex-1-enecarboxylic acid	0.38 ± 0.20	2.07 ± 0.09	2.48 ± 0.21	0.990	0.11	168	14
2-Methylcyclohex-1-enecarboxylic acid	0.52 ± 0.16	1.66 ± 0.07	2.35 ± 0.17	0.989.	0.09	162	14
2-Ethylcyclohex-1-enecarboxylic acid	0.87 ± 0.21	1.24 ± 0.10	1.51 ± 0.22	0.972	0.12	58	14
2-Chlorocyclohex-1-enecarboxylic acid	0.75 ± 0.21	1.07 ± 0.10	1.42 ± 0.22	0.960	0.12	39	14
2-Bromocyclohex-1-enecarboxylic acid	0.64 ± 0.22	1.04 ± 0.10	1.42 ± 0.23	0.954	0.13	20	14
2-Iodocyclohex-1-enecarboxylic acid	0.65 ± 0.22	1.07 ± 0.10	1.40 ± 0.23	0.957	0.13	36	14
Benzoic acid	1.34 ± 0.47	1.51 ± 0.22	1.98 ± 0.49	0.915	0.26	17	14
2-Methylbenzoic acid	1.05 ± 0.44	1.64 ± 0.20	1.75 ± 0.46	0.932	0.25	22	14
2-Ethylbenzoic acid	0.92 ± 0.29	1.81 ± 0.13	1.79 ± 0.31	0.973	0.10	75	14
2-Chlorobenzoic acid	0.93 ± 0.19	1.28 ± 0.09	1.33 ± 0.20	0.978	0.10	75	14
2-Bromobenzoic acid	0.83 ± 0.19	1.28 ± 0.09	1.25 ± 0.20	0.976	0.11	70	14
2-Iodobenzoic acid	0.89 ± 0.19	1.31 ± 0.09	1.27 ± 0.21	0.977	0.11	71	14

[a]Calculated solvatochromic coefficient; [b]correlation coefficient; [c]standard deviation of the estimate; [d]Fisher's test; [e]number of points used in the calculation

TABLE VIII. The percentage contributions of Kamlet–Taft's solvatochromic parameters to the reactivity for the studied cyclohex-1-enecarboxylic acids and benzoic acids

Acid	P_{π^*} / %	P_{α} / %	P_{β} / %
Cyclohex-1-enecarboxylic acid	8	42	50
2-Methylcyclohex-1-enecarboxylic acid	11	37	52
2-Ethylcyclohex-1-enecarboxylic acid	24	34	42
2-Chlorocyclohex-1-enecarboxylic acid	23	33	44
2-Bromocyclohex-1-enecarboxylic acid	21	34	46
2-Iodocyclohex-1-enecarboxylic acid	21	34	45
Benzoic acid	28	31	41
2-Methylbenzoic acid	24	37	39
2-Ethylbenzoic acid	20	40	40
2-Chlorobenzoic acid	26	36	38
2-Bromobenzoic acid	25	38	37
2-Iodobenzoic acid	26	38	36

Considering the results presented in Table IX, the solvation models of the reactants and the transition state, considered separately for the 2-substituted cyclohex-1-enecarboxylic and 2-substituted benzoic acid systems, can be represented as:

2-Substituted cyclohex-1-enecarboxylic acids:

Reactants	$\Rightarrow$	Transition state	$\Rightarrow$	Products
HBA salvation (≈ 46 %)		HBD and solvation by non--specific interactions (≈ 54 %)		

2-Substituted benzoic acids:

Reactants   ⇒   Transition state   ⇒   Products

HBA salvation (≈ 38 %)

HBD and solvation by non-
-specific interactions (≈ 62 %)
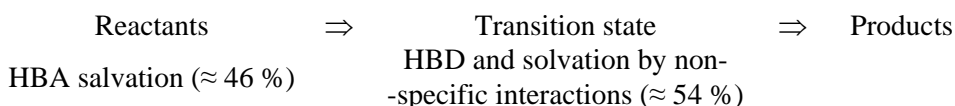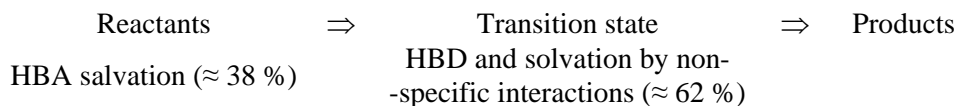
TABLE IX. The solvent effects for the studied cyclohex-1-enecarboxylic acids and benzoic acids

Acid	HBA solvation (β)/ % (effect on the reactants)	HBD solvation (α) + non-specific interactions (π^*)/ % (effect on the transition state)
Cyclohex-1-enecarboxylic acid	50	50
2-Methylcyclohex-1-enecarboxylic acid	52	48
2-Ethylcyclohex-1-enecarboxylic acid	42	58
2-Chlorocyclohex-1-enecarboxylic acid	44	56
2-Bromocyclohex-1-enecarboxylic acid	46	54
2-Iodocyclohex-1-enecarboxylic acid	45	55
Benzoic acid	41	59
2-Methylbenzoic acid	39	61
2-Ethylbenzoic acid	40	60
2-Chlorobenzoic acid	38	62
2-Bromobenzoic acid	37	63
2-Iodobenzoic acid	36	64

The results presented here show that the proton-acceptor solvent effects are somewhat more pronounced in the ground state for cyclohex-1-enecarboxylic acid and its 2-substituted derivatives than for benzoic acids, supporting the fact that the reaction rates were higher for the benzoic acids. The dominant solvent effects for the benzoic acid type are proton-donor and non-specific interactions, characteristic for the transition state. This fact is likely to be a consequence of the degree of conjugation of the carboxylic group of the benzoic acids with the ring; in other words, the charge distribution in the carboxylic group, which is the result of the conjugation, makes the anion more stable and, therefore, the reaction faster. However, a more general conclusion that arises from these results is that the substituents at the C-2 position in both carboxylic acid types have a secondary influence on the reaction with DDM, and seem not to cause steric hindrance between the reactants and the solvent. The principal influences on these reaction rates are apparently the properties of the solvent and the general form of the molecule of the carboxylic acid.

3.3. 2-Substituted cyclohex-1-eneacetic and 2-substituted phenylacetic acids

The values of second-order rate constants for the reaction of the examined 2-substituted cyclohex-1-eneacetic and 2-substituted phenylacetic acids with DDM in 11 aprotic and 3 protic solvents are given in Tables X and XI.

Available online at www.shd.org.rs/JSCS/
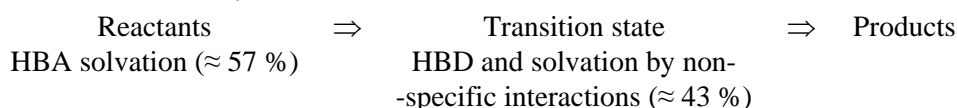
TABLE X. The second-order rate constants, dm^3 mol^{-1} min^{-1}, for the reaction of 2-substituted cyclohex-1-eneacetic acids with diazodiphenylmethane at 30 °C in various solvents

Solvent	2-Methyl-cyclohex-1--eneacetic acid	2-Ethyl-cyclohex-1--eneacetic acid	2-Chloro-cyclohex-1--eneacetic acid	2-Bromo-cyclohex-1--eneacetic acid	2-Iodocy-clohex-1--eneacetic acid	2-Nitro-cyclohex-1--eneacetic acid
Methyl acetate	0.087	0.092	0.285	0.290	0.331	1.461
Cyclohexanone	0.092	0.097	0.286	0.289	0.329	1.357
Diethyl ketone	0.133	0.141	0.406	0.411	0.467	1.880
Carbon tetrachloride	1.117	1.178	3.251	3.251	3.716	14.13
Ethyl acetate	0.078	0.083	0.249	0.251	0.288	1.230
Cyclopen-tanone	0.066	0.071	0.216	0.217	0.251	1.096
Dioxane	0.077	0.081	0.229	0.229	0.262	1.020
Acetonitrile	0.803	0.849	2.469	2.472	2.841	11.57
Acetone	0.118	0.125	0.380	0.385	0.440	1.898
Methanol	0.890	0.942	2.479	2.669	3.212	9.682
Ethanol	0.350	0.362	0.963	1.080	1.269	4.230
Ethylene glycol	1.550	1.607	3.775	4.197	4.932	12.36
Dimethyl sulfoxide	0.018	0.019	0.038	0.042	0.067	0.242
Tetrahydro-furan	0.034	0.036	0.111	0.117	0.129	0.578

In order to explain the obtained kinetic results through solvent dipolarity/polarizability and basicity or acidity, the rate constants were correlated with the solvatochromic parameters π^*, α and β,[11] using the total solvatochromic equation, Eq. (2). The correlations of the kinetic data were realized by means of multiple linear regression analysis. It was found that the rate constants in the 14 selected solvents showed satisfactory correlation with the π^*, α and β solvent parameters. The obtained correlation results are given in Tables XII and XIII.

The percentage contribution of each solvent effect for each acid is given in Table XIV. The specific interactions, the HBA and HBD effects, are dominant and have a rather similar share for both acid types, but the classical solvation effects are somewhat higher for the phenylacetic acids, especially for its halogen- and nitro-substituted derivatives. To obtain a complete view of the solvent interaction with the molecules of the examined acids, the solvent effects are expressed quantitatively for both carboxylic acid systems and the ground and the transition state are referred to separately.

2-Substituted cyclohex-1-eneacetic acids:

Reactants	$\Rightarrow$	Transition state	$\Rightarrow$	Products
HBA solvation (≈ 57 %)		HBD and solvation by non--specific interactions (≈ 43 %)		

TABLE XI. The second-order rate constants, dm^3 mol^{-1} min^{-1}, for the reaction of 2-substituted phenylacetic acids with diazodiphenylmethane at 30 °C in various solvents

Solvent	2-(2-Methyl-phenyl)acetic acid	2-(2-Ethyl-phenyl) acetic acid	2-(2-Chloro-phenyl) acetic acid	2-(2-Bromo-phenyl) -acetic acid	2-(2-Iodophe-nyl)acetic acid	2-(2-Nitro-phenyl) acetic acid
Methyl acetate	0.063	0.066	0.169	0.182	0.198	0.290
Cyclohexanone	0.089	0.096	0.232	0.240	0.252	0.316
Diethyl ketone	0.165	0.168	0.358	0.364	0.376	0.560
Carbon tetra-chloride	4.041	5.153	7.816	7.880	8.126	12.86
Ethyl acetate	0.109	0.124	0.273	0.286	0.294	0.462
Cyclopentanone	0.058	0.061	0.157	0.184	0.199	0.264
Dioxane	0.102	0.140	0.239	0.248	0.259	0.342
Acetonitrile	3.802	3.955	10.57	11.03	11.16	16.28
Acetone	0.101	0.113	0.348	0.360	0.384	0.486
Methanol	2.420	2.460	3.329	3.500	3.790	5.110
Ethanol	1.010	1.020	1.440	1.559	1.670	2.470
Ethylene glycol	5.333	5.457	6.761	7.261	8.035	8.750
Dimethyl sul-foxide	0.008	0.007	0.021	0.034	0.040	0.164
Tetrahydrofuran	0.033	0.033	0.092	0.098	0.134	0.198

TABLE XII. The results of the correlations of the kinetic data for 2-substituted cyclohex-1--eneacetic acids with Eq. (2)

Acid	s^a	a^a	b^a	R^b	s^c	F^d	n^e
Cyclohex-1-eneacetic acid	0.40 ± 0.21	1.67± 0.10	2.73 ± 0.22	0.985	0.12	112	14
2-Methylcyclohex-1-eneacetic acid	0.50 ± 0.25	1.61± 0.12	2.71 ± 0.28	0.977	0.14	71	14
2-Ethylcyclohex-1-eneacetic acid	0.50 ± 0.25	1.60± 0.12	2.70 ± 0.27	0.977	0.14	70	14
2-Chlorocyclohex-1-eneacetic acid	0.38 ± 0.28	1.55± 0.13	2.72 ± 0.30	0.972	0.16	55	14
2-Bromocyclohex-1-eneacetic acid	0.39 ± 0.28	1.58± 0.13	2.67 ± 0.29	0.973	0.16	59	14
2-Iodocyclohex-1-eneacetic acid	0.46± 0.26	1.57± 0.12	2.60 ± 0.28	0.975	0.15	63	14
2-Nitrocyclohex-1-eneacetic acid	0.36 ± 0.30	1.58± 0.14	2.50 ± 0.32	0.962	0.17	41	14

[a]Calculated solvatochromic coefficient; [b]correlation coefficient; [c]standard deviation of the estimate; [d]Fisher's test; [e]number of points used in the calculation

2-Substituted phenylacetic acids:

Reactants $\Rightarrow$ Transition state $\Rightarrow$ Products
HBA solvation (≈ 58 %) HBD and solvation by non--specific interactions (≈ 42 %)
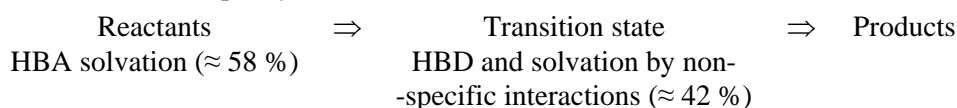
TABLE XIII. The results of the correlations of the kinetic data for 2-substituted phenylacetic acids with Eq. (2)

Acid	s^a	a^a	b^a	R^b	s^c	F^d	n^e
Phenylacetic acid	0.66 ± 0.52	2.08 ± 0.24	3.99 ± 0.55	0.952	0.29	32	14
2-(2-Methylphenyl)acetic acid	0.55 ± 0.47	2.36 ± 0.22	3.93 ± 0.49	0.966	0.26	47	14
2-(2-Ethylphenyl)acetic acid	0.45 ± 0.45	2.35 ± 0.21	4.04 ± 0.48	0.969	0.25	51	14
2-(2-Chlorophenyl)acetic acid	0.67 ± 0.49	2.03 ± 0.23	3.85 ± 0.52	0.983	0.12	96	14
2-(2-Bromophenyl)acetic acid	0.76 ± 0.47	1.98 ± 0.22	3.71 ± 0.50	0.954	0.28	34	14
2-(2-Iodophenyl)acetic acid	0.75 ± 0.46	1.96 ± 0.21	3.61 ± 0.48	0.952	0.26	35	14
2-(2-Nitrophenyl)acetic acid	0.82 ± 0.54	1.79 ± 0.25	3.31 ± 0.56	0.929	0.30	22	14

[a]Calculated solvatochromic coefficient; [b]correlation coefficient; [c]standard deviation of the estimate; [d]Fisher's test; [e]number of points used in the calculation
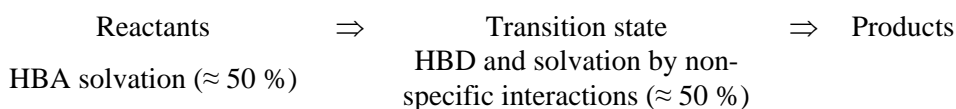
TABLE XIV. The percentage contributions of the Kamlet-Taft solvatochromic parameters to the reactivity

Acid	$P_{\pi*}$ / %	P_{α} / %	P_{β} / %
Cyclohex-1-eneacetic acid	8	35	57
2-Methylcyclohex-1-eneacetic acid	10	33	57
2-Ethylcyclohex-1-eneacetic acid	10	33	57
2-Chlorocyclohex-1-eneacetic acid	8	33	59
2-Bromocyclohex-1-eneacetic acid	8	34	58
2-Iodocyclohex-1-eneacetic acid	10	34	56
2-Nitrocyclohex-1-eneacetic acid	8	36	56
Phenylacetic acid	10	31	59
2-(2-Methylphenyl)acetic acid	8	35	57
2-(2-Ethylphenyl)acetic acid	7	35	58
2-(2-Chlorophenyl)acetic acid	10	31	59
2-(2-Bromophenyl)acetic acid	12	31	57
2-(2-Iodophenyl)acetic acid	12	31	57
2-(2-Nitrophenyl)acetic acid	14	30	56

It can be noticed that the two examined carboxylic acid types behave similarly, as can be seen from the distributions of solvent effects that are practically the same. However, the more general conclusion that arises from these results is that the substituents at the C-2 position in both carboxylic acid types have a very weak influence on the solvation effects during reaction with DDM. The phenylacetic acids are somewhat faster than the corresponding cyclohexeneacetic ones, which makes sense, as their structure is more approachable for the other reactant as well as for solvent, but there seems to be no great difference. On the contrary, in the case of the α,β-unsaturated cyclic carboxylic acids there was a considerable difference between the reaction rate constants of benzoic and cyclohex-1--enecarboxylic acids regardless of the presence of substituents.[42,43] In other

words, the ring type determines the reactivity of a carboxylic acid. For β,γ-unsaturated acids, the ring is sufficiently far removed from the reaction center (the carboxylic group) to have much influence on it, hence the steric and electronic effects of substituents in the γ-position are more visible. Regarding the geometric properties, the 2-substituted cyclohex-1-eneacetic acids and 2-substituted phenylacetic acids have similar torsion angles, as well as the reactivity, but the α,β-unsaturated cyclic carboxylic acids (benzoic and cyclohex-1-enecarboxylic) have completely a different geometry and, subsequently, behave differently in the same reaction. The torsion angle (C_2–C_3–C_4) for benzoic acid is –16.60° and for cyclohex-1-enecarboxylic acid 142.0°. Their values are very different and the carboxylic groups are orientated in opposing directions.[43]

3.4. 2-Phenylcyclohex-1-enecarboxylic, 2-phenylbenzoic and 2-phenylacrylic acids

The transmission of substituent effects through three types of double bond, *i.e.*, in a ring, open chain and delocalized double bonds, were investigated previously in the case of 2-(4-substitutedphenyl)cyclohex-1-enecarboxylic acids,[33,35] 2-(4-substitutedphenyl)benzoic acids[33,48] and 2-(4-substitutedphenyl)acrylic acids.[33,35] The results showed that there were differences in the composition of the electronic effect depending on the type of double bond through which the substituent effects were transmitted. The considerable difference between the reaction constants, ρ, of the investigated acids indicates that, regardless of the identical possibility of steric interactions of the phenylene and the carboxylic group, there is probably a different interaction of the phenylene group with the rest of the molecule. This assumption was confirmed with Dreiding models.

In the present review, the values of the second order rate constants for the reaction of 2-phenylcyclohex-1-enecarboxylic, 2-phenylbenzoic and 2-phenylacrylic acids with DDM in 11 aprotic and 3 protic solvents (Table XV) were correlated with the solvatochromic parameters π^*, α and β using the total solvatochromic equation. The correlation of the kinetic data was realized by means of multiple linear regression analysis.

It was found that the rate constants in 14 solvents showed satisfactory correlation with the solvatochromic parameters π^*, α and β. The obtained correlation results were as follows:

2-Phenylcyclohex-1-enecarboxylic acid:

$$\log k = -0.14 + (0.35 \pm 0.22)\pi^* + (2.34 \pm 0.10)\alpha - (2.70 \pm 0.24)\beta \quad (6a)$$
$$(R = 0.991, \ s = 0.13, \ F = 175, \ n = 14).$$

2-Phenylbenzoic acid:

$$\log k = -0.34 + (0.99 \pm 0.41)\pi^* + (2.11 \pm 0.19)\alpha - (1.90 \pm 0.44)\beta \quad (6b)$$
$$(R = 0.961, \ s = 0.24, \ F = 40, \ n = 14).$$

Available online at www.shd.org.rs/JSCS/

2-Phenylacrylic acid:

$$\log k = 0.24 + (0.29 \pm 0.19)\pi^* + (1.92 \pm 0.09)\alpha - (2.23 \pm 0.21)\beta \qquad (6c)$$
$$(R = 0.989,\ s = 0.11,\ F = 151,\ n = 14).$$

TABLE XV. The second-order rate constants, dm^3 mol^{-1} min^{-1}, for the reaction of 2-phenyl-cyclohex-1-enecarboxylic, 2-phenylbenzoic and 2-phenylacrylic acids with diazodiphenylme-thane at 30 °C in various solvents

Solvent	2-Phenylcyclohex-1--enecarboxylic acid	2-Phenylbenzoic acid	2-Phenylacrylic acid
Methyl acetate	0.068	0.316	0.244
Cyclohexanone	0.038	0.246	0.151
Diethyl ketone	0.133	0.268	0.424
Carbon tetrachloride	0.873	1.010	2.001
Ethyl acetate	0.054	0.236	0.201
Cyclopentanone	0.049	0.338	0.186
Dioxane	0.142	0.110	0.447
Acetonitrile	0.839	5.500	1.937
Acetone	0.103	0.400	0.343
Methanol	2.790	11.61	5.219
Ethanol	1.279	5.000	2.743
Ethylene glycol	6.367	15.37	10.31
Dimethyl sulfoxide	0.014	0.162	0.066
Tetrahydrofuran	0.037	0.147	0.147

From all the equations above, it can be concluded that two opposing solvent effects influence the carboxylic acid – DDM reaction. The opposite signs of the electrophilic and the nucleophilic parameters are in accordance with the descri-bed mechanism (Fig. 1). The positive signs of the coefficients *s* and *a* prove that classical solvation and the HBD effects dominate the transition state and increase the reaction rate, and the negative sign of the coefficient *b* indicates that HBA effects stabilize the initial state before the reaction commences and are res-ponsible for a decrease in the reaction rate. From the values of the regression co-efficients, the contribution of each parameter to the reactivity, on a percentage basis, were calculated and are listed in Table XVI. The percentage contribution of the solvatochromic parameters for the reaction of the examined acids with DDM show that most of the solvatochromism is due to solvent basicity and aci-dity rather than to the solvent dipolarity/polarizability. Considering these results, the solvation models of the reactants and the transition states, separately for 2-phenylcyclohex-1-enecarboxylic, 2-phenylbenzoic and 2-phenylacrylic acids can be represented as:

2-Phenylcyclohex-1-enecarboxylic acids:
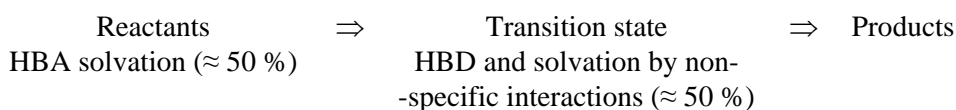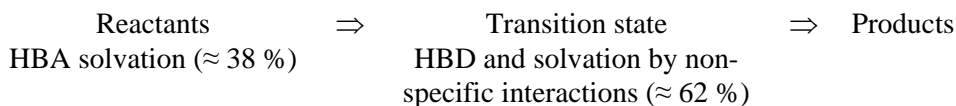
Reactants	$\Rightarrow$	Transition state	$\Rightarrow$	Products
HBA solvation (≈ 50 %)		HBD and solvation by non--specific interactions (≈ 50 %)		

Available online at www.shd.org.rs/JSCS/

2-Phenylbenzoic acids:

Reactants	$\Rightarrow$	Transition state	$\Rightarrow$	Products
HBA solvation ($\approx 38\ \%$)		HBD and solvation by non-specific interactions ($\approx 62\ \%$)		

2-Phenylacrylic acids:

Reactants	$\Rightarrow$	Transition state	$\Rightarrow$	Products
HBA solvation ($\approx 50\ \%$)		HBD and solvation by non-specific interactions ($\approx 50\ \%$)		

TABLE XVI. The percentage contributions of the Kamlet–Taft solvatochromic parameters to the reactivity

Acid	P_{π^*}/ %	P_α/ %	P_β/ %
2-Phenylcyclohex-1-enecarboxylic	6.50	43.50	50.00
2-Phenylbenzoic	20.00	42.00	38.00
2-Phenylacrylic	6.50	43.50	50.00

The suggested solvation models indicate that the 2-phenylcyclohex-1-ene-carboxylic and the 2-phenylacrylic acid systems are more sensitive to HBA solvent interactions than the 2-phenylbenzoic acid system (Table XVI) and less sensitive to the HBD solvent ability. The same results were obtained for a comparative LSER study of the reactivity of 2-substituted cyclohex-1-enecarboxylic and 2-substituted benzoic acids[43] and 2-substituted cyclohex-1-eneacetic and 2-substituted phenylacetic acids[44] presented in this review.

Generally, the presence of a substituent at the C-2 position in all types of examined acids affects the orientation of the carboxylic group. The degree of these interactions is in agreement with the obtained kinetic data, solvation models and characteristics of the examined carboxylic acid molecules.[42–44]

4. CONCLUDING REMARKS

The results of the presented investigations show that the solvatochromic concept of Kamlet and Taft (LSER) is applicable to the kinetic data for the reaction of more than 50 different carboxylic acids with diazodiphenylmethane in various solvents, meaning that this model gives the correct interpretation of the solvating effects on the carboxylic group in the selected solvents. For these reasons, it is considered that the results presented in this review may be used to quantitatively estimate and separate the overall solvent effects into the contributions of the initial and the transition state in the reaction of diazodiphenylmethane with carboxylic acids, and the solvation models are proposed. The results show that substituents at the C-2 position of the ring in all types of the investigated acids have a secondary influence on the reaction with DDM and do not seem to cause steric hindrance between the reactants and the solvent. The reactivities of the examined

Available online at www.shd.org.rs/JSCS/

carboxylic acids in the reaction with DDM are in agreement with their geometric characteristics.

И З В О Д

ПРОУЧАВАЊЕ РЕАКТИВНОСТИ КАРБОКСИЛНИХ КИСЕЛИНА СА ДИАЗОДИФЕНИЛМЕТАНОМ У АПРОТИЧНИМ И ПРОТИЧНИМ РАСТВАРАЧИМА ПОМОЋУ ЛИНЕАРНЕ КОРЕЛАЦИЈЕ СОЛВАТАЦИОНИХ ЕНЕРГИЈА

ГОРДАНА С. УШЋУМЛИЋ и ЈАСМИНА Б. НИКОЛИЋ

Катедра за органску хемију, Технолошко–металурщки факултет Универзитета у Београду, Карнегијева 4, п. пр. 3503, 11120 Београд

Утицај растварача на реактивност циклоалкенкарбонских, циклоалкенсирћетних, 2-супституисаних циклохекс-1-енкарбонских, 2-супституисаних циклохекс-1-енсирћетних, 2-супституисаних бензоевих, 2-супституисаних фенилсирћетних, 2-фенилциклохекс-1-енкарбон-ске, 2-фенилбензоеве и 2-фенилакрилне киселине са диазодифенилметаном је проучаван у низу протичних и апротичних растварача. Да би се кинетички резултати објаснили помоћу ефеката растварача, добијене константе брзине реакције другог реда су корелисане помоћу Камлет–Тафтове солватохромне једначине. Корелације кинетичких података су извршене помоћу методе вишеструке линеарне регресионе анализе, а ефекти растварача су посебно анализирани у односу на основно и прелазно стање. Аритметички знаци испред коефиције-ната солватохромних параметара одговарају претпостављеном механизму испитиване реак-ције. Предложен је солватациони модел за све проучаване киселине, који је показао да пос-тоји квантитативни однос молекулске структуре и њихове реактивности.

(Примљено 15. јуна 2009)

REFERENCES

1. E. D. Hughes, C. K. Ingold, *J. Chem. Soc.* (1935) 244
2. J. G. Kirkwood, *J. Phys. Chem.* **2** (1934) 351
3. E. Grunwald, S. Winstein, *J. Am. Chem. Soc.* **70** (1948) 846
4. M. H. Abraham, *Prog. Phys. Org. Chem.* **11** (1974) 1
5. E. F. Caldin, *Pure Appl. Chem.* **51** (1979) 2067
6. C. Reichardt, *Pure Appl. Chem.* **54** (1982) 1867
7. D. Mather, J. Shorter, *J. Chem. Soc. Perkin Trans. 2* (1983) 1179
8. I. A. Koppel, V. A. Palm, in *Advanced Linear Free Energy Relationships*, N. B. Chapman, J. Shorter, Eds., Plenum Press, London, 1972, Ch. 5
9. M. J. Kamlet, J. L. M. Abboud, R. W. Taft, *Prog. Phys. Org. Chem.* **13** (1981) 485
10. M. H. Abraham, R. W. Taft, M. J. Kamlet, *J. Org. Chem.* **46** (1981) 3053
11. M. J. Kamlet, J. L. M. Abboud, M. H. Abraham, R. W. Taft, *J. Org. Chem.* **48** (1983) 2877
12. M. H. Abraham, *Pure Appl. Chem.* **57** (1985) 1055
13. M. H. Aslan, A. G. Burden, N. B. Chapman, J. Shorter, *J. Chem. Soc. Perkin Trans. 2* (1981) 500
14. M. H. Aslan, G. Collier, J. Shorter, *J. Chem. Soc. Perkin Trans. 2* (1981) 1572
15. K. Bowden, N. B. Chapman, J. Shorter, *J. Chem. Soc.* (1963) 5329

16. J. Shorter, *Correlation Analysis of Organic Reactivity,* Wiley, Chichester, UK, 1982, p. 130
17. M. H. Abraham, L. P. Grellier, J. L. M. Abboud, M. R. Doherty, R. W. Taft, *Can. J. Chem.* **66** (1988) 2673
18. G. S. Ušćumlić, V. V. Krstić, M. D. Muškatirović, *J. Serb. Chem. Soc.* **54** (1989) 119
19. G. S. Ušćumlić, V. V. Krstić, M. D. Muškatirović *J. Chem. Soc. Perkin Trans. 2* (1993) 999
20. G. S. Ušćumlić, J. B. Nikolić, V. V. Krstić, *Indian J. Chem. B* **44** (2005) 1283
21. G. S. Ušćumlić, M. D. Muškatirović, *J. Serb. Chem. Soc.* **59** (1994) 803
22. G. S. Ušćumlić, M. D. Muškatirović *J. Chem. Soc. Perkin Trans. 2* (1994) 1799
23. J. B. Nikolić, G. S. Ušćumlić, V. V. Krstić, *J. Serb. Chem. Soc.* **69** (2004) 601
24. G. S. Ušćumlić, V. V. Krstić, M. D. Muškatirović, *J. Serb. Chem. Soc.* **50** (1985) 343
25. J. B. Nikolić, G. S. Ušćumlić, V. V. Krstić, *Indian J. Chem. B* **43** (2004) 1995
26. J. B. Nikolić, G. S. Ušćumlić, V. V. Krstić, in *Recent Progress in Medicinal Plants,* Stadium Press, Houston, TX, Vol. 14, 2006, p. 71
27. G. S. Ušćumlić, V. V. Krstić, M. D. Muškatirović, *J. Serb. Chem. Soc.* **58** (1993) 881
28. G. S. Ušćumlić, J. B. Nikolić, V. V. Krstić, *J. Serb. Chem. Soc.* **67** (2002) 77
29. N. B. Chapman, M. R. J. Dack, J. Shorter, *J. Chem. Soc. B* (1971) 834
30. G. S. Ušćumlić, V. V. Krstić, M. D. Muškatirović, *J. Mol. Struct.* **174** (1988) 521
31. V. V. Krstić, G. S. Ušćumlić, M. D. Muškatirović, *J. Mol. Struct.* **174** (1988) 247
32. G. S. Ušćumlić, V. V. Krstić, M. D. Muškatirović, *J. Serb. Chem. Soc.* **59** (1994) 889
33. G. S. Ušćumlić, V. V. Krstić, *J. Serb. Chem. Soc.* **61** (1996) 411
34. G. S. Ušćumlić, V. V. Krstić, *J. Serb. Chem. Soc.* **61** (1996) 621
35. G. S. Ušćumlić, V. V. Krstić, M. D. Muškatirović, *Quant. Struct. Act. Relat.* **10** (1991) 216
36. G. S. Ušćumlić, V. V. Krstić, M. D. Muškatirović, *J. Serb. Chem. Soc.* **60** (1995) 181
37. G. S. Ušćumlić, V. V. Krstić, *Indian J. Chem. B* **37** (1998) 85
38. G. S. Ušćumlić, V. V. Krstić, *Org. React.* **31** (1997) 181
39. G. S. Ušćumlić, M. D. Muškatirović, *J. Serb. Chem. Soc.* **56** (1991) 707
40. G. S. Ušćumlić, M. D. Muškatirović, *J. Serb. Chem. Soc.* **57** (1992) 19
41. J. B. Nikolić, G. S. Ušćumlić, V. V. Krstić, *Int. J. Chem. Kinet.* **37** (2005) 361
42. J. B. Nikolić, G. S. Ušćumlić, I. O. Juranić, *Int. J. Chem. Kinet.* **39** (2007) 664
43. J. B. Nikolić, G. S. Ušćumlić, *J. Serb. Chem. Soc.* **72** (2007) 1217
44. J. B. Nikolić, G. S. Ušćumlić, I. O. Juranić, *Int. J. Chem. Kinet.* **41** (2009) 613
45. N. B. Chapman, M. R. J. Dack, D. J. Newman, J. Shorter, R. Wilkinson, *J. Chem. Soc. Perkin Trans. 2* (1974) 962
46. N. B. Chapman, D. J. Newman, J. Shorter, *J. Chem. Soc. Perkin Trans. 2* (1976) 847
47. C. Reinchart, *Solvents and Solvent Effects in Organic Chemistry,* Wiley-VCH, Weinheim, Germany, 2003, p. 447
48. K. Bowden, M. Hojatti, *J. Chem. Soc. Perkin Trans. 2* (1990) 1201.

Effects of solvent and structure on the reactivity of 6-substituted nicotinic acids with diazodiphenylmethane in aprotic solvents

SAŠA Ž. DRMANIĆ*# , ALEKSANDAR D. MARINKOVIĆ#
and BRATISLAV Ž. JOVANOVIĆ#

Department of Organic Chemistry, Faculty of Technology and Metallurgy, University of Belgrade, Karnegijeva 4, P.O. Box 3503, 11121 Belgrade, Serbia

Abstract: The rate constants for the reactions of diazodiphenylmethane (DDM) with 6-substituted nicotinic acids in aprotic solvents at 30 °C were determined. The obtained second order rate constants in aprotic solvents, together with literature data for benzoic and nicotinic acids in protic solvents, were used for the calculation of solvent effects, employing the Kamlet-Taft solvatochromic equation (linear solvation energy relationship – LSER) in the form: $\log k = \log k_0 + s\pi^* + a\alpha + b\beta$. The correlations of the kinetic data were performed by means of multiple linear regression analysis taking appropriate solvent parameters. The sign of the equation coefficients (*s*, *a* and *b*) were in agreement with the postulated reaction mechanism, and the mode of the solvent influences on the reaction rate is discussed based on the correlation results. A similar contribution of the non-specific solvent effect and electrophilic solvation was observed for all acids, while the highest contribution of nucleophilic solvation was influenced by their high acidity. Correlation analysis of the rate data with substituent σ_p parameters in an appropriate solvent using the Hammett equation was also performed. The substituent effect on the acid reactivity was higher in aprotic solvents of higher dipolarity/polarizability. The mode of the transmission of the substituent effect is discussed in light of the contribution of solute––solvent interaction on the acid reactivity.

Keywords: pyridine carboxylic acids; diazodiphenylmethane; rate constants; solvatochromic parameters; aprotic solvents.

INTRODUCTION

The relationship between the structure of carboxylic acids and their reactivity with diazodiphenylmethane (DDM) has been studied by many authors, with particular regard to the influence of the solvent.[1–5] Related to previous studies[6–9]

---

* Corresponding author. E-mail: drmana@tmf.bg.ac.rs

Serbian Chemical Society member.

1359

of the transmission of substituent effects in pyridine carboxylic acids, this paper describes the transmission of those effects in 6-substituted nicotinic acids, with the following substituents: Cl (chloro), OH (hydroxy), CH_3 (methyl), Br (bromo) and SH (mercapto). The kinetics of these acids was studied in a series of aprotic solvents and the results were compared with the data for nicotinic and benzoic acid in protic solvents.

The kinetic data were correlated with the solvatochromic parameters π^*, α and β corresponding to the solvents used, in the form of the following LSER equation:

$$\log k = \log k_0 + s\pi^* + a\alpha + b\beta \qquad (1)$$

where π^* is an index of the solvent dipolarity/polarizability, which measures the ability of the solvent to stabilize a charge or a dipole by virtue of its dielectric effect, the α parameter is the HBD acidity (hydrogen bond donor), and the β parameter is the HBA basicity (hydrogen bond acceptor) of the solvent in a solute to solvent hydrogen bond and log k_0 is the regression value of the solute property in a reference solvent. The regression coefficients s, a, and b measure the relative susceptibilities of the solvent-dependent solute property (rate constant) to the indicated solvent parameter. The rate data for all the compounds studied show a satisfactory correlation with solvent parameter *via* the above LSER equation (Eq. (1)). Such a correlation indicates the existence of both specific and non-specific solute–solvent interactions in the studied reaction.

The reactivity of the investigated acids with DDM related to the electronic substituent effects was also studied using the Hammett equation (linear free energy relationship – LFER) of the type:

$$\log k_2 = \rho\sigma + \log k_0 \qquad (2)$$

where ρ is a reaction constant reflecting the sensitivity of the rate constant to the substituent effect, and σ is the substituent constant. The analysis included in the discussion concerning the contribution of the electronic substituent effects shows that these effects have a definite influence on the reactivity of the investigated acids. Some other factors, such as the coplanarity of nicotinyl ring and the carboxylic group could be significant for the reactivity and therefore geometry optimization of all investigated acids in three solvents was preformed.

<div align="center">EXPERIMENTAL</div>

Materials

The acids were commercial samples of *p.a.* quality, used without further purification. Diazodiphenylmethane was prepared by the Smith and Howard method.[10] A stock solution of *ca*. 0.06 mol dm^{-3} was stored in a refrigerator and diluted before use.

The solvents were purified as described in the literature.[11] All the solvents used for the kinetic studies were examined by GC and no impurities were detected.

Kinetic measurements

The rate constants, *k*, for the reactions of the investigated acids with DDM were determined as reported previously by the spectroscopic method of Roberts and co-workers[12] using a Shimadzu 1700A spectrophotometer. The optical density measurements were performed at 525 nm with 1 cm cells at 30±0.05 °C.

Three to five rate determinations were made on each acid and in every case, the individual second-order rate constants agreed within 3 % of the mean.

Geometry optimization

The reported conformations of the molecular forms were obtained by the semi-empirical MO PM6 method,[13] with implicit chosen solvent solvation (COSMO) (keywords: EF, GNORM = 0.01, EPS = 48 (DMSO), EPS = 4.8 (CHCl$_3$), EPS = 37.5 (acetonitrile) and NSPA = 92) using the MOPAC2009[TM] program package. A VEGA ZZ 2.3.2 was used as the graphical user interface (GUI).[14]

RESULTS AND DISCUSSION

The mechanism of the reaction between carboxylic acids and DDM, in both protic and aprotic solvents was found to involve the rate-determining proton transfer from the acids to DDM, thereby forming a diphenylmethanediazonium carboxylate ion-pair (Fig. 1.).[15–22] Chapman *et al.*[23] established that the solvent effects are best interpreted in the form of the contributions of the initial and transition state to the specific (α and β) and non-specific (π^*) solvent–solute interactions (Fig. 1).

Fig. 1. The mode of the solvent effects in 6-substituted nicotinic acids in
a) the initial state and b) the transition state.

The reaction rate constants (as log k_2) for the reaction of the examined acids with DDM in the employed solvents are given in Table I.

The results from Table I show that the influence of a solvent on the reactivity is complex, due to the many types of solvent to solute interactions (dipolarity, HBD and HBA effects), acting not only at the electrophilic and nucleo-

philic acid sites (Fig. 1), but also they could cause modifications of electronic properties of a substituent. Solvents of high dipolarity/polarizability and/or high proton-acceptor capability cause a significant decrease of the reaction rate. The highest value of the reaction rates in chloroform could be explained by the highest proton-donor ability of this solvent ($\alpha = 0.2$), as well as by the lowest proton--acceptor capability ($\beta = 0.1$).[24]

TABLE I. Logarithm of the second order rate constants (dm^3 mol^{-1} min^{-1}) for the reaction of 6-substituted nicotinic acids with DDM at 30 °C in aprotic solvents (NMF: *N*-methylformamide; DMSO: dimethyl sulfoxide; DMAC: *N,N*-dimethylacetamide; DMF: *N,N*-dimethylformamide; NMP: *N*-methylpyrrolidone)

Solvent	H[a]	6-Cl	6-OH	6-CH$_3$	6-Br	6-SH
Acetophenone	0.714	0.878	–[b]	0.350	0.920	0.790
Acetone	0.190	0.370	–	0.142	0.400	0.320
Chloroform	1.610	2.320	–	1.500	2.450	2.200
Ethyl benzoate	0.528	0.640	–	0.450	0.653	0.482
Isobutyl methyl ketone	0.143	0.550	–	–0.052	0.614	0.350
NMF	–0.027	0.180	–0.310	–0.117	0.150	0.008
DMSO	–0.678	–0.379	–1.200	–0.900	–0.350	–0.380
DMAC	–0.940	–0.600	–1.500	–1.120	–0.560	–0.460
DMF	–0.611	–0.238	–1.280	–0.780	0.200	–0.160
NMP	–0.921	–0.480	–1.370	–1.070	–0.303	–0.450

[a]From reference 1; [b]insoluble

As was stated in the literature,[19] carboxylic acids dissolved in chloroform exist in the form of dimers. A dimer could appear in two forms, cyclic and open, the latter being a very reactive form, because it can easily lose a proton and convert into a resonance stabilized anion. As the carboxylic anion is the reacting species in this system, it is continuously converted into the product and this is a probable reason why the open chain dimer, which stabilizes the anion, is the dominant form.[19] Being a solvent of low polarity, chloroform influences a weaker stabilisation of the ion pair intermediate making it easily convertible into the final product. Solvation of an ion-pair intermediate with a solvent of lower polarizability could have a higher contribution than with one of higher polarizability to a less negative activation entropy and thus to a more spontaneous reaction.

Generally, the results of the kinetic studies show that reaction rates for all acids with DDM were of second order, which was confirmed by the high correlation coefficients, *r*, which were in the range 0.95–0.99.

Solvent–reactivity relationship

In order to explain the obtained kinetic results based on the polarity, acidity and basicity of the solvent, the log k_2 were correlated with the solvatochromic parameters π^*, α and β using the solvatochromic Eq. (1). The correlation of the kinetic data was realized by means of multiple regression analysis, which is very

useful in separating and quantifying such interactions in the examined reaction. The correlation results are presented in Table II. The values for π^*, α and β were taken from the literature.[24]

TABLE II. Statistical results for the correlations of the reaction rate constants (log k_2) of 6-substituted nicotinic acids with DDM with the Kamlet–Taft solvatochromic parameters

Acid	$s(\pi^*)$	$a(\alpha)$	$b(\beta)$	log k_0	R^b	F^c	SD^d	n
NA	2.05±1.08	1.61±0.39	−(4.63±0.67)	0.80±0.60	0.974	38	0.22	10
Cl–NA	1.70±0.70	1.58±0.27	−(4.77±0.47)	1.48±0.41	0.990	91	0.16	10
HO–NA	2.37±0.36	1.99±0.09	−(2.20±0.51)	−1.92±0.37	0.999	320	0.03	5[a]
CH$_3$–NA	1.35±0.97	1.73±0.35	−(4.34±0.61)	1.02±0.54	0.980	49	0.20	10
Br–NA	1.68±0.77	1.50±0.28	−(4.91±0.48)	1.64±0.42	0.989	92	0.16	10
HS–NA	1.89±0.77	1.40±0.28	−(4.56±0.48)	1.18±0.43	0.986	72	0.16	10

[a]See Table I; [b]correlation coefficient; [c]Fischer's test; [d]standard error

The correlation equations obtained by polylinear regression for all the examined acids showed that the best approach, which aids in the understanding of the effects of aprotic solvents in the reaction, could be the usual correlation of the kinetic data with the contribution of the hydrogen bond donating (HBD) and hydrogen bond accepting (HBA) ability of a solvent to the transition and initial states. From the values of regression coefficients (s, a and b), the contribution of each parameter to the reactivity of the investigated compounds on the percentage basis was calculated and the results are listed in Table III.

TABLE III. Percentage contribution of the Kamlet–Taft solvatochromic parameters (P) to the reactivity of the investigated acids in aprotic solvent

Acid	P_{π^*} / %	P_{α} / %	P_{β} / %
NA	27	23	60
Cl–NA	21	20	59
HO–NA	36	30	34
CH$_3$–NA	18	23	59
Br–NA	21	19	60
HS–NA	24	18	58

The results from Tables II and III, lead to the following conclusions:

1) The rate of the reaction is strongly influenced by specific solute–solvent interactions, as indicated by the percentage contributions of the α and β parameters ($P_{\alpha} + P_{\beta}$).

2) The positive sign of the coefficient of the α term suggests that the specific interaction between the transition state and the solvent (see Fig. 1), through HBD properties is stronger than that between the reactant and solvent, *i.e.*, the HBD solvent effect or electrophilic solvation increases the reaction rate.

3) The negative sign of the coefficient of the β term suggest that the specific interaction between the reactant and solvent, through HBA properties, is stronger than that between the transition state and the solvent, *i.e.,* the HBA effect or nucleophilic solvation decreases the reaction rate.

4) The solvent dipolarity/polarizability, as indicated by $P_{\pi*}$ also plays an appreciable role in governing the reactivity. The positive sign of the coefficient of this term proves that classical or non-specific solute–solvent interactions dominate in the transition state and increase the reaction rate.

One correlation was found in the literature[25] which includes all three solvent parameters in a correlation for benzoic acid for solvents that do not possess HBD character:

$$\log k_2 = 0.20 + 1.21\pi* + 2.71\alpha - 3.70\beta \qquad (3)$$
$$R = 0.980; \; SD = 0.171; \; n = 44$$

The correlation coefficients for this equation also indicate a high contribution of the HBD solvent effect or electrophilic stabilization of the carboxylate anion in forming. The calculated percent contributions of particular solvent effects for benzoic acid are $P_{\pi*}$ (16 %), P_α (35 %) and P_β (49 %).

Generally, the higher contribution of the HBA solvent effect for substituted nicotinic acids is affected by their higher acidity and the strong proton accepting character of some aprotic solvents. Classical solvation has a higher influence on the reactivity of 6-hydroxynicotinic acid, while the electrophilic stabilization, respectively the HBD solvent effect, is more pronounced for benzoic acid. The significant contribution of the HBD solvent effect, reflected in value of the coefficient *a* for aprotic solvents, in all previous equations, and especially for benzoic acid, indicate an important role of the HBD solvent effect. The proton donor ability of a solvent to stabilize nucleophilic sites at an acid anion in forming increases the reaction rate, while stabilization of the initial state decreases it. These results could be supported by the observation that dipolar non-HBD solvents, in spite of their high relative permittivities and dipole moments, could favour acid ionisation and charge separation, and the created carboxylate anion–diazodiphenylmethane cation ion pair could be stabilized by aprotic solvents.

Furthermore, the significantly higher value of P_α for benzoic acid leads to the conclusion that the strong electron-accepting character of the pyridine nitrogen has an undesirable contribution to HBD solvent stabilization in the transition state. The small and definitely increased contribution of the HBD solvent effect for 6-hydroxynicotinic acid could probably be a manifestation of the specific solvation of the acidic hydrogen of the hydroxy group, causing stabilization and a definite modification of the electron-donating properties of that group.

A better understanding of the contribution of solvent effects could be attained by comparing the results from the present study with correlation results of data published for nicotinic and benzoic acids[8] in protic solvents.

The kinetic data for nicotinic acid from a previous paper[8] were correlated with the solvent parameter for eleven protic solvents, giving the following results:

$$\log k_2 = (-0.14\pm0.20) + (1.34\pm0.52)\pi^* + (0.78\pm0.21)\alpha - (0.51\pm0.76)\beta \quad (4)$$
$$R = 0.960; \; SD = 0.12; \; n = 11$$

All the coefficients are in agreement with the mechanism of this reaction but not all of them are statistically correct. The negative value of coefficient b indicates that nucleophilic solvation decreased the reaction rate, which corroborates the established reaction mechanism, but this parameter is disputable, making the three-parameters equation useless for interpretation of the kinetic data, because of a statistical deficiency.

Therefore, the best interpretation of solvent effects in protic solvents is described by a simplified system of a two-parameter equation of the following type:

$$\log k_2 = (-0.76\pm0.17) + (1.65\pm0.22)\pi^* + (0.85\pm0.16)\alpha \quad (5)$$
$$R = 0.960; \; SD = 0.11; \; n = 11$$

The results of the above correlation corroborate the reaction mechanism, and the influence of solvent by classical solvation and electrophilic solvation. It is evident that the HBD effect increases the reaction rate, stabilizing the transition state more than the initial state.

The calculation of the percent contribution of particular solvent effects gave the following results: for nicotinic acid P_{π^*} (66 %) and P_α (34 %); for benzoic acid the effect of electrophilic solvation is the main effect (21 and 79 %, respectively). The large differences in the contributions of the same solvent effects for these two acids can be explained by the significant increase in the influence of classical solvation because of the more polar structure of nicotinic acid in the transition state, caused by the negative inductive and resonance effects of the pyridine nitrogen.

Structure–reactivity relationship

The relationship between the molecular structure and chemical reactivity gives additional insight into the electronic effect of substituents and the influence of solvent on the electronic distribution in the initial and transition states. Correlation results obtained using the Hammett equation (2) are given in Table IV for aprotic solvents.

The magnitude of the obtained reaction constants indicates that the reaction is significantly susceptible to substituent effects. Furthermore, the positive reaction constant suggests that the positive charge at the reaction centre may disap-

Available online at www.shd.org.rs/JSCS/

pear. Generally, the Hammett equation predicts[27] that the reaction constant for this type of reaction appears to increase with decreasing relative permittivity of the medium. In the present study, however, there is a very marked deviation from the relationship between ρ and the relative permittivity of the medium (ε_r) (macroscopic solvent parameter). This suggests that the ρ values are influenced by both non-specific and specific solvent effects.

TABLE IV. Hammett ρ values for the reaction of 6-substituted nicotinic acids with DDM in aprotic solvents at 30 °C (σ values for Cl, OH, CH$_3$, Br and SH are from literature[26])

Solvent	ρ	$\log k_0$	r	SD	F	n
Acetophenone	0.96±0.17	0.65±0.17	0.94	0.06	32	5
Acetone	1.29±0.26	0.32±0.05	0.93	0.09	26	5
Chloroform	1.91±0.42	1.84±0.08	0.92	0.16	20	5
Ethyl benzoate	1.13±0.23	0.53±0.05	0.93	0.09	24	5
Isobutyl methyl ketone	1.62±0.14	0.10±0.03	0.98	0.05	128	5
NMF	1.37±0.17	0.03±0.04	0.96	0.09	61	6
DMSO	2.09±0.24	−0.66±0.05	0.97	0.12	77	6
DMAC	2.25±0.32	−0.82±0.07	0.95	0.16	48	6
DMF	2.11±0.24	−0.56±0.05	0.97	0.12	78	6
NMP	2.36±0.29	−0.83±0.06	0.96	0.15	64	6

Taking into consideration the assumption of similarity in the transmitting cavities for 6-substituted nicotinic acids and benzoic acid, the differences in the transmission of substituent effects through the benzene and pyridine ring depend on the polarizability of these ring systems and also on the contribution of electrons from the pyridine nitrogen. The higher sensitivity of the reaction constant to solvent effects in aprotic dipolar solvent may be explained in the way that at high relative permittivities of the surrounding solvent molecules, the energy necessary to bring about charge separation in the transition state is relatively small, which gives rise to a higher susceptibility to the electronic substituent effect. Aprotic highly dipolar solvents (DMSO, DMF, DMAC and NMP) tend to be poor anion solvators, while they are usually better for larger and softer anions. The extended conjugated system of the investigated acids, considering their planarity shown by the semi-empirical PM6 method, having delocalized electronic densities could be more susceptible to the influence of substituents on reactivity. The classical solvent effect is not necessarily only achieved through dipolar attraction but also by the repulsion of the negative end of solvent dipole and, consequently, the π-electronic densities could have more influence on the reactivity of the acids. An exception is NMF which contributes less to the substituent influences, probably because of its possibility of hydrogen bonding and self-association. Other aprotic dipolar solvents (acetophenone, acetone and ethyl benzoate) of lower dipolarity/polarizability and HBA basicity show lower substituent influence on reactivity, primarily because of their lower polarizability.[25]

The consideration of the influences of solvent and substituent is based on the macroscopic solvent and substituent characteristics, which do not separate specific reactant/solvent interaction and the contribution of substituent/solvent interactions. The interaction modes presented in Fig. 1 approximate the regiospecific interactions of the solvent with the actual electrophilic and nucleophilic sites in an acid. The overall solvent effect is achieved by the joint interactions, presented in Fig. 1, of the contribution of non-specific and specific solvent effects to the electron density at the site. The solvent or substituent causes electron density changes of the most polarisable molecular orbitals, which indeed transmit these effects to the reaction centre. The reasons why some irregularities were observed in the correlation results may be associated with the choice and analysis of the HOMO molecular orbitals, occupied with electrons, available for reactant/solvent interactions. The optimized geometries of all 6-substituted nicotinic acids show small or no deviation from planarity and thus electron transfer could be achieved without suppression of these effects. Analysis of the three highest occupied levels showed that only HOMO orbitals give an adequate explanation of the interaction and transmission modes of solvent and substituent effects to the reaction centre. The HOMO orbitals for 6-hydroxynicotinic and nicotinic acid are presented in Fig. 2.
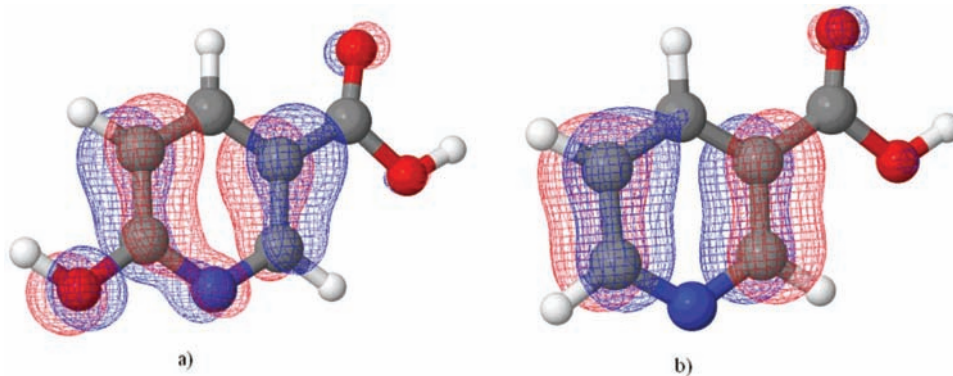
Fig. 2. HOMO orbitals of 6-hydroxynicotinic (a) and nicotinic acid (b) obtained by the semi-empirical MO PM6 method, with implicit DMSO solvation using the MOPAC2009[TM] program package.

Electron densities of the most polarized HOMO orbitals in both acids show some important differences which indeed have the highest contribution to the transmission of the substituent effect and influence of solvent on the reactivity. The pyridine nitrogen in 6-hydroxynicotinic acid belongs to the π-polarized system with a C_5–C_6 double bond, which is susceptive to electronic shifts, being sensitive to substituent and solvent influences at these atoms. The electronic effects of the pyridine nitrogen, as a part of this π-polarisable system, have a signi-

ficant contribution to the solvent and substituent effects on the reactivity of the investigated nicotinic acids. Aprotic solvents of high dipolarity/polarizability interfere with the electron-accepting capability of the pyridine nitrogen, causing lower acidity of the investigated acids. Opposed to this, solvents of lower dipolarity/polarizability and higher proton-donor ability contribute to the higher electrophilic solvation of the nitrogen in both the initial and transition state, enhancing the electron-accepting power and thus increasing the acidity of the acids.

CONCLUSIONS

The overall solvent effects on the reactivity are complicated by several possible modes of interactions between the solvent, either protic or aprotic, with several active sites on the reacting acid molecules. The results of the present investtigation show that these diverse solvent effects could be generally quantified by use of the Kamlet–Taft equation. The quantitative separation of these effects into individual contributions in the initial and transition states is not completely possible. Secondary solvent effects are operative, causing modifications originating from both the pyridine ring and substituent electronic effects on the reactivity of the investigated acids. Generally, the pyridine nitrogen has a significant influence on the reactivity of 6-substituted nicotinic acids, considering the possibilities of different solvent interactions with this atom. Thus, for example, a stronger electrophilic solvation of the pyridine nitrogen in the transition state causes a decrease of the electrophilic solvation of the carboxylate anion in forming. In addition, the high contribution of nucleophilic solvation of the carboxylic hydrogen in the initial state is caused by the strong electron-accepting character of the pyridine nitrogen. The substituent electronic effect on the reactivity is of greatest influence in highly dipolar aprotic solvents which interfere with the strong electron-accepting character of the pyridine nitrogen.

И З В О Д

УТИЦАЈ РАСТВАРАЧА И СТРУКТУРЕ НА РЕАКТИВНОСТ 6-СУПСТИТУИСАНИХ НИКОТИНСКИХ КИСЕЛИНА СА ДИАЗОДИФЕНИЛМЕТАНОМ У АПРОТИЧНИМ РАСТВАРАЧИМА

САША Ж. ДРМАНИЋ, АЛЕКСАНДАР Д. МАРИНКОВИЋ и БРАТИСЛАВ Ж. ЈОВАНОВИЋ

Катедра за органску хемију, Технолошко-металуршки факултет, Универзитет у Београду, п. пр. 3503, Карнегијева 4, 11120 Београд

Константе брзина 6-супституисаних никотинских киселина са диазодифенилметаном (ДДМ) су одређене у различитим протичним и апротичним растварачима на 30 °C. Израчунате константе брзина, као и литературни подаци, коришћени су за израчунавање ефеката растварача коришћењем Kamlet–Taft-ове солватохромне једначине. Константе брзина су корелисане са параметрима растварача коришћењем Kamlet–Taft-ове једначине облика: log k

$= \log k_0 + + s\pi^* + a\alpha + b\beta$. Корелације добијених кинетичких резултата са одговарајућим параметрима растварача су изведене применом методе вишеструке линеарне регресионе анализе. Знак коефицијената (*s*, *a* и *b*) у добијеним корелацијама је у сагласности са реакционим механизмом. Сличан допринос неспецифичних ефеката и електрофилне солватације растварача је уочен за све испитиване киселине, а највећи допринос нуклеофилне солватације полазног стања је последица високе киселости испитиваних киселина. Утицај растварача на вредности реакционих константи је дискутован на основу добијених корелационих резултата. Корелациона анализа константи брзина са σ_p константама супституената, у испитиваном растварачу, извршена је применом Hammett-ове једначине. Ефекти супституената на реактивност испитиваних киселина су значајнији у апротичним растварачима високе диполарности/поларизабилности. Начин преноса ефеката супституената је дискутован у светлу доприноса интеракција растворак–растварач на реактивност испитиваних киселина.

REFERENCES

1. M. H. Aslam, A. G. Burden, N. B. Chapman, J. Shorter, *J. Chem. Soc. Perkin Trans. 2* (1981) 500
2. N. B. Chapman, D. J. Newman, J. Shorter, *J. Chem. Soc. B* (1976) 847
3. M. Kamlet, J. Abboud, R. W. Taft, in *Progress in Physical Organic Chemistry*, S. G. Kohen, A. Streitwieser, R. W. Taft, Eds., Wiley, New York, Vol 13, 1981, p. 485
4. D. Mather, J. Shorter, *J. Chem. Soc. Perkin Trans. 2* (1983) 1179
5. N. B. Chapman, J. R. Lee, J. Shorter, *J. Chem. Soc. B* (1969) 769
6. B. Jovanović, S. Drmanić, M. Mišić-Vuković, *J. Chem. Res.* (1998) 2581 (M); 554 (S)
7. S. Drmanić, B. Jovanović, M. Mišić-Vuković, *J. Serb. Chem. Soc.* **65** (2000) 481
8. A. Marinković, S. Drmanić, B. Jovanović, M. M. Mišić-Vuković, *J. Serb. Chem. Soc.* **70** (2005) 557
9. S. Drmanić, B. Jovanović, A. Marinković, M. Mišić-Vuković, *J. Serb. Chem. Soc.* **68** (2003) 515
10. L. I. Smith, K. L. Howard, *Org. Synth. Coll.* Vol **3** (1955) 351
11. W. L. F. Armarego, C. L. L. Chai, *Purification of laboratory chemicals*, Elsevier Science, Burlington, USA, 2003
12. J. D. Roberts, E. A. McElhill, R. Armstrong, *J. Am. Chem. Soc.* **71** (1949) 2923
13. J. J. P. Stewart, *J. Mol. Mod.* **13** (2007) 1173
14. A. Pedretti, L. Villa, G. Vistoli, *J. Comput-Aided Mol. Des.* **18** (2004) 167; VEGA ZZ 2.1.0. (http://www.ddl.unimi.it)
15. A. Buckley, N. B. Chapman, M. R. J. Dack, J. Shorter, H. M. Wall, *J. Chem. Soc. B* (1968) 631
16. B. Ž. Jovanović, A. D. Marinković, Ž. Vitnik, I. O. Juranić, *J. Serb. Chem. Soc.* **72** (2007) 1191
17. J. B. Nikolić, G. S. Ušćumlić, *J. Serb. Chem. Soc.* **72** (2007) 1217
18. A. Buckley, N. B. Chapman, J. Shorter, *J. Chem. Soc. B* (1969) 195
19. N. B. Chapman, M. R. J. Dack, D. J. Newman, J. Shorter, R. Wilkinson, *J. Chem. Soc. Perkin Trans. 2* (1974) 962
20. K. Bowden, A. Buckley, N. B. Chapman, J. Shorter, *J. Chem. Soc.* (1964) 3380
21. R. A. More O'Ferrall, W. K. Kwok, S. I. Miller, *J. Am. Chem. Soc.* **86** (1964) 5553

Available online at www.shd.org.rs/JSCS/

22. B. Jovanović, I. Juranić, M. Mišić-Vuković, D. Brkić, Ž. Vitnik, *J. Chem. Res. (S)* (2000) 506
23. N. B. Chapman, D. J. Newman, J. Shorter, H. M. Wall, *J. Chem. Soc. Perkin Trans. 2* (1976) 847
24. Y. Marcus, *Chem. Soc. Rev.* (1993) 409
25. C. Reichardt, *Solvents and Solvent Effects in Organic Chemistry*, VCH, Weinheim, 2003, pp. 458, 472
26. H. Kubinyi, in *QSAR: Hansch Analysis and Related Approaches*, R. Mannhold, P. Krogs-gaard-Larsen, H. Timmerman, Eds., Wiley, Weinheim, 1993, p. 23
27. J. Shorter, *Correlation Analysis of Organic Reactivity*, Research Study Press, Letchworth, 1982.

SHORT COMMUNICATION

Synthesis and characterization of a series of 1,3,5-trisubstituted-2-pyrazolines derivatives using methanoic acid under thermal condition

BEHROOZ MALEKI[1]*, DAVOOD AZARIFAR[2], MONA KHODAVERDIAN MOGHADDAM[1], SEYEDEH FATEMEH HOJATI[1], MOSTAFA GHOLIZADEH[1] and HAFEZEH SALEHABADI[1]

[1]*Department of Chemistry, Sabzevar Tarbiat Moallem University, Sabzevar-397, Khorasan and* [2]*Department of Chemistry, Bu-Ali Sina University, Hamadan-65178, Iran*

Abstract: An efficient and practical synthesis of 1,3,5-trisubstituted 2-pyrazoline structures was achieved through cyclization of phenylhydrazine with α,β-unsaturated ketones (chalcones) using methanoic acid (formic acid) as catalyst under thermal condition.

Keywords: 1,3,5-trisubstituted-2-pyrazoline; phenylhydrazine; chalcone; methanoic acid; heterocyclic synthesis.

INTRODUCTION

Chalcones constitute an important class of naturally occurring flavonoid compounds that exhibit a wide spectrum of biological activities and are well-known intermediates for the synthesis of various heterocycles. Chalcones are useful synthons in the synthesis of a large number of bioactive molecules, such as pyrazolines and isoxazoles that are well-known nitrogen-containing heterocyclic compounds.[1–5]

The discovery of this class of compounds provides an outstanding case history of modern drug development and also emphasizes the unpredictability of biological activity from structural modification of a prototype drug molecule. Considerable interest has been focused on the pyrazoline structure, which is known to possess a broad spectrum of biological activities, such as antitumor,[6] immunosuppressive,[7] antibacterial,[8] anti-inflammatory,[9] anticancer,[10] antidiabetic[11] and antidepressant.[12] Thus, the synthesis of the 1,3,5-trisubstituted 2-pyrazolines moiety is always a great challenge.

Among various pyrazolines derivatives, 2-pyrazolines seem to be the most frequently studied pyrazoline type of compounds. Various procedures have been developed for the synthesis of pyrazolines.[13–15] After the pioneering work of Fischer and Knoevenagel in the 19th century, the reaction of α,β-unsaturated aldehydes and ketones with phenylhydrazine in acetic acid under reflux became one of the most popular methods for the preparation of 2-pyrazolines.[16–18]

In continuation of our research on the synthesis of 1,3,5-trisubstituted-2-pyrazolines,[19–21] a facile synthesis of a range of 1,3,5-trisubstituted-2-pyrazolines from α,β-unsaturated ketones (chalcones) and phenylhydrazine in the presence of methanoic acid is described herein (Scheme 1).
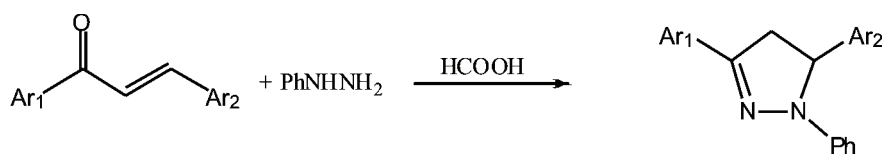
Scheme 1. General reaction for the preparation of 1,3,5-trisubstituted-2-pyrazolines.

RESULTS AND DISCUSSIONS

Methanoic acid (HCOOH, pK_a = 3.744) is a versatile organic compound. It is well known as a natural product and as a one-carbon source in organic chemistry.[22] Under appropriate conditions, it decomposes to carbon dioxide and hydrogen and the generated hydrogen can be used under transfer hydrogenation conditions for the reduction of a wide variety of functional groups.[23–25] Furthermore, methanoic acid has found extensive use as an oxidizing agent.[26]

First, 3-(4-chlorophenyl)-1-(2-naphthyl)prop-2-en-1-one (1.0 mmol) was chosen as the trial substance for reaction with phenylhydrazine (2.0 mmol) in the presence of methanoic acid. Different solvents were screened for the synthesis of 2-pyrazolines and the results are summarized in Table I, from which it can be seen that EtOH was the best solvent in terms of reaction time and yield (Entry 1). Then, the effect of the amount of the catalyst, methanoic acid, on the yield and time of the same reaction was investigated. In the absence of catalyst, no product was obtained after 2 h (Table I, Entry 4). It was found that 2.5 ml of the catalyst was sufficient to mediate the reaction towards the formation of the 1,3,5-trisubstituted-2-pyrazoline in terms of time and yield (Table I, Entry 5).

Having established the reaction conditions, various chalcones (**1a–q**), prepared by Claisen–Schmidt condensation of aromatic ketones with aromatic aldehydes, were treated with phenylhydrazine in the presence of methanoic acid to investigate the scope of the reaction. The obtained 1,3,5-trisubstituted-2-pyrazolines (**2a–q**) are presented in Table II, together with their melting points and the reaction times and yields.

TABLE 1. Optimization of the reaction conditions
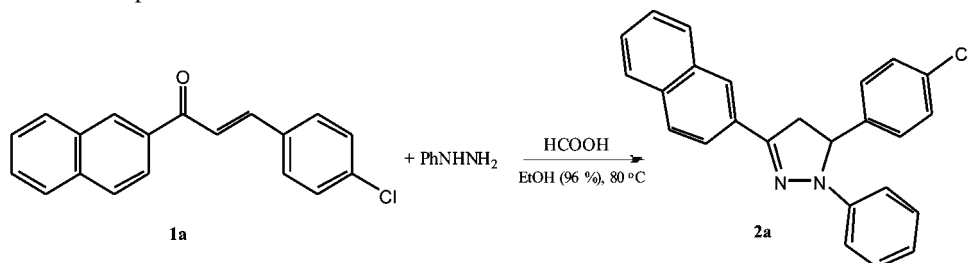
Entry	Catalyst amount/ ml	Solvent	Time/ min	Yield[a]/ %
1	1	EtOH	30	80
2	1	MeOH	45	60
3	1	CH3CN	50	50
4	–	EtOH	120	–
5	2.5	EtOH	15	90
6	3.5	EtOH	15	62
7	4.5	EtOH	35	48

[a]Isolated yield

TABLE II. Synthesis of 1,3,5-trisubstituted 2-pyrazolines in the presence of methanoic acid

Product	Ar1	Ar2	Time/ min	Yield[a]/ %	M.p./ °C	
					Found	Reported[b]
2a	2-naphthyl	$4\text{-ClC}_6\text{H}_4$	15	90	128–130	129–130
2b	2-naphthyl	$2\text{-ClC}_6\text{H}_4$	10	80	123–125	124–126
2c	C_6H_5	$4\text{-CH}_3\text{C}_6\text{H}_4$	15	90	130–132	128–130
2d	C_6H_5	$2\text{-ClC}_6\text{H}_4$	15	72	134–136	134–135
2e	$4\text{-MeOC}_6\text{H}_4$	C_6H_5	15	80	139–140	134–136
2f	C_6H_5	$4\text{-MeOC}_6\text{H}_4$	15	75	108–110	110–112
2g	C_6H_5	C_6H_5	25	82	132–134	134–135
2h	$4\text{-ClC}_6\text{H}_4$	C_6H_5	15	84	140–142	143–145
2i	2-naphthyl	$3\text{-CH}_3\text{C}_6\text{H}_4$	15	90	150–151	152–154
2j	2-naphthyl	$2\text{-CH}_3\text{C}_6\text{H}_4$	20	92	170–172	169–171
2k	C_6H_5	$3\text{-BrC}_6\text{H}_4$	20	88	134–136	135–136
2l	$4\text{-MeOC}_6\text{H}_4$	$2\text{-ClC}_6\text{H}_4$	15	82	149–150	148–150
2m	2-naphthyl	$4\text{-MeOC}_6\text{H}_4$	20	90	134–136	135–136
2n	$4\text{-CH}_3\text{C}_6\text{H}_4$	$3\text{-CH}_3\text{C}_6\text{H}_4$	25	80	125–126	124–126
2o	$4\text{-MeOC}_6\text{H}_4$	$2\text{-CH}_3\text{C}_6\text{H}_4$	25	80	90–92	88–90
2p	$4\text{-MeOC}_6\text{H}_4$	$3\text{-CH}_3\text{C}_6\text{H}_4$	25	74	110–112	112–114
2q	$3\text{-CH}_3\text{C}_6\text{H}_4$	$4\text{-(CH}_3)_2\text{NC}_6\text{H}_4$	35	80	142–144	New

[a]Isolated yield; [b]literature data[17,19-21]

All the isolated products were characterized based on their physical properties and IR, ^{1}H-NMR and mass spectral data, and by direct comparison with authentic materials. All the synthesized compounds gave the expected spectral

Available online at www.shd.org.rs/JSCS/

data. As a representative product, the spectroscopic data for 5-[4-(dimethyl-amino)phenyl]-3-(3-methylphenyl)-1-phenyl-2-pyrazoline (**2q**) are given below.

IR (KBr, cm^{-1}): 3020 (C–H stretching of aromatic ring), 2880 (C–H stretching of aliphatic), 1614 (C=N stretching of pyrazoline ring), 1595, 1520, 1499 (C=C stretching of aromatic ring), 1219 (C–N stretching of pyrazoline ring), 745 (C–H bending).

^{1}H-NMR (90 MHz, CDCl$_3$, δ / ppm): 2.28 (3H, *s*, CH$_3$), 2.81 (6H, *s*, N(CH$_3$)$_2$), 3.05 (1H, *dd*, –CH$_{2pyraz.}$), 3.63 (1H, *dd*, –CH$_{2pyraz.}$), 5.05 (1H, *dd*, –CH$_{pyraz.}$), 6.62–7.48 (13H, *m*, Ar-H).

MS (m/z, (relative abundance, %)): 355 (M$^+$, 82.35), 235 (M–120, 16.87), 208 (M–27), 20.58), 147 (M–61, 55.88), 91 (M–56, 76.47) (see Scheme 2).
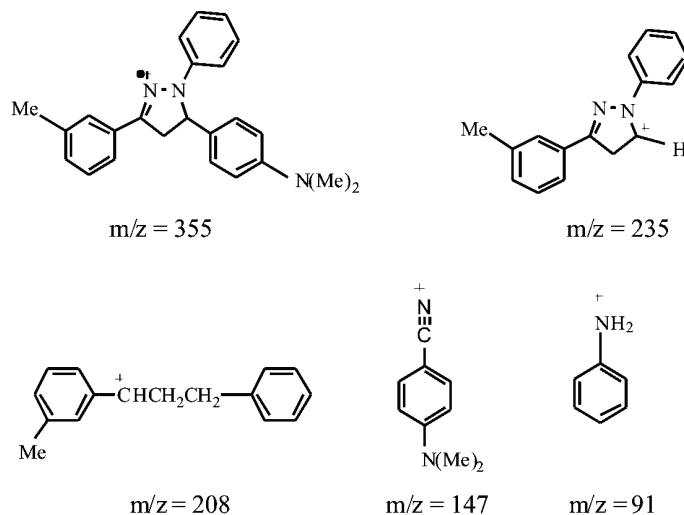
Scheme 2.

Methanoic acid is a source of H$^+$, the following sequence of reaction appears to afford a satisfactory explanation of the mode of formation of the products (Scheme 3). This reaction involves the initial formation of an arylhydrazone (**I**) with the subsequent attack of the nitrogen on the carbon-carbon double bond.[17,19–21]

EXPERIMENTAL

The IR spectra as KBr discs were recorded on a Shimadzu 435-U-04 spectrophotometer. The ^{1}H-NMR and ^{13}C-NMR spectra were obtained using a Jeol FT NMR 90 MHz spectrometer in CDCl$_3$ with TMS as the internal reference. The melting points were determined on a Stuart SMP3 apparatus and are uncorrected. Mass spectra were recorded on a GCMS--QP1100EX spectrometer.

$$HCOOH \rightleftharpoons H^+ + HCOO^-$$
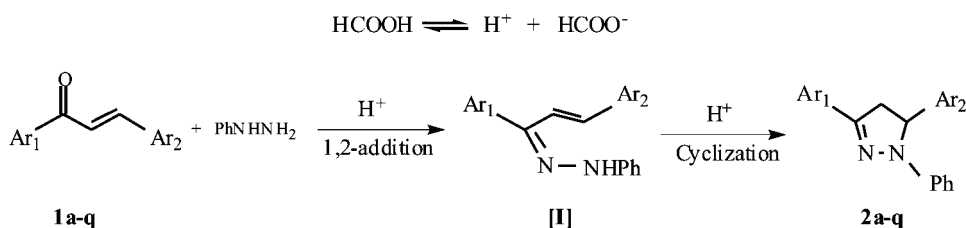
Scheme 3.

*General procedure for the synthesis of 1,3,5-trisubstituted-2-pyrazolines (**2a**–**q**)*

To a stirred solution of chalcone (**1a**–**q**, 1.0 mmol) in 10 ml EtOH (96 %) was added phenylhydrazine (2.0 mmol) and methanoic acid (2.5 ml) at room temperature. The reaction mixture was heated to reflux for an appropriate time (see Table II). The progress of the reaction was monitored by TLC (ethyl acetate/hexane, 8:2). The EtOH was removed under reduced pressure and residue recrystalized from EtOH (2 × 5 ml) to afford the pure products (**2a**–**q**).

CONCLUSIONS

In conclusion, a rapid, high yield, simple, practical, economic, readily available system, and convenient procedure for the synthesis of 1,3,5-trisubstituted-2--pyrazolines, which compares well with the similar acetic acid system under the same conditions, has been developed.

ИЗВОД

СИНТЕЗА И КАРАКТЕРИЗАЦИЈА 1,3,5-ТРИСУПСТИТУИСАНИХ-2-ПИРАЗОЛИН ДЕРИВАТА СА МЕТАНСКОМ КИСЕЛИНОМ КАО КАТАЛИЗАТОРОМ УЗ ЗАГРЕВАЊЕ

BEHROOZ MALEKI[1], DAVOOD AZARIFAR[2], MONA KHODAVERDIAN MOGHADDAM[1], SEYEDEH FATEMEH HOJATI[1], MOSTAFA GHOLIZADEH[1] и HAFEZEH SALEHABADI[1]

[1]Department of Chemistry, Sabzevar Tarbiat Moallem University, Sabzevar-397, Khorasan and [2]Department of Chemistry, Bu-Ali Sina University, Hamadan-65178, Iran

Ефикасна и практична синтеза 1,3,5-трисупституисаних 2-пиразолин структура изведена је циклизацијом фенилхидразина са α,β-незасићеним кетонима (халконима) са метанском (мрављом) киселином као катализатором уз загревање.

REFERENCES

1. L. W. Wattenberg, M. A. Page, J. L. Leong, *Cancer Res.* **28** (1968) 2539
2. T. Shah, V. Desi, *J. Serb. Chem. Soc.* **72** (2007) 443
3. S. Mostahar, S. Alam, A. Islam, *J. Serb. Chem. Soc.* **72** (2007) 329
4. V. N. Patange, R. K. Pardeshi, B. R. Arbad, *J. Serb. Chem. Soc.* **73** (2008) 1073
5. M. S. Yar, A. A. Siddqui, M. S. Ali, *J. Serb. Chem. Soc.* **72** (2007) 5

6. E. Taylor, H. Patel, H. Kumar, *Tetrahedron* **48** (1992) 8089
7. M. S. Karthikeyan, B. S. Holla, N. S. Kumari, *Eur. J. Med. Chem.* **42** (2007) 30
8. B. S. Holla, P. M. Akberali, M. K. Shivananda, *Farmaco* **55** (2000) 256
9. E. Bansal, V. K. Srivatsava, A. Kumar, *Eur. J. Med. Chem.* **36** (2001) 81
10. F. Manna, F. Chimenti, R. Fioravanti, A. Bolasco, D. Secci, P. Chimenti, C. Ferlini, G. Scambia, *Bioorg. Med. Chem. Lett.* **15** (2005) 4632
11. J. H. Ahn, H. M. Kim, S. H. Jung, S. K. Kang, K. R. Kim, S. D. Rhee, S. D. Yang, H. G. Cheon, S. S. Kim, *Bioorg. Med. Chem. Lett.* **14** (2004) 4461
12. Y. R. Prasad, R. A. Lakshmana, L. Prasoona, K. Murali, K. P. Ravi, *Bioorg. Med. Chem. Lett.* **15** (2005) 5030
13. J. Elguero, in *Comprehensive Heterocyclic Chemistry*, Vol. 5, A. R. Katritzky, C. W. Rees, Eds., Pergamon Press, Oxford, 1984, pp. 167–302
14. J. Elguero, in *Comprehensive Heterocyclic Chemistry II*, A. R. Katritzky, C. W. Rees, E. F. Scriven, Eds., Pergamon Press, Oxford, 1996, pp. 1–75
15. V. V. Dabholkar, R. P. Gavande, *J. Serb. Chem. Soc.* **68** (2003) 723
16. A. Levai, *Arkivoc* **9** (2005) 344
17. J. T. Li, X. H. Zhang, Z. P. Lin, *Beilstein J. Org. Chem.* **3** (2007) 1
18. R. R. Kamble, B. S. Sudha, D. G. Bhadregowda, *J. Serb. Chem. Soc.* **73** (2008) 131
19. D. Azarifar, M. Saebanzadeh, *Molecules* **7** (2002) 885
20. D. Azarifar, H. Ghasemnejad, *Molecules* **8** (2003) 642
21. D. Azarifar, B. Maleki, *J. Heterocycl. Chem.* **52** (2005) 157
22. W. Reutemann, H. Kieczka, in *Ullmann's Encyclopedia of Industrial Chemistry,* 5th Ed., VCH, Weinheim, 1983, pp. 13–33
23. H. W. Gibson, *Chem. Rev.* **69** (1969) 673
24. R. A. W. Johnstone, A. H. Wilby, I. D. Entwistle, *Chem. Rev.* **85** (1985) 129
25. G. Brieger, T. J. Nestrick, *Chem. Rev.* **74** (1974) 567
26. H. S. P. Rao, S. Jothilingam, K. Vasantham, H. W. Scheeren, *Tetrahedron Lett.* **48** (2007) 4495.

Synthesis and biological activities of some indoline derivatives

MILIND A. RODE[1]*, SAHEBRAO S. RINDHE[1] and BHAUSAHEB K. KARALE[2]

[1]*Department of Chemistry, New Arts, Commerce and Science College, Ahmednagar-414001 and* [2]*Department of Chemistry, Radhabai Kale Mahila Mahavidyalaya, Ahmednagar-414001, India*

Abstract: The reaction of indoline with a substituted benzoyl chloride in the presence of K_2CO_3 in THF gave compound **4**. Compound **4** was subjected to chlorosulphonation to obtain compound **5**. Condensation of aromatic amines with compound **5** led to the synthesis of indoline derivatives **6(a–f)**. Similarly, 5-nitroindoline was treated with a substituted benzoyl chloride to obtain the nitro compound **9**, which was reduced using stannous chloride and reacted further with aromatic sulphonyl chloride to obtain the indoline derivatives **11(a–e)**. These compounds were tested for antibacterial, anti-tuberculosis and antifungal activity. Some of them showed very good activity against some gram-positive and gram negative bacteria, fungal strains and also *Mycobacterium tuberculosis*. All of the synthesized compounds were subjected to antioxidant activity testing using the *in vitro* DPPH assay and most of them showed very good activity.

Keywords: indoline; antioxidant activity; antifungal; anti-tuberculosis and antibacterial activity.

INTRODUCTION

Indoline and other related ring systems possess several interesting biological activities. The indolines are also interesting structural scaffolds and have, for example, been evaluated as 5-HT$_{2C}$ receptor agonists for the treatment of obesity.[1] Factor Xa (FXa) is well known to play a pivotal role in blood coagulation; hence, an FXa inhibitor is a promising drug candidate for prophylaxis and treatment of thromboembolic diseases. Some indoline derivatives have been found to show very good FXa inhibitory activities.[2] Indoline derivatives have also been found to show an antagonistic effect on progesterone receptors.[3] In addition, indolines have been evaluated for antimicrobial activity.[4] Owing to the biological importance of indolines and in continuation of our work on the synthesis of biologically important heterocyclic compounds, the synthesis of some indolines is reported herein.

---

* Corresponding author. E-mail: milindrode@yahoo.com

Available online at www.shd.org.rs/JSCS/

RESULTS AND DISCUSSION

In present work, the synthesis of novel indoline derivatives is reported starting with the substituted benzoyl chloride **2**, which was prepared by the reaction of 4-(aminosulfonyl)benzoic acid with $SOCl_2$ and DMF. Treatment of **2** with indoline **3** in the presence of K_2CO_3 in THF afforded compound **4**. Compound **4** was subjected to chlorosulphonation to obtain compound **5**, which on reaction with aromatic amines in presence of pyridine and a catalytic amount of DMAP using THF as the solvent yielded the indoline derivatives **6(a–f)**. The synthetic scheme to **6(a–f)** is shown in Scheme 1 and the structural data of **6(a–f)** are given in Table I.
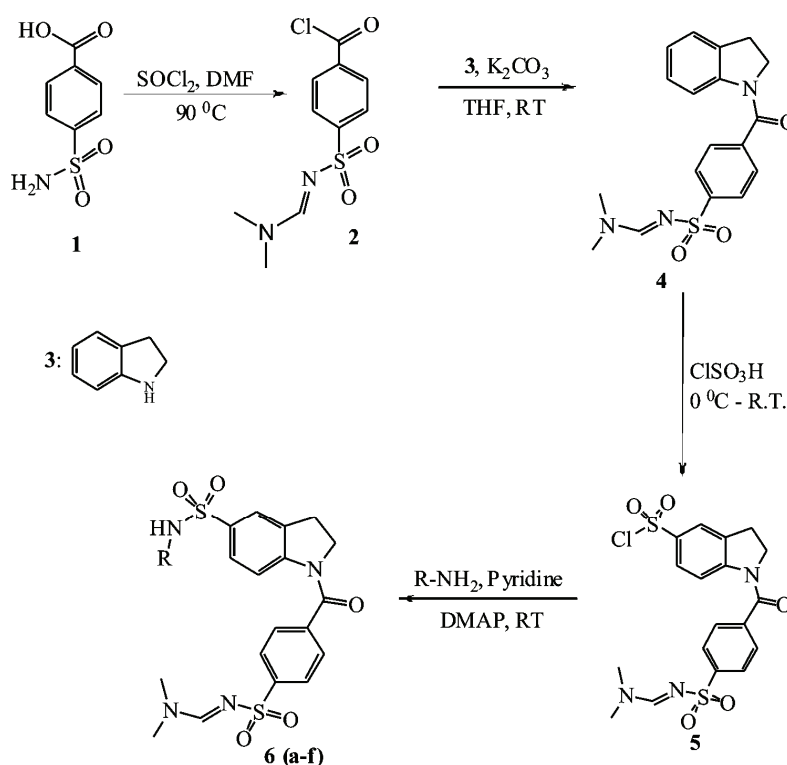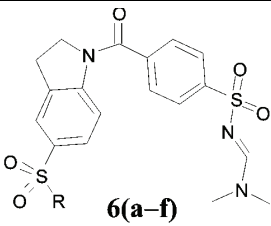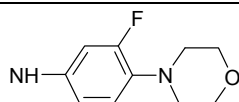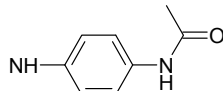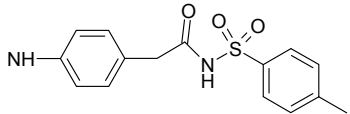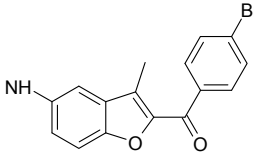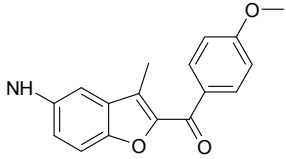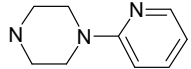
Scheme 1.

Similarly, 5-nitroindoline (**8**) on treatment with compound **7** gave the nitro derivative **9**, which was further reduced by stannous chloride to the amino derivative **10**. The amino derivative on treatment with aromatic sulphonyl chlorides gave the indoline derivatives **11(a–e)**. The synthetic scheme to **11(a–e)** is shown in Scheme 2 and the structural data of **11(a–e)** are given in Table II.

The compounds **6(a–f)** and **11(a–e)** were characterized by FTIR, ^{1}H-NMR and mass spectroscopy.

TABLE I. Structure of the synthesized compounds **6(a–f)**

6(a–f)

Compound	R
6a	
6b	
6c	
6d	
6e	
6f	

*Compound **6a***. Yield: 89 %; white crystalline; m.p. 119 °C; Anal. Calcd. for $C_{28}H_{30}FN_5O_6S_2$: C, 54.62; H, 4.91; N, 11.37 %. Found: C, 54.61; H, 4.90; N, 11.36 %. IR (KBr, cm^{-1}): 3452 (stretching of NH), 3047 (stretching of N=C–H), 2937, 2840 (stretching of C–H), 1634 (stretching of amide C=O), 1246 (stretching of C–F), 1050 (stretching of C–O). ^{1}H-NMR (400 MHz, DMSO-d_6, δ / ppm) 2.85 (4H, *t*, morpholine CH$_2$), 2.90 (3H, *s*, NCH$_3$), 3.09 (2H, *t*, indoline CH$_2$), 3.16 (3H, *s*, NCH$_3$), 3.68 (4H, *t*, morpholine CH$_2$), 4.01 (2H, *t*, indoline CH$_2$), 6.53–7.88 (10H, *m*, aromatic protons), 8.26 (1H, *s*, N=CH), 10.52 (1H, *s*, NH). MS (*m/z*): 615 (M$^+$) with all isotopic and other peaks.
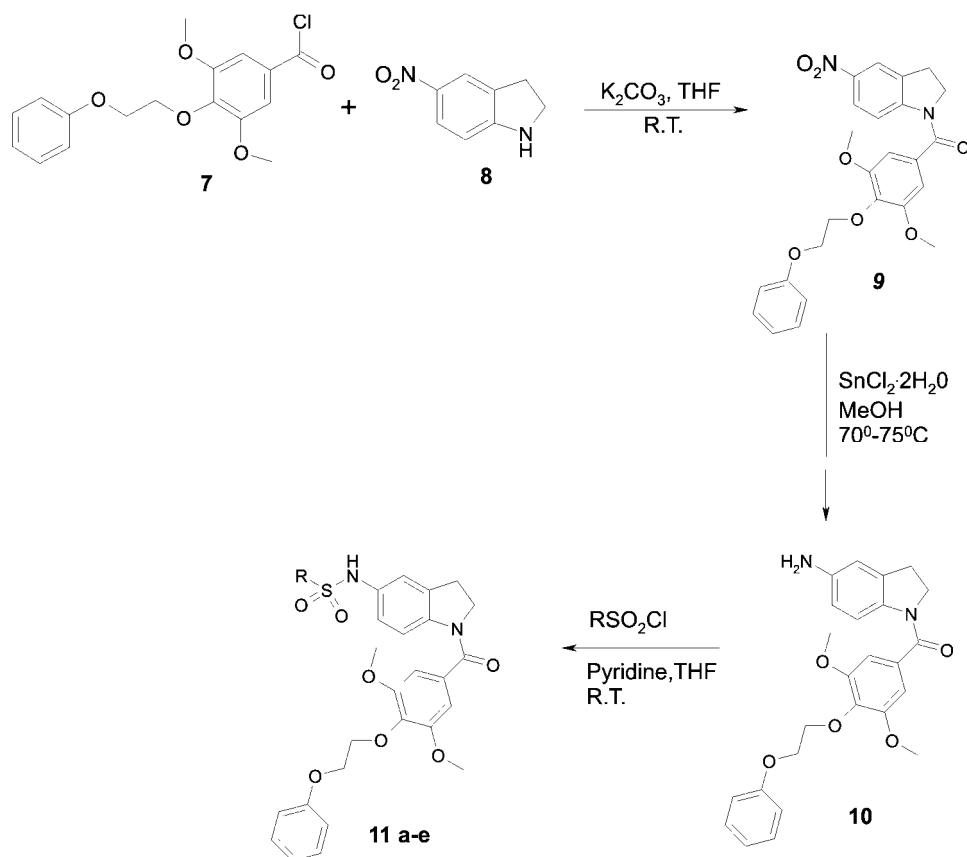
Scheme 2.

Compound 6b. Yield: 76 %; grey microcrystalline; m.p; 146 °C. Anal. Calcd. for $C_{26}H_{27}N_5O_6S_2$: C, 54.82; H, 4.78; N, 12.29 %. Found: C, 54.81; H, 4.77; N, 12.28 %. IR (KBr, cm^{-1}): 3455 (stretching of NH), 3050 (stretching of N=C–H), 2927, 2830 (stretching of C–H), 1632 (stretching of amide C=O). ^{1}H-NMR (400 MHz, DMSO-d_6, δ/ ppm): 2.67 (3H, *s*, NHCOC**H₃**), 2.71 (2H, *t*, indoline CH₂), 2.90 (3H, *s*, NCH₃), 3.16 (3H, *s*, NCH₃), 3.90 (2H, *t*, indoline CH₂), 6.83–8.25 (11H, *m*, aromatic protons), 8.28 (1H, *s*, N=CH), 8.72 (1H, *s*, NHCO), 10.25 (1H, *s*, NHSO₂). MS (*m/z*): 569 (M$^+$) with all isotopic and other peaks.

Compound 6c. Yield: 90 %; red powder; m.p. 132 °C; Anal. Calcd. for $C_{33}H_{33}N_5O_8S_3$: C, 54.76; H, 4.60; N, 9.68 %. Found: C, 54.75; H, 4.61; N, 9.67 %. IR (KBr, cm^{-1}): 3450 (stretching of NH), 3048 (stretching of N=C–H), 2929, 2832 (stretching of C–H), 1633 (stretching of amide C=O). ^{1}H-NMR (400 MHz, DMSO-d_6, δ/ ppm): 2.37 (3H, *s*, ArCH₃), 2.92 (3H, *s*, NCH₃), 3.09 (2H, *t*, indoline CH₂), 3.16 (3H, *t*, NCH₃), 3.42 (2H, *s*, CH₂CO), 3.98 (2H, *t*, indoline CH₂),

6.99–8.25 (15H, *m*, aromatic protons), 8.26 (1H, *s*, N=CH), 8.57 (1H, *s*, NHSO$_2$), 10.52 (1H, *s*, CONHSO$_2$). MS (*m/z*): 723 (M$^+$) with all isotopic and other peaks.

TABLE II. Structure of the synthesized compounds **11(a–e)**

11(a–e)

Compound	R
11a	
11b	
11c	
11d	
11e	

Compound 6d. Yield: 85 %; brown crystalline; m.p. 124 °C. Anal. Calcd. for C$_{34}$H$_{29}$BrN$_4$O$_7$S$_2$: C, 54.47; H, 3.90; N, 7.47 %. Found: C, 54.46; H, 3.89; N, 7.46 %. IR (KBr, cm^{-1}): 3450 (stretching of NH), 3048 (stretching of N=C–H), 2929, 2832 (stretching of C–H), 1682 (stretching of Ar–C=O), 1633 (stretching of amide C=O). ^{1}H-NMR (400 MHz, DMSO-d_6, δ / ppm): 2.51 (3H, *s*, ArCH$_3$), 2.76 (2H, *t*, indoline CH$_2$), 3.07 (3H, *s*, NCH$_3$), 3.15 (3H, *s*, NCH$_3$), 4.00 (2H, *t*, indoline CH$_2$), 7.41–8.01 (14H, *m*, aromatic protons), 8.26 (1H, *s*, N=CH), 10.52 (1H, *s*, NH). MS (*m/z*): 749 (M$^+$) with all isotopic and other peaks.

Available online at www.shd.org.rs/JSCS/

Compound 6e. Yield: 88 %; brown microcrystalline; m.p. 132 °C. Anal. Calcd. for $C_{35}H_{32}N_4O_8S_2$: C, 59.99; H, 4.60; N, 7.99 %. Found: C, 59.98; H, 4.59; N, 7.99 %. IR (KBr, cm^{-1}): 3438 (stretching of NH), 3052 (stretching of N=C–H), 2928, 2842 (stretching of C-H), 1685 (stretching of Ar–C=O), 1635 (stretching of amide C=O). ^{1}H-NMR (400 MHz, DMSO-d_6, δ/ ppm): 2.53 (3H, *s*, ArCH$_3$), 3.08 (2H, *t*, indoline CH$_2$), 3.15 (6H, *s*, N(CH$_3$)$_2$), 3.88 (3H, *s*, OCH$_3$), 4.03 (2H, *t*, indoline CH$_2$), 7.10–8.05 (14H, *m*, aromatic protons), 8.26 (1H, *s*, N=CH), 10.52 (1H, *s*, NH). MS (*m/z*): 700 (M$^+$) with all isotopic and other peaks.

Compound 6f. Yield: 95 %; white needles; m.p. 160 °C; Anal. Calcd. for $C_{27}H_{30}N_6O_5S_2$: C, 55.65; H, 5.19; N, 14.42 %. Found: C, 55.64; H, 5.18; N, 14.42 %. IR (KBr, cm^{-1}): 3434 (stretching of NH), 3050 (stretching of N=C–H), 2927, 2852 (stretching of C–H), 1631 (stretching of amide C=O). ^{1}H-NMR (400 MHz, DMSO-d_6, δ/ ppm): 2.94 (6H, *s*, N(CH$_3$)$_2$), 3.05 (2H, *t*, indoline CH$_2$), 3.19 (4H, *t*, piperazine CH$_2$), 3.63 (4H, *t*, piperazine CH$_2$), 4.06 (2H, *s*, indoline CH$_2$), 6.89–8.45 (11H, *m*, aromatic protons), 8.26 (1H, *s*, N=CH). MS (*m/z*): 582 (M$^+$) with all isotopic and other peaks.

Compound 11a. Yield: 76 %; red crystals; m.p. 155 °C; Anal. Calcd. for $C_{30}H_{28}ClN_3O_7S$: C, 59.06; H, 4.63; N, 6.89 %. Found: C, 59.05; H, 4.62; N, 6.88 %. IR (KBr, cm^{-1}): 3486 (stretching of NH), 2902, 2852 (stretching of C–H), 1632 (stretching of amide C=O), 1240 (stretching of C–O). ^{1}H-NMR (400 MHz, DMSO-d_6, δ/ ppm): 2.98 (2H, *t*, indoline CH$_2$), 3.73 (6H, *s*, OCH$_3$), 3.97 (2H, *t*, indoline CH$_2$), 4.22 (4H, *m*, OCH$_2$), 6.83–9.03 (13H, *m*, aromatic protons), 10.52 (1H, *s*, NH). MS (*m/z*): 609 (M$^+$) with all isotopic and other peaks.

Compound 11b. Yield: 65 %; white needles; m.p. 99 °C; Anal. Calcd. for $C_{31}H_{29}BrN_2O_7S$: C, 56.97; H, 4.47; N, 4.29 %. Found: C, 56.96; H, 4.46; N, 4.28 %. IR (KBr, cm^{-1}): 3488 (stretching of NH), 2922, 2852 (stretching of C–H), 1632 (stretching of amide C=O), 1246 (stretching of C–O). ^{1}H-NMR (400 MHz, DMSO-d_6, δ/ ppm): 3.00 (2H, *t*, indoline CH$_2$), 3.73 (6H, s, OCH$_3$), 3.98 (2H, *t*, indoline CH$_2$), 4.22 (4H, *m*, OCH$_2$), 6.84–7.79 (14H, *m*, aromatic protons), 10.25 (1H, *s*, NH). MS (*m/z*): 653 (M$^+$) with all isotopic and other peaks.

Compound 11c. Yield: 78 %; grey crystals; m.p. 106 °C; Anal. Calcd. for $C_{37}H_{34}N_2O_7S$: C, 68.29; H, 5.27; N, 4.30 %. Found: C, 68.28; H, 5.26; N, 4.29 %. IR (KBr, cm^{-1}): 3488 (stretching of NH), 2922, 2852 (stretching of C–H), 1632 (stretching of amide C=O), 1246 (stretching of C–O). ^{1}H-NMR (400 MHz, DMSO-d_6, δ/ ppm): 3.00 (2H, *t*, indoline CH$_2$), 3.71 (6H, *s*, OCH$_3$), 3.97 (2H, *t*, indoline CH$_2$), 4.22 (4H, *m*, OCH$_2$), 6.82–7.85 (19H, *m*, aromatic protons), 10.52 (1H, *s*, NH). MS (*m/z*): 650 (M$^+$) with all isotopic and other peaks.

Compound 11d. Yield: 80 %; yellow crystals; m.p. 105 °C; Anal. Calcd. for $C_{34}H_{30}N_2O_9S$: C, 63.54; H, 4.71; N, 4.36 %. Found: C, 63.54; H, 4.71; N, 4.35 %. IR (KBr, cm^{-1}): 3486 (stretching of NH), 2902, 2852 (stretching of C–H), 1690 (stretching of coumarin CO), 1633 (stretching of amide C=O), 1245 (stretching

of C–O). ^{1}H-NMR (400 MHz, DMSO-d_6, δ / ppm): 3.00 (2H, *t*, indoline CH$_2$), 3.80 (6H, *s*, OCH$_3$), 3.98 (2H, *t*, indoline CH$_2$), 4.41 (4H, *m*, OCH$_2$), 6.60–8.21 (15H, *m*, aromatic protons), 10.52 (1H, *s*, NH). MS (*m/z*): 642 (M$^+$) with all isotopic and other peaks.

Compound 11e. Yield: 81 %; yellow crystals; m.p. 111 °C; Anal. Calcd. for C$_{33}$H$_{32}$N$_2$O$_8$S: C, 64.27; H, 5.23; N, 4.54 %. Found: C, 64.27; H, 5.22; N, 4.53 %. IR (KBr, cm^{-1}): 3445 (stretching of NH), 3198, 2935, 2842 (stretching of C–H), 1720 (stretching of COCH$_3$), 1632 (stretching of amide C=O), 1250 (stretching of C–O). ^{1}H-NMR (400 MHz, DMSO-d_6, δ / ppm): 2.04 (3H, *s*, COCH$_3$), 3.00 (2H, *t*, indoline CH$_2$), 3.77 (6H, *s*, OCH$_3$), 4.02 (2H, *t*, indoline CH$_2$), 4.24 (4H, *m*, OCH$_2$), 6.81–7.71 (14H, *m*, aromatic protons), 10.17 (1H, *s*, NH); MS (*m/z*): 616 (M$^+$) with all isotopic and other peaks.

The compounds **6(a–f)** and **11(a–e)** were tested for their antioxidant, antibacterial, antifungal and anti-tuberculosis activities.

Amongst the compounds screened for antioxidant activity, **6a**, **6b**, **6e**, **6f** and **11 (a–e)** showed very good antioxidant activities, as shown in Table III.

All the screened compounds, except **6b**, **6c**, **11d** and **11e**, exhibited very good antifungal and antibacterial activities, as shown in Tables IV and V, respectively.

TABLE III. Antioxidant activity (%) of the compounds

Compound	Concentration / μg ml^{-1}		
	200	100	50
L-Ascorbic acid	99.2	99	98.8
6a	93.5	92.00	88.05
6b	90.00	88.05	85.00
6c	28.05	24.36	20.7
6d	57.9	48.0	28.2
6e	98.6	98.5	89.8
6f	98.4	98.0	85.8
11a	99.00	97.2	93.6
11b	94.2	93.2	92.6
11c	95.00	92.40	78.05
11d	94.55	92.40	85.05
11e	91.70	83.25	70.22

TABLE IV. Antifungal activity of the compounds

Compound	Concentration / μg ml^{-1}														
	5	25	50	100	250	5	25	50	100	250	5	25	50	100	250
	A. niger					*A. clavatus*					*C. albicans*				
Griseofulvin	19	23	25	25	28	18	21	22	22	24	–	–	–	–	–
Nystatin	18	19	24	29	29	18	21	24	25	26	–	–	–	–	–
6a	–	10	15	17	19	–	11	16	17	19	–	14	16	17	20
6d	–	12	16	19	21	–	12	15	19	22	–	12	15	20	22
6e	–	13	17	19	22	–	13	17	18	20	–	15	17	19	21

TABLE IV. Continued

Compound	Concentration / µg ml^{-1}														
	5	25	50	100	250	5	25	50	100	250	5	25	50	100	250
	A. niger					A. clavatus					C. albicans				
6f	–	14	16	18	19	–	13	15	18	19	–	15	17	19	20
11a	–	14	16	19	20	–	11	17	18	19	–	12	17	18	21
11b	–	12	15	18	20	–	12	15	18	19	–	13	15	18	19
11c	–	13	16	20	21	–	13	16	18	20	–	15	16	19	20

TABLE V. Antibacterial activity of the compounds

Compound	Concentration / µg ml^{-1}															
	25	50	100	250	25	50	100	250	25	50	100	250	25	50	100	250
	E. coli				P. aeruginosa				S. aureus				S. pyogenes			
Ampicillin	15	16	19	20	15	15	18	20	14	16	18	19	13	14	16	20
Ciprofloxacin	23	28	28	28	23	24	26	27	19	21	21	22	19	21	22	22
Norfloxacin	25	26	27	29	19	21	23	23	19	20	21	21	22	25	26	28
6a	13	15	17	21	12	14	18	21	12	14	17	19	11	12	15	17
6d	16	18	20	22	15	17	19	22	11	12	15	17	12	14	17	20
6e	13	13	15	17	11	12	15	16	15	18	20	22	11	14	16	18
6f	11	11	14	15	11	12	13	15	12	14	15	17	11	13	15	17
11a	11	14	16	17	11	14	17	19	12	14	15	15	11	13	14	15
11b	11	13	17	17	10	12	15	18	14	16	19	23	12	14	16	17
11c	11	13	15	15	10	13	14	16	17	19	19	24	12	15	17	19

Compounds **6a** (*MIC* = 100 µg/ml) and **6f** (*MIC* = 62.5 µg/ml) showed promising anti-tuberculosis activity, as shown in Table VI.

TABLE VI. Anti-tuberculosis activity of the compounds

Compound	*MIC* / µg ml^{-1}
Steptomycin	4
Isoniazid	0.2
Rifampicin	40
Ethambutol	2
6a	100
6d	250
6e	250
6f	62.5
11a	500
11b	1000
11c	>1000

EXPERIMENTAL

All the recorded melting points were determined in an open capillary and are uncorrected. The IR spectra were recorded on a Perkin-Elmer FTIR spectrophotometer in KBr discs. The ^{1}H-NMR spectra were recorded on a 400 MHz spectrophotometer in DMSO-d_6 as solvent and TMS as the internal standard. The mass spectra were obtained using a Waters mass spectrometer.

4-(2,3-Dihydro-1H-indol-1-ylcarbonyl)-N-[(1E)-(dimethylamino)methylene]-
benzenesulphonamide (4)

Compounds **2** (0.010 mol) and **3** (0.010 mol) were dissolved in THF together with K_2CO_3. The reaction mixture was stirred at room temperature for 4 h. The reaction mixture was then poured into water and extracted with EtOAc. The organic layer was separated, dried over Na_2SO_4 and concentrated under vacuum.

Compound 4. Yield: 85 %, red crystalline, m.p. 161 °C. Anal. Calcd. for $C_{18}H_{19}N_3O_3S$: C, 60.49; H, 5.36; N, 11.76 %. Found: C, 60.48; H, 5.35; N, 11.76 %. IR (KBr, cm^{-1}): 3047 (stretching of N=C–H), 2937, 2840 (stretching of C–H), 1634 (stretching of amide C=O). ^{1}H--NMR (400 MHz, DMSO-d_6, δ / ppm): 2.94 (3H, *s*, NCH$_3$), 3.09 (2H, *t*, indoline CH$_2$), 3.17 (3H, *s*, NCH$_3$), 3.98 (2H, *t*, indoline CH$_2$), 7.07–7.87 (8H, *m*, aromatic protons), 8.27 (1H, *s*, N=CH). MS (*m/z*): 357 (M$^+$) with all isotopic and other peaks.

1-[4-({[(1E)-(Dimethylamino)methylene]amino}sulphonyl)benzoyl]indoline-5-sulphonyl
chloride (5)

Compound **4** (0.010 mol) was added in portions to a solution of chlorosulphonic acid (10 ml) at 0 °C and stirred for 30 min. The reaction mixture was cooled to room temperature and stirred for a further 1 h. The reaction mixture was then poured into cold water and the formed solid was separated by filtration.

Compound 5. Yield: 65 %, grey microcrystalline, m.p. 131 °C. Anal. Calcd. for $C_{18}H_{18}ClN_3O_5S_2$: C, 47.42; H, 3.98; N, 9.22 %. Found: C, 47.41; H, 3.97; N, 9.21 %. IR (KBr, cm^{-1}): 3047 (stretching of N=C–H), 2937, 2840 (stretching of C–H), 1634 (stretching of amide C=O). ^{1}H-NMR (400 MHz, DMSO-d_6, δ / ppm): 2.94 (3H, *s*, NCH$_3$), 3.09 (2H, *t*, indoline CH$_2$), 3.17 (3H, *s*, NCH$_3$), 3.98 (2H, *t*, indoline CH$_2$), 7.49–8.14 (7H, *m*, aromatic protons), 8.27 (1H, *s*, N=CH). MS (*m/z*): 455 (M$^+$) with all isotopic and other peaks.

General procedure for the synthesis of 6(a–f)

Compound **5** (0.010 mol) and the required amine (0.010 mol) were dissolved in THF, together with DMAP and pyridine (0.030 mol). The reaction mixture was stirred at room temperature for 4 h, after which the reaction mixture was poured into dilute HCl and extracted with EtOAc. The organic layer was washed with water, separated, dried over Na_2SO_4 and concentrated under vacuum. The so-obtained crude product was crystallized from a mixture of CH_2Cl_2 and hexane.

[3,5-Dimethoxy-4-(2-phenoxyethoxy)phenyl](5-nitro-2,3-dihydro-1H-indol-1-yl)methanone (9)

Compound **7** (0.010 mol) and **8** (0.010 mol) were dissolved in THF, together with K_2CO_3. The reaction mixture was stirred at room temperature for 4 h and then poured into water and extracted with EtOAc. The separated, organic layer was dried over Na_2SO_4 and concentrated under vacuum.

Compound 9. Yield: 80 %; yellow needles; m.p. 93 °C; Anal. Calcd. for $C_{25}H_{24}N_2O_7$: C, 64.65; H, 5.21; N, 6.03 %. Found: C, 64.64; H, 5.20; N, 6.02 %. IR (KBr, cm^{-1}): 2902, 2852 (stretching of C–H), 1632 (stretching of amide C=O), 1515 (stretching of NO$_2$), 1240 (stretching of C–O). ^{1}H-NMR (400 MHz, DMSO-d_6, δ / ppm): 3.20 (2H, *t*, indoline CH$_2$), 3.77 (6H, *s*, OCH$_3$), 4.17 (2H, *t*, indoline CH$_2$), 4.27 (4H, *m*, OCH$_2$), 6.92–8.16 (10H, *m*, aromatic protons); MS (*m/z*): 464 (M$^+$) with all isotopic and other peaks.

(5-Amino-2,3-dihydro-1H-indol-1-yl)[3,5-dimethoxy-4-(2-phenoxyethoxy)phenyl]methanone (10)

To a suspension of the nitro derivative **9** (0.10 mol) in methanol (50 ml) were added 5 equivalents SnCl$_2$·2H$_2$O and the reaction mixture was heated at 70 °C for 4 h. Then the

Available online at www.shd.org.rs/JSCS/

mixture was cooled to room temperature, poured into aqueous NH_3 and filtered through celite. The filtrate was extracted with EtOAc. The separated organic layer was dried over Na_2SO_4 and concentrated under vacuum. The product was recrystallized from ethanol.

Compound 10. Yield: 66 %; brown powder; m.p. 65 °C; Anal. Calcd. for $C_{25}H_{26}N_2O_5$: C, 69.11; H, 6.03; N, 6.45 %. Found: C, 69.10; H, 6.02; N, 6.44 %. IR (KBr, cm[-1]): 3445 (stretching of NH_2), 2902, 2852 (stretching of C–H), 1632 (stretching of amide C=O), 1240 (stretching of C–O). ^{1}H-NMR (400 MHz, DMSO-d_6, δ / ppm): 2.94 (2H, *t*, indoline CH_2), 3.75 (6H, *s*, OCH_3), 3.95 (2H, *t*, indoline CH_2), 4.22 (4H, *m*, OCH_2), 4.95 (2H, *bs*, NH_2), 6.40–7.78 (10H, *m*, aromatic protons). MS (*m/z*): 434 (M+) with all isotopic and other peaks.

General procedure for the synthesis of 11(a–e)

Compound **10** (0.010 mol) and the required aromatic sulphonyl chloride (0.010 mol) were dissolved in THF, together with DMAP and pyridine (0.030 mol). The reaction mixture was stirred at room temperature for 4 h, after which it was poured into dilute HCl and extracted with EtOAc. The organic layer was washed with water, separated, dried over Na_2SO_4 and concentrated under vacuum. The crude product was crystallized from a mixture of CH_2Cl_2 and hexane mixture.

Anti-oxidant activity

The *in vitro* antioxidant activity of the test compounds was determined by the DPPH method[5]using L-ascorbic acid (an antioxidant agent) as the positive control. The compounds were tested for antioxidant activity at concentrations of 200, 100 and 50 μg/ml.

Antimicrobial activity

The *in vitro* antimicrobial activity of the test compounds was assessed against 24 h cultures of several selected bacteria and fungi. The employed gram positive and gram negative bacteria were *Escherichia coli*, *Pseudomonas aeruginosa*, *Streptococcus pyogenes* and *Staphylococcus aureus* and the used fungi were *Candida albicans*, *Aspergillus niger* and *Aspergillus clavatus*.

The antimicrobial activity of all the compounds was tested using Müller Hinton broth (Hi Media M 391) as the nutrient medium for bacterial and Sabouraud Dextrose broth for fungal growth. The media were prepared using distilled-deionized water and dispensed in 25 ml amounts into 100-mm Petri dishes.The activity was determined by measuring the diameter of inhibition zone in millimetres.

Anti-tuberculosis activity

All the compounds were screened for their in vitro antimycobacterial activity against Mycobacterium tuberculosis by the broth macro dilution method. The activity of the compounds was confirmed by MIC determination against M. tuberculosis. A stock solution of each compound (1 mg/ml) was diluted in sterile distilled water to test the range. Each tube contained 4 ml sterile Middle Brook 7H9 broth containing albumin-dextrose-catalase, Tween 80, glycerol and 4 ml of the compound solution was added to make serial double dilutions. The tubes were incubated at 37 °C for 7 days and then read visually. The MIC was determined as the lowest concentration of the test substance that prevented turbidity. Streptomycin, isoniazid, rifampicin and ethambutol were used as the reference standards.

<div align="center">CONCLUSIONS</div>

In conclusion, a series of novel indoline derivatives were synthesized and subjected to various biological activity tests, *viz.* antioxidant, antifungal, anti-tu-

berculosis and antibacterial activity. Most of the compounds showed very good antioxidant and anti-infective activities, which suggest that the indoline core has a very high therapeutic value and needs to be explored in further studies.

И З В О Д

СИНТЕЗА И БИОЛОШКА АКТИВНОСТ НЕКИХ ДЕРИВАТА ИНДОЛИНА

MILIND A. RODE[1], SAHEBRAO S RINDHE[1] и BHAUSAHEB K KARALE[2]

[1]*Department of Chemistry, New Arts, Commerce and Science College, Ahmednagar- 414001 и* [2]*Department of Chemistry, Radhabai Kale Mahila Mahavidyalaya, Ahmednagar-414001, India*

Реакцијом индолина са супституисаним бензоил-хлоридом, у присуству K_2CO_3 у THF, добијено је једињење **4** које је, након хлоросулфоновања, преведено у једињење **5**. Кондензацијом ароматичних амина са молекулом **5** добијени су индолински деривати **6(a–f)**. Сличан третман 5-нитроидолина супституисаним бензоил-хлоридом дао је нитро дериват **9**, који је прво редукован калај(II)-хлоридом, а резултујући амин је затим кондензован са ароматичним сулфонил-хлоридом, при чему су добијени индолински деривати **11(a–e)**. Финални производи, **6(a–f)** и **11(a–e)** су тестирани на антибактеријску, антитуберкулозну и антигљивичну активност. Неки од синтетизованих деривата су се показали веома активним према одабраним грам-позитивним и грам-негативним микро-ораганизмима, према одређеним сојевима гљива, као и према *Mycobacterium tuberculosis*. Применом *in vitro* DPPH теста испитане су антиоксидативне особине свих синтетизованих индолина, при чему је код већине деривата детектована запажена антиоксидативна активност.

(Примљено 14. априла 2009)

REFERENCES

1. J. M. Bentley, S. P. Vickers, D. R. Adams, D. Bebbington, K. R. Benwell, M. J. Bickerdike, J. E. P. Davidson, C. E. Dawson, C. T. Dourish, M. A. J. Duncton, S. Gaur, A. R. George, P. R. Giles, R. J. Hamlyn, G. A. Kennett, A. R. Knight, C. S. Malcolm, H. L. Mansell, A. Misra, N. J. T. Monck, R. M. Pratt, K. Quirk, J. R. A. Roffey, S. P. Vickers, I. A. Cliffe, *Bioorg. Med. Chem. Lett.* **14** (2004) 2367
2. T. Noguchi, N. Tanaka, T. Nishimata, R. Goto, M. Hayakawa, A. Sugidachi, T. Ogawa, F. Asai, T. Ozeki, K. Fujimoto, *Chem. Pharm. Bull.* **55** (2007) 393
3. A. Fensome, W. R. Adams, A. L. Adams, T. J. Berrodin, J. Cohen, C. Huselton, A. Illenberger, J. C. Kern, V. A. Hudak, M. A. Marella, E. G. Melenski, C. C. McComas, C.A. Mugford, O. D. Slayden, M. Yudt, Z. Zhang, P. Zhang, Y. Zhu, R. C. Winneker, J. E. Wrobel, *J. Med. Chem.* **51** (2008) 1861
4. A. H. Abdel-Rahman, E. M. Keshk, M. A. Hanna, S. M. El-Bady, *Bioorg. Med. Chem.* **12** (2004) 2483
5. O. P. Sharma, T. K. Bhat, *Food Chem.* **113** (2009) 1202.

Flavonoids from mango leaves with antibacterial activity

QUDSIA KANWAL[1], ISHTIAQ HUSSAIN[1], HAMID LATIF SIDDIQUI[1]
and ARSHAD JAVAID[2]*

[1]*Institute of Chemistry, University of the Punjab, Quaid-e-Azam Campus, Lahore and*
[2]*Institute of Mycology and Plant Pathology, University of the Punjab,*
Quaid-e-Azam Campus, Lahore, Pakistan

Abstract: Five flavonoids, *viz.* (–)-epicatechin-3-*O*-β-glucopyranoside (**1**), 5-hydroxy-3-(4-hydroxylphenyl)pyrano[3,2-*g*]chromene-4(8*H*)-one (**2**), 6-(*p*-hydroxybenzyl)taxifolin-7-*O*-β-D-glucoside (tricuspid) (**3**), quercetin-3-*O*-α-glucopyranosyl-(1→2)-β-glucopyranoside (**4**) and (–)-epicatechin(2-(3,4-dihydroxyphenyl)-3,4-dihydro-2*H*-chromene-3,5,7-triol) (**5**), were isolated from the leaves of mango (*Mangifera indica* L.). The antibacterial activity of different concentrations of these flavonoids (100, 300, 500, 700, 900 and 1000 ppm) was evaluated against four bacterial species, namely *Lactobacillus* sp., *Escherichia coli*, *Azospirillium lipoferum* and *Bacillus* sp. All the tested concentrations of the five flavonoids significantly reduced the growth of all the five tested bacterial species. However, differences in the antibacterial activity of the flavonoids were evident. Compound **1** exhibited the lowest antibacterial activity, resulting in a 7–75 % reduction in the growth of the different bacterial species. Compound **5** showed the greatest antibacterial activity and the different concentrations reduced the bacterial growth by 45–99.9 %. *A. lipoferum* and *Bacillus* sp. showed the highest susceptibility to this compound. Compounds **2**–**4** also depicted pronounced antibacterial activity. Different concentrations of these compounds decreased bacterial growth by 52–96 %. From the present study, it can be concluded that compound **5** is the most effective of the tested flavonoids against *A. lipoferum* and *Bacillus* sp.

Keywords: antibacterial; *Mangifera indica*; mango; flavonoids; leaves.

INTRODUCTION

Flavonoids are a major class of oxygen-containing heterocyclic natural products that are widespread in green plants.[1] Generally, they are found as plant pigments in a broad range of fruits and vegetables.[2] These are C_{15} compounds composed of two aromatic rings linked through a three-carbon bridge with a carbonyl

---

functional gr oup located at one end o f th e bridge. Flavonoids h ave been reco-gnized as having a protective effect in plan ts against microbial invasion by plant pathogens.[3,4] Flavono id-rich plant extr acts have been used for centuries to tre at human disease.[5] Isolated flavonoids have been shown to possess a host of impor-tant biol ogical activities, including antif ungal and ant ibacterial activities.[6–8] The potential of n aturally occurring flavo noids as anti-infective agents has been re-cognized.[9] However, reports of activit y in t he field of antibacterial flavono id re-search are widely conflicting, probably owing to inte r- and intra-assay variations in the susceptibility testing.[5]

Mango (*Mangifera indica* L.) is an econom ically im portant tro pical fruit found throughout the world. It is ver y popular due to its excellent eating qualit y (bright colour, sweet taste and luscious flavour) and nutritional com position (vi-tamins, minerals, fibre an d other ph ytochemical compounds).[10] Mango contains various class es of poly phenols, carote noids, and ascorbic acid, which de mons-trate different health-promoting pr operties, mainly fr om their anti oxidant activi-ties.[11] The present study was aimed at investigating the antibacte rial activity of five flavonoids isolated from mango leaves, against four bacterial species.

EXPERIMENTAL

General procedure

All the reagents and the solve nts used in the present study were procured from E. Merck Germany, Fluka Switzerla nd, BDH Chemicals England and Sig ma-Aldrich Che micals Co . USA. The solv ents u sed were of analy tical grade. For colu mn chromatography, silica gel 60 (Merck 23 0–400 mesh) wa s u sed and TLC was performed on sili ca gel (Merck, K eiselgel 60F256). The melting points were determined by the sealed capillary method using a Gallen-kamp m elting point apparatus. However, the melting point s were uncorrected. The optical rotation was measured by a polarimeter (modal wxg-4 Dise polarimeter).

The IR spe ctra of the co mpounds in K Br discs were re corded on a Fourier Transfor m Shimadzu 4200 instru ment. Th e ^{1}H- and ^{13}C-NMR spectra were recorded on a Bruker 14.1 TNMR spectrometer, operating at a frequenc y of 600 MHz. The DEPT experi ments w ere performed u sing polarization t ransfer pulses of 90 and 135 °. The EI–MS spectra were mea-sured with a JEOL JMS-AX 505 HAD mass spectrometer at an ionization voltage of 70 eV.

Isolation of bioactive compounds from mango leaves

Five hundred g rams of fresh m ango leav es (equivalent to 2 20 g dry weigh t) were col-lected fro m th e Univer sity of the Punj ab, Qua id-e-Azam Campus, Lahore, Pakistan in May 2007. The leav es were w ashed with distilled water, dried in the shad e an d soake d in 1 L methanol for 15 min to re move chlorophy ll. The leaves we re then blended with 1.5 L m e-thanol, left overnight, filtered with Whatman No. 1 filter paper under vacuu m, centrifuged at 2000 rpm for 5 min and the supernatant was concentrated to 100 mL under vacuum at 50 °C. The concentrated solution was diluted with water (1:1), for p recipitation to o ccur. These pre -cipitates were filtered, washed with ether, dried in a vacuu m desiccator to y ield compound **1** (215 mg). The filtrate was then concentrated to reduce the volume to 100 mL, extracted with 100 mL of acet one, filtered and the residue w as re moved. The residue wa s p urified by pre-paratory TLC (MeOH:CHCl$_3$, 1:99) and recry stallized in CH Cl$_3$:MeOH (4:1) to y ield com-

pound **2** (323 mg). The remaining filtrate was successively extracted with 150 mL $CHCl_3$ and *n*-butanol each. The $CHCl_3$ extract was subjected to silica gel column chromatography using a solvent system of ethyl acetate:MeOH:H_2O (4:1:1). From this column, compound **3** (1.75 g) was isolated and subsequently purified by preparative TLC using the solvent system EtOAc:MeOH (1:4). The butanolic extract was fractionated by silica gel column (90×4 cm) chromatography using an isocratic solvent system of MeOH:$CHCl_3$:H_2O (3:1:1) to yield compounds **4** (720 mg) and **5** (1.1 g).

Acid hydrolysis

Each flavonoid glycoside (3 mg) was refluxed with 2 M HCl (3 ml) for one hour. The aglycon part was extracted with EtOAc and identified with the help of IR, UV and NMR spectral analysis. The sugar part was isolated from the aqueous layer and identified by co-TLC and comparison with authentic samples.

Antibacterial activity

Four bacterial species, *viz. Lactobacillus* sp. 004, *Escherichia coli* 019, *Azospirillium lipoferum* 022 and *Bacillus* sp. 018, were procured from the Fungal Culture Bank, Institute of Mycology and Plant Pathology, University of the Punjab, Lahore, Pakistan. After autoclaving at 121 °C, LBA broth medium was cooled to room temperature and 10 mL aliquots of the medium were added to 20 mL culture tubes. Appropriate quantities of the five flavonoids were added to the LBA broth medium in the culture tubes to achieve final concentrations of 100, 300, 500, 700, 900 and 1000 ppm. The test compounds were not added to the control tube. One drop of overnight broth culture of each bacterial species was added to the culture tubes prior to incubation at 37 °C for 24 h. Each treatment was performed in triplicate. Afterwards, the optical density of each suspension was recorded at 630 nm on a modal UT 2100UV spectrophotometer (Utechproducts Inc., USA). The effectiveness of the substances was inversely related to the optical density of the suspension.

Statistical analysis

All the data were subjected to analysis of variance followed by the Student–Newman––Keuls test ($p \leq 0.05$) to separate the treatment means using computer software COSTAT.

RESULTS AND DISCUSSION

Structures of the isolated compounds

*Compound **1***. Greenish brown powder; m.p. 202–205 °C. IR (KBr, cm^{-1}): 3431, 2923, 2922, 1650,1600. ^{1}H-NMR (600 MHz, MeOH-d_4, δ / ppm): 5.10 (1H, *d*, *J* = 2.2 Hz, H-2), 4.45 (1H, *dtd*, *J* = 2.2, 5.0, 3.4 Hz, H-3), 2.75 (2H, *d*, *J* = 3.4 Hz, H-4), 6.03 (1H, *d*, *J* = 2.2 Hz, H-6), 5.89 (1H, *d*, *J* = 2.2 Hz, H-8), 6.78 (1H, *br s*, H-2'), 6.97 (1H, *d*, *J* = 10.0 Hz, H-5'), 6.60 (1H, *dd*, *J* = 10.0, 1.8 Hz, H-6'), 6.54 (1H, *br s*, H-1"), 4.83 (1H, *br s*, H-2"), 4.65 (1H, *t*, *J* = 8.1 Hz, H-3"), 4.34 (1H, *t*, *J* = 8.2 Hz, H-4'), 4.77 (1H, *m*, H-5"), 4.20 (1H, *m*, H-6"α), 4.46 (1H, *m*, H-6"β). ^{13}C-NMR (MeOH-d_4, δ / ppm): 78.9 (C-2), 68.0 (C-3), 30.4 (C-4), 160.5 (C-5), 99.1 (C-6), 155.1 (C-7), 95.9 (C-8), 155.8 (C-9), 104.0 (C-10), 132.9 (C-1'), 115.1(C-2'), 146.3 (C-3'), 146.4 (C-4'),116.0 (C-5'), 115.5 (C-6'), 106.0 (C-1"), 73.0 (C-2"), 75.9 (C-3"), 71.8 (C-4"), 78.4 (C-5"), 62.9 (C-6").

EI–MS (*m/z*): 452 (M$^+$), 256, 213, 170, 153, 125, 97. UV (MeOH) (λ_{max} / nm):
212, 280. [α]^{20} (589 nm) = –30.4° (*c* = 0.1 g/100 ml, MeOH).

Compound **2**. Brown solid; m.p. 220–221 °C. IR (KBr, cm^{-1}): 3410 (*br*),
2923, 2916, 1670, 1650, 1600. ^{1}H-NMR (600 MHz, CDCl$_3$, δ / ppm): 7.83 (1H, *s*,
H-2), 6.34 (1H, *s*, H-8), 7.35 (1H, *dd*, *J* = 8.6, 2.6 Hz, H-2'), 6.83 (1H, *dd*, *J* = 8.3
Hz, 2.6 Hz, H-3', H-5'), 7.37 (1H, *dd*, *J* = 8.3, 2.6 Hz, H-6'), 4.72, 4.89 (2H, *dd*, *J* =
= 3.5 Hz, 16.4 Hz, H-2''), 6.71 (1H, *m*, H-3''), 5.81 (1H, *d*, *J* = 3.0 Hz, H-4''). ^{13}C-
-NMR (CDCl$_3$, δ / ppm): 148.8 (C-2), 125.5 (C-3), 197.7 (C-4), 161.9 (C-5), 105.4
(C-6), 160.9 (C-7), 96.9 (C-8), 158.0 (C-9), 104.9 (C-10), 126.2 (C-1'), 132.3 (C-2'),
115.3 (C-3'), 146.2 (C-4'), 116.2 (C-5'), 132.2 (C-6'), 77.0.(C-2''), 132.6 (C-3''),
115.2 (C-4''). UV (MeOH) (λ_{max} / nm): 270, 256; (NaOAc) (λ_{max} / nm): 276.
EI–MS (*m/z*): 308 (M$^+$), 245, 184, 170, 153, 129, 109, 108, 107, 79, 55.

Compound **3**. Yellow brown crystalline, m.p. 145 °C. IR (KBr, cm^{-1}): 2914,
2724, 2357, 1697, 1610, 1454, 1376, 1202, 1030. ^{1}H-NMR (600 MHz, MeOH-
d_4, δ / ppm): 4.97 (1H, *d*, *J* =11.4 Hz, H-2), 4.45 (1H, *d*,
J =11.4 Hz, H-3), 6.25 (1H, *s*, H-8), 6.90 (1H, *d*, *J* = 1.82, H-2'), 6.77 (1H, *d*, *J* =
= 7.4 Hz, H-5'), 6.76 (1H, *dd*, *J* = 7.4, 1.82 Hz, H-6'), 3.55 (2H, *s*, H-1''), 6.62
(2H, *dd*, *J* = 8.4, 2.1 Hz, H-3'', H-7''), 6.61 (2H, *dd*, *J* = 8.4, 2.1 Hz, H-4'', H-6''),
6.52 (1H, *br s*, H-1'''), 4.80 (1H, *br s*, H-2'''), 4.62 (1H, *t*, *J* = 8.1 Hz, H-3'''), 4.31
(1H, *t*, *J* = 8.2 Hz, H-4'''), 4.73 (1H, *m*, H-5'''), 3.55 (1H, *m*, H-6'''α), 4.52 (1H, *m*,
H-6'''β). ^{13}C-NMR (MeOH-d_4, δ / ppm): 82.8 (C-2), 71.5 (C-3), 198.8 (C-4), 160.7
(C-5), 110.9 (C-6), 96.4 (C-8), 162.5 (C-7), 160.7 (C-9), 104.5 (C-10), 130.7 (C-1'),
115.4 (C-2'), 146.0 (C-3'), 146.4 (C-4'), 114.9 (C-5'), 114.7 (C-6'), 31.6 (C-1''),
136.1 (C-2''), 132.8 (C-3'') 115.8 (C-6'', C-4''), 160.7 (C-5''), 133.1 (C-7''), 102.8
(C-1'''), 73.6 (C-2'''), 76.4 (C-3'''), 69.7 (C-4'''), 77.6 (C-5'''), 62.6 (C-6'''). EI–MS
(*m/z*): 595 (M$^+$), 184, 170, 153, 134.9, 125, 109, 108, 107, 97, 79. UV (MeOH)
(λ_{max} / nm): 228, 287. [α]^{25} (589 nm) = –7.62° (*c* 0.5 g/100 ml, MeOH)

Compound **4**. Reddish pink powder; m.p. 210–214 °C. IR (KBr, cm^{-1}):
3332, 2950, 2922, 1652, 1600, 1300, 1210, 1147, 1050, 878. ^{1}H-NMR (600
MHz, MeOH-d_4, δ / ppm): 6.32 (1H, *d*, *J* = 2.1Hz, H-6), 6.51 (1H, *d*, *J* = 2.10
Hz, H-8), 6.78 (1H, *d*, *J* = 1.8 Hz, H-2'), 7.63 (1H, *d*, *J* = 10.0 Hz, H-5'), 7.62
(1H, *dd*, *J* = 10.0, 1.8 Hz, H-6'), 5.71 (1H, *d*, *J* = 7.6 Hz, H-1''), 4.83 (1H, *br s*,
H-2''), 4.65 (1H, *t*, *J* = 8.1 Hz, H-3''), 4.34 (1H, *t*, *J* = 8.2 Hz, H-4''), 4.77 (1H, *m*,
H-5''), 3.50 (1H, *m*, H-6''α), 4.46 (1H, *m*, H-6''β), 5.10 (1H, *d*, *J* = 7.8 Hz, H-1'''),
4.28 (1H, *d*, *J* = 8.2 Hz, H-2'''), 4.63 (1H, *br s*, H-3'''), 4.13 (1H, *t*, 8.2 Hz, H-4'''),
4.52 (1H, *m*, H-5'''), 4.36, 4.50 (2H, *m*, H-6'''α, H-6'''β). ^{13}C-NMR (MeOH-d_4,
δ / ppm): 160.0 (C-2), 133.3 (C-3), 198.9 (C-4), 162.1 (C-5), 100.4 (C-6), 162.8
(C-7), 96.4 (C-8), 161.1 (C-9), 104.6 (C-10), 132.9 (C-1'), 115.4 (C-2'), 146.4 (C-
3'), 146.2 (C-4'), 115.8 (C-5'), 123.9 (C-6'), 105.6 (C-1''), 101.5 (C-1'''), 72.6 (C-
4'', C-4'''), 62.5 (2C, C-6'', C-6''') 79.9 (C-5''), 78.1 (C-5'''), 77.7 (C-2''), 72.3 (C-
2'''), 77.7 (C-3''), 72.8 (C-3'''). EI–MS (*m/z*): 626 (M$^+$), 390, 354, 327, 302, 299,

192, 153, 12 5,121, 9 3. U V (λ_{max} / nm) (MeOH): 357,   30 7, 2 56, (λ_{max} / nm) (NaOAc): 372, 260.

Compound 5. Off-white powder, m.p. 241– 245 °C. IR (KBr, cm $^{-1}$): 333 1, 2923, 1 650, 1240, 1 070, 880. ^{1}H-NMR (600 MHz , MeOH-d_4, δ / ppm): 4. 87 (1H, *d*, *J* = 2.4 Hz, H-2), 3.98 (1H, *m*, H-3), 2.85 (1H, *dd*, *J* = 5.4, 16.2 Hz, H-4α), 2.51 (1H, *dd*, *J* = 4.2, 16.2 Hz, H-4β), 5.88 (1H, *d*, *J* = 2.1 Hz, H-8), 6.03 (1H, *d*, *J* = 2.1 Hz, H-6), 6.89 (1H, *d*, *J* = 1.7 Hz, H-2'), 6.77 (1H, *d*, *J* = 7.4 Hz, H-5'), 6.73 (1H, *dd*, *J* = 7.4, 1.7 Hz, H-6'). ^{13}C-NMR (MeOH-d_4, δ / ppm): 74.8 (C-2), 71.8 (C-3), 31.4 (C-4), 160 .1 (C-5), 96.8 (C-6), 156. 1 (C-7), 96.5 (C-8), 155.3 (C-9), 104.0 (C-10), 132.1 (C-1'), 110.1 (C-2'), 145.5 (C-3') 146.4 (C-4'), 116.0 (C-5'), 115.2 (C-6'). EI–MS (*m/z*): 2 90 (M $^+$), 24 5, 227, 1 70, 153, 12 6. UV (MeOH) (λ_{max} / nm): 280, 212. $[\alpha]^{25}$ (589 nm) = –14.90°.

Compound **1** was obtained as a greenish brown amorpho us pow der having m.p. 202–205 °C, positive to the butanol/HCl   and vanillin/HCl tests. It gave   a dark greenish black colour with FeCl $_3$. A positive   molecular i on peaks (M $^+$) appeared at *m/z* 452. The IR spectrum showed bonded OH at (343 1 cm^{-1}) and an aromatic group at   1600 a nd 1 650^{-1}. T he ^{1}H-NMR spectru m showed a pair of doublets at δ 2.7 and 2.8 ppm, assigned to the H-4 protons (coupled to each other with *J* = 16.7 Hz and to H-3 with *J* = 4.5 and 2.5 Hz), a doublet at 5.10 p pm (*J* = = 2.2 Hz, H-2), a *dtd* signal at 4.45 ppm (*J* = 2.2, 3.4 Hz, H-3) and a pair of meta coupled doublets (*J* = 2.2 Hz) at 6.0 ppm (H-6) and 5.89 ppm (H-8). The ^{1}H-NMR spectrum showed a resonance due to   an anom eric proton at 6. 54 ppm (*br, s*, H-1"), a broad signal at 4. 80 ppm (H-2") and four other peaks, indicating that the glucose moiety is a β-D-glucopyranosyl group. The glucosidation at position 3 was also concluded from   a ^{1}H-heteronuclear multiple band correlation (MBC) correlation between the anom eric proton of glucose at 6.54 ppm and the C-3   at 68.0 ppm. Also, the ^{13}C-NMR signals at C-2 and C-3 confirm that the compound suggested is (–)-epicatechin with a glucose moiety at C-3.[12]

Compound **2** was isolated as a brown s olid having a m .p. 220–221 °C. The molecular form ula C $_{18}$H$_{12}$O$_5$ was deduced from el emental analy sis and the EI– –MS mass spectrum, which exhibited a (M $^+$) at *m/z* 308. The co mpound gave a bluish black colour with F eCl$_3$. Bands at 3410 (OH), 167 0 (C=O) and 16 50 and 1600 cm^{-1} (phenyl group) were observed in the IR spectrum. The ^{1}H-NMR spec- trum exhibited a singlet at 7.83 ppm (H-2) and the ^{13}C-NMR spectrum, a signa l at 148.8 ppm (C-2), which are charact eristic for the isoflavone skeleton. ^{13} This was further supported b y the UV spectrum with λ_{max} at 270 nm. The ^{1}H-NMR data indicated a doublet of doublets (*J* = 8.6, 2.6 Hz) at 7.35 (H-2'), 6.83 (H-3',H-5') and 7.37 ppm (H-6'), showing the presence of a 4'-OH on ring B of isoflavonoid. The OH at   C-7 was not free as   NaOAc fail ed to produce any   bathochromi c shift.[14] The ^{1}H-NMR and ^{13}C-NMR spectra showed the presence of a pyran ring at 4.72 and 4.89 (2H, H-2"), 6.71 (H-3") and 5.81 ppm (H-4") and at 76.9 (H-2"),

Available online at www.shd.org.rs/JSCS/

132.6 (H-3") and 115 ppm (H-4"), respectively. These data suggested that compound **2** was 5-hydroxy-3-(4-hydroxylphenyl)pyrano[3,2-*g*]chromene-4(8*H*)-one. This compound was previously reported form *Erythrina lysistemon*.[15]

Compound **3** was isolated as a yellow powder, m.p. 145 °C. EI-MS gave the (M⁺) peak at *m/z* 595. Its UV and IR data were similar to that of the reported data.[16] The ^{1}H-NMR signals at 4.97 (1H, *d*, *J* = 11.4 Hz, H-2) and 4.45 ppm (1H, *d*, *J* = 11.4 Hz, H-3) are specific for trans stereochemistry of the dihydroflavonol skeleton. Two sets of doublets *(J* = 8.4, 2.1 Hz) at 6.62 (H-3", H-7") and 6.61 ppm (H-4", H-6") indicate the presence of a *p*-substituted phenyl group. The proton ^{1}H-NMR resonance of the anomeric carbon at 6.52 ppm (1H, *br s*, H-1''') suggest the glucose moiety has the *β*-configuration. The ^{13}C-NMR upfield signals of C-8 and C-6 and the downfield resonance of C-7 indicate that the glucose moiety was attached with that of (C-7). Regarding the data described, compound **3** is suggested to be 6-(*p*-hydroxybenzyl)taxifolin-7-*β*-D-glucoside. This compound was previously identified from *Cudrania tricuspidata*.[17]

Compound **4** was isolated as a reddish pink powder, m.p. 210–214 °C. The UV, IR and NMR data resembled those of a reported flavonol.[18] The IR spectrum showed bands at 3332 (OH) and 1652 cm⁻¹ (C=O). The UV spectrum showed a maximum absorbance with NaOAc at 260 and 372 nm, indicating the presence of free OH groups at position 5 and 7 of ring A.[19] In the ^{1}H-NMR spectrum, two anomeric protons appeared at 5.71 ppm (1H, *d*, *J* = 7.7, H-1'') and 5.10 (1H, *d*, *J* = 7.8, Hz H-1'''), indicating the presence of glucose moieties having a *β*-configuration. The ^{1}H-NMR and ^{13}C-NMR data of model sugars identified that the sugar moiety may be D-glucopyranoside. The ^{13}C-NMR upfield signal at 77.7 (C-2") and downfield signal at 105.6 ppm (C-1") confirmed the presence of a 1→2 interglucoside linkage.[20] This compound was previously isolated from *Cadaba glandulosa*.[21]

Compound **5** was isolated as an off-white amorphous powder, m.p. 241–245 °C. The compound was positive to butanol/HCl and vanillin/HCl reagents. The UV spectrum (MeOH) showed maximum absorbance at 280 and 212 nm. Its EI––MS *m/z* 313 (Na+M)⁺ indicates a monomeric unit of *m/z* 290. Bands at 3331, 2923 and 1650 cm⁻¹ were observed in the IR spectrum. The ^{1}H-NMR spectrum showed a pair of doublets at 2.51 and 2.85 ppm, assigned to H-4 proton (coupled to each other with *J* = 16.2 Hz and to H-3 with 5.4 and 4.2 Hz). A doublet at 4.87 ppm (*J* = 2.4 Hz, H-2), a signal at 3.98 ppm (1H, *m*, H-3) and a pair of meta coupled doublets (*J* = 2.1 Hz) at 6.03 (H-6) and 5.88 ppm (H-8) were observed. The ^{1}H-NMR data suggest that the compound was epicatechin, which was further supported by ^{13}C-NMR signals, especially at 74.8 (C-2) and 71.8 ppm (C-3).[12] This compound was previously isolated from *Adansonia digitata*.[22]

The structures of the five isolated compounds are given in Fig. 1.
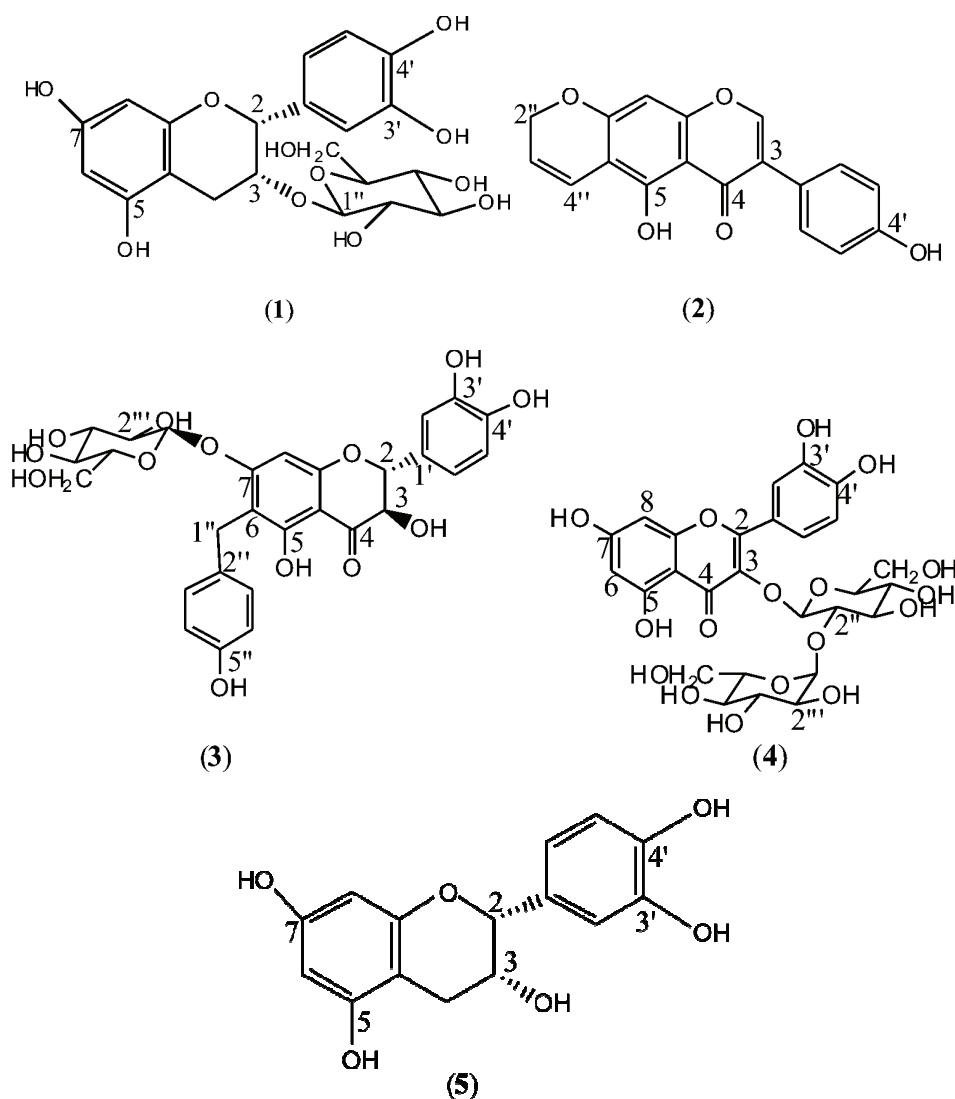
Fig. 1. Structures of flavonoids isolated from mango leaves.

Antibacterial activity

Analysis of v ariance showed that the effect of flavonoids, bacterial species, concentration and their interaction was highly significant ($p \leq 0.001$) for bacterial growth (Table I). The data presented in Fig. 2 indicates that all the concentrations of the five isolated flavonoids significantl y suppressed the growt h of all the f our tested bacterial species, however, variation in antibacterial activity of the isolated compounds was evident. Co mpound **1** exhibited the least antibacterial activit y. Various concentrations of co mpound **1** reduced the b acterial growth b y 7–75 %

(Fig. 2A). In contrast, co mpound **5** was found to b e the most effective in co n-trolling bacterial growth. This com pound was highl y toxic t o *A. lipoferum* and *Bacillus* sp. growth, resul ting in 94–99.9 % and 73 –99 % decreases in bacterial growth over corresponding control treatments, respectively. *Lactobacillus* sp. and *E. coli* were comparatively less suscep tible to com pound **5** where 59–9 6 % and 45–83 % suppression in bacterial growth, respectively, was recor ded over the corresponding control trea tments (Fig. 2E). Com pounds **2**–**4** exhi bited inter me-diate antibacterial activity between compound **1** and **5**. Different concentrations of compound **2**–**4** reduced the bacterial growth by 65–96 %, 52–80 % and 68–92 %, respectively (Figs. 2B–2D). Recently, similar antibacterial activities were also re-ported for o ther flavonoid s isolated from different plant species. [8,23,24] Various antibacterial mechanisms of action of different flavonoids have been propose d, including inhibition of nucleic a cid sy nthesis,[25] inhibition of c ytoplasmic mem-brane function[26] and inhibition of energy metabolism.[27] Earlier compound **2** was known for its antimicrobial and radical scavenging activities.[15] In conclusion, the results of the present study revealed that the flavonoids isolated from mango leaves possess antibacterial activity. Co mpound **5** is the most effective flavonoi d against *A. lipoferum* and *Bacillus* sp.

TABLE I. Analysis of variance for the effect o f different concentrations of th e five flavonoids isolated from mango leaves against four bacterial species

Sources of variation	df	SS	MS	F values[a]
Treatment 139		121	0.87	2285
Flavonoids (F)	4	26	6.54	17147
Bacterial species (B)	3	4.1	1.35	3554
Concentration (C)	6	77	12.91	33882
F×B 12		4.2	0.35	922
F×C 24		6.2	0.26	678
B×C 18		1.0	0.06	147
F×B×C 72		1.9	0.03	70
Error 280		0.1	0.0004	–
Total 420		335	–	–

[a]Significant at $p \leq 0.001$
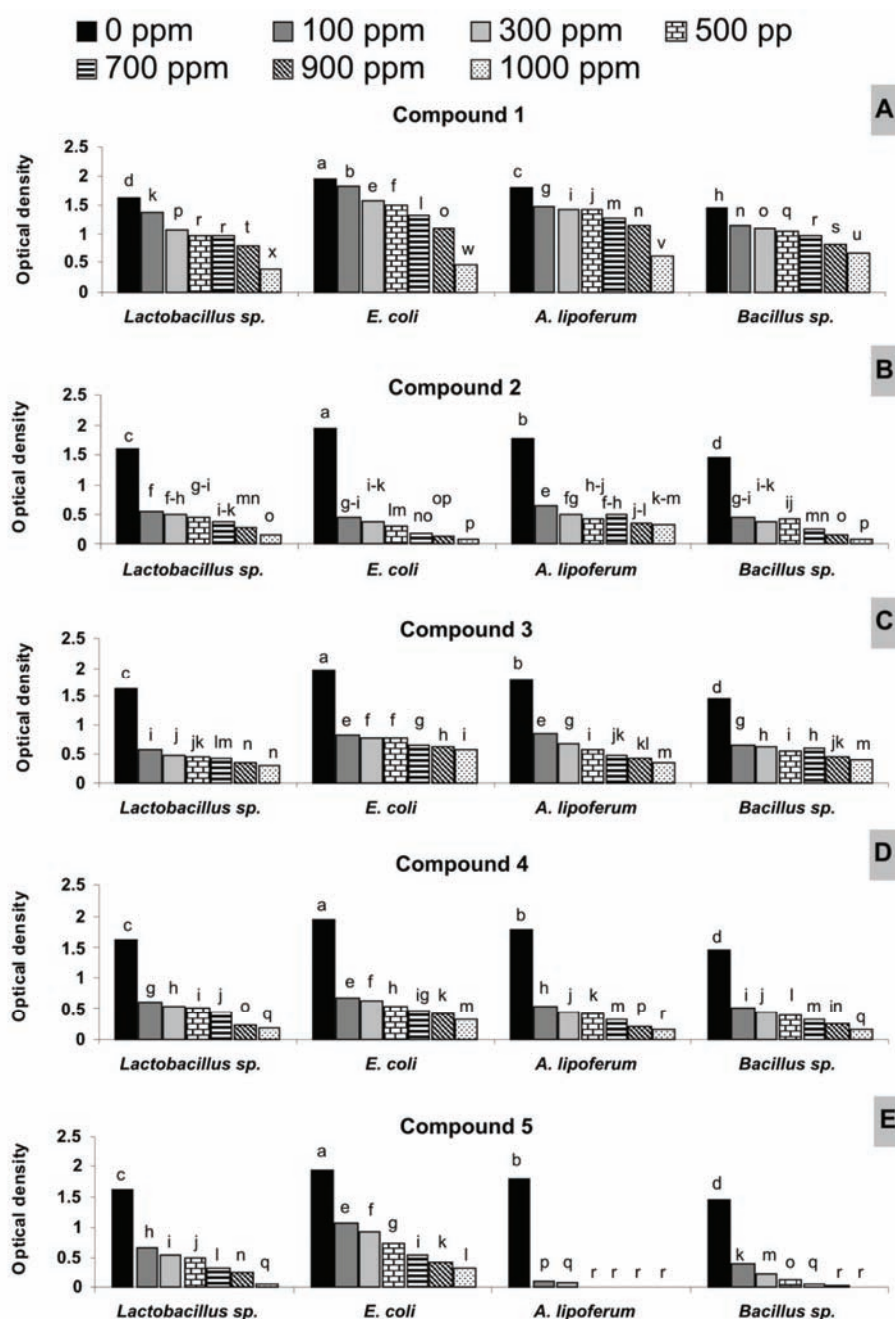
Fig. 2. Effect of different concentrations of five flavonoids on the growth of bacteria. In each graph, bars with different letters show significant difference ($p \leq 0.05$) as determined by the Student–Newman–Keuls test.

Available online at www.shd.org.rs/JSCS/

ИЗВОД

АНТИБАКТЕРИЈСКА АКТИВНОСТ ФЛАВОНОИДА ЛИСТА МАНГА

QUDSIA KANWAL[1], ISHTIAQ HUSSAIN[1], HAMID LATIF SIDDIQUI[1] и ARSHAD JAVAID[2]

[1]*Institute of Chemistry, University of the Punjab, Quaid-e-Azam Campus, Lahore u* [2]*Institute of Mycology and Plant Pathology, University of the Punjab, Quaid-e-Azam Campus, Lahore, Pakistan*

Из листа манга (*Mangifera indica* L.) изоловано је пет флавоноида: (–)-епикатехин-3-*O*- -*β*-глукопиранозид (**1**), 5- хидрокси-3-(4-хидроксифенил)пирано[3,2-*g*]хромен-4(8*H*)-он (**2**), 6-(*p*-хидроксибензил)таксифолин-7-*O*-*β*-D-глукозид (**3**), кверцетин-3-*O*-*α*-глукопиранозил- -(1→2)-*β*-глукопиранозид (**4**) и (–)- епикатехин (2-(3,4- дихидроксифенил)-3,4-дихидро-2*H*- -хромен-3,5,7-триол) (**5**). Антибактеријска активност различитих концентрација флавоноида (100, 300, 500, 700, 900 и 1000 ppm) је одређивана спрам четири бактеријске врсте: *Lactobacillus* sp., *Escherichia coli*, *Azospirillium lipoferum* и *Bacillus* sp. Сви флавоноиди су значајно смањивали раст тестираних бактерија, мада је постојала разлика у њиховој ефикасности. Једињење **1** је имало најмању антибактеријску активност (смањење раста различитих врста бактерија 7–75 %). Једињење **5** је имало највећу антибактеријску активност (редукција раста бактерија 45–99,9 %). Бактерије *A. lipoferum* и *Bacillus* sp. су биле најосетљивије на ово једињење. Једињења **2–4** су, такође, испољила изражену антибактеријску активност (редукција раста 52–96 %). На основу резултата ове студије може се закључити да је једињење **5** најефикасније од свих тестираних флавоноида и да је ефекат најизраженији спрам *A. lipoferum* и *Bacillus* sp.

(Примљено 18. априла, ревидирано 1. јуна 2009)

REFERENCES

1. B. A. Bohm, *Introduction to Flavonoids*, Gordon & Breach, Amsterdam, Netherlands, 1998
2. J. A. Joule G. F. Smith, *Heterocyclic Chemistry*, Van Nostrand Reinhold Company, London, 1972
3. J. B. Harborne, C. A. Williams, *Phytochemistry* **55** (2000) 481
4. D. Treutter, *Environ. Chem. Lett.* **4** (2006) 147
5. T. P. T. Cushnie, A. J. Lamb, *Int. J. Antimicrob. Agents* **26** (2005) 343
6. F. Galeotti, E. Barile, P. Curir, M. Dolci, V. Lanzotti, *Phytochem. Lett.* **1** (2008) 44
7. B. Sathiamoorthy, P. Gupta, M. Kumar, A. K. Chaturvedi, P. K. Shukla, R. Maurya, *Bioorg. Med. Chem. Lett.* **17** (2007) 239
8. R. Alarcón, R. C. Flores, S. Ocampos, A. Lucatti, L. F. Galleguillo, C. Tonn, V. Sosa, *Planta Med.* **74** (2008) 1463
9. B. H. Havsteen, *Pharmacol. Ther.* **96** (2002) 67
10. Y. Kim, A. J. Lounds-Singleton, S. T. Talcott, *Food Chem.* **115** (2009) 989
11. S. T. Talcott, J. P. Moore, A. J. Lounds-Singleton, S S. Percival, *J. Food Sci.* **70** (2005) 337
12. L. J. Porter, R. H. Newman, L. Y. Foo, H. Wong, *J. Chem. Soc. Perkin Trans. 1* (1982) 1217
13. J. Wijindi, Z. T. Fomum, F. Tillequin, E. Seguim, M. Kock, *Phytochemistry* **35** (1994) 245
14. S. EI-Masry, M. E. Amer, M. S. Abdel-Kader, H. H. Zaatout, *Phytochemistry* **60** (2002) 783
15. B. F. Juma, R. R. T. Majinda, 11th NAPRECA *Symposium Book of Proceedings*, 2005, Antananarivo, Madagascar, 2005, p. 97
16. I. K. Lee, C. J. Kim, K. S. Song, H. M. Kim, H. Koshino, M. Uramoto, I. D. Yoo, *Phytochemistry* **48** (1996) 213

17. Z. P. Zheng, J. Y. Liang, L. H. Hu, *J. Integrative Plant Biol.* **48** (2006) 97
18. A. Debella, O. Kunert, M. G. Sch mi, G. Mi chl, F. Bucar, D. Abebe, E. Hasling er, *Monatsh. Chem.* **131** (2000) 401
19. T. J. Mabr y, K. R. Mar kham, M. V. T homas, *Systematic Identification of flavonoids*, Springer Publ., New York, 1970
20. F. Imperato, R. Nazzarot, *Phytochemistry* **41** (1996) 337
21. A. A. Gohar, *Z. Naturforsch.* **57c** (2002) 216
22. A. A. Shahat, *Pharm. Biol.* **44** (2006) 445
23. Y. C. Wang, H. W. Hsu, W. L. Liao, *LWT – Food Sci. Technol.* **41** (2008) 1793
24. L. Zhou, D. Li, J. Wang, Y. Liu, J. Wu, *Nat. Prod. Res.* **21** (2007) 283
25. A. Mori, C. Nishino, N. Enoki, S. Tawata, *Phytochemistry* **26** (1987) 2231
26. H. Tsuchiya, M. Iinuma, *Phytomedicine* **7** (2000) 161
27. H. Haraguchi, K. Tani moto, Y. Ta mura, K. Mizuta ni, T. Kinoshita, *Phytochemistry* **48** (1998) 125.

Available online at www.shd.org.rs/JSCS/

Mechanochemical synthesis and electrical conductivity of nanocrystalline δ-Bi$_2$O$_3$ stabilized by HfO$_2$ and ZrO$_2$

MIODRAG ZDUJIĆ[1*#], DEJAN POLETI[2#], ČEDOMIR JOVALEKIĆ[3]
and LJILJANA KARANOVIĆ[4]

[1]*Institute of Technical Sciences of the Serbian Academy of Science and Arts, Knez Mihailova 35, 11000 Belgrade,* [2]*Department of General and Inorganic Chemistry, Faculty of Technology and Metallurgy, University of Belgrade, Karnegijeva 4, 11000 Belgrade,* [3]*Institute for Multidisciplinary Research, Kneza Višeslava 1a, 11000 Belgrade and* [4]*Laboratory of Crystallography, Faculty of Mining and Geology, University of Belgrade, Đušina 7, 11000 Belgrade, Serbia*

Abstract: A powder mixture of α-Bi$_2$O$_3$ and HfO$_2$, in the molar ratio 2:3, was mechanochemically treated in a planetary ball mill under air, using zirconium oxide vials and balls as the milling medium. After 50 h of milling, the mechanochemical reaction led to the formation of a nanocrystalline δ-Bi$_2$O$_3$ phase (fluorite-type solid solution Bi$_{0.78}$Hf$_{0.59}$Zr$_{0.63}$O$_{3.61}$), with a crystallite size of 20 nm. The mechanochemical reaction started at a very beginning of milling accompanied by an accumulation of ZrO$_2$ arising from the milling tools. The samples prepared after various milling times were characterized by X-ray powder diffraction and DSC analysis. The electrical properties of the as-milled and pressed Bi$_{0.78}$Hf$_{0.59}$Zr$_{0.63}$O$_{3.61}$ powder were studied using impedance spectroscopy in the temperature range from 100 to 700 °C under air. The electrical conductivity was determined to be 9.43×10^{-6} and 0.080 S cm^{-1} for the temperatures of 300 and 700 °C, respectively.

Keywords: bismuth(III) oxide; milling; X-ray diffraction; electrical conductivity; fuel cells.

INTRODUCTION

In recent years, there has been considerable interest in the study of materials based on Bi$_2$O$_3$ owing to their physical properties, such are ionic conductivity, ferroelectricity, photoconductivity and photoluminescence. The ferroelectric nature of some bismuth-rich compounds, *e.g.*, Bi$_4$Ti$_3$O$_{12}$, CaBi$_3$Ti$_3$O$_{12-x}$ and

---

$SrBi_2(Ta,Nb)_2O_9$, make them important materials for the manufacture of ferro-electric random access memories,[1] while the δ-Bi_2O_3 polymorph, with a fluorite--type structure, has the highest oxide–ion conductivity of all known compounds,[2] providing useful properties for its application in solid oxide fuel cells and gas sensors.[3,4]

Bismuth(III) oxide, Bi_2O_3, is known to appear in five polymorphs, as the α-, β-, γ-, δ- and ε-phase.[5–7] The room-temperature monoclinic α-Bi_2O_3 transforms upon heating at 729 °C to the high-temperature cubic δ-Bi_2O_3, which is stable up to the melting point at 825 °C.[8] Upon cooling, two metastable phases may occur depending on the applied thermal treatment, *i.e.*, the tetragonal β-phase near 650 °C and the body-centered cubic γ-phase near 640 °C. Usually these phases transform into the α-phase on further cooling.[5]

The structure of the δ-phase is based on a face-centered cubic cation sublattice and can be described as a defective fluorite structure where one quarter of the available anion sites are vacant.[6,9] The disorder of the oxide ions in the structure has been investigated in detail,[10–12] and it was found that a high concentration of oxygen vacancies, combined with the high polarizability of the Bi^{3+} $6s^2$ lone electron pairs, increases the oxide ion mobility in this compound.[13]

Pure δ-Bi_2O_3 cannot be quenched to room temperature.[14] Nevertheless, the stability of the δ-Bi_2O_3 phase at low temperatures can be achieved by substituting Bi^{3+} with different mono to pentavalent cations.[15–17] However, the stability improvement is usually accompanied by a decrease in the ionic conductivity. Thus, the substitution of Bi^{3+} by higher-valent cations, such as Ti^{4+}, Zr^{4+} and Hf^{4+} should result in a reduction of the vacancy concentration.[13]

Knowing that mechanochemical treatment is a process producing metastable (amorphous, nanocrystalline, supersaturated solid solutions) materials, this technique has already been employed for the study of various Bi_2O_3-containing systems.[18,19] One of the recent studies showed that mechanochemical treatment applied to the $2Bi_2O_3·3ZrO_2$ system led to the gradual formation of a nanocrystalline phase which resembles δ-Bi_2O_3.[20] Following this line, it seemed quite reasonable to undertake an examination of the analogous $2Bi_2O_3·3HfO_2$ system. However, after prolonged milling for 50 h, a significant amount of ZrO_2, originating from the milling medium, accumulated in the system yielding a final sample with the formula $Bi_{0.78}Hf_{0.59}Zr_{0.63}O_{3.61}$. Herein, structural, thermal and electrical investigations of a hafnium/zirconium-substituted bismuth oxide that adopts a fluorite-type δ-Bi_2O_3 structure, a material with very promising electrical properties, are presented.

EXPERIMENTAL

A mixture of commercial Bi_2O_3 (> 99 % purity) and HfO_2 (> 98.5 % purity) powders in a 2:3 molar ratio was used as the starting material. By the X-ray powder diffraction (XRPD) technique, the Bi_2O_3 was identified as being in the stable α-Bi_2O_3, bismite form (JCPDS card

Available online at www.shd.org.rs/JSCS/

41-1449), whereas the HfO_2 was in the monoclinic modification (JCPDS card 34-0104), but contained about 1.5 wt. % of ZrO_2. Mechanochemical treatment was performed in a Fritsch Pulverisette 5 planetary ball mill. Zirconia vials of 500 c m^3 volume charged with 93 zirconia balls of a nominal diameter of 10 mm were used as the milling medium. The mass of the powder mixtures was 15 g, giving a ball-to-powder mass ratio of 20:1. The angular velocities of the supporting disc and vials was 33.2 (317) and 41.5 rad s $^{-1}$ (396 rpm), respectively. The mixtures were milled for 10 and 30 min, as well as for 1, 10, 20 and 50 h in an air atmosphere with no addition of lubricant (dry milling). Each milling run was realized with a fresh powder mixture and without opening the vials for the specified milling period.

The X-ray powder diffraction data were collected on a Rigaku PH 1050 diffractometer with Cu-Kα graphite-monochromatized radiation ($\lambda = 1.5418$ Å) in the 2θ range 10–80° (step-length: 0.02° 2θ, scan time: 5 s). The program PowderCell,[21] was used for an approximate phase analysis in a Rietveld-like refinement. Unit cell parameters were obtained by the least-squares method using the program LSUCRIPC.[22] The mean crystallite size, $<D>$, of the sample milled for 50 h was calculated by the Scherrer formula.[23] The sample milled for 50 h was tested using the EDXR fluorescence technique, which confirmed the presence of Bi, Hf and Zr only. The composition of the sample was determined by EDAX and re-checked by ICP analysis. The mean Zr content was 15.2 wt. %, yielding the formula $Bi_{0.78}Hf_{0.59}Zr_{0.63}O_{3.61}$. The particle morphology of the prepared material can be seen in Fig. 1.
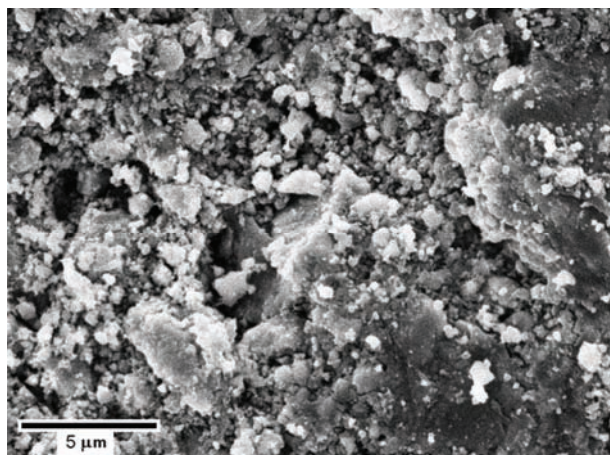
Fig. 1. SEM of the $Bi_{0.78}Hf_{0.59}Zr_{0.63}O_{3.61}$ solid solution (δ-Bi₂O₃ phase) after 50 h of milling.

The thermal behavior of the initial mixture and powders milled for 1, 20 and 50 h was investigated from room temperature to 900 °C using an SDT Q600 simultaneous DSC–TGA instrument (TA Instruments) with a heating and cooling rate of 20 °C min^{-1} under a dynamic (100 cm^3 min^{-1}) N₂ atmosphere.

The electrodes for the electrical measurements were applied to polished disc surfaces (diameter 8 mm, thickness 1 mm) pressed under 1 MPa, by the screen printing method. The silver paste was polymerized at 200 °C for 30 min. AC impedance measurements were performed over the frequency range from 10^{-2} to 3×10^5 Hz using a Gamry Potentiostat EIS 300. The amplitude of the input sine-wave signal was 10 mV. The ionic conductivity was measured up to 700 °C under an air atmosphere. The values of grain and grain boundary resistivity were

determined from the intersection of the semicircles with the Z' axis, while grain capacitance was calculated from the condition $\omega RC = 1$.

<div align="center">RESULTS AND DISCUSSION</div>

Structural changes

As can be seen from Fig. 2, significant structural changes had already occurred after 10 min of milling. The XRPD pattern exhibits broad low intensity peaks, implying a very deformed and disordered structure. Both constituents mainly preserve their original monoclinic structure. In addition, some peaks may be assigned to β-Bi$_2$O$_3$ in an amount of about 15 wt. %, indicating that the mechanochemical reaction starts at the very beginning of milling. Such an early appearance of β-Bi$_2$O$_3$ is in accordance with the observed tendency for ZrO$_2$ and HfO$_2$ to stabilize this phase.[24–26]
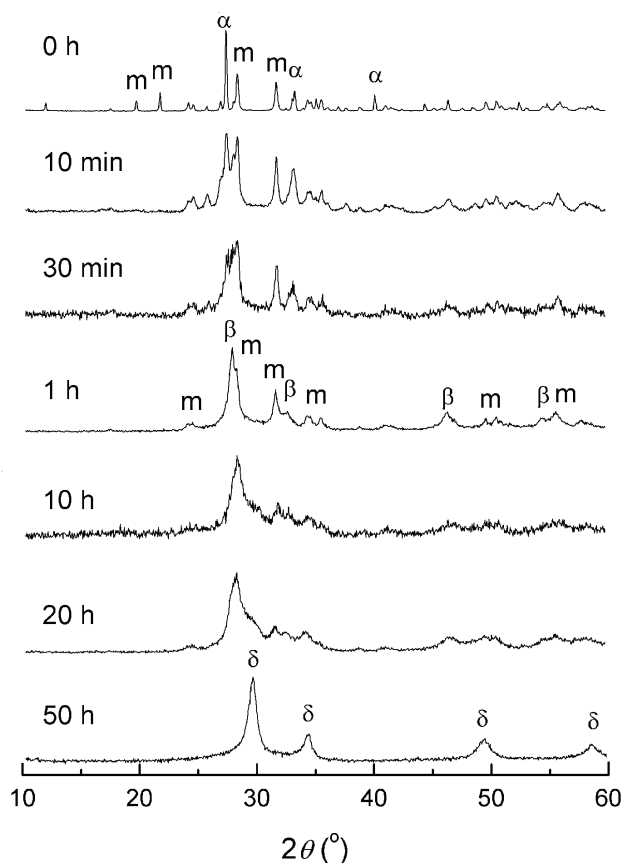
Fig. 2. XRPD Patterns of the powder mixtures after various milling times. Main maxima of the phases present are denoted as: m – monoclinic HfO$_2$, α, β and δ – α-Bi$_2$O$_3$, β-Bi$_2$O$_3$ and δ-Bi$_2$O$_3$, respectively.

As milling continued, the formation of the β-Bi$_2$O$_3$ phase progressed. Thus, the XRPD pattern of the sample milled for 30 min revealed that the strongest maxima of α-Bi$_2$O$_3$ (120 at 27.37° 2θ) and HfO$_2$ ($\bar{1}$11 at 28.34° 2θ) merge into one broad peak at around 28° 2θ. This peak is the most pronounced in the pattern of the sample milled for 1 h, and represents the main, (201) peak of the β-Bi$_2$O$_3$ phase. After 1 h of milling, the approximate β-Bi$_2$O$_3$ content was 50 wt. %.

Such a situation was maintained over a broad interval of mechanochemical treatment, so that differences in the patterns of samples milled for 10 and 20 h were hardly visible. Finally, in the XRPD pattern of the sample milled for 50 h, all peaks may be assigned to the δ-Bi$_2$O$_3$ phase. Therefore, mechanochemical treatment produced and stabilized the δ-Bi$_2$O$_3$ structure through the formation of a solid solution with HfO$_2$, as well as with ZrO$_2$ introduced into the system as a consequence of vial and ball debris during prolonged milling. The obtained composition, *i.e.*, a solid solution of the formula Bi$_{0.78}$Hf$_{0.59}$Zr$_{0.63}$O$_{3.61}$, is in a nanocrystalline form with a crystallite size of about 20 nm. The microstructure of this sample (Fig. 1) is typical for milled ceramic materials showing small primary particles of about 0.1 μm, as well as much larger aggregates of up to 10 μm.

The high solubility of HfO$_2$ and ZrO$_2$ in Bi$_2$O$_3$ can be explained by structural similarity of the high-temperature, cubic HfO$_2$/ZrO$_2$ and δ-Bi$_2$O$_3$. Cubic HfO$_2$ and ZrO$_2$ both have the fluorite structure (space group $Fm\bar{3}m$) with a = 5.115(10) and 5.065(10) Å, respectively. [27] In these phases, each cation is surrounded by eight equidistant oxygens. As already described in the Introduction, δ-Bi$_2$O$_3$ also has a fluorite-type structure, but with partially vacant oxide positions making space for the lone electron pair on Bi^{3+}. High-temperature Hf$_{1-x}$Bi$_x$O$_{2-x/2}$ (x = 0.4–0.75) and Zr$_{1-x}$Bi$_x$O$_{2-x/2}$ (x = 0.50–0.75) phases with a defect fluorite structure have already been observed. At temperatures above 750 °C, both phases decompose giving different products.[25] The unit cell parameter of the present Bi$_{0.78}$Hf$_{0.59}$Zr$_{0.63}$O$_{3.61}$ sample was a = 5.221(4) Å. This is between the values for HfO$_2$ and ZrO$_2$ unit cell parameters (see above) and the unit cell parameter of undoped δ-Bi$_2$O$_3$ (5.6549(9)−5.665(8) Å).[6,10]

Thermal behavior

The DSC examination of the powders milled for various milling times gave further understanding of the structures achieved with the progress of mechanochemical treatment. On heating, the starting powder mixture (before milling) exhibits two endothermic heat effects (Fig. 3a): the first is at about 740 °C (with an enthalpy change, ΔH, of 30.5 J per gram of the powder mixture), which arises from the α-Bi$_2$O$_3$ → δ-Bi$_2$O$_3$ phase transition and the second at about 860 °C (ΔH = 11.6 J g^{-1}) is assigned to the melting of δ-Bi$_2$O$_3$.[20] Mechanochemical treatment for 1 h induced significant structural changes (Fig. 2), hence during heating, the temperature of the first heat effect was shifted to a lower temperature

of about 713 °C ($\Delta H = 2\ 2.5$ J g^{-1}), while during cooling, the δ-Bi$_2$O$_3$ transformed to the β-phase at about 576 °C ($\Delta H = 20.7$ J g^{-1}) (Fig. 3b). The fact that the sample milled for 1 h consisted of β-Bi$_2$O$_3$ and HfO$_2$, as revealed by XRPD analysis, implies that first heat effect should be attributed to the $\beta \rightarrow \delta$ phase transition.
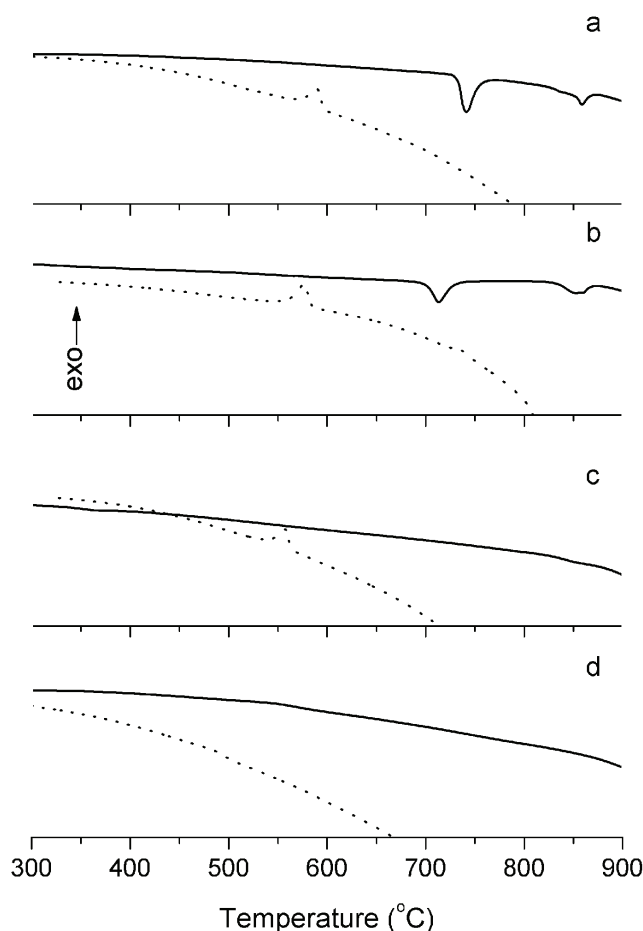
Fig. 3. DSC Curves (full line – heating, dotted line – cooling) of the powder mixtures: before (a) and after mechanochemical treatment for 1 (b), 20 (c), and 50 h (d).

Milling up to 20 h gradually deformed and mixed the constituents on the atomic level, and the powder milled for 20 h was stable during heating up to 900 °C, *i.e.*, no significant heat effect could be resolved on the DSC curve (Fig. 3c). However, on cooling, the $\delta \rightarrow \beta$ phase transition occurred at about 556 °C ($\Delta H = 16.7$ J g^{-1}). Prolonged milling for 50 h, further refined and stabilized the structure, hence no recognizable heat effects may be detected during either heating or

cooling. This finding confirms that a single δ-Bi$_2$O$_3$ phase had been obtained, i n agreement with the XRPD analy sis. A similar thermal behavior was observed fo r the Bi$_{0.85}$Eu$_{0.1}$V$_{0.05}$O$_{1.55}$ compound with a fluorite-type δ-Bi$_2$O$_3$ structure.[15]

Electrical measurements

Impedance spectroscopy was us ed to deter mine th e electri cal p roperties of the material mechanochemically synthesized for 50 h of milling. For such measu-rements, co mpacts wer e prepared by pressing only . No heat treat ment was ap -plied in order to preserve the structure attained after 50 h of milling, *i.e.*, to avoid possible phase transitions of δ-Bi$_2$O$_3$, which could occur at high er temperatures. The density of the pressed samples was about 65 % of the theoretical density ($\rho_x =$ = 8.94 g cm^{-3}). Therefore, a high porosity plausibly implies considerably higher impedance values than if fully dense sa mples were used for the measurements. Moreover, the mechanochemical treat ment cr eated highly activated powders , which during pressing may form specific in tergranular lay ers influencing, espe-cially at low temperatures, the electrical characteristics.

Selected impedance spectra recorded in the temperature interval from 100 to 700 °C and in the frequency range from 300 kHz to 0.01 Hz are shown in Fig. 4. As can be seen, the curves are somewhat flattened, which may indicate deviation
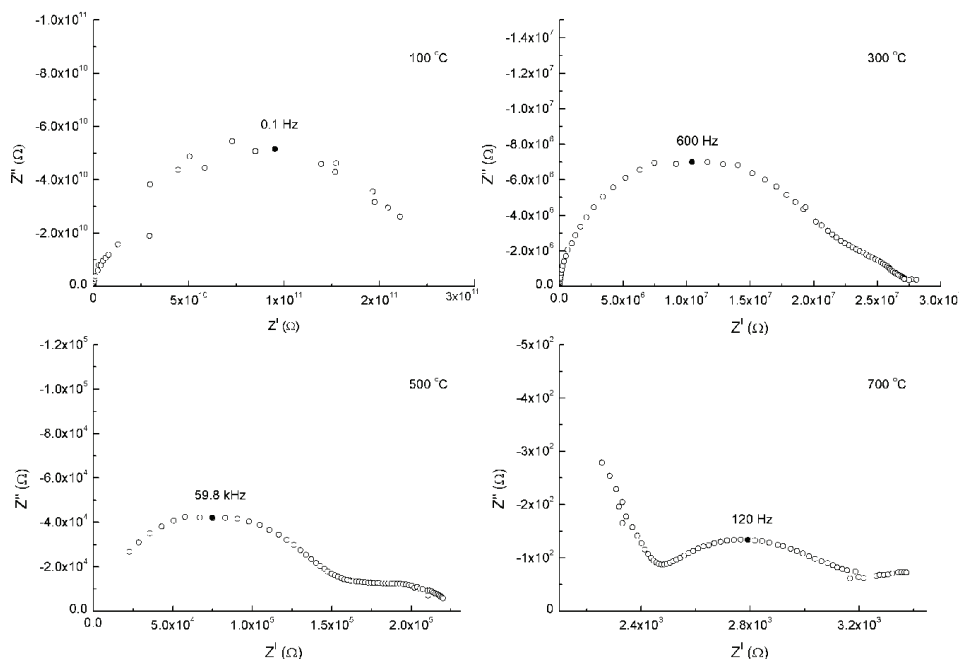
Fig. 4. Selected complex impedance plots measured at different temperatures of the Bi$_{0.78}$Hf$_{0.59}$Zr$_{0.63}$O$_{3.61}$ solid solution (δ-Bi$_2$O$_3$ phase) powder prepared by mechanochemical treatment for 50 h, and compacted by pressing.

from Debye character of the samples.[28] With increasing temperature from 400 to 700 °C, the resistivity of the sample-to-electrode contact had a greater influence on the overall sample resistivity. This was most obvious at 700 °C, where the semicircle arising from the resistivity of the bulk sample material at higher frequency significantly declines.

It should be emphasized that no detectable structural changes were observed by XRPD analysis of the samples after the impedance–temperature measurements. This observation showed that prolonged heating does not cause any phase transition up to at least 700 °C, *i.e.*, the prepared δ-Bi$_2$O$_3$ samples were stable under these conditions. On the other hand, after a heat treatment (attempting to increase the density of the samples) at 820 °C for 24 h followed by slow (furnace) cooling or quenching, such metastable solid solutions transform into complex mixtures of either δ-Bi$_2$O$_3$, γ-Bi$_2$O$_3$ and monoclinic HfO$_2$/ZrO$_2$ or δ-Bi$_2$O$_3$, β-Bi$_2$O$_3$ and monoclinic HfO$_2$/ZrO$_2$, respectively. (Monoclinic HfO$_2$ and ZrO$_2$ are indistinguishable by XRPD analysis because of their very similar unit cell parameters.)

The bulk resistivity is equal to the sum of the grain, R_g, and grain boundary, R_{gb}, resistivities. The specific resistivity, ρ, for various temperatures was calculated from the total resistivity, and the specific conductivity, $\sigma = 1/\rho$, as a function
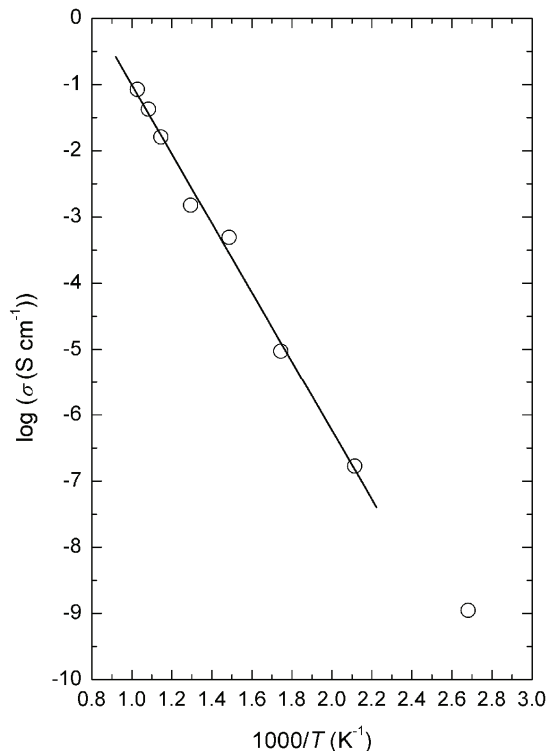
Fig. 5. Arrhenius plot of the δ-Bi$_2$O$_3$ (Bi$_{0.78}$Hf$_{0.59}$Zr$_{0.63}$O$_{3.61}$) powder prepared by mechanochemical treatment for 50 h, and compacted by pressing.

Available online at www.shd.org.rs/JSCS/

of 100 0/T is presented in Fig. 5. T he obtained values of the electrical conductivity are σ_{300} = 9.43×10^{-6} and σ_{700} = 0.08 0 S cm^{-1} for the tem peratures 300 and 700 °C, r espectively (Table I). In c omparison with som e Bi-containing phases, the conductivity of Bi$_{0.78}$Hf$_{0.59}$Zr$_{0.63}$O$_{3.61}$ was lower than the electrical conductivity of pure δ-Bi$_2$O$_3$ (σ_{bulk} = 1 S cm^{-1} at 730 °C),[4] and those of som e Bi$_3$Nb$_{1-x}$Zr$_x$O$_{7-x/2}$ compounds (σ_{600} = 0.11 4 and 0.123 S cm^{-1} for x = 0.80 and 0.90, respectively),[16] as well as of some compositions in the of Bi $_2$O$_3$–Er$_2$O$_3$––PbO system (σ_{750} = 0.49 and 0.72 S cm^{-1} for (BiO$_{1.5}$)$_{0.80}$(ErO$_{1.5}$)$_{0.11}$(PbO)$_{0.09}$ and (BiO$_{1.5}$)$_{0.85}$(ErO$_{1.5}$)$_{0.12}$(PbO)$_{0.03}$, respect ively).[29] Moreover, it is comparable with that for the Bi $_{23}$V$_4$O$_{44.5}$ compound (σ_{600} = 10^{-2} S cm^{-1}),[30] or even higher in comparison to som e other sy stems. For exam ple, the electrical conductivities at 800 °C of the isostructural SrBi $_6$V$_2$O$_{15}$ and PbBi $_6$V$_2$O$_{15}$ are 1.96×10^{-3} and 1.72×10^{-3} S cm^{-1}, respectively,[31] while for the Bi $_9$SO$_{16.5}$ compound, conductivities from ≈10^{-3} to ≈10^{-2} S cm^{-1} were found at 600 and 700 °C.[32] In addition, σ_{690} = 3.41×10^{-2} S cm^{-1} was obtained for the Pb$_2$BiVO$_6$ compound.[33]

For the temperature range 200−700 °C, the calculated value of the activation energy, E_a = 1.03 eV, was higher than t he values for som e other bismuth oxide compounds with sim ilar grain sizes, for exam ple, E_a = 0.7 eV, for Bi$_4$Ti$_3$O$_{12}$,[34] and E_a ≈ 0.78 eV for Bi$_{23}$V$_4$O$_{44.5}$.[30]

As can be seen from Table I, the grain re sistivity change with te mperature is not so pronounced as it for the grain bou ndary resistivity. The drastic decrease of the grain boundary resistivity from 0.19 GΩ to ≈ 6.5 kΩ between 373 and 973 K is a consequence of an activation of defects, in first place oxygen vacancies located in the grain bounda ries and gene rated during the mechanochemical treatment. A high am ount of oxy gen vacancies arises fr om the large density of the grain boundaries of nanocrystalline structures. It is a well known that the inherent feature of nanostructured m aterials is a significant fraction of atom s residing in the grain boundaries.[35] T herefore, it may be conc luded t hat m echanochemical treatment, thr ough the for mation of sig nificant defect structure(s), has an effect on the ionic conductivity.

TABLE I. Grain, R_g, and grain boundary , R_{gb}, resistivities, grain boundary capacita nce, C_{gb}, specific r esistivity, ρ, and spe cific condu ctivity, σ, at various te mperatures of th e pre ssed Bi$_{0.78}$Hf$_{0.59}$Zr$_{0.63}$O$_{3.61}$ sample mechanochemically synthesized by 50 h of milling

Parameter	t / °C						
	100	200	300 400	500		600	700
R_g / kΩ	25	24.5	23	22.5 ≈5		≈4	≈2
R_{gb} / kΩ	0.19×10^9	1.2×10^6	21.1×10^3 4.1 ×10^2	≈1.4×10^2		≈16	≈6.5
C_{gb} / pF	13	25	25.5	31.8 ≈35		≈48	–
ρ / Ω cm	9.01×10^8	5.99 ×10^6	1.06×10^5 2.02 ×10^3	6.6×10^2	62		12.5
σ/ S cm^{-1}	1.11×10^{-9}	1.67 ×10^{-7}	9.43×10^{-6} 4.94×10^{-4}	1.52×10^{-3}	1.62×10^{-2}		8.00 ×10^{-2}

CONCLUSIONS

A nanocrystalline $Bi_{0.78}Hf_{0.59}Zr_{0.63}O_{3.61}$ solid solution with a fluorite-type δ-Bi_2O_3 structure was synthesized by prolonged mechanochemical treatment of a $2Bi_2O_3·3HfO_2$ powder mixture in a zirconia medium.

The reaction commenced at the very beginning of milling through the formation of a β-Bi_2O_3 phase, which grew with the advancement of milling and was finely transformed to a single δ-Bi_2O_3 phase. The final phase transition was very likely assisted by the accumulation of ZrO_2 arising from the milling tools. Thus, contamination of the milled materials, which in many situations must be judged as undesirable, presents here a favorable process.

According to DSC results, the $Bi_{0.78}Hf_{0.59}Zr_{0.63}O_{3.61}$ solid solution was stable on heating and cooling between room temperature and 900 °C. This fact and the relatively high value of the electrical conductivity, close to 0.1 S cm^{-1} for a temperature of 700 °C, make the mechanochemically synthesized $Bi_{0.78}Hf_{0.59}Zr_{0.63}O_{3.61}$ solid solution a promising high oxide ion conductivity material.

ИЗВОД

МЕХАНОХЕМИЈСКА СИНТЕЗА И ЕЛЕКТРИЧНА ПРОВОДНОСТ НАНОКРИСТАЛНОГ δ-Bi_2O_3 СТАБИЛИСАНОГ СА HfO_2 И ZrO_2

МИОДРАГ ЗДУЈИЋ[1], ДЕЈАН ПОЛЕТИ[2], ЧЕДОМИР ЈОВАЛЕКИЋ[3] и ЉИЉАНА КАРАНОВИЋ[4]

[1]Институт техничких наука САНУ, Кнез Михаилова 35, Београд, [2]Катедра за општу и неорганску хемију, Технолошко–металуршки факултет, Универзитет у Београду, Карнегијева 4, Београд, [3]Институт за мултидисциплинарна истраживања, Кнеза Вишеслава 1а, Београд и [4]Лабораторија за кристалографију, Рударско–геолошки факултет, Универзитет у Београду, Београд

Смеша прахова α-Bi_2O_3 и HfO_2 у моларном односу 2:3 механохемијски је третирана у планетарном млину у атмосфери ваздуха, користећи цирконијумске посуде и куглице као медијум за млевење. После 50 h млевења, механохемијска реакција доводи до стварања нанокристалне δ-Bi_2O_3 фазе (чврсти раствор флуоритске структуре $Bi_{0.78}Hf_{0.59}Zr_{0.63}O_{3.61}$), величине кристалита 20 nm. Механохемијска реакција отпочиње у самом почетку млевења и праћена је акумулацијум ZrO_2 који потиче од медијума за млевење. Узорци добијени после различитих времена млевења карактерисани су рендгенском структурном и термијском анализом. Електрична својства млевених и пресованих $Bi_{0.78}Hf_{0.59}Zr_{0.63}O_{3.61}$ прахова испитивана су импедансном спектроскопијом у температурном опсегу од 100 до 700 °C. Добијена електрична проводност је 9,43·10^{-6} и 0,080 S cm^{-1} за температуру 300 и 700 °C, редом.

REFERENCES

1. H. Ishiwara, M. Okuyama, Y. Arimoto, Eds., *Ferroelectric Random Access Memories – Fundamentals and Applications* (Topics in Applied Physics, Vol. 93), Springer-Verlag, Berlin, 2004

Available online at www.shd.org.rs/JSCS/

2. A. R. West, *Basic Solid State Chemistry*, 2nd ed., Wiley, Chichester, 2004, p. 345
3. P. Shuk, H. -D . Wiemhofer, U. Guth, W . Gopel, M . Greenblatt, *Solid State Ionics* **89** (1996) 179
4. J. C. Boivin, G. Mairesse, *Chem. Mater.* **10** (1998) 2870
5. E. M. Levin, R. S. Roth, *J. Res. Natl. Bur. Stand.* **68A** (1964) 189
6. H. A. Harwig, Z. *Anorg. Allg. Chem.* **444** (1978) 151
7. N. Cornei, N. Tancret, F. Abraham, O. Mentré, *Inorg. Chem.* **45** (2006) 4886
8. A. Helfen, S. Merkourakis, G. W ang, M. G. Walls, E. Roy , K. Yu-Zhang, Y. Leprince- -Wang, *Solid State Ionics* **176** (2005) 629
9. G. Gattow, H. Schröder, Z. *Anorg. Allg. Chem.* **318** (1962) 176
10. S. Kashida, K. Nakamura, *Philos. Mag. Lett.* **73** (1996) 279
11. U. Pirnat, M. Valant, B. Jančar, D. Suvorov, *Chem. Mater.* **17** (2005) 5155
12. M. Valant, B. Jančar, U. Pirnat, D. Suvorov, *J. Eur. Ceram. Soc.* **25** (2005) 2829
13. M. Yashima, D. Ishimura, *Chem. Phys. Lett.* **378** (2003) 395
14. C. D. Ling, M. Johnson, *J. Solid State Chem.* **177** (2004) 1838
15. N. Portefaix, P. Conflant, J. C. Boivin, J. P. Wignacourt, M. Drache, *J. Solid State Chem.* **134** (1997) 219
16. F. Krok, I. Abraha ms, W . Wrobel, S. C. M . Chan, A. K ozanecka, T. O ssowski, J. R. Dygas, *Solid State Ionics* **175** (2004) 335
17. O. Labidi, M. Drache, P. Roussel, J. P. Wignacourt, *Solid State Sci.* **10** (2008) 1074
18. D. Poleti, Lj. Karanović, M. Zdujić, Č. Jovalekić, Z. Branković, *Solid State Sci.* **6** (2004) 239
19. M. Zdujić, D. Poleti, Č. Jovalekić, Lj. Karanović, *J. Non-Cryst. Solids* **352** (2006) 3058
20. Č. J ovalekić, M. Zdujić, D. Poleti, Lj . Karanovi ć, M. Mitrić, *J. Solid State Chem.* **181** (2008) 1321
21. W. Kraus, G. Nolze, *PowderCell for Windows*, V.2.4, Federal Ins titute for M aterials Research and Testing, Berlin, Germany, 2000.
22. R. G. Garwey, *Powder Diff.* **1** (1986) 114
23. H. P. Klug, L. E. Alexander, *X-Ray Diffraction Procedures*, 2nd ed., Wiley, New York, 1974, p. 687
24. I. Abrahams, A. J. Bush, S. C. M. Chan, F. Krok, W. Wrobel, *J. Mater. Chem.* **11** (2001) 1715
25. S. L. Sorokina, A. W. Sleight, *Mater. Res. Bull.* **33** (1998) 1077
26. A. Ayala, A. López-Garcia, A. G. Leyva, M. A. R. De Benyacar, *Solid State Commun.* **99** (1996) 451
27. L. Passerini, *Gazz. Chim. Ital.* **60** (1930) 762
28. *Impedance Spectroscopy: Emphasizing Solid Materials and Systems*, J. R. Mac Donald, Ed., Wiley, New York, 1987, p. 33
29. N. A. S. Webster, C. D. Ling, C. L. Raston, F . J. Lincoln, *Solid State Ionics* **178** (2007) 1451
30. A. Watanabe, *Solid State Ionics* **96** (1997) 75
31. C. K. Lee, C. S. Lee, A. Watanabe, D. C. Sinclair, *Solid State Ionics* **171** (2004) 237
32. V. I. S mirnov, V. G. Pono mareva, Yu. M. Yukhin, N. F. Uv arov, *Solid State Ionics* **156** (2003) 79
33. O. Labidi, P. Roussel, M. Huve, M. Dr ache, P. Conflant, J. P. Wignacourt, *J. Solid State Chem.* **178** (2005) 2247
34. Z. S. Macedo, C. R. Ferrari, A. C. Hernandes, *J. Eur. Ceram. Soc.* **24** (2004) 2567
35. E. Gaffet, G. Le Caër, in *Encyclopedia of Nanoscience and Nanotechnology*, Vol. 10, H. S. Nalwa, Ed., American Scie ntific Publis hers: Steven son Ranch, Californi a, 2004, pp. 1−39.

Spectroscopic and biological approach in the characterization of Cr(III), Mn(II) and Co(II) complexes with a novel hexaaza-macrocyclic ligand derived from semicarbazide

SULEKH CHANDRA* and ARCHANA GAUTAM

Department of Chemistry, Zakir Husain College, University of Delhi, J. L. N. Marg, New Delhi – 110002, India

Abstract: Complexes of Cr(III), Mn(II) and Co(II) with a novel 5,7,12,14-tetraphenyl-1,2,4,8,10,11-hexaazacyclotetradecane-3,9-dione macrocyclic ligand, THTD (L), were synthesized and characterized by elemental analysis, molar conductance and magnetic susceptibility measurements, as well as by mass, ^{1}H-NMR, IR, electronic and EPR spectral studies. Based on the spectral studies, an octahedral geometry was assigned for the Cr(III), Mn(II) and Co(II) complexes. The ligand and its complexes were screened *in vitro* against some species of bacteria and plant pathogenic fungi. The metal complexes were found to be more active antimicrobial agents than the free ligand from which they were derived.

Keywords: hexaazamacrocycle; Cr(III), Mn(II), Co(II) complexes; characterization; antimicrobial activity.

INTRODUCTION

Enormous progress has been made in macrocyclic chemistry because of the potential applications of macrocyclic compounds in the area of coordination chemistry.[1,2] The macrocyclic ligands and their metal complexes play an important role as potential catalysts. Macrocyclic ligands and their transition metal complexes have a wide range of biological activities,[3–10] including antimicrobial, antifertility, antimalarial, anticancer, antiviral and anti-HIV activities. Such biological activities of these compounds were associated with the formation of chelates with essential metal ions, bonding through N as well as S/O donor atoms. Many of these transition metal ions in living systems play the role of enzymes carriers in a macrocyclic ligand field environment.

In this paper, the synthesis, spectral characterization and antimicrobial activities of Cr(III), Mn(II) and Co(II) complexeswith a novel hexaazamacrocyclic ligand, THTD (L) (Fig. 1) are described.
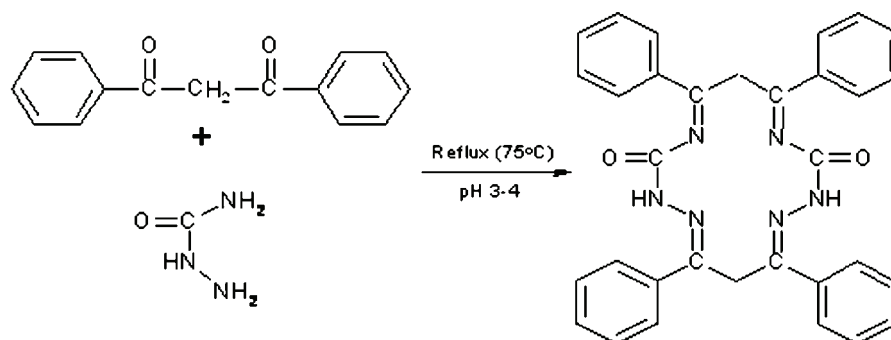
Fig. 1. Preparation and structure of the ligand (L).

EXPERIMENTAL

All the used chemicals were of AnalaR grade and procured from Sigma-Aldrich. The metal salts were purchased from E. Merck and were used as received. All the used solvents were of standard spectroscopic grade.

Synthesis of the ligand

A hot ethanolic solution (20 mL) of dibenzoylmethane (4.48 g, 0.020 mol) and a hot ethanolic solution (20 mL) of semicarbazide (2.22 g, 0.020 mol) were mixed slowly with constant stirring. The mixture was refluxed at 75 °C for 6 h in the presence of few drops of hydrochloric acid. On cooling, a white solid precipitate formed. It was filtered, washed with cold EtOH and dried under vacuum over P_4O_{10}. Yield: 62 %; m.p. 165 °C. Anal. Calcd. for $C_{32}H_{26}N_6O_2$ (FW = 526): C, 73.00; H, 4.94; N, 15.96 %. Found C, 73.12; H, 4.87; N, 15.88 %.

Synthesis of the complexes

A hot ethanolic solution (20 mL) of the ligand (0.526 g, 0.0010 mol) and a hot ethanolic solution (20 mL) of the required metal salt $CrCl_3·6H_2O$, $Cr(NO_3)_3·9H_2O$, $MnCl_2·4H_2O$, $Mn(NO_3)_2·2H_2O$, $CoCl_2·6H_2O$ or $Co(NO_3)_2·2H_2O$ (0.0010 mol) were mixed together under constant stirring. The mixture was refluxed for ≈ 8 h at ≈ 80 °C. On cooling, a coloured precipitate formed, which was filtered, washed with cold EtOH and dried under vacuum over P_4O_{10}.

Physical measurements

The analytical data were obtained using a Carlo-Erba 1106 elemental analyzer. The molar conductance was measured on an ELICO (CM82T) conductivity bridge. The magnetic susceptibility was measured at room temperature on a Gouy balance using $CuSO_4·5H_2O$ as the callibrant. Diamagnetic corrections were made using Pascal constants.[11] The electron impact mass spectra were recorded on a TOF MS ES+ mass spectrometer. The ^{1}H-NMR spectra were recorded on a Hitachi FT-NMR, model R-600 spectrometer using DMF as the solvent. The chemical shifts are given in ppm relative to tetramethylsilane. The IR spectra (in KBr discs) were recorded on a FTIR Spectrum BX-II spectrophotometer. The electronic spectra were

recorded in DMF on a Shimadzu UV mini-1240 spectrophotometer. The EPR spectra of the complexes were recorded as polycrystalline samples at room temperature on an E_4-EPR spectrometer using DPPH as the *g*-marker.

Antimicrobial screening

The preliminary fungi-toxicity screening of the compounds at different concentrations was performed *in vitro* by the agar plate technique.[12-14] The chosen fungi strains were *Aspergillus niger*, *A. glaucus* and *A. flavus*. Chlorothalonil was used as the commercial fungicide. Appropriate quantities of the compounds were mixed in autoclaved and adequately cooled potato dextrose agar medium in order to obtain concentrations of 125 and 250 ppm. The medium was dispensed into sterilized Petri plates. Mycelial discs (0.5 cm in diameter) of the test pathogens were taken from 7 days old culture with the help of a sterilized cork and placed at the centre of the Petri plates. Then, they were incubated at 27 °C until fungal growth in the control plate was almost complete.

The mycelial growth of the fungi (mm) in each Petri plate was measured diametrically and the growth inhibition (*I*) was calculated using the formula:

$$I = 100(C - T)/C$$

where *C* is the growth of the fungus (mm) in the control plate and *T* is the growth in the presence of the test compounds.

The antibacterial activity of the ligand and its metal complexes were tested using the disc diffusion method[4,15–20] against *Sarcina lutea* (gram-positive) and *Escherichia coli* (gram-negative). The nutrient agar (NA) medium was prepared using peptone, beef extract, NaCl, agar-agar and distilled water. The NA medium (25 mL) was poured into Petri plates. After solidification, 0.10 mL of test bacteria was spread over the medium using a spreader. The test compounds in measured quantities were dissolved in DMF to obtain concentrations of 125 and 250 ppm of the compounds. Whatmann No. 1 filter paper discs, 5.0 mm in diameter, each containing 1.5 mg cm^{-1} of the test compounds were placed at 4 equidistant places at a distance of 2 cm from the centre of the inoculated Petri plates. Streptomycin was used as the standard drug. The plates were kept in a refrigerator for 24 h for pre-diffusion. Finally, they were incubated for 28 h at 30 °C. The zone of inhibition was carefully measured in mm. All determinations were made in duplicate for each of the compounds. The average of two independent readings for each compound was recorded.

RESULTS AND DISCUSSION

The analytical data and some physical properties of the complexes are given in Table I. The spectral data are presented in Tables II and III.

Based on elemental analyses, the complexes were found to have compositions shown in Table I. The Cr(III) complexes in DMSO showed a molar conductance corresponding to 1:1 electrolytes. Thus, these complexes may be formulated as [Cr(L)X$_2$]X, whereas the complexes of Mn(II) and Co(II) were found to be non-electrolytes and may be formulated as [M(L)X$_2$], where M is Mn(II) or Co(II), and X = Cl$^-$ and NO$_3^-$.

Free ligand

The electron impact mass spectrum of the metal free ligand (L) (Fig. 2), confirmed the proposed formula by showing the molecular ion peak at *m/z* 548

(*i.e.*, an atomic mass of 526 corresponding to the macrocyclic moiety ($C_{32}H_{26}N_6O_2$) + 23 atomic mass of Na^+).

TABLE I. Molar conductance, colour, m.p., yield and elemental analysis data of the complexes

Complex	Λ S cm^2 mol^{-1}	Colour	M.p. °C	Yield %	Found (calcd.)/ %			
					M	C	H	N
[Cr(L^a)Cl$_2$]Cl CrC$_{32}$H$_{26}$N$_6$O$_2$Cl$_3$	108	Light green	285	65	7.48 (7.60)	56.21 (56.14)	3.87 (3.80)	12.19 (12.28)
[Cr(L)(NO$_3$)$_2$]NO$_3$ CrC$_{32}$H$_{26}$N$_9$O$_{11}$	105	Light green	280	63	6.93 (6.80)	50.35 (50.26)	3.51 (3.40)	16.41 (16.49)
[Mn(L)Cl$_2$] MnC$_{32}$H$_{26}$N$_6$O$_2$Cl$_2$	14	Cream	275	60	8.50 (8.42)	58.97 (58.89)	4.04 (3.98)	12.79 (12.88)
[Mn(L)(NO$_3$)$_2$] MnC$_{32}$H$_{26}$N$_8$O$_8$	12	Cream	280	62	7.87 (7.78)	54.38 (54.46)	3.76 (3.68)	15.95 (15.88)
[Co(L)(NO$_3$)$_2$] CoC$_{32}$H$_{26}$N$_8$O$_8$	7	Pink	268	60	8.37 (8.31)	54.11 (54.16)	3.72 (3.66)	15.85 (15.79)
[Co(L)]SO$_4$ CoC$_{32}$H$_{26}$N$_6$O$_6$S	208	Pink	260	58	8.72 (8.64)	56.45 (56.38)	3.76 (3.81)	12.41 (12.33)

[a]5,7,12,14-tetraphenyl-1,2,4,8,10,11-hexaazacyclotetradecane-3,9-dione macrocyclic ligand (THTD)

TABLE II. Magnetic moments, electronic spectral data and extinction coefficients of the complexes

Complex	μ_{eff} / μ_B	λ_{max} / cm^{-1}	ε / 1 mol^{-1} cm^{-1}
[Cr(L^a)Cl$_2$]Cl	3.72	13623, 18621, 32362	41, 55, 127
[Cr(L)(NO$_3$)$_2$]NO$_3$	3.76	13605, 18621, 32150	39, 54, 125
[Mn(L)Cl$_2$]	6.00	18621, 24272, 28011, 37453	32, 42, 67, 134
[Mn(L)(NO$_3$)$_2$]	5.97	18621, 24198, 28169, 36900	32, 41, 65, 131
[Co(L)Cl$_2$]	5.03	10775, 14814, 18621	54, 63, 121
[Co(L)(NO$_3$)$_2$]	4.91	10341, 15360, 18621	52, 68, 121

[a]5,7,12,14-tetraphenyl-1,2,4,8,10,11-hexaazacyclotetradecane-3,9-dione macrocyclic ligand (THTD)

TABLE III. EPR spectral data and ligand field parameters of the complexes

Complex	Dq / cm^{-1}	B / cm^{-1}	C / cm^{-1}	β	LFSE / kJ mol^{-1}	g
[Cr(L)Cl$_2$]Cl	1362	487	–	0.53	222	1.9493
[Cr(L)(NO$_3$)$_2$]NO$_3$	1361	489	–	0.53	195	1.9493
[Mn(L)Cl$_2$]	1862	534	3787.4	0.67	–	1.8726
[Mn(L)(NO$_3$)$_2$]	1862	567	3705.6	0.72	–	2.1601
[Co(L)Cl$_2$]	1346	748	–	0.67	129	2.1649
[Co(L)(NO$_3$)$_2$]	1292	718	–	0.64	124	2.0389

[a]5,7,12,14-tetraphenyl-1,2,4,8,10,11-hexaazacyclotetradecane-3,9-dione macrocyclic ligand (THTD)

The ^{1}H-NMR spectrum of the ligand exhibits no signals corresponding to a primary amine and alcoholic protons. The signal at δ 1.76–2.18 ppm may be assigned to (4H, C–CH$_2$–C) and the strong triplet at δ 7.89–8.21 ppm to (20H, C–C$_6$H$_5$).
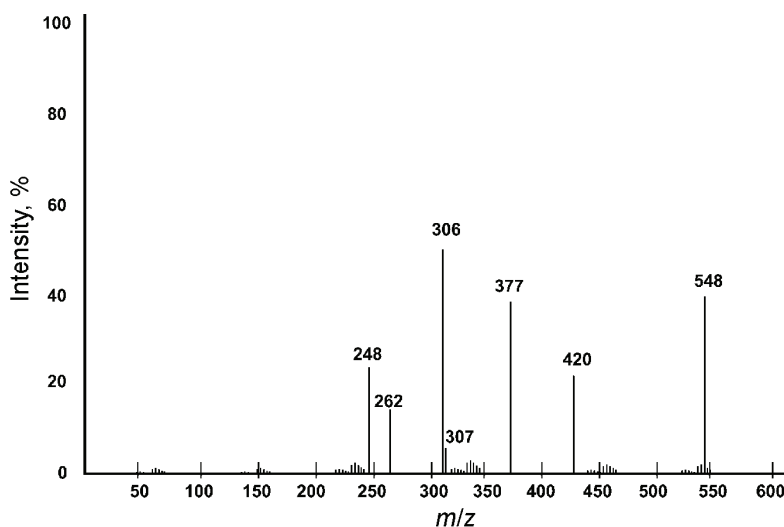
Fig. 2. Electron-impact mass spectra of the ligand (L).

The main characteristic strong band in the IR spectrum of the free ligand, appearing at 1597 cm^{-1}, is due to the >C=N group. The position of this band confirmed the reaction between the primary amine group, –NH$_2$, of the diamine and the carbonyl group, >C=O, of the diketone. It also confirmed the elimination of a water molecule and complete condensation. The bands appearing in the region 1662, 1597, 1272 and 785 cm^{-1} are assignable to amide I ν(C=O), amide II ν((C–N) + δ(N–H)), amide III δ(N–H) and IV (ϕ(C=O)), respectively. The bands at 754 and 1461 cm^{-1} are due to the presence of the phenyl ring in the macrocycle.[21,22]

Chromium(III) complexes

The Cr(III) complexes showed a magnetic moment in the range 3.72–3.76 μ_B. These values are close to the spin-only value, suggesting an octahedral geometry around the Cr(III) ion.[23] The IR spectrum of the Cr(III) nitrate complex shows three bands at 1452 (ν_5), 1315 (ν_1) and 1066 cm^{-1} (ν_2). The difference of two highest frequency bands ($\nu_5 - \nu_1$) is 137 cm^{-1}, which suggests that both the nitrate groups are attached to Cr(III) in a unidentate fashion. However, the presence of the band at 1367 cm^{-1} suggests that one nitro group is uncoordinated.[24] The electronic spectra of the Cr(III) complexes recorded in DMF (Table II) display three bands in the range 13605–13623, 18621, and 32150–32362 cm^{-1}. The first two bands may be assigned to the transitions $^4A_{2g}(F) \rightarrow {}^4T_{2g}(F)$ and $^4A_{2g}(F) \rightarrow {}^4T_{1g}(F)$, respectively, and the third band may be due to charge transfer. The EPR spectra of the complexes were recorded as polycrystalline samples at room temperature[25] (Table III). The EPR spectra of Cr(III) complexes show a broad line and the *g* value was found to be 1.9493.

Various ligand field parameters for the Cr(III) complexes were calculated, which are listed in Table III. The first spin allowed transition directly gives the value of $10Dq$. The Racah interelectronic repulsion parameter B was calculated from the equation:

$$B = (2\nu_1^2 + \nu_2^2 - 3\nu_1\nu_2) / (15\nu_2 - 27\nu_1).$$

The nephelauxetic parameter β was calculated by the relation:

$$\beta = B(\text{complex})/B(\text{free ion})$$

where B(free ion) is 918 cm^{-1} for Cr(III). The β values indicate that there is an appreciable covalent character in the metal–ligand σ bond.

Manganese(II) complexes

The magnetic moments of the Mn(II) complexes lay in the range 5.97–6.00 μ_B, corresponding to five unpaired electrons. The IR spectrum of the Mn(II) nitrate complex displays three bands in the region 1404 (ν_5), 1294 (ν_1) and 1056 cm^{-1} (ν_2). The separation of the two highest frequency bands ($\nu_5-\nu_1$) is 110 cm^{-1}. This suggests that the nitrate group is coordinated to the metal ion in an unidentate manner.[24] The electronic spectra of the Mn(II) complexes (Table II) exhibit four absorption bands in the range 18621, 24198–24272, 28011–28169 and 36900–37453 cm^{-1}.[26] These bands may be assigned to the transitions $^6A_{1g} \rightarrow$ $^4T_{1g}(^4G)$, $^6A_{1g} \rightarrow {}^4E_g(^4G)$, $^6A_{1g} \rightarrow {}^4E_g(^4D)$ and $^6A_{1g} \rightarrow {}^4T_{1g}(^4P)$, respectively. The EPR spectra were recorded as polycrystalline sample at room temperature. The polycrystalline spectra gave one broad isotropic signal and exhibit g values in the range 1.8726–2.1601.

The ligand field parameter values Dq, B, C and β for Mn(II) were calculated and are given in Table III.

$$^6A_{1g} \rightarrow {}^4E_g, {}^4A_{1g}(^4G) = 10B + 5C$$
$$^6A_{1g} \rightarrow {}^4T_{1g}(^4P) = 17B + 5C$$

The energies of these transitions are independent of the crystal field splitting and depend only on the parameters B and C.[27] The values of B and C were calculated from the second and third transitions.[28] The numerical value of 786 cm^{-1} for B for the Mn(II) free ion was used to calculate the value of β.

Cobalt(II) complexes

The Co(II) complexes showed magnetic moments in the range 4.91–5.03 μ_B, indicating a hexa-coooordinated octahedral geometry around the Co(II). The IR spectrum of the Co(II) nitrate complex displayed three bands in the region 1448 (ν_5), 1309 (ν_1) and 1042 cm^{-1} (ν_2). The separation of the two highest frequency bands ($\nu_5-\nu_1$) is 139 cm^{-1}, indicating unidentate coordination of the nitrate group. The electronic spectra of the Co(II) complexes displayed three well-defi-

ned bands in the range 10341–10775, 14814–15360 and 18621 cm^{-1}, corresponding to the $^4T_{1g}(^4F) \rightarrow {}^4T_{2g}(^4F)$ (ν_1), $^4T_{1g}(^4F) \rightarrow {}^4A_{2g}(^4F)$ (ν_2) and $^4T_{1g}(^4F) \rightarrow {}^4T_{1g}(^4P)$ (ν_3) transitions,[29] respectively, characteristic of an octahedral geometry.[30,31] The EPR spectra of the Co(II) complexes were recorded as polycrystalline samples at liquid nitrogen temperature (LNT), because the rapid spin lattice relaxation of Co(II) broaden the lines at higher temperatures. The g values lie in the range 2.0389–2.1649.

Various ligand field parameters, *viz. Dq*, *B*, β and *LFSE* were calculated and are reported in Table III. The *Dq* values were evaluated using the Orgel diagram.[32] The value for *B*(free ion) for Co(II) is 1120 cm^{-1}. The values of β lie in the range 0.64–0.67, indicating an appreciable covalent character in the complexes.

Based on the above spectral studies, the structures shown in Fig. 3 may be suggested for the complexes.
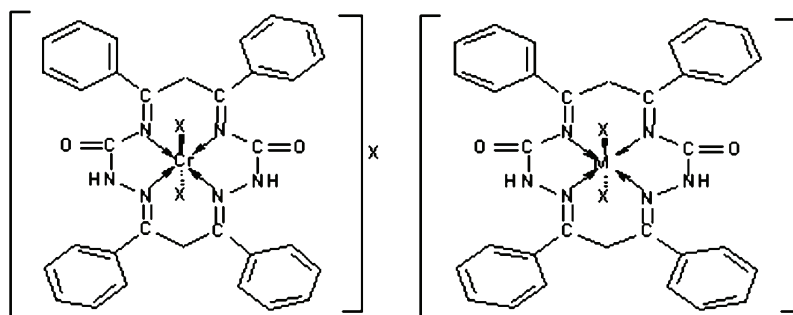
Fig. 3. Suggested structures of complexes (M = Mn(II) or Co(II); X = Cl$^-$ or NO$_3^-$).

The results of the antifungal and antibacterial activity are given in Tables IV and V, respectively.

TABLE IV. Antifungal screening data of the ligand (L) and its complexes

Compound	Fungal inhibition / %					
	Aspergillus niger		*Aspergillus glaucus*		*Aspergillus flavus*	
	c / µg ml^{-1}					
	125	250	125	250	125	250
L[a]	29	49	–	38	35	50
[Cr(L)Cl$_2$]Cl	29	47	10	40	36	53
[Cr(L)(NO$_3$)$_2$]NO$_3$	31	50	–	38	35	52
[Mn(L)Cl$_2$]	33	54	26	41	38	57
[Mn(L)(NO$_3$)$_2$]	31	51	23	39	36	53
[Co(L)Cl$_2$]	37	58	29	45	45	59
[Co(L)(NO$_3$)$_2$]	34	61	31	47	49	64
Chlorothalonil (standard)	52	76	48	67	61	82

[a]5,7,12,14-tetraphenyl-1,2,4,8,10,11-hexaazacyclotetradecane-3,9-dione macrocyclic ligand (THTD)

TABLE V. Antibacterial screening data of the ligand (L) and its complexes

Compound	Inhibition diameter / mm			
	Sarcina lutea		*Escherchia coli*	
	c / µg ml^{-1}			
	125	250	125	250
L^a	6	11	–	10
[Cr(L)Cl$_2$]Cl	–	14	6	9
[Cr(L)(NO$_3$)$_2$]NO$_3$	8	15	7	10
[Mn(L)Cl$_2$]	7	16	–	9
[Mn(L)(NO$_3$)$_2$]	–	14	6	11
[Co(L)Cl$_2$]	12	20	14	21
[Co(L)(NO$_3$)$_2$]	10	19	12	19
Streptomycin (standard)	24	28	20	25

[a] 5,7,12,14-tetraphenyl-1,2,4,8,10,11-hexaazacyclotetradecane-3,9-dione macrocyclic ligand (TH T)D

The antimicrobial screening data show that the metal chelates exhibit a higher inhibitory effect than the free ligand. The increased activity of the metal chelates can be explained based on the chelation theory.[33,34]

The ligand and its metal complexes show fungal growth inhibition in the following order: Co(II) > Mn(II) > Cr(III) ≅ ligand. The bacterial growth inhibitory capacity of the ligand and its metal complexes show the following order: Co(II) > > Mn(II) ≅ Cr(III) > ligand.

CONCLUSIONS

In the present study, a novel 5,7,12,14-tetraphenyl-1,2,4,8,10,11-hexaazacyclotetradecane-3,9-dione macrocyclic ligand, HTTD (L), derived from dibenzoylmethane and semicarbazide, was synthesized. Based on the above-described spectral studies, the ligand was found to be tetradentate and an octahedral geometry was assigned for the Cr(III), Mn(II) and Co(II) complexes. The antimicrobial screening indicated that the metal chelates showed greater inhibitory effects than the metal free ligand. It is also proposed that concentration plays a vital role in increasing the degree of inhibition, *i.e.*, as the activity increased with increasing concentration of the compounds.

И З В О Д

СПЕКТРОСКОПСКИ И БИОЛОШКИ ПРИСТУП У КАРАКТЕРИЗАЦИЈИ Cr(III), Mn(II) И Co(II) КОМПЛЕКСА СА НОВИМ ХЕКСААЗАМАКРОЦИКЛИЧНИМ ЛИГАНДОМ ИЗВЕДЕНИМ ИЗ СЕМИКАРБАЗИДА

SULEKH CHANDRA* и ARCHANA GAUTAM

Department of Chemistry, Zakir Husain College, University of Delhi, J.L.N. Marg, New Delhi – 110002, India

Синтетисани су комплекси Cr(III), Mn(II) и Co(II) са новим макроцикличним лигандом 5,7,12,14-тетрафенил-1,2,4,8,10,11-хексаазациклотетрадекан-3,9-дионом, THTD (L). Они су

окарактерисани елементалном анализом, моларном проводљивошћу и мерењима магнетне сусцептибилности, масеном спектроскопијом, ^{1}H-NMR, IR, електронским и EPR спектро-скопским проучавањима. На основу спектара, октаедарска геометрија је приписана Cr(III), Mn(II) и Co(II) комплексима. Лиганд и комплекси су тестирани *in vitro* према неким сојевима бактерија и биљних патогених гљивица. Нађено је да су метални комплекси активнији антимикробни агенси у поређењу са слободним лигандом из кога су изведени.

REFERENCES

1. S. Chandra, S. D. Sharma, *Transition Met. Chem.* **27** (2002) 732
2. S. Chandra, R. Kumar, *Transition Met. Chem.* **29** (2004) 269
3. S. Chandra, Sangeetika, *Spectrochim. Acta* **60A** (2004) 2153
4. N. Raman, A. Kulandaisamy, C. Thangaraja, K. Jeyasubramanian, *Transition Met. Chem.* **28** (2003) 29
5. D. P. Singh, R. Kumar, V. Malik, P. J. Tyagi, *J. Enzyme Inhib. Med. Chem.* **22** (2007) 177
6. F. M. A. M. Aqra, *Transition Met. Chem.* **28** (2003) 224
7. Y. S. Kim, R. Song, C. O. Lee, Y. S. Sohn, *Bioorg. Med. Chem. Lett.* **14** (2004) 2889
8. T. M. Hunter, S. J. Paisey, H. S. Park, *J. Inorg. Biochem.* **98** (2004) 713
9. S. J. Laulloo, M. Witvrouw, *Indian J. Chem.* **30B** (2000) 842
10. J. A. Parkinson, M. Weishaupl, R. O. Gould, *J. Am. Chem. Soc.* **124** (2002), 9105
11. R. S. Drago, *Physical Methods in Chemistry*, W. B. Saunders Company, London, 1977, p. 413
12. A. Hooda, V. K. Garg, N. K. Sangwan, K. S. Dhindsa, *Proc. Natl. Acad. Sci.USA* **66A** (1996) 223
13. N. K. Singh, M. K. Biyala, R. V. Singh, *Transition Met. Chem.* **29** (2004) 681
14. R. K. Agarwal, S. Prasad, *Bioinorg. Chem. Appl.* **3** (2005) 271
15. Z. H. Chohan, A. Munawar, C. T. Supuran, *Met. Based Drugs* **8** (2001)137
16. J. R. Anacona, G. D. Sillva, *J. Chil. Chem. Soc.* **50** (2005) 447
17. S. Zivanovic, S. Chi, A. F. Draughon, *J. Food Sci.* **70** (2005) **M**45
18. Z. H. Chohan, C. T. Supuran, *Main Group Met. Chem.* **24** (2001) 399
19. R. V. Singh, M. K. Biyala, N. Fahmi, *Phosphorus Sulfur Silicon Relat. Elem.* **180** (2005) 425
20. R. F. F. Costa, A. P. Rebolledo, *J. Coord. Chem.* **58** (2005) 1307
21. S. Chandra, K. Gupta, *Transition Met. Chem.* **27** (2002) 329
22. S. Chandra, L. K. Gupta, *J. Indian Chem. Soc.* **82** (2005) 454
23. B. N. Figgis, *Introduction to Ligand Field Theory*, Wiley, New York, 1978
24. S. Chandra, M. Pundir, *Spectrochim. Acta* **69A** (2008) 1
25. S. Chandra, S. Sharma, *Transition Met. Chem.* **32** (2007) 150
26. S. Chandra, L. K. Gupta, *Spectrochim. Acta* **61A** (2005) 2139
27. J. E. Huheey, *Principles of Structure and Reactivity*, Harper and Row, New York, 1972, p. 363
28. S. Chandra, R. Kumar, *Spectrochim. Acta* **67A** (2007) 188
29. A. B. P. Lever, *Crystal Field Spectra. Inorganic Electronic Spectroscopy*, 1st ed., Elsevier, Amsterdam, 1968
30. K. Nakamoto, *Infrared Spectra of Inorganic and Coordination Compounds*, Wiley Interscience, New York, 1970
31. S. Chandra, L. K. Gupta, *J. Saudi Chem. Soc.* **7** (2003) 243

32. H. J. Emeleus, A. G. Sharpe, *Modern Aspects of Inorganic Chemistry*, ELBS and Rout-ledge & Kegan Paul, Delhi, 1973
33. S. K. Sengupta, O. P. Pandey, B. K. Srivastava, V. K. Sharma, *Transition Met. Chem.* **23** (1998) 349
34. S. Chandra, M. Tyagi, *J. Serb. Chem. Soc.* **73** (2008) 727.

Obtaining the Varshni potential function using the 2-body Kaxiras–Pandey parameters

TEIK-CHENG LIM*

School of Science and Technology, SIM University, 535A Clementi Road, S 599490, Republic of Singapore

*Abstrac*t: A generalized version of the Varshni potential function was adopted by Kaxiras and Pandey for describing the 2-body energy portion of multi-body condensed matter. The former's simplicity and resemblance to a Morse potential allows faster computation while the latter's greater number of parameters allows better curve-fitting of spectroscopic data. This paper shows one set of parameter conversion from the Varshni function to the 2-body portion of the Kaxiras–Pandey function, and *vice versa* two sets of parameter conversion. The latter two sets reveal good correlation between plotted curves, and were verified by the imposition of equal energy curvatures at equilibrium and equal energy integral from equilibrium to dissociation. These parameter conversions can also be attained more easily by equating the product of indices (for short range) and the summation of index reciprocals (for long range).

Keywords: derivative; integral; Kaxiras–Pandey; parameter conversion; potential function; Varshni.

INTRODUCTION

The simulation of mechanical properties (such as modulus and strength), fluid flow (such as flow rate and flow profile), mass transport (such as particle diffusion), heat transfer (such as convection), or novel properties at the nano--scale would require molecular modeling[1–3] that is either based on the molecular dynamics method[4–6] or the Monte Carlo method.[7–9] In both approaches, the interaction energy between bonded atoms (including bond stretching, bending and torsion), non-bonded energy of interaction (for both van der Waals and Coulombic interactions), and between molecules are described in terms of potential energy functions. A comprehensive review of the classical potential energy functions of diatomic molecules was written by Varshni.[10] In addition, Varshni[10]

---

*Corresponding author. E-mail: alan_tc_lim@yahoo.com

Available online at www.shd.org.rs/JSCS/

proposed seven potential energy functions of his own, whereby the first one is written as:

$$U_V = D(1 - \exp(-b(r^2 - R^2)))^2 \tag{1}$$

where D, r and R are the dissociation energy, the internuclear distance and the equilibrium bond length, respectively. The parameter b controls the shape of the potential energy curve. One may note that $(U_V)_{r=R} = 0$ and $(U_V)_{r \to \infty} = D$. The Varshni function can also be alternatively written in a modified form:

$$U_{MV} = U_{MV} - D = D\left(\exp\left(2bR^2\left(1 - \frac{r^2}{R^2}\right)\right) - 2\exp\left(bR^2\left(1 - \frac{r^2}{R^2}\right)\right)\right) \tag{2}$$

so that $(U_{MV})_{r=R} = -D$ and $(U_{MV})_{r \to \infty} = 0$. It can be shown that the Varshni function is a special case of the Kaxiras–Pandey[11] potential energy function for a multi-body condensed matter system. The 2-body portion of the Kaxiras–Pandey function:

$$U_{KP} = A_1 \exp(-\alpha_1 r^2) - A_2 \exp(-\alpha_2 r^2) \tag{3}$$

can be converted to an equivalent form that allows comparison to be made with the Varshni potential. Suppose one lets:

$$(U_{KP})_{r=R} = -D \tag{4}$$

and

$$\left(\frac{\partial U_{KP}}{\partial r}\right)_{r=R} = 0 \tag{5}$$

then Eq.(3) can be recast as:

$$U_{KP} = D\frac{\alpha_2}{\alpha_1 - \alpha_2}\left(\exp\left(\alpha_1 R^2\left(1 - \frac{r^2}{R^2}\right)\right) - \exp\left(\alpha_2 R^2\left(1 - \frac{r^2}{R^2}\right)\right)\right) \tag{6}$$

Comparing the indices of Eqs. (2) and (6) gives:

$$\alpha_i = jb, \; (i,j = 1,2) \tag{7}$$

and

$$A_i = iD\exp(jbR^2), \; (i,j = 1,2) \tag{8}$$

Hence, extraction of the Kaxiras–Pandey 2-body parameters from the Varshni parameters can be easily obtained from Eqs. (7) and (8). However this conversion is meaningless because the former is more flexible and, hence, more accurate than the latter. The next section proposes three approaches for reducing a 2-body Kaxiras–Pandey function into a Varshni potential. Two of the methods give good correlation and are elucidated in the discussion section.

COMPARISON OF INDICES

The extraction of the Varshni parameter from the Kaxiras–Pandey function is not straightforward due to the former's fewer number of parameters compared to the latter's. One possible way of obtaining the Varshni parameter is to take the average, or mean, value from Eq. (7), *i.e.*, by using:

$$2b = \alpha_1 \tag{9}$$

and

$$b = \alpha_2 \tag{10}$$

Taking the arithmetic average of Eqs. (9) and (10) gives:

$$2b + b = \alpha_1 + \alpha_2 \Rightarrow b = (\alpha_1 + \alpha_2)/3 \tag{11}$$

while taking the geometric mean leads to:

$$2b \times b = \alpha_1 \times \alpha_2 \Rightarrow b = \sqrt{\frac{\alpha_1 \alpha_2}{2}} \tag{12}$$

It can be seen that taking the arithmetic average of the reciprocals yields:

$$\frac{1}{2b} + \frac{1}{b} = \frac{1}{\alpha_1} + \frac{1}{\alpha_2} \Rightarrow b = \frac{3}{2} \frac{\alpha_1 \alpha_2}{\alpha_1 + \alpha_2} \tag{13}$$

Taking the geometric mean of the reciprocals also leads to Eq. (12). It is of interest to note that dividing the square of Eq. (12) with Eq. (11) also gives Eq. (13).

RESULTS

The Kaxiras and Pandey parameterized values[11] for silicon are: $A_1 = 57.316072$ eV, $A_2 = 6.4373054$ eV, $\alpha_1 = 0.8233523$ Å^{-2} and $\alpha_2 = 0.19061589$ Å^{-2}. Based on the imposition of zero slopes at the minimum well-depth, *i.e.*, Eq. (5), the equilibrium bond length can be calculated from:

$$R = \sqrt{\frac{1}{\alpha_1 + \alpha_2} \ln \left(\frac{\alpha_1 A_1}{\alpha_2 A_2}\right)} \tag{14}$$

to give $R = 2.401656627$ Å. From this value of R, the dissociation energy can be easily calculated using either:

$$D = \frac{\alpha_1 - \alpha_2}{\alpha_2} A_1 \exp(-\alpha_1 R^2) \tag{15a}$$

or

$$D = \frac{\alpha_1 - \alpha_2}{\alpha_2} A_2 \exp(-\alpha_2 R^2) \tag{15b}$$

to give D = 1.6475939 eV. Using Eqs. (11)–(13), the Varshni shape parameter, b, was calculated as 0.33798940, 0.28012857 and 0.23217301 Å^{-2}, respectively. With the obtained potential function parameters, the Varshni and the 2-body portion of the Kaxiras–Pandey potential functions, as depicted in Eqs. (2) and (6), respectively, can be plotted. For the purpose of comparison, the dimensionless interatomic energy, (U/D) was plotted against the dimensionless bond length, (r/R). Figures 1–3 show the 2-body energy portion of the Kaxiras-Pandey function, as bold curves, while the Varshni potential energy curves are based on the parameters obtained from Eqs. (11)–(13).
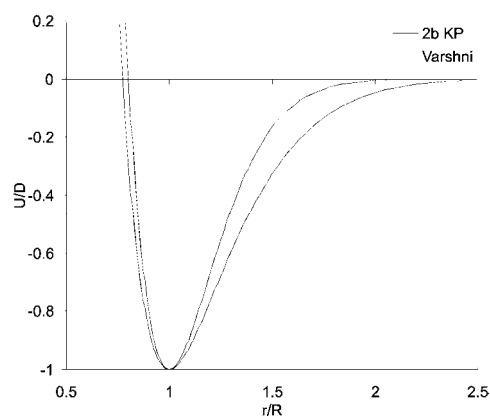
Fig. 1. The 2-body energy portion of silicon according to the Kaxiras–Pandey potential and the Varshni approximation using Eq. (11).
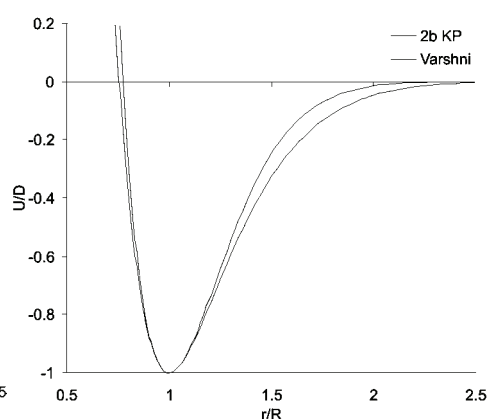
Fig. 2. The 2-body energy portion of silicon according to the Kaxiras–Pandey potential and the Varshni approximation using Eq. (12).
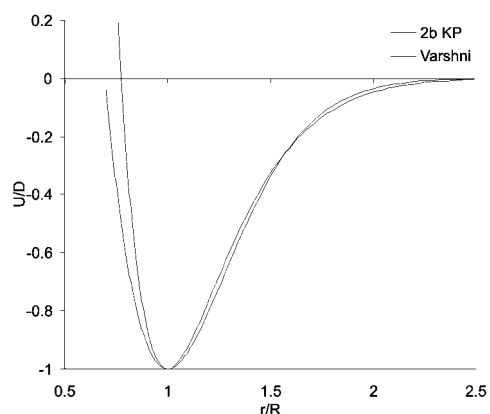
Fig. 3. The 2-body energy portion of silicon according to the Kaxiras–Pandey potential and the Varshni approximation using Eq. (13).

DISCUSSION

It is clear that good correlations were found in Figs. 2 and 3, but not in Fig.1. Why? To answer this question, let:

$$\left(\frac{\partial^2 U_{\mathrm{MV}}}{\partial r^2}\right)_{r=R} = \left(\frac{\partial^2 U_{\mathrm{KP}}}{\partial r^2}\right)_{r=R} \tag{16}$$

and

$$\int_R^\infty U_{\mathrm{MV}}\mathrm{d}r = \int_R^\infty U_{\mathrm{KP}}\mathrm{d}r \tag{17}$$

analogous to references[12–15] and,[16–20] respectively. It is clear that Eq. (16) imposes equal curvatures for both potential functions, while Eq. (17) imposes an equal area between the potential energy curves with the bond length axis from equilibrium to dissociation. The impositions laid down by Eqs. (16) and (17) lead to Eqs. (12) and (13), respectively. For this reason, the Varshni curve agrees well with the 2-body portion of the Kaxiras–Pandey energy near the minimum well--depth, *i.e.*, from $0.8 < (r/R) < 1.2$ (see Fig. 2) on the basis of Eq. (12). The imposition of equal energy integral in Eq. (17) gives a generally good approximation for $(r/R) > 1$ (see Fig. 3) due to the integral range from $r = R$ to $r \rightarrow \infty$. The correlation in Fig. 1 is unsatisfactory due to the lack of a mathematical basis for Eq. (11), unlike Eqs. (12) and (13). The conversion of the 2-body Kaxiras––Pandey parameters into the Varshni shape parameters, excluding the common initial conversion of A_1 and A_2 to R and D, as denoted by Eqs. (14) and (15), is summarized in Table I.

TABLE 1. Conversion of 2-body Kaxiras–Pandey parameters[2] into Varshni parameter[1]

Range	Rigorous approach	Simplified approach	Conversion
Short range	$\left(\frac{\partial^2 U_{MV}}{\partial r^2}\right)_{r=R} = \left(\frac{\partial^2 U_{KP}}{\partial r^2}\right)_{r=R}$	$2b \times b = \alpha_1 \times \alpha_2$	$b = \sqrt{\dfrac{\alpha_1 \alpha_2}{2}}$
Long range	$\int_R^\infty U_{MV}\mathrm{d}r = \int_R^\infty U_{KP}\mathrm{d}r$	$\dfrac{1}{2b} + \dfrac{1}{b} = \dfrac{1}{\alpha_1} + \dfrac{1}{\alpha_2}$	$b = \dfrac{3}{2}\left(\dfrac{\alpha_1 \alpha_2}{\alpha_1 + \alpha_2}\right)$

CONCLUSIONS

The 2-body energy portion of Kaxiras–Pandey function is a generalized version of the Varshni potential function. While the former possesses better flexibility for curve-fitting of spectroscopic data and higher accuracy, the resemblance of the latter to the Morse potential suggests its ease of execution in computational chemistry software. Hence the conversion of the 2-body parameters of the Kaxiras–Pandey function into Varshni parameters. Although rigorous under-

standing for converting the 2-body Kaxiras–Pandey parameters into Varshni parameters can be approached using equated minimum well-depth curvatures (for short range) and equated energy integral from equilibrium to dissociation (for long range), a more convenient approach can be performed by assuming $2b \times b = \alpha_1 \times \alpha_2$ (for short range) and $(2b)^{-1} + b^{-1} = \alpha_1^{-1} + \alpha_2^{-1}$ (for long range).

ИЗВОД

ИЗРАЧУНАВАЊЕ ПОТЕНЦИЈАЛНЕ ФУНКЦИЈЕ ВАРШНИЈЕВОГ ТИПА ПОМОЋУ ДВОЧЕСТИЧНИХ КАКСИРАС–ПАНДЕЈЕВИХ ПАРАМЕТАРА

TEIK-CHENG LIM

School of Science and Technology, SIM University, 535A Clementi Road, S 599490, Republic of Singapore

Kaxiras и Pandey су применили једну генерализовану верзију Varshni-јеве потенцијалне функциије да би описали двочестичне доприносе енергији многочестичне кондензоване материје. Једноставност Varshni-јевог потенцијала и његова сличност са Морзеовим потенцијалом омогућује брже рачунање, док Kaxiras–Pandey-ев поступак омогућује лакше усклађивање са спектроскопским подацима. У овом раду је показано како се Varshni-јева функције може конвертовати у двочестични део Kaxiras–Pandey-еве функције, и обратно.

(Примљено 23. јуна 2009)

REFERENCES

1. H. D. Holtje, W. Sippl, D. Rognan, G. Folkers, *Molecular modeling: basic principles and applications*. 3rd ed., Wiley-VCH, New York, 1997
2. F. Jensen, *Introduction to Computational Chemistry*, 2nd ed., Wiley, New York, 2006
3. A. Hinchcliffe, *Modelling molecular structures*, Wiley, New York, 1996
4. L. Verlet, *Phys. Rev.* **159** (1967) 98
5. J. M. Haile, *Molecular dynamics simulation: elementary methods*, Wiley, New York, 1997
6. T. Schlick, *Molecular modeling and simulation*, Springer, Heidelberg, 2002
7. N. Metropolis, S. Ulam, *J. Am. Stat. Assoc.* **44** (1949) 335
8. N. Metropolis, A. E. Rosenbluth, M. N. Rosenbluth, A. H. Teller, E. Teller, *J. Chem. Phys.* **21** (1953) 1087
9. B. A. Berg, Markov chain Monte Carlo simulations and their statistical analysis, World Scientific, Singapore, 2004
10. Y. P. Varshni, *Rev. Mod. Phys.* **29** (1957) 664
11. E. Kaxiras, K. C. Pandey, *Phys. Rev. B* **38** (1988) 12736
12. T. C. Lim, *J. Math. Chem.* **41** (2007) 135
13. T. C. Lim, *J. Serb. Chem. Soc.* **72** (2007) 159
14. T. C. Lim, *Chem. Phys.* **331** (2007) 270
15. T. C. Lim, *MATCH Commun. Math. Comput. Chem.* **59** (2008) 499
16. T. C. Lim, *Mol. Phys.* **105** (2007) 1013
17. T. C. Lim, *MATCH Commun. Math. Comput. Chem.* **58** (2007) 647
18. T. C. Lim, *Mol. Simul.* **33** (2007) 1029
19. T. C. Lim, *MATCH Commun. Math. Comput. Chem.* **61** (2009) 313
20. T. C. Lim, *J. Math. Chem.* **46** (2009) 569.

Temperature imposed textural and surface synergism affecting the isomerization activity of sulfated zirconia catalysts

ALEKSANDRA ZARUBICA[1≠], BRANISLAV JOVIĆ[2], ALEKSANDAR NIKOLIĆ[2], PAULA PUTANOV[3#] and GORAN BOŠKOVIĆ[1*#]

[1]Faculty of Technology, University of Novi Sad, 21000 Novi Sad, [2]Faculty of Sciences, Department of Chemistry, University of Novi Sad, 21000 Novi Sad and [3]Serbian Academy of Sciences and Arts, Knez Mihailova 10, 11000 Belgrade, Serbia

Abstract: Using sulfuric acid as the sulfating agent, two catalyst series were obtained from hydroxide and nitrate precursor with a sulfate loading identical to commercial sulfated hydroxide, *i.e.*, 4.2 mass %. After calcination at 500, 600 and 700 °C, all nine samples had various contents of residual sulfates depending on the origin of the catalyst. Accordingly, their surface properties were different, which, together with various textural properties, govern the formation of the active phase and their catalytic activity in the *n*-hexane isomerization reaction. The dominant activity and yield of mainly mono-branched isomers were attained in reaction at 200 °C with a commercially sulfated zirconia catalyst calcined at 500 °C. Among the SZ catalyst series synthesized from hydroxide and nitrate, the second according to its activity profile was similar to that of the commercially sulfated one, while samples originating from hydroxide showed some activity only after calcination at 600 °C. This is due to the poorer textural properties of the hydroxide series, necessitating a higher calcination temperature in order to promote the simultaneous decomposition of S-containing species and their re-adsorption into the zirconia matrix following interaction and active phase formation. It seems that the tetragonal zirconia phase was not responsible for the catalytic activity but a synergistic effect of the textural properties of the samples and the sulfate loadings, which determine different acid strengths on the catalyst surface.

Keywords: active phase formation; calcination temperature; isomerization activity; sulfated zirconia catalyst; synergism of textural and surface properties.

INTRODUCTION

Strong legislative restrictions eliminated harmful but at the same time high octane number (ON) substances, making the production of motor gasoline of required quality a challenging task for refineries. Hydro-isomerization of straight C_5–C_7 paraffins, thereby producing high-ON isomers for gasoline blending, is one possibility of solving the ON-issue.[1] The reaction requires a bifunctional catalyst: a noble metal on an acidic support, *i.e.*, chlorinated alumina or zeolites. The former, however, faces environmental and expense drawbacks, while the latter, although resistant to impurities, are not satisfactory due to their relatively low activity.[2] Therefore, for the near future, an important challenge is to develop a new environmental friendly and active catalyst.

Solid acids, such as sulfated zirconia (SZ), are potential candidates for the isomerization of light alkanes.[3] Zirconia modified with sulfates exhibits superior catalytic activity. The presence of sulfates increases the stability of zirconia as well as the content of the tetragonal crystal phase, which is the one believed to be catalytically active.[4] Several detailed investigations indicated, however, that the type of zirconia phase is only of secondary importance and emphasized the significance of labile sulfate groups for catalytic activity.[5–8] Generally speaking, the properties of SZ depend on the preparation method, the type of precursor and the activation procedure.[8–12] Although a number of methods and various zirconium compounds have been suggested for the preparation of SZ, there is still no consensus on the correlation of activity with the fraction of tetragonal phase, the quality and content of sulfates or textural and surface properties.

In the present study, three series of SZ catalysts were synthesized from different precursors by suitable preparation methods, followed by calcination at different temperatures. The catalytic activities of the prepared catalysts were measured in the isomerization of *n*-hexane, as a model reaction, and the results were correlated with their physico-chemical properties, which emphasized the importance of the textural environment for the utilization of their surface properties in the formation of the active phase.

EXPERIMENTAL

Catalysts preparation and characterization

Three types of SZ catalysts were prepared, two as self-made from materials of different origin and the third from a commercial sulfated zirconia. The same procedures required to obtain SZ samples with the same temperature history were applied using the following precursors: sulfated zirconium hydroxide, SO_4–$Zr(OH)_4$ (Aldrich); zirconium hydroxide, $Zr(OH)_4$ (97 %, Aldrich) and zirconium oxynitrate, $ZrO(NO_3)_2 \cdot xH_2O$ (Aldrich). Different steps were performed for each particular precursor: a) lone calcination of the commercially sulfated Zr hydroxide; b) sulfation and calcination when starting from the Zr hydroxide precursor and c) precipitation of the nitrate precursor (with 25 % NH_4OH) to Zr hydroxide, followed by its sulfation and calcination in order to obtain the third catalyst. The sulfating procedure was realized by wet-impregnation using 0.50 M H_2SO_4 for the intended content of sulfates (4.2 mass

%). The subsequent calcination was performed at different temperatures for 3 h in a synthetic air flow of 25 cm^3/min. Consequently, a total of nine SZ-catalyst samples were obtained, denoted as: SZ-C-X, SZ-H-X or SZ-N-X, where C, H and N reveal the catalyst origin, *i.e.*, commercially sulfated hydroxide, hydroxide and nitrate, respectively, and X (X = 5, 6 or 7) stands for the applied calcination temperature: 500, 600 or 700 °C, respectively.

The specific surface area of the catalysts was investigated by the BET procedure following low temperature N$_2$ adsorption on a Micromeritics ASAP 2010 apparatus. X-Ray diffraction analysis (XRD, Philips APD-1700 diffractometer with a Cu-anticathode and monochromator) was used for the zirconia determination of the crystal structure. The fraction of sulfates removed during the calcination was measured by thermogravimetric analysis (TG) in a manner explained previously.[13] The density of sulfates was calculated from the amount of remaining SO$_4^{2-}$ obtained by TG and BET data, assuming a surface area of 0.25 nm^2 for a sulfate group.[14] The related acid strength properties of the catalysts were evaluated by following the change of color of Hammett indicators in contact with the surface of the catalyst samples. The following indicators were used: *p*-dimethylaminoazobenzene, 2-amino-5-azotoluene, benzeneazodiphenylamine and crystal violet, covering the range of pK_a values from 3.3 to 0.8.[15] The nature of acidic sites present was studied by Fourier transformed infrared spectrophotometry of the catalyst samples with previously adsorbed pyridine by means of a Thermo Nicolet Nexus 670 FTIR spectrophotometer. Preceding the IR analysis, the samples were evacuated in order to remove physically adsorbed pyridine.

Catalysts activity measurements

The isomerization of *n*-hexane was used as the test reaction to probe the activity and selectivity of the catalysts. The reaction conditions were as follows: 200–300 °C, atmospheric pressure, the molar ratio of He, as the carrier gas, and *n*-C$_6$ was 1 5.5 at a constant partial pressure of *n*-C$_6$ of 60.5 mbar and a space velocity of 6×10^{-2} mmol *n*-C$_6$/g$_{cat}$·min. As a rule, 0.50 g of a fresh catalyst sample was loaded into a quartz microreactor and *in situ* activated at 500 °C for 1 h in a synthetic air flow of 20 cm^3/min. By switching the carrier gas stream to the saturator with *n*-hexane, the reaction commenced and the products were analyzed in the GC jet after 5 min (initial activity). The procedure provided catalyst activity testing free of deactivation, which usually occurs under similar conditions due to intensive coking.[16] The reaction products were separated on the 30 m long PONA GC-capillary column and analyzed by gas chromatograph (GC-HP 5 890, Series II) equipped with an FID detector. Conversion of *n*-hexane was measured to each of the individual gas-phase products and normalized by the number of C-atoms in both the reactant and product. The corresponding selectivity for the formation of an individual product was calculated by dividing the normalized conversion of *n*-hexane to the particular product with the total *n*-hexane conversion. Finally, the catalysts were classified by their yields, calculated by means of the product of the conversion and the selectivity.

RESULTS

The basic textural properties of the sulfated zirconia catalyst samples are given in Table I. Obviously, these properties are functions of the precursor of the catalysts and the thermal history of the samples. Catalysts of SZ-C and SZ-N series were characterized with high BET surface areas, while the series of catalyst samples from hydroxide (SZ-H) showed significantly lower surface areas. Very high specific surface areas (far above 100 m^2/g) are due to the presence of mic-

ropores in the case of the samples from SZ-C and SZ-N series calcined at 500 °C. Moreover, the latter is characterized with a bim odal pore distribution, having, simultaneously, a substantial fraction of mesopores, which are resp onsible for the considerable pore volum e of the sam ple. Samples of SZ-H series had the lowest total pore vol ume compared to their counterparts from different o rigins. The general feature of the textural characteristics of all sa mples is that the surface areas were not proportional to t he total pore volum es, since the porosities and the pore size distributions were different among the series. The mean pores size decreased with increasi ng calcination tem perature, transfor ming the pores with diam eters close to those of micro- to the meso-pore size. This was followed by an increase in the pore volume and a decrea se in th e specific surface are a; this trend was, however, the slowest in the SZ-H series.

TABLE I. Specific surface are a (BET), total pore volume and mean pore di ameter of the SZ samples as a function of their origin and calcination temperature

Sample Surface	area, m^2/g	Pore volume, cm^3/g	Mean pore diameter, nm
SZ-C-5	130	0.059	$< 2.0^a$
SZ-C-6	103	0.096	3.3
SZ-C-7	69	0.105	5.7
SZ-H-5	82	0.053	2.6
SZ-H-6	68	0.064	3.9
SZ-H-7	67	0.089	5.0
SZ-N-5	144	0.139	< 2.0; 3.2
SZ-N-6	117	0.139	4.4
SZ-N-7	89	0.141	6.0

[a]Pores smaller than 2 nm were beyond the limit of the equipment

The sim ilar properties were found b y Matsuhashi *et al.*,[12] wh o rep orted values of the specific surface area and mean pore dia meter in the range of 60–90 m^2/g and 2–20 nm, respectively, for SZ sam ples differing in origin, as well as in sulfating agent and sulfation procedure.

From Table I I, it can be c oncluded that all the sam ples calcined at 500 °C were characterized by only the tetrag onal zirconia phase, while increasing the calcination temperature resulted in an increasing fr action of the monoclinic crystal phase. The latter phase prevailed in the catalysts pretreated at the highest temperature; the highest value of 72. 7 % w as in the cata lyst sample p repared from the hydroxide precursor.

The range of acid strength, H_0, of the catalyst samples relative to color changes of applied Hammett indicators are given in Table II. Although quite a modest range of pK_a values was covered with the available indicators, all the sa mples, except SZ-C-5, were within the acidity range $3.3 \geq H_0 \geq 0.8$. The sample SZ-C-5 possessed a higher acid strength, characterized with $H_0 < 0.8$. For a m ore a ccu-

Available online at www.shd.org.rs/JSCS/

rate acidity categorization, probes with indicators of basicity higher than that of the most basic available crystal violet would be required.[15]

TABLE II. Crystal phase composition, content of remaining sulfates, sulfates density and H_0 values of the SZ samples as a function of their origin and calcination temperature

Sample	Fraction of sulfates removed during the calcination step[a] %	Sulfates remaining after calcination, %	Sulfate density (per nm^2 of surface)	H_0	Volume fraction of tetragonal/ /monoclinic phases, %
SZ-C-5	0	4.2	2.03	$H_0 < 0.8$	100
SZ-C-6	7.2 (7.2)	3.9	2.38	$3.3 > H_0 \geq 0.8$	93.3/6.7
SZ-C-7	55.9 (48.7)	2.0	1.81	$H_0 > 3.3$	48.3/51.7
SZ-H-5	45.2	2.3	1.76	$3.3 > H_0 \gg 0.8$	100
SZ-H-6	45.2 (0)	2.3	2.12	$3.3 > H_0 \geq 0.8$	71.9/28.1
SZ-H-7	66.9 (21.7)	1.8	1.69	$3.3 \gg H_0 \ggg 0.8$	27.3/72.7
SZ-N-5	28.6	3.0	1.31	$3.3 > H_0 \geq 0.8$	100
SZ-N-6	31.9 (3.3)	2.9	1.55	$3.3 > H_0 \gg 0.8$	80.3/19.7
SZ-N-7	42.2 (10.3)	2.6	1.83	$3.3 \gg H_0 \ggg 0.8$	37.5/62.5

[a]Calculated based on the identical initial sulfates loading of 4.2 mass % for all samples determined by TGA;[13] the fraction of sulfates released for the applied calcination temperature gradient of 100 °C are given in parentheses

The initial activity and selectivity to total isomers of the catalysts are given in Table III as a function of the origin of the SZ samples and of both calcination and reaction temperatures. Catalyst SZ-C-5 showed the maximal initial activity of all the prepared catalysts at both applied reaction temperatures. The selectivity to i-C$_6$ of the same catalyst was also considerable; altogether resulting in the highest isomer yield, Fig. 1. The samples from the SZ-N and SZ-C series exhibited similar catalytic properties when exposed to the most favorable calcination and reaction temperatures, *i.e.*, 500 and 200 °C, respectively, resulting in a more or less comparable isomer yield, given in Fig. 1. Increasing the calcination temperature generally led to a decline in the catalyst activity, except for the sample SZ-H-6, for which a considerable increase in the yield relative to the same sample calcined at 500 °C was registered, Fig. 1. However, the substantially lower activity of the samples of the SZ-H series relative to other two catalyst series of different origin should be emphasized. The product distribution was similar for all tested catalysts regardless of their origin, showing a lack of the highly desirable di-branched isomers, *i.e.*, 2,2- and 2,3-dimethylbutane, with methylpentanes as the major isomers. In the absence of a metallic dehydrogenation function, which produces olefins as intermediates of isoparaffins, direct isomerization of paraffins is possible on acidic sites throughout a carbonium ion, which additionally requires higher reaction temperatures.[17]

TABLE III. Initial activity and s electivity of th e catalys ts as a function of the precurs or and both the calcination and reaction temperatures

Sample	Conversion of *n*-hexane (%)/selectivity to *i*-C_6 (%)	
	200 °C 300	°C
SZ-C-5	14.0/45.8	50.4/11.9
SZ-C-6	13.8/36.8	22.1/13.6
SZ-C-7	0	0
SZ-H-5	0	2.2/90.9
SZ-H-6	4.4/66.4	11.5/26.0
SZ-H-7	0	3.7/87.5
SZ-N-5	20.0/15.4	40.0/22.5
SZ-N-6	3.1/89.8	10.5/21.5
SZ-N-7	6.2/39.4	8.5/38.6
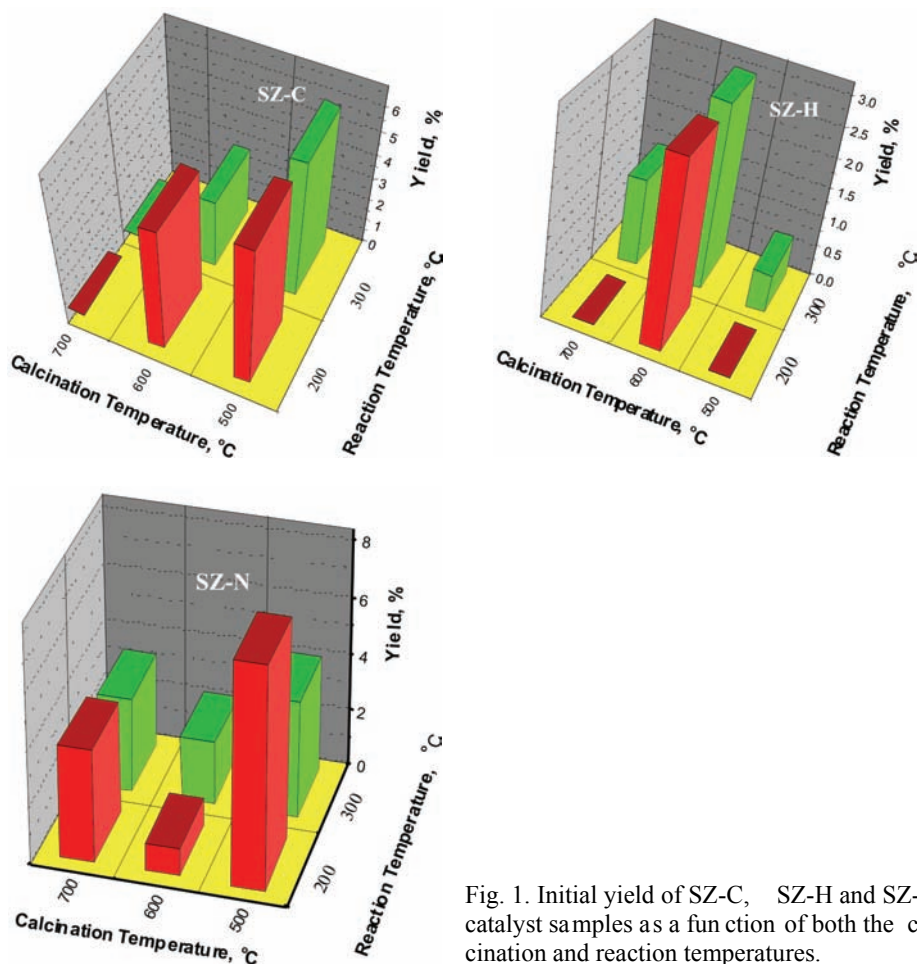
Fig. 1. Initial yield of SZ-C, SZ-H and SZ-N catalyst samples as a fun ction of both the cal-cination and reaction temperatures.

DISCUSSION

All the catalyst sa mples of series SZ-C and SZ-N calcined at the two lower temperatures had high BET surface ar eas, greater th an usually reported in the literature for SZ with the sam e temperature history.[4–7,9,10,12,14,17,18] Samples of the series SZ-H had a low surface area range which was not affected significantly by the pretreatment temperature, Table I. Transformation of the pore structure a s a function of calcination temperature is predictable; the mean pore diameter was doubled whe n the tem perature was increased f rom 500 to 700 °C, indicating a broadening of the pores openings for a ll the investigated sa mples regardless of their origin. This, coupled with the decr ease in the specific surface area, usually indicates the sintering process occurring at higher temperatures.

The volume fraction of the cry stal phases of all samples calcined at 500 °C showed the presence of only the tetragonal zirconia phase, the one which is widely referred to as the a ctive cataly tic phase in the scientific lit erature,[4,5,18–20] Table II. When higher calcination temperatures were applied, both tetragonal and monoclinic phases existed, the last final ly prevailing at 700 °C reg ardless of the catalyst precursor type. This phase tra nsformation was the fastest with the S Z-H catalyst series, showing it s lowest stab ility am ong all the cataly st samples. Fo r example, the SZ sample originating from hydroxide when calcined at 700 °C was left with the lowest tetrag onal phase frac tion, which coincided with its lowest content of sul fates, Table II. This is in agreement with claims that the tetragonal zirconia phase aids the for mation of labile sulfates gi ving the active sites r esponsible for a high *n*-butane isomerization activity.[7] The phase structure of the SZ-H-7 sample, *i.e.*, with the monoclinic phase dom inant, might be responsible for the abundant release of sulfate, which gives no chance f or the sulfates to react wit h the zirconia matrix and consequently provide active sites, Tables II and III. Correspondingly, the prevailing tetragonal phase struct ure of the SZ sy nthesized from the other two precursors (SZ-C and SZ-N) demonstrated values which seem to be fully utilized in terms of cataly tic activity. Quite opposed to this, there was no registered activity for the SZ-C-7 sam ple that still had a consi derable fraction of the tetrag onal phase, im plying that so me other characteristics other than t he SZ phase structure governs the catalytic activity, Tables I–III.

Comparing surface, textural and structural properties of the catalysts, Tabl es I and II, wit h their cataly tic effici ency, Table III and Fig. 1, some correlations might be im posed. Firstly, it is obvious that there is a direct propor tion between the fraction of the tetragonal zirconia p hase and cat alyst activity, however, this property may not be suffic ient to deliver activity, as can be seen f rom the case of sample SZ-C-7. Nam ely, this sam ple, having t he hi ghest fraction of t he tetragonal phase relative to the other samples calcined at the same temperature nevertheless exhibited no cataly tic activity, Table II. Thus, so me other factors, such as the am ount and qualit y of sulfates remain ing o n the sam ples after calcination,

might be equally or even more responsible for the efficiency of the cataly sts. After calcination, the remaining sulfate groups stay embedded in the zirconia matrix and form certain densi ties of sulfates on the surface,[13] which might require a minimal value to act as catalytically active sites. Finally, the surface acid strength may also play a vital role in determining the catalytic efficiency of the samples.

It was recently fo und t hat the acidic strength of residual Lewis acidic sites (coordinative unsaturated site Zr^{4+} in the vicinit y of sulfate groups) was significantly en hanced b y sulfation, provided that the sample had been calcined at a proper temperature.[21] In fact, active sites are claimed to have been created throug h the selective elimination of sulfates loc ated on the side ter minations of the cry stallites following tetragonal phase formation only as a coincidence. [5] Other a uthors also indicated the importance of la bile sulfate groups for activity. However, they assum ed the formation of active s ites on both monoclinic and tetragonal phases of SZ, the latter case resulting in pr eferentially higher concentrations of such sites. [7] In addition, t he procedure of the calcination step seems to be important. Thus sulfate decom position providing an adequate contac t time between the released SO_3 and zirconia is a necessity for the formation of active sites.[22]

Contrary to s ome zirconia sa mples, sul fated by a procedure si milar to that applied in thi s work, in which the am ount of incorporated sulfate s we re directly proportional t o the surface area of the SZ, [20] all the samples investigated in this study had the same amount of sulfates, *i.e*., 4.2 mass % , Table II. This and the dynamics of sulfate re moval during calcination at a particular temperature we re calculated from TG data reported earlier. [13] In contr ast to the same am ount o f initial sulfates, their stabil ity was quite different, which, togethe r with textural and structural properties, as w ell as th e magnitude of the applied calcination temperature determined the formation of the active phase resulting in catalyst activity, Tables I–III. The loss of a significant fraction of the sulfates in a single calcination step at the lower te mperature may not re sult in the same activity , as can be s een from the c ases of the SZ- N-5 and SZ-H-5 sa mples. Obviously, sulfates of si milar stability behave differen tly depending on their environm ent defined by its textural rather than its stru ctural characteristics. Namely, the presence of the full amount of tetragonal zirconia phase in both samples calcined at 500 °C did not guara ntee the same activity output, as seen fr om Tables II and III. Thus, the superior activity perfo rmance of the SZ-N-5 sam ple might be the conse - quence of its good textural properties (high specific surface area), providing conditions for the re-adsorption of S-containing species on the zirconia matrix, their interaction and active sites formation. The textural properties of the samples from the SZ-H s eries required, however, higher te mperatures for the same mechanism of active sites formation. Since there w as no extra s ulfate removal when the ca l-cination temperature differed by 100 °C (co mparison of the sample SZ-H-6 an d SZ-H-5), as s hown in Table II, a question arises as t o the origin of the cataly tic

activity of the SZ-H sa mple exposed to the higher te mperature. Obviously, the magnitude of the calcination tem perature has to be a co mpromise between the dynamics of sulfate deco mposition and the rate of interaction of the released S-containing species and the zirconia host. While for the SZ-N series 500 °C was the preferential tem perature, for their c ounterparts fr om the hy droxide series, a minimum of 600 °C was required for both processes to occur si multaneously. Thus, the same fraction o f sulfates was liberated at 600 an d 500 °C, however, at the higher temperature, the sulfates underwent interaction with the zirconia h ost, formed active sites and the SZ-H-6 sam ple perfor med with satisfactory activity for this particular series, T able III. The behavior of SZ-C-5, showing at the same time no sulfate release and the maximal activity, casts doubts on the association of the release of labile sulfate groups with the formation of the active phase. However, the sulfating procedure and, possibly, s ome additional stabilizati on process during sulfation re main unrevealed by the manufacturer of the SZ-C series. This fact makes comparison with samples of this series partly impossible, at least when the sulfating agent and sulfating proc edure are concerned. How- ever, the same original sulfate loading as in the cases of the cataly sts of other origin makes all of them interesting for co mparing the i mpact of temperature on the dynamics of sulfate release. It has to be understood, however, t hat the release of a s mall fr action of the sulfates, as i n the favorable cas es of the SZ-N serie s, does not necessarily mean the presence of inactive sulfates. Again, it is a conse- quence of the sy nergistic effect of the calcination te mperature and prefera ble textural properties allowing the released sulfates to interact with the zirconia host thereby forming active centers for iso merization. The magnitude of the calcina- tion temperature is nevert heless one of the main fac tors deter mining the forma - tion of t he active phase; thus 700 °C i s too high tem perature regardless of the sample origin, leaving in all cases, exce pt in the case of SZ-N-7, amounts of sul- fates lower than the critical value necessary to contribute to the activity.

The sulfates density has been considere d in the past as a clue for the expla- nation of t he activity of S Z.[23] Considering this characteristi c in the case of the SZ-N series, it seems, however, that the sulfate density is not a cr ucial factor for SZ-catalyst a ctivity, at lea st not in a w ay the density of sulfates was defined [14] and calculated in the present work, Tabl es II and III, Fig. 1. Namely , from the textural chara cteristics of the whole series of SZ-N s amples, it se ems that so me fraction of su lfates located within the zi rconia matrix can participate in the cata- lytic reaction once there are pores of certain openin gs and volume providin g the environment for the operation of the active sites. Indeed, the mean pore diameters and total por e volumes of the series of SZ-N samples leave roo m for such a spe- culation, giving recognition to the textural characteristics of a cata lyst as the pre- vailing factor in determ ining its cataly tic properties.[11] Accordingly, the consid e- rable sulfate density obtained for the only active catalyst in hydroxide series, *i.e.*,

the SZ-H-6 s ample, is just a coincidenc e due to the low surface area of all the SZ-H series. The previously mentioned mechanism of sulfate relea se at a certai n temperature preceding the interaction is equally valid, requiring a critical mini-mal amount of sulfate to r eact with the zirconia host and form acti ve sites. From Fig. 2, a d irect correlation between sulfate loading and the am ount of tetragon al SZ phase can be assumed, while the sulfate density function is ambiguous. Given the fact that t he specific s urface ar ea d irectly contributes to the sulfates density calculation, the latter indi cates that the textural properties of SZ, although f ol-lowing the same tem perature dependence, ar e not directly correlated to its phase structure.
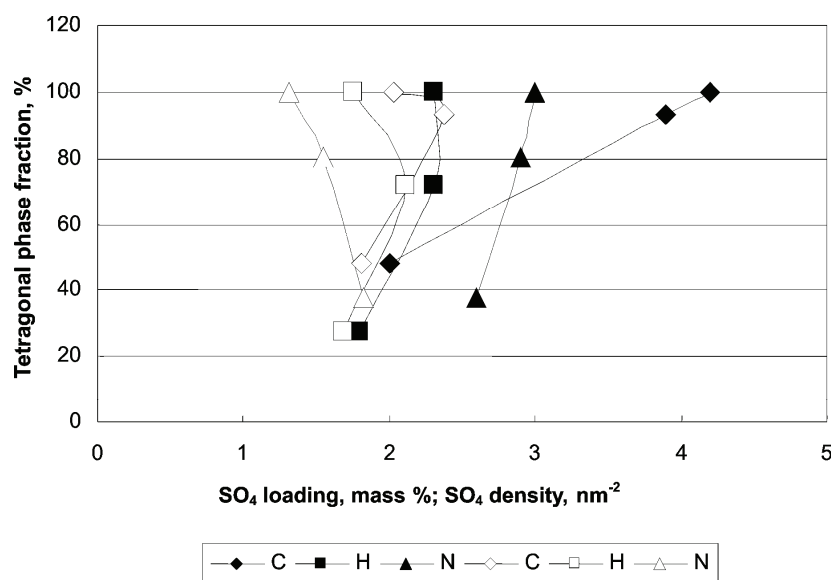
Fig. 2. Sulfate loading (filled patterns) and sulfate density (empty patterns) as a function of the fraction of tetragonal phase in the SZ.

From the ap plied Hammett indicators, althou gh c overing a quite m odest range of acidity, some interesting points can be extracted. First of all, there is the peculiar behavior of the S Z-C series of samples exhibiting two extrem es: sample SZ-C-5 showing t he highest and sam ple SZ-C-7 the l owest acid strength am ong all the sa mples.[15] Simultaneously, the d ynamics of sulfates rem oval during cal-cination showed the full amount of remaini ng sulfates in the sample calcined at 500 °C and one of the lowest sulfate loading for its counterpart exposed to 700 °C. While the dynamics of sulfate removal relative to the acid–base pr operties is dif-ficult to discuss due to th e unknown (post)sulfating procedure in this particular series, the acid strength of the SZ-C samples directly reflects the am ount of re-maining sulfate. The acid s trength correlation for the other series i s rather diffi-

cult. Thus, the nitrate and hydroxide samples calcined at 600 °C exhibited similar activities and had m ore or less equal a cid strength, the first, however, having a significantly higher am ount of rem aining sulfates and simultaneously the lowest sulfate density.

The quite irregular catalytic behavior of the applied samples in terms of their structural, te xtural and surface properti es i mposes t he considerat ion of the pre-sence of acid sites of different nature as being partly responsible for differences in cataly tic activity . The results of so me investigat ions advocate the pres ence both Brønste d (BAS) and Lewis a cid site (LAS) o n SZ. These sites being of different acid strength would, consequently, have different abilities for the isome-rization of linear or branched alkanes.[24] The FTIR spectra of s everal samples are given in Fig. 3, which sh ow different bands of previousl y adsor bed p yridine.
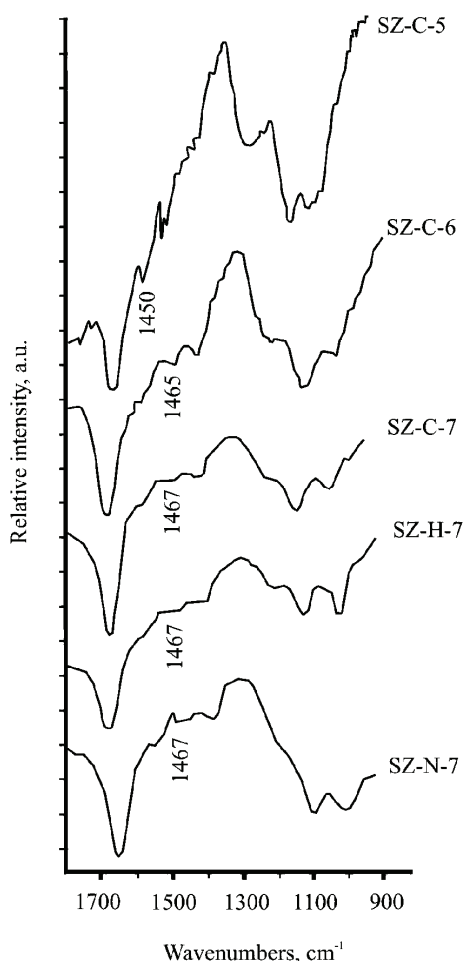
Fig. 3. FTIR Spectra of py ridine pre-adsorbed on the SZ sa mples as a functio n of origin and calcination temperature: a) ZS-C-5; b) SZ-C-5; c) SZ-C-5; d) SZ-H-7 and e) SZ-N-7.

From the literature, in most instances, the band around 1540 cm^{-1} is assumed to be characteristic for a pyridinium ion sitting on BAS, while bands between 1445 and 1460 cm^{-1} are attributed to pyridine coordinative adsorbed on a LAS.[25] According to literature data,[26,27] the formation of both BAS and LAS is connected to surface bonded sulfate groups imposing electron shifts and changes in the electron densities in the proximity of Z^{4+}, as shown in Fig. 4. In contrast, other authors see LAS not sitting on the zirconia matrix but on S-additive, comprising both ionic, S–O–Zr, and coordination, S=O, bonds.[28] According to the FTIR spectra shown in Fig. 3, there is a direct correlation between the activities of the catalyst samples and presence of acidic centers of different nature, as well as the acid strength of the samples given in Table II. Namely, the band at 1450 cm^{-1} witnesses the presence of BAS in the sample with the highest acid strength, Table II, while the band at 1466 cm^{-1} indicates the presence of LAS, the concentration of which rapidly decrease with increasing calcination temperature. Other results from the literature claim, however, that the acid strength of BAS is lower than that of LAS,[29] but the temperature history of the catalysts was quite different from that applied in the present investigation. Some other studies, nevertheless, do report on the importance of the presence of strong BAS in SZ in order to obtain high catalytic activity in reaction with *n*-heptane.[30] In any case, the obtained distribution of the isomeric products, *i.e.*, mainly mono-branched hydrocarbons at the expense of the more desirable 2,2- and 2,3-dimethylbutane, indicates a monomolecular isomerization mechanism, including the carbenium ion.[24]
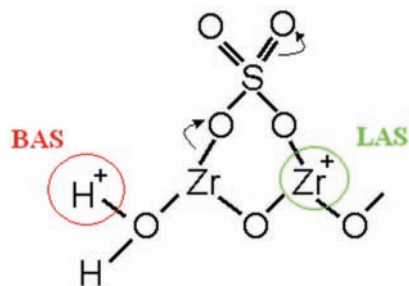
Fig. 4. Model of the BAS and LAS formed upon sulfate incorporation into the zirconia matrix.[26,27]

CONCLUSIONS

The presence of the tetragonal phase of zirconia probably only coincides with the real formation of the active phase as a consequence of zirconia phase transformation at the calcination temperature being responsible for the development of the active phase at the first place. The existence of thermally labile sulfates in the zirconia matrix is a necessity for active phase formation; however, it must be coupled with preferable textural properties. A large surface area and total pore volume, as well as larger pore openings, provide the environment for the formation and operation of effective active sites. The magnitude of the calci-

nation temperature has to be a co mpromise between the dy namics of sulfate decomposition and the rate of interaction of the rel eased S-containing species and the zirconia host in order for an active phase to be formed. The active phase might partly include acidic cent ers of Brønsted and Lewis nature initiated by incorporation of S-c ontaining species into the zi rconia host. However, some critical su lfate loading above 2 mass % is required for catalytic activity in the *n*-hexane isomerization reaction under the conditi ons a pplied in this work.   Nonetheless, it seems difficu lt to correlate sulfate densi ty with cataly tic activity , indicating tha t the catalytic activity is a complex function of textural and surface (acid strength) characteristics of the samples.

ИЗВОД

СИНЕРГИЗАМ ТЕКСТУРАЛНИХ И ПОВРШИНСКИХ СВОЈСТАВА СУЛФОНОВАНОГ КАТАЛИЗАТОРА НА БАЗИ ЦИРКОНИЈУМ-ОКСИДА ПРОУЗРОКОВАН ТЕМПЕРА-ТУРОМ И ЊЕГОВ УТИЦАЈ НА АКТИВНОСТ КАТАЛИЗАТОРА У РЕАКЦИЈИ ИЗОМЕРИЗАЦИЈЕ

АЛЕКСАНДРА ЗАРУБИЦА[1], БРАНИСЛАВ ЈОВИЋ[2], АЛЕКСАНДАР НИКОЛИЋ[2], ПАУЛА ПУТАНОВ[3] и ГОРАН БОСКОВИЋ[1]

[1]*Технолошки факулѿеѿ, Универзиѿеѿ у Новом Саду, 21000 Нови Сад,* [2]*Природно−маѿемаѿички факулѿеѿ, Дейарѿман за хемију, Универзиѿеѿ у Новом Саду, 21000 Нови Сад и* [3]*Срйска академија наука и умеѿносѿи, 11000 Беоѓрад*

Коришћењем сумпорне киселине као агенса за сулфоновање, синтетисане су две серије катализатора из хидроксидног и нитратног прекурсора са идентичним садржајем сулфата од 4,2 mas. %.   Исти садржај сулфата установљен је и у сулфонованом цирконијум-оксиду комерцијалног порекла, који је чинио основу за трећу серију узорака. Након калцинације на 500, 600 и 700 °C, девет узорака катализатора садржали су различите количине сулфата у зависности од примењене температуре и порекла катализатора. Као резултат, њихова површинска својства се разликују, и заједно са текстуралним својствима воде формирању активне фазе у различитом степену, а самим тим и различитој активности у тест реакцији изомеризације нормалног хексана. Највећа активност и највећи принос, превасходно моно-разгранатих изомера, постиже се на температури од 200 °C у случају примене комерцијално синтетисаног сулфонованог ZrO$_2$ калцинисаног на 500 °C. Узимајући у обзир следеће две серије катализатора, добијене из хидроксида и нитрата, ова друга је по свом профилу активности ближа комерцијално сулфонованом узорку, док узорци који за прекурсор имају хидроксид показују веома ниску активност, али тек након калцинације на 600 °C. Ова ниска активност одговара најнеповољнијим текстуралним својствима ове серије катализатора, а последица је веће температуре калцинације потребне за симултану разградњу сулфатних врста, њихове реадсорпције на матрици цирконијум-оксида, и на крају интеракције са њом и настанак активне фазе. Намеће се закључак да тетрагонална фаза сама по себи није одговорна за каталитичку активност, већ да синергија текстуралних и површинских својстава, одређених садржајем сулфата, одређује јачину активних центара катализатора, а тиме и интензитет његове активности.

(Примљено 15. октобра, ревидирано 29. октобра 2009)

REFERENCES

1. I. E. Maxwell, J. E. Naber, K. P. De Jong, *Appl. Catal. A: General*. **113** (1994) 153
2. G. Bošković, R. Mićić, P. Pavlović, P. Putanov, *Catal. Today* **65** (2001) 123
3. T. Yamaguchi, *Appl. Catal. A* **222** (2001) 237
4. J. M. Parera, *Catal. Today* **15** (1992) 481
5. C. Morterra, G. Cerrato, M. Signoretto, *Catal. Lett*. **41** (1996) 101
6. C. Morterra, G. Cerrato, S. Di Ciero, M. Signoretto, F. Pinna , G. St rukul, *J. Catal.* **165** (1997) 172
7. X. Li, K. Nagaoka, R. Olindo, J. A. Lercher, *J. Catal.* **238** (2006) 39
8. A. Zarubica, P. Putanov, G. Boskovic, *J. Serb. Chem. Soc.* **72** (2007) 679
9. G. D. Yadav, J. J. Nair, *Micropor. Mesopor. Mater.* **33** (1999) 1
10. A. Corma, J. M. Serra, A. Chica, *Catal. Today* **81** (2003) 495
11. G. Bošković, A. Zarubica, P. Putanov, *J. Optoelect. Adv. Mater.* **9** (2007) 2251
12. H. Matsuhashi, H. Nakamura, T. Ishihara, S. Iwamoto, Y. Kamiya, J. Kobayashi, Y. Ku-bota, T. Ya mada, T. Mat suda, K. Mat sushita, K. Nakai, H. Nishi guchi, M. Ogura, N . Okazaki, S. Sato, K. Shi mizu, T. Shishido, S. Yamazoe, T. Takeguchi, K. Tomishige, H. Yamashita, M. Niwa, N. Katada, *Appl. Catal. A* **360** (2009) 89
13. G. C. Bošković, A. R. Zarubica, M. N. Kova čević, P. S. Putanov, *J. Therm. Anal. Cal*. **91** (2008) 849
14. K. Föttinger, G. Kinger, H. Vinek, *Appl. Catal. A* **266** (2004) 195
15. K. Tanabe, *Solid Acid and Base Catalysts, Catalysis: Science and Technology*, J . R. Anderson, M. Boudart, Eds., Springer-Verlag, Berlin, 1981, p. 231–273
16. A. R. Zarubica, M. N. Miljković, E. E. Kiss, G. C. Bošković, *React. Kinet. Catal. Lett.* **90** (2007) 145
17. P. A. Jacobs, J. A. Martens, *Stud. Surf. Sci. Catal.* **58** (1991) 445
18. M. Benaissa, J. G. Santiesteban, G. Diaz, C. D. Chang, M. Jose-Yacaman, *J. Catal.* **161** (1996) 694
19. M. Signoretto, F. Pinna, G. St rukul, P. Chie s, G. Cerrato, S. Di Ciero, C. Morterra, *J. Catal.* **167** (1997) 522
20. J. B. Laizet, A. K. Søiland, J. Leglise, J. C. Duchet, *Top. Catal.* **10** (2000) 89
21. V. Bolis, G. Magnacca, G. Cerrato, C. Morterra, *Top. Catal.* **19** (2002) 229
22. X. Li, K. Nagaoka, L. J. Simon, R. Olindo, J. A. Lercher, *Catal. Lett.* **113** (2007) 34
23. F. R. Chen, G. Coudurier, J. F. Joly, J. C. Vedrine, *J. Catal.* **143** (1993) 616
24. T. Wakayama, H. Matsuhashi, *J. Mol. Catal. A: Chem.* **239** (2005) 32
25. J. A. Lercher, C. Gründling, G. Eder-Mirth, *Catal. Today* **27** (1996) 353
26. T. Yamaguchi, K. Tanabe, Y. C. Kung, *Mater. Chem. Phys.* **16** (1986) 67
27. K. Arata, M. Hino, *Mater. Chem. Phys.* **26** (1990) 213
28. M. Hino, M. Kurashige, H. Matsuhashi, K. Arata, *Thermochim. Acta* **441** (2006) 35
29. N. Katada, J. E ndo, K. Not su, N. Yasunobu, N. Naito, M. Niwa, *J. Phys. Chem. B* **104** (2000) 10321
30. N. Katada, T. Tsubaki, M. Niwa, *Appl. Catal. A* **340** (2008) 76.

Electrochemical detection of carbidopa using a ferrocene-modified carbon nanotube paste electrode

HALIMEH YAGHOUBIAN[1], HASSAN KARIMI-MALEH[2*],
MOHAMMAD ALI KHALILZADEH[2] and FATEMEH KARIMI[2]

[1]Islamic Azad University, Branch of Bam, Bam and [2]Department of Chemistry, Islamic Azad University, Qaemshahr, Iran

Abstract: A chemically modified carbon paste electrode (MCPE) containing ferrocene (FC) and carbon nanotubes (CNT) was constructed. The electrochemical behavior and stability of the MCPE were investigated by cyclic voltammetry. The electrocatalytic activity of the MCPE was investigated and it showed good characteristics for the oxidation of carbidopa (CD) in phosphate buffer solution (PBS). A linear concentration range of 5 to 600 μM CD, with a detection limit of 3.6±0.17 μM CD, was obtained. The diffusion coefficient of CD and the transfer coefficient (α) were also determined. The MCPE showed good reproducibility, remarkable long-term stability and especially good surface renewability by simple mechanical polishing. The results showed that this electrode could be used as an electrochemical sensor for the determination of CD in real samples, such as urine samples.

Keywords: carbidopa; ferrocene; carbon nanotube; modified electrode; voltammetry.

INTRODUCTION

Carbon nanotubes (CNTs) are new kinds of porous nanostructured carbon materials, which are promising as immobilization substances because of their significant mechanical strength, excellent electrical conductivity, high surface area and good chemical stability.[1] CNTs can be used to promote electron transfer reactions when used as electrode materials in electrochemical devices, in electrocatalysis and electroanalysis processes due to their significant mechanical strength, high electrical conductivity, high surface area, good chemical stability, as well as relative chemical inertness in most electrolyte solutions and a wide operation potential window.[2–5] Both redox mediators and CNTs exhibited excellent electrochemical performance for the fabrication of sensors or biosensors. Synergistic ef-

1443

fects in the enhanced current response were observed when both CNTs and redox mediators were employed.[6,7]

Parkinson's disease victims show a significant depletion of dopamine in the brain. Since this neurotransmitter can not cross the blood–brain barrier into the central nervous system and it can not be employed to restore its normal level, levodopa (LD) (a precursor of dopamine) has been successfully used and is the most widely prescribed drug for the treatment of such patients.[8] After its administration, LD is converted into dopamine *via* an enzymatic reaction catalyzed by dopa-decarboxylase.

However, since the metabolism of LD is also extra cerebral, several side effects of systemic dopamine can arise if LD is administered in high dosages. In order to achieve better a therapeutic effect and lower toxicity, CD is administered in association with LD in pharmaceutical preparations, which contain 10–25 % CD. This catecholamine acts as an inhibitor for the decarboxylase activity.[8] Hence, a combination of LD with CD leads to a control of the dopamine concentration at suitable levels, reducing the side effects and improving the efficiency of the therapy.

Accordingly, the development of an analytical method is very important to control the content of these catecholamines in pharmaceuticals. Different techniques have been employed for the determination of CD in pharmaceutical formulations.[9–15] Long analysis times, the use of organic solvents and high costs are some of the drawbacks associated with these techniques. Voltammetry is considered an important electrochemical technique utilized in electroanalytical chemistry because it provides low cost, sensitivity, precision, accuracy, simplicity and rapidity.[16–18]

To the best of our knowledge, no study has reported the electrocatalytic determination of CD using carbon nanotube paste electrodes. In addition, no paper has reported FC as a catalyst for the electrocatalysis of CD. Thus, in continuation of studies concerning the preparation of chemically modified electrodes,[19–22] in this paper, initially the preparation and suitability of a FC modified carbon nanotube paste electrode (FCMCNPE) as a new electrocatalyst in electrocatalysis and the determination of CD in an aqueous buffer solution are described. Finally, in order to demonstrate the catalytic ability of the modified electrode in the electro--oxidation of CD in real samples, this method was examined for the voltammetric determination of CD in urine samples.

EXPERIMENTAL

Apparatus and reagents

All the cyclic voltammetric measurements were performed using a BHP 2063[+] electrochemical analysis system, Behpajooh, Iran, comprising the potentiostat/galvanostat coupled with a Pentium IV personal computer connected to a HP laser jet 6L printer.

An Ag/AgCl/3 M KCl, a platinum wire, and a FCMCNPE were used as the reference, auxiliary and working electrodes, respectively. A digital pH/mV-meter (Metrohm model 710)

was applied for pH measurements. Graphite fine powder, paraffin oil and reagents were analytical grade from Merck. CD was purchased from Merck. Multi-walled carbon nanotubes (purity more than 95 %) with *o.d.* between 10 and 20 nm, *i.d.* between 5 and 10 nm and tube length from 0.5 to 200 nm were prepared by Nanostructured & Amorphous Materials (USA). The buffer solutions were prepared from orthophosphoric acid and its salts in the pH range 2.0–11.0.

Preparation of the electrode

Modified carbon nanotube paste electrodes were prepared by dissolving 0.010 g of FC in diethyl ether and hand mixing with 89-times its weight of graphite powder and 10-times its weight of carbon nanotubes with a pestle and mortar. The solvent was evaporated by stirring. A 70:30 (w/w) mixture of FC spiked carbon nanotube powder and paraffin oil was blended by hand mixing for 20 min until a uniformly-wetted paste was obtained. The paste was then packed into the end of a glass tube (*ca.* 2 mm *i.d.* and 10 cm long). Electrical contact was made by inserting a copper wire into the glass tube at the back of the mixture. When necessary, a new surface was obtained by pushing an excess of paste out of the tube and polishing it on a weighing paper. Unmodified carbon paste, prepared in the same way but without the addition of FC and carbon nanotubes to the mixture, was used for comparison purposes.

Preparation of a real sample

The urine sample was stored in a refrigerator immediately after collection. Ten milliliters of the sample was centrifuged for 10 min at 1000 rpm. The supernatant was filtered through a 0.45 μm filter and then diluted 10-times with 0.10 M phosphate buffer solution (pH 7.0). The solution was transferred into a voltammetric cell to be analyzed without any further pretreatment. The standard addition method was used for the determination of CD in real samples.

RESULTS AND DISCUSSION

Electrochemical behavior of the FCMCNPE

Cyclic voltammetry was employed for the investigation of the electrochemical properties of the FCMCNPE in a pure buffered aqueous solution (pH 7.0). The cyclic voltammogram (Fig. 1) exhibits an anodic and corresponding cathodic peaks with $E_{pa} = 0.370$ V and $E_{pc} = 0.265$ V *vs.* Ag/AgCl/3 M KCl. The experimental results showed well-defined and reproducible anodic and cathodic peaks related to the FC/FC$^+$ redox couple with quasi-reversible behavior, because the peak separation potential, $\Delta E_p = (E_{pa} - E_{pc})$, was greater than the 59/n mV expected for a reversible system. In addition, the result obtained from cyclic voltammetry of this modified electrode in various buffered solutions did not show any shift in the anodic and cathodic peak potentials. Therefore, the electrochemical behavior of the redox process of FC/FC$^+$ in the FCMCNPE is independent of the pH of the aqueous solution.

The capability of the electrode for the generation of a reproducible surface was examined by cyclic voltammetric data obtained in the optimum solution pH from five separately prepared FCMCNPEs (Table I). The calculated RSDs for various parameters accepted as the criteria for a satisfactory surface reproduce-

bility were 1–4 %. This degree of reproducibility is virtually the same as that expected for a renewed or ordinary carbon paste surface.
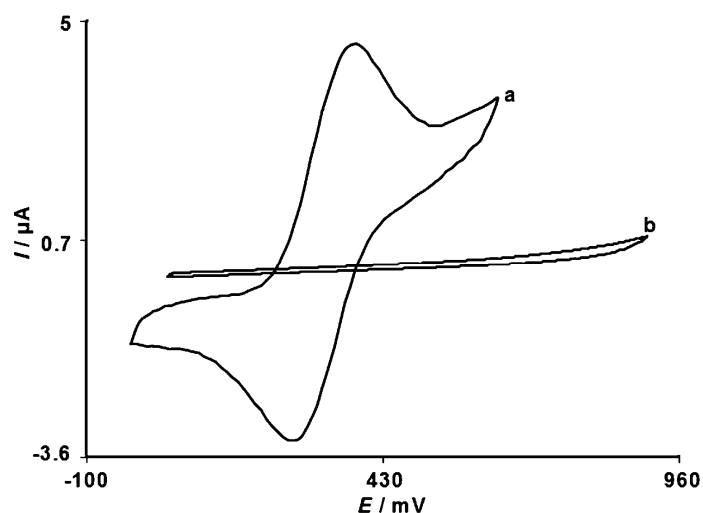
Fig. 1. Cyclic voltammograms of a) FCMCNPE and b) bare CPE in 0.1 M PBS (pH 7.0) at a scan rate 20 mV s⁻¹.

In addition, the long term stability of the FCMCNPE was tested over a three--week period. Cyclic voltammetry of the CD at the surface of the FCMCNPE after the modified electrode had been stored under ambient conditions showed that the oxidation peak potential of the CD was unchanged and the anodic peak current was only decreased by less than 2.1 % of the initial oxidation peak current. The antifouling properties of modified electrode toward CD and its oxidetion product were investigated by recording the cyclic voltammograms of this modified electrode before and after using in the presence of CD.

TABLE I. Cyclic voltammetric data obtained for the constructed FCMCNPE in 0.10 M PBS (pH 7.0) at 20 mV s⁻¹([a]: *vs.* Ag/AgCl/3 M KCl as the reference electrode; [b]: the values in parenthesis indicate the calculated *RSD*)

E_{pa} / V [a]	E_{pc} / V [a]	$E_{1/2}$ / V [a]	ΔE_{pa} /V [a]	I_{pa} / μA	I_{pc} / μA	Γ_a / mol cm⁻²	Γ_c / mol cm⁻²
0.370	0.265	0.3175	0.105	4.55	3.27	1.85×10^{-9}	1.45×10^{-9}
(0.75) [b]	(0.67) [b]	(0.78) [b]	(0.81) [b]	(2.45) [b]	(2.12) [b]	(3.4) [b]	(2.8) [b]

The cyclic voltammetry of the CD at the surface of the FCMCNPE after 10 repetition cycles at a scan rate of 20 mV s⁻¹ showed that the oxidation peak potential of CD was not changed and the anodic peak current was decreased by less than 3.3 %. However, it should be emphasized that the surface of the FCMCNPE was regenerated before each experiment.

Available online at www.shd.org.rs/JSCS/

Optimization of the pH of the solution

The electrochemical behavior of CD is dependent on the pH value of the aqueous solution, whereas the electrochemical properties of the FC/FC$^+$ redox couple are independent of pH. Therefore, pH optimization of the solution seemed to be necessary in order to realize the electrocatalytic oxidation of CD. Thus, the electrochemical behavior of CD in 0.10 M phosphate buffer solutions of different pH values (2.0 < pH < 11.0) at the surface of the FCMCNPE by cyclic voltammetry was examined. It was found that the electrocatalytic oxidation of CD at the surface of the FCMCNPE was more favored under neutral conditions than in acidic media. This appears as a gradual growth in the anodic peak current and a simultaneous decrease in the cathodic peak current in the cyclic voltammograms recorded at the surface of the FCMCNPE. The results showed that the anodic peak potential of CD at the surface of the FCMCNPE was shifted to a less-positive potential. In addition, the anodic peak current and the shifted potential value for the electro-oxidation of CD are high at physiological pH values. Thus, pH 7.0 was chosen as the optimum pH for electrocatalysis of CD oxidation at the surface of the FCMCNPE.

Electrochemistry of CD at the FCMCNPE

The cyclic voltammetric responses from the electrochemical oxidation of 250 μM CD at the FCMCNPE (curve f), the FC modified CPE (FCMCPE) (curve e), CNPE (curve d) and the bare CPE (curve a) are depicted in Fig. 2. As can be seen, the anodic peak potentials for the oxidation of CD at the FCMCNPE (curve f) and the FCMCPE (curve e) are about 370 mV, while at the CNPE (curve d), the peak potential is about 720 mV and at the bare CPE (curve b), the peak potential is about 750 mV for CD. From these results, it was concluded that the best electrocatalytic effect for CD oxidation was observed at the FCMCNPE (curve f). For example, the results showed that the peak potential of CD oxidation at the FCMCNPE (curve f) shifted by about 350 and 380 mV toward negative values compared with that at the CNPE (curve d) and the bare CPE (curve b), respectively. Similarly, when the oxidation of CD at the FCMCPE (curve e) and the FCMCNPE (curve f) are compared there is a dramatic enhancement of the anodic peak current at the FCMCNPE relative to the value obtained at the FCMCNPE. In the other words, the obtained data clearly showed that the combination of carbon nanotubes and mediator (FC) definitely improve the characteristics of CD oxidation. The FCMCNPE in 0.10 M phosphate buffer (pH 7.0) without CD in the solution exhibited a well-behaved redox reaction (curve c) upon the addition of 250 μM CD, the anodic peak current of mediator was greatly increased, while the corresponding cathodic peak disappeared on the reverse scan of the potential (curve f). This behavior is typical of that expected for electrocatalysis at chemically modified electrodes.[23]
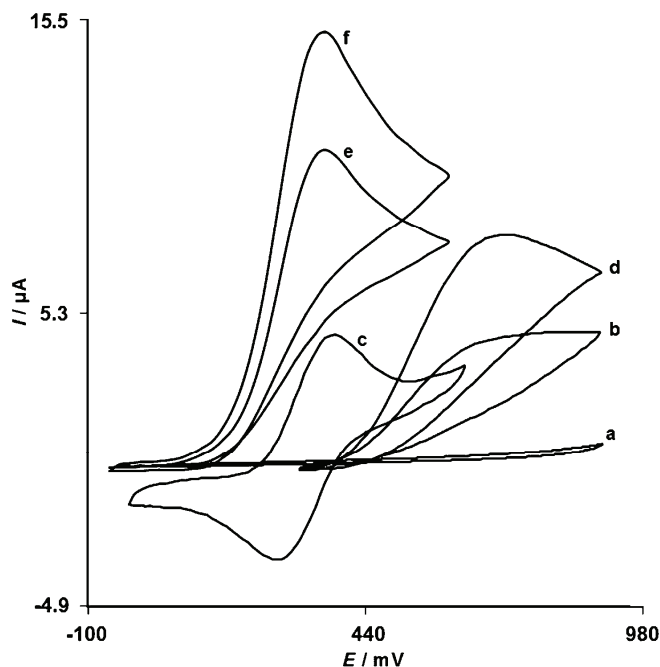
Fig. 2. Cyclic voltammograms of a) CPE in 0.1M PBS (pH 7.0) at a scan rate 20 mV s^{-1} and b) as a) + 250 μM CD; c) as a) and d) as b) at the surface of the FCMCNPE and CNPE, respectively; e) and f) as b) at the surface of the FCMCPE and FCMCNPE, respectively.

The effect of scan rate on the electrocatalytic oxidation of 250 μM CD at the FCMCNPE was investigated by cyclic voltammetry. The oxidation peak potential shifted with increasing scan rate towards more positive potentials, confirming the kinetic limitation of the electrochemical reaction. In addition, a plot of peak height (I_p) against the square root of the scan rate ($v^{1/2}$) was linear in range of 10–90 mV s^{-1} (Fig. 3A, curve a), suggesting that at a sufficient overpotential, the process is diffusion rather than surface controlled. A plot of the sweep rate normalized current ($I_p/v^{1/2}$) *vs.* sweep rate (Fig. 3A, curve b) exhibited the characteristic shape typical of an EC$_{cat}$ process.

From the slope of the E_p *vs.* log v curve, as shown in Fig. 3B, curve b, the Tafel slope can also be obtained from the following equation:[24]

$$E_p = (b/2) \log v + \text{constant} \qquad (1)$$

The slope of E_p *vs.* log v plot is $b/2$, where b indicates the Tafel slope. The slope of the E_p *vs.* log v plot is $\partial E_p/\partial(\log v)$, which was found to be 0.050 V in this work; hence, $b = 2 \times 0.050 = 0.100$ V. The value of Tafel slope indicates that a one-electron transfer process is the rate limiting step assuming a transfer coefficient, α, of about 0.41.

A Tafel plot constructed from data of the rising part of the current–voltage curve recorded at a scan rate of 20 mV s^{-1} is shown in Fig. 3B, curve a. This part of the voltammogram, known as the Tafel region, is affected by the kinetics of the electron transfer between CD and FC, assuming deprotonation of the substrate is a sufficiently fast step. Under this condition, the number of electrons involved in the rate determining step can be estimated from the slope of the Tafel plot. A slope of 0.100 V dec^{-1} was obtained, indicating that a one electron transfer is rate limiting assuming a transfer coefficient of $\alpha = 0.41$.
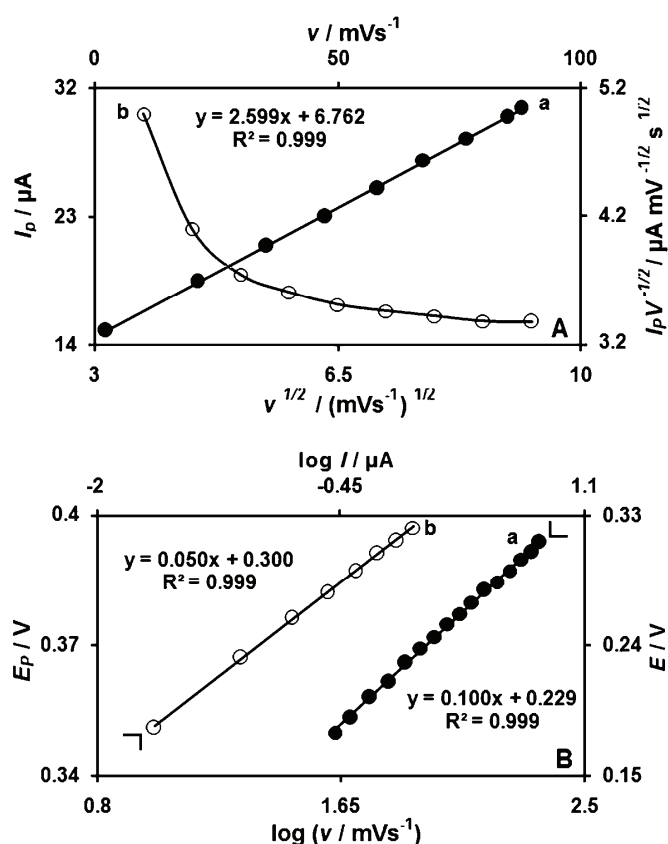
Fig. 3. A) Curve a, variation of the electrocatalytic current (I_p) with the square root of scan rate and curve b, variation of the scan rate- normalized current ($I_p/v^{1/2}$) with scan rate; B) curve a, Tafel plot derived from the rising part of the voltammogram recorded at a scan rate 20 mV s^{-1} and curve b, plot of E_p vs. log v.

Chronoamperometric studies

The catalytic oxidation of CD by a FCMCNPE was also studied by chronoamperometry. Chronoamperometric measurements of different concentrations of

CD at the FCMCNPE were performed by setting the working electrode potential at 450 mV. From the chronoamperometric studies, we have determined the diffusion coefficient, D, of CD was determined. The experimental plots of I *vs.* $t^{-1/2}$ with the best fits for different concentrations of CD were employed. The slopes of the resulting straight lines were then plotted *vs.* the CD concentration. From the slope of the resulting plot and using the Cottrell Equation:[20]

$$I = nFAD^{1/2}c_b\pi^{-1/2}t^{-1/2} \qquad (2)$$

a diffusion coefficient of $(2.65\pm0.4)\times10^{-6}$ cm^2 s^{-1} was determined for CD.

Calibration plot and limit of detection

Differential pulse voltammetry was used to determine the concentration of CD (Fig. 4A). The responses were linear with CD concentration in the range from 5.0×10^{-6} to 6.0×10^{-4} M and the current sensitivity was 0.0414 µA/µM (Fig. 4B). The detection limit (3σ) was 3.6 ± 0.17 µM.
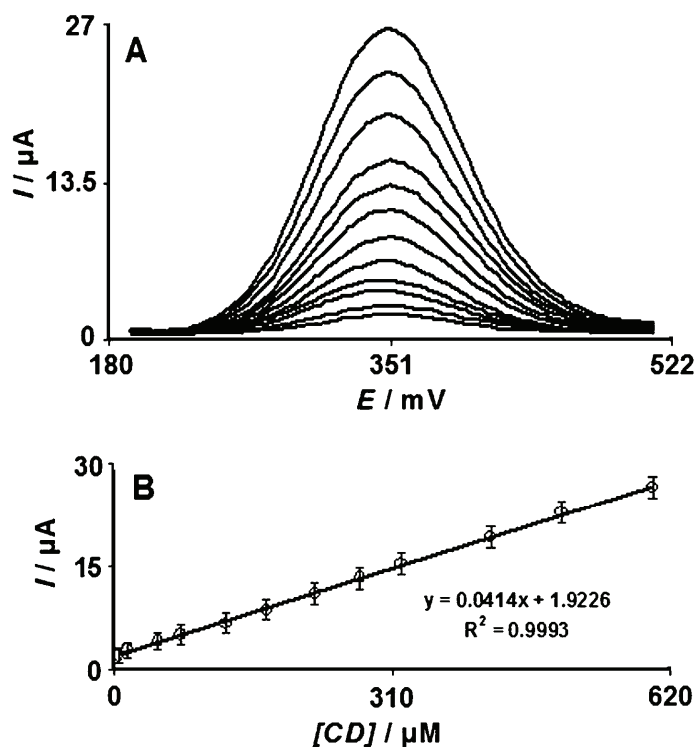
Fig. 4. A) Differential pulse voltammograms of the FCMCNPE in 0.10 M PBS (pH 7.0) containing different concentrations of CD, from inner to outer corresponding to 5, 15, 50, 75, 125, 170, 225, 275, 320, 420, 500 and 600 µM of CD; B) plots of the electrocatalytic peak current as a function of CD concentration.

Interference studies

The influence of various substances as compounds potentially interfering with the determination of CD was studied under optimum conditions with 10 μM CD at pH 7.0. The potentially interfering substances were chosen from the group of substances commonly found with CD in pharmaceuticals and/or in biological fluids. The tolerance limit was defined as the maximum concentration of the interfering substance that caused an error of less than ±5 % in the determination of CD. According to the results, neither an 800-fold excess of glucose, sucrose, lactose, fructose or citric acid, nor a 600-fold excess of methanol, ethanol, Ca^{2+}, Mg^{2+}, SO_4^{2-}, Al^{3+}, NH_4^+, Fe^{2+}, Fe^{3+}, CO_3^{2-}, Cl^- or F^-, nor a 200-fold excess of alanine, methionine, phenylalanine, glycine, or folic acid (vitamin B_9) affected the selectivity. In addition, neither a saturated starch solution nor a 50-fold excess of urea interfered with the determination of CD. Although ascorbic acid showed interference, this interference could be minimized, if necessary, by using ascorbic oxidase enzyme, which exhibits a high selectivity to the oxidation of ascorbic acid. Also, LD interfered with the determination of CD.

Determination of CD in a real sample

To evaluate the applicability of the proposed method to real samples, it was applied to the determination of CD in urine samples. The CD contents were measured after sample preparation using the standard addition method. The results are given in Table II.

TABLE II. Concentration values obtained from the proposed and the reference method (spectrophotometric method) for CD analysis of urine samples using the proposed method under optimum conditions ($n = 3$)

Sample	Added, μM	Proposed method[a], μM	Standard method[a], μM	F_{ex}	F_{tab}[b]	t_{ex}	$t_{tab(98\%)}$
Urine[c]	10.0	10.1±1.2	10.3±1.5	4.2	19	2.8	3.3
Urine[c]	10.0	10.2±1.4	10.5±1.8	3.7	19	2.5	3.3
Urine[d]	10.0	10.6±1.5	10.8±2.1	4.3	19	2.9	3.3
Urine[d]	10.0	10.4±2.1	10.5±2.2	3.9	19	2.7	3.3

[a]±Standard deviation; [b]$F_{tab(0.05),(2,2)}$; [c]a man who is safe; [d]a woman who is safe

CONCLUSIONS

This work demonstrates the construction of an FCMCNPE and its application in the determination of CD. The results showed that the oxidation of CD was catalyzed at pH 7.0, whereas the peak potential of CD was shifted by 380 mV to a less positive potential at the surface of the FCMCNPE. The catalytic peak currents obtained using DPV, were linearly dependent on the CD concentrations and the detection limit for CD was 3.6±0.17 μM. The high current sensitivity, low detection limit and high selectivity of the FCMCNPE for the detection of CD

Available online at www.shd.org.rs/JSCS/

proved its potential as a sensor. In addition, the FCMCNPE was employed for the determination of CD in some urine samples.

И З В О Д

ЕЛЕКТРОХЕМИЈСКА ДЕТЕКЦИЈА КАРБИДОПЕ КОРИШЋЕЊЕМ ЕЛЕКТРОДЕ ОД ПАСТЕ УГЉЕНИЧНИХ НАНОЦЕВИ МОДИФИКОВАНИХ ФЕРОЦЕНОМ

HALIMEH YAGHOUBIAN[1], HASSAN KARIMI-MALEH[2], MOHAMMAD ALI KHALILZADEH [2] и FATEMEH KARIMI[2]

[1]*Islamic Azad University, Branch of Bam, Bam* и [2]*Department of Chemistry, Islamic Azad University, Qaemshahr, Iran*

Направљена је хемијски модификована електрода на бази угљеничне пасте која садржи угљеничне наноцеви и фероцен. Електрохемијско понашање и стабилност ове електроде су испитивани цикличном волтаметријом. Показана је добра активност електроде за електрохемијску оксидацију карбидопе у фосфатном пуферу. Добијена је линеарна зависност у опсегу концентрација од 5 до 600 μM карбидопе са границом осетљивости од 3,6±0.17 μM. Такође су одређени коефицијент дифузије карбидопе и коефицијент прелаза (α) за његову оксидацију. Електрода је показала добру репродуктивност, изузетну стабилност током дугих времена и посебно добру репродуктивност површине након механичког полирања. Резултати су показали да се испитивана електрода може користити као електрохемијски сензор за одређивање карбидопе у реалним системима, као што су узорци урина.

(Примљено 1. маја, ревидирано 6. августа 2009)

REFERENCES

1. H. Ma, L. Zhang, Y. Pan, K. Zhang, Y. Zhang, *Electroanalysis* **20** (2008) 1220
2. G. G. Wildgoose, C. E. Banks, H. C. Leventis, R. G. Compton, *Microchim. Acta* **152** (2006) 187
3. J. Wang, *Electroanalysis* **17** (2005) 7
4. J. U. Yan, L. Y. Feng, R. W. Zhong, *J. Serb. Chem. Soc.* **70** (2005) 277
5. J. J. Gooding, *Electrochim. Acta* **50** (2005) 3049
6. Y. L. Yao, K. K. Shiu, *Electrochim. Acta* **52** (2007) 278
7. H. Beitollahi, H. Karimi-Maleh, H. Khabazzadeh, *Anal. Chem.* **80** (2008) 9848
8. P. Gomes, P. Soares-da-Silva, *Neuropharmacology* **38** (1999)1371
9. M. Chamsaz, A. Safavi, J. Fadaee, *Anal. Chim. Acta* **603** (2007) 140
10. P.C. Damiani, A. C. Moschetti, A. J. Rovetto, F. Benavente, A. C. Olivieri, *Anal. Chim. Acta* **543** (2005) 192
11. A. Safavi, M. Tohidi, *J. Pharm. Biomed. Anal.* **44** (2007) 313
12. M. Grünhut, M. E. Centurión, W. D. Fragoso, L. F. Almeida, M. C. U. de Araújo, B. S. Fernández Band, *Talanta* **75** (2008) 950
13. W. H. Kim, M. M. Karim, S. H. Lee, *Anal. Chim. Acta* **619** (2008) 2
14. M. Karimi, J. L. Carl, S. Loftin, J. S. Perlmutter, *J. Chromatogr. B* **836** (2006) 120
15. K. A. Sagar, M. R. Smyth, *J. Pharm. Biomed. Anal.* **22** (2000) 613
16. K. Stulik, V. Pacakova, *Electroanalytical Measurements in Flowing Liquids*, Halsted Press, New York, 1987
17. P. T. Kissinger, W. R. Heineman, *Laboratory Techniques in Electroanalytical Chemistry*, Marcel Dekker, New York, 1984
18. R. E. Sabzi, A. Hassanzadeh, K. Ghasemlu, P. Heravi, *J. Serb. Chem. Soc.* **72** (2007) 993

19. J. B. Raoof, R. Ojani, H. Karimi-Maleh, *Electroanalysis* **20** (2008) 1259
20. H. Karimi-Maleh, A. A. Ensafi, A. R. Allafchian *J. Solid State Electrochem.* **14** (2010) 9
21. E. Mirmomtaz, A. A. Ensafi, H. Karimi-Maleh, *Electroanalysis* **20** (2008) 1973
22. J. B. Raoof, R. Ojani, H. Karimi-Maleh, *J. Appl. Electrochem.* **39** (2009) 1169
23. A. J. Bard, L. R. Faulkner, *Electrochemical methods, fundamentals and applications*, Wiley, New York, 2001
24. C. P. Andrieux, J. M. Saveant, *J. Electroanal. Chem.* **93** (1978) 163.

A rapid spectrophotometric determination of imidacloprid in selected commercial formulations in the presence of 6-chloronicotinic acid

VALÉRIA J. GUZSVÁNY[1*#], ZSIGMOND J. PAPP[1#], SANJA D. LAZIĆ[2#], FERENC F. GAÁL[1#], LUKA J. BJELICA[1#] and BILJANA F. ABRAMOVIĆ[1#]

[1]*Department of Chemistry, Biochemistry and Environmental Protection, Faculty of Sciences, University of Novi Sad, Trg D. Obradovića 3, 21000 Novi Sad and* [2]*Faculty of Agriculture, University of Novi Sad, Trg D. Obradovića 8, 21000 Novi Sad, Serbia*

Abstract: A simple first-order derivative spectrophotometric method was developed for the simultaneous determination of imidacloprid and 6-chloronicotinic acid (6-CNA). By using the zero-crossing approach, imidacloprid was determined at 249 nm and 6-CNA at 236 nm with detection limits of 0.32 and 0.17 μg mL^{-1}, respectively, and relative standard deviations not exceeding 1.2 % in the case of model systems. The proposed method was applied for the determination of imidacloprid and 6-CNA in commercial formulations. A conventional spectrophotometric method (at 270 nm) was also employed for the determination of the content of imidacloprid in the same commercial formulations. The results of the developed spectrophotometric methods were in good agreement with those obtained by the high-performance liquid chromatographic method.

Keywords: derivative spectrophotometry; imidacloprid; 6-chloronicotinic acid; insecticide formulations.

INTRODUCTION

Imidacloprid ((*EZ*)-1-(6-chloro-3-pyridylmethyl)-*N*-nitroimidazolidin-2-ylideneamine, Fig. 1a) belongs to the most efficient class of insecticides nowadays, called neonicotinoids, which account for about 17 % of the total insecticide market.[1,2] Since its launch in 1991, products containing imidacloprid have gained registration in about 120 countries and are marketed for use in agriculture (for over 140 agricultural crops), on turf, on pets and for household pests.[2] The mechanism of imidacloprid action has been extensively studied and is relatively well known.

1455

It acts as an agonist by binding to nicotinic acetylcholine receptors in the nervous system of insects. This leads to an accumulation of acetylcholine, resulting in the paralysis and death of insects.[1–3] Imidacloprid is marketed under variety of names, including Gaucho, Merit, Admire, Confidor, Macho and Winner. Although imidacloprid has been in use for a relatively short period compared to other common pesticides, it is now considered to be the most widely used insecticide globally.[1,2]

One of the synthetic precursors, and also an intermediate of imidacloprid decomposition, is 6-chloronicotinic acid (6-CNA), Fig. 1b.[4,5] Recent investigations showed positive effects of imidacloprid on the stress resistance of several plants, which was probably due to 6-CNA. This substance is known to stimulate the defense systems of plants and thus protect them against disease.[5]
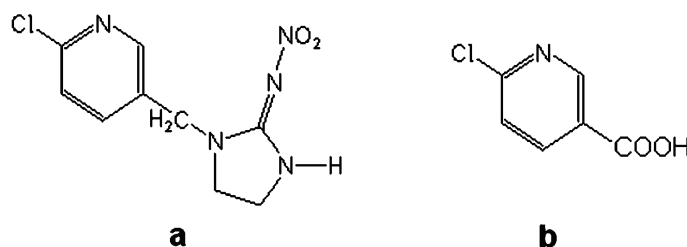
Fig. 1. Structure of imidacloprid (**1**) and 6-CNA (**2**).

All the above facts impose the necessity for reliable analytical methods for the determination of these two compounds in their mixtures. Analytical techniques used for imidacloprid determination include high-performance liquid chromatography (HPLC) with diode array (DA),[6–8] mass spectrometric (MS)[9,10] and thermal lens spectrometric[11] detection. Some alternative techniques, such as an enzyme-linked immunosorbent assay,[12,13] fluorimetry,[14] Fourier transform infrared spectroscopy[15] and voltammetry,[16–20], have also been employed to analyze different imidacloprid-containing samples.

Several methods were developed to determine both imidacloprid and 6-CNA. Thus, capillary electrophoresis with DA[21] and LC with DA,[22,23] pulsed reductive amperometric[24] and MS[25] detection are used for this purpose. Matrix solid phase dispersion combined with LC–APCI–MS[26] and column switching LC with post--column photochemical fluorescence detection[27] was also applied for the simultaneous determination of imidacloprid and 6-CNA. Monitoring of 6-CNA in human urine by GC–MS, as indication of exposure to the pesticide imidacloprid, was also described.[28]

Due to common availability of the instrumentation, simplicity of procedures, speed, precision and accuracy, spectrophotometric methods enjoy wide popularity. In addition, they are more economic and simpler, compared to methods such as chromatography and electrophoresis.[29] Hitherto, no spectrophotometric me-

Available online at www.shd.org.rs/JSCS/

thods have been reported for the simultaneous determination of imidacloprid and 6-CNA. Namely, highly overlapped spectra of these compounds in the UV range complicate their determination in mixtures.

Several techniques have been proposed for the treatment of spectrophotometric data, with the objective of extracting a largest amount of analytical information from spectra composed of unresolved bands. Undoubtedly, a major success was achieved by derivative treatment of the absorbance curves, in which the first- or a higher-order mathematical derivative of the absorbance is plotted against the wavelength ($dA/d\lambda$). Derivative spectrophotometry offers a convenient solution to a number of analytical problems, such as resolution of multicomponent systems, removal of sample turbidity, matrix background and enhancement of spectral details. Due to this, it was applied in the analysis of different pharmaceuticals, foods, cosmetics, and environmental samples.[29,30] The same method was also applied for the simultaneous determination of pesticides or pesticides and their degradation products.[31–37]

In this work, a rapid, environmentally acceptable and inexpensive first-order derivative spectrophotometric method was developed for the determination of imidacloprid and 6-CNA in their mixtures, both in model solutions and commercial formulations (Macho 200 SL and Confidor 200 SL). The conventional spectrophotometric method was also tested for the determination of imidacloprid in these two formulations. The results of the spectrophotometric methods developed were compared with those obtained by HPLC with DA detection, HPLC–DAD.

EXPERIMENTAL

Chemicals and solutions

All employed chemicals were of the analytical reagent grade. The analytical standard of imidacloprid and 6-CNA was of Pestanal quality (Riedel de Haën, Germany). Stock solutions were prepared by dissolving the compounds in doubly distilled water to obtain a concentration of 0.50 mg mL^{-1}, which did not change over a long period when the solutions were kept in the dark at 4 °C. Britton–Robinson buffer solutions were prepared from a stock solution containing 0.040 mol L^{-1} phosphoric (Merck, Darmstadt, Germany), boric (Merck) and acetic (Merck) acids by adding 0.20 mol L^{-1} sodium hydroxide (Merck) to the required pH values, covering the pH range of approx. 2.0–10. Commercial formulations of imidacloprid were Confidor 200 SL (Bayer CropScience, Germany) and Macho 200 SL (Hemovet, Serbia), both with a declared imidacloprid content of 200±12 g L^{-1}. The amount of 6-CNA in spiked commercial formulations was 115.0 g L^{-1}.

Apparatus

The spectrophotometric measurements were performed on an Anthelie Data UV–visible single-beam spectrophotometer (SECOMAM, France) with a fixed slit width (2 nm) operated *via* Anthelie Data software. The chromatograms were recorded on an Agilent 1100 liquid chromatograph (Agilent Technologies Inc., USA) furnished with an Agilent Hypersil ODS--C18 column (2.0 mm×250 mm, 5 μm). A digital pH-meter (PHM 62, Radiometer, Denmark) and a combined glass electrode were used for pH measurements.

Procedures

Spectrophotometry. Characterization of the individual optical behavior of imidacloprid and 6-CNA was performed at the same molar concentration (1×10^{-4} mol L^{-1}), *i.e.*, 25.57 μg mL^{-1} and 15.76 μg mL^{-1}, respectively, in the pH range 2.0–10 and in the wavelength range 200–400 nm. Standard solutions for the calibration curves were prepared by the stepwise dilution of the stock solution to obtain concentrations in the 1.6–22.5 μg mL^{-1} for both compounds. The conventional spectrophotometric determination of imidacloprid was performed at a working wavelength of 270 nm, while the simultaneous derivative spectrophotometric determination was realized at 249 nm (imidacloprid) and 236 nm (6-CNA).

Chromatography. The mobile phase was 80:20 v/v water (containing 0.2 % phosphoric acid):acetonitrile. The wavelength of the DA-detector was 270 nm for imidacloprid and 224 nm for 6-CNA, with a reference wavelength of 360 nm. Other parameters were: flow rate 0.8 mL min^{-1}, column temperature 25 °C and injection volume 20.0 μL. The linearity of the detector response was checked in the concentration range 1.61–22.5 μg mL^{-1} for both analytes.

Procedure for the commercial formulations. For both the spectrophotometric and HPLC measurements, 0.25 mL of the commercial formulation was diluted stepwise to 1:50000 with doubly distilled water. The standard addition method was used for the determination in order to eliminate the matrix effect. In the case of the HPLC measurements, the solutions were filtered through Millex 0.22 μm syringe filters.

Validation of the analytical method. The linearity of both the spectrophotometric and comparative chromatographic method was checked in the concentration range 1.6–22.5 μg mL^{-1}. The limit of detection (LOD) and the limit of quantification (LOQ) were calculated using the following equations: $LOD = 3s/m$ and $LOQ = 10s/m$, where s is the standard deviation of the blank and m is the slope of the calibration curve.

RESULTS AND DISCUSSION

Optimization of the conventional and derivative spectrophotometric methods

To study the optical characteristics of the investigated compounds, the corresponding spectra were recorded in Britton–Robinson buffers (pH 2.0–10.0) in the wavelength range 200–400 nm. Representative spectra of imidacloprid and 6-CNA obtained at pH 7.0 are shown in Fig. 2a. The spectra of imidacloprid have two discrete absorption bands with maxima at 212 and 270 nm, whereby the latter is much more intense. No significant changes in the absorption spectra were observed in dependence on the pH of the solution. The spectra of 6-CNA also have two discrete, well-defined absorption bands with maxima at 224 and 269 nm, the former band being more intense. The shape of the spectra and their maxima depended significantly on the pH, especially at pH < 4.0. At higher pH values, no significant changes were observed. In this context, pH 7.0 was selected for the further investigations. As can be seen from Fig. 2a, the strong overlapping of the spectra of the investigated compounds hindered their conventional spectrophotometric determination in the mixture. Hence, derivative spectrophotometry was investigated to develop a method for their simultaneous determination. The derivative spectra of solutions containing the individual analytes were investigated in order to optimize the derivative order. As can be seen from Fig. 2, the first-

-order derivative spectrum (b) showed a high sensitivity and a good resolution for the simultaneous determination. Higher derivative orders (c, d) were discarded because the noise attenuation was less effective and the signal became distorted.
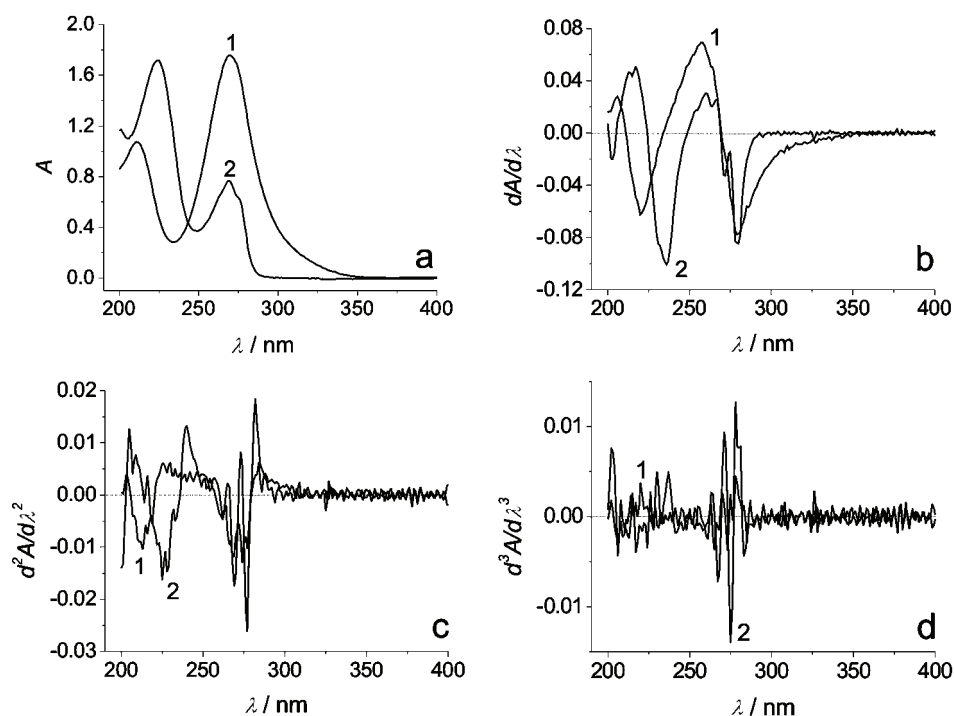
Fig. 2. Absorption spectra (a), first- (b), second- (c) and third-order (d) derivative spectra of imidacloprid (**1**) and 6-CNA (**2**). Measurement parameters: $c(\mathbf{1}) = 16.9$ μg mL^{-1}, $c(\mathbf{2}) = 11.6$ μg mL^{-1}, pH 7.0.

The main disadvantage of the derivative technique is that the signal-to-noise ratio worsens with increasing order of the derivative. Therefore, the practical derivative technique includes a certain degree of low-pass filtering or smoothing, to control the noise increase, which is an inevitable consequence of the noise signal differentiation. The effect of smoothing a peak-type signal is that the noise is reduced, which is desirable. However, it distorts the signal, which is undesirable but unavoidable. Thus, optimization of the smoothing factor is very important in order to obtain appropriate signals.[38] In the present study, the adjacent averaging method was tested, using smoothing factors of 2, 5 and 8 (Fig. 3). The obtained curves were then compared with unsmoothed ones (Fig. 2b). The smoothing factor 5 was selected because this yielded good sensitivity without a significant sacrifice of the signal to noise ratio.
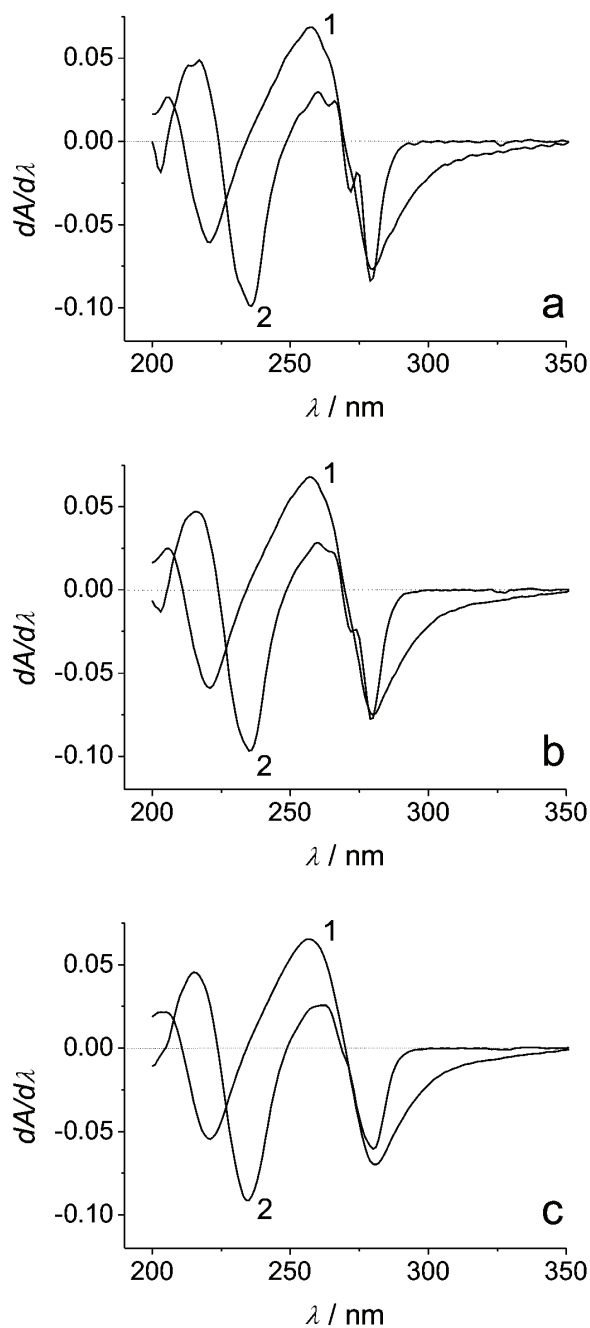
Fig. 3. Effect of smoothing on the first-order derivative spectra of imidacloprid (**1**) and 6-CNA (**2**). Measurement parameters: $c(\mathbf{1}) = 16.9$ μg mL^{-1}, $c(\mathbf{2}) = 11.6$ μg mL^{-1}, pH 7.0, smoothing factors: 2 (a), 5 (b) and 8 (c).

The smoothed first derivative spectrum of both compounds have more zero-crossings, of which those at 236 nm in case of imidacloprid and 249 nm in case of 6-CNA offer better sensitivity for the determination of the second compound (Fig. 3b). At these wavelengths, all the absorption is attributed to a single compound. The effect of the concentration of the analytes on both zero-crossing points was studied in the concentration range 1.61–22.5 µg mL^{-1}. The selected zero-crossing values were independent of the concentration.

In the case of the conventional spectrophotometric determination of imidacloprid, the absorbance was measured at the absorption maximum (270 nm).

Determination of imidacloprid in a model solution and commercial formulations

The simultaneous determination of imidacloprid and 6-CNA in the model solution is demonstrated in Fig. 4a. Using the selected conditions, linear graphs of dA/dλ versus the analyte concentration were obtained in the concentration range of 1.6–22.5 µg mL^{-1} for both analytes. The calculated values of the *LOD* were 0.32 and 0.17 µg mL^{-1} for imidacloprid and 6-CNA, respectively. The relative standard deviations (*RSD*s) did not exceed 1.2 %. The results of the first--order spectrophotometric method were compared with those of the HPLC–DAD method. The retention times of 6-CNA and imidacloprid were 7.85 and 9.04 min, respectively. The repeatability of the retention times and peak areas were checked by injecting the standard mixture solution six times and the *RSD* of the retention times and that of the peak areas were less than 0.1 and 1.1 %, respectively. The analytical parameters for both methods are presented in Table I.

Preliminary HPLC analysis did not confirm the presence of 6-CNA in the investigated commercial formulations (Confidor 200 SL, and Macho 200 SL). Hence, before applying the developed derivative spectrophotometric method for the determination of imidacloprid and 6-CNA (Fig. 4c), the formulations were spiked with a defined amount of 6-CNA. The standard addition method was used for the determination in order to eliminate the matrix effect. As can be seen from Table II, the determined amounts of imidacloprid and 6-CNA agreed well with the supplier's data (imidacloprid) or with the added amount (6-CNA). The HPLC–DAD measurements confirmed the results of the spectrophotometric measurements. On the other hand, the conventional spectrophotometric analysis of imidacloprid in commercial formulations by the standard addition method (205.0 g L^{-1}, 2.27 % *RSD* in case of Confidor 200 SL (Fig 4b) and 194.5 g L^{-1}, 3.93 % *RSD* in case of Macho 200 SL) agreed well with the derivative spectrophotometric and HPLC data (Table II), confirming that simple conventional spectrophotometry can also give valuable insight into the content of the active compound of some commercial formulations.

The sufficiently good recoveries and low RSDs reflect the high accuracy and precision of the proposed derivative spectrophotometric method. The method is sen-
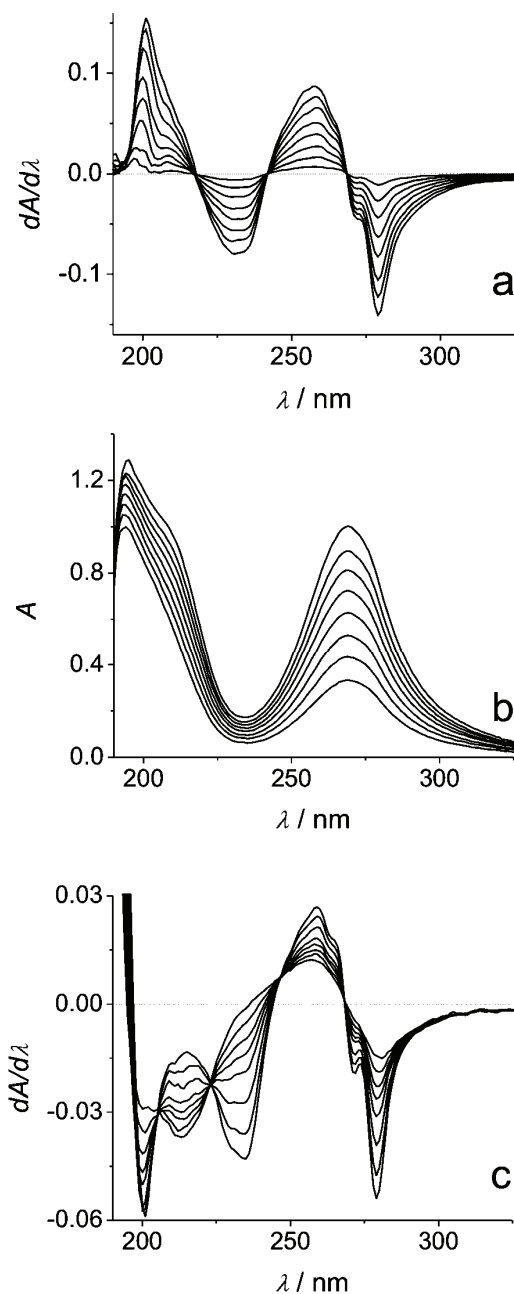
Figure 4. Simultaneous derivative spectrophotometric determination of imidacloprid and 6-CNA in a model solution (a), conventional spectrophotometric determination of imidacloprid in Confidor 200 SL (b) and derivative spectrophotometric determination of 6-CNA in spiked Confidor 200 SL (c).

sitive, simple, relatively rapid and inexpensive, thus making it a convenient alternative tool for the fast determination of imidacloprid in commercial formulations, even in the presence of 6-CNA.

TABLE I. Analytical parameters for the derivative spectrophotometric and HPLC–DAD determination of imidacloprid and 6-CNA in model systems

Parameter	Method of determination			
	Derivative spectrophotometry		HPLC–DAD	
	Imidacloprid	6-CNA	Imidacloprid	6-CNA
Concentration interval, μg mL^{-1}	1.1–22.5	0.58–22.5	0.19–22.5	0.24–22.5
Slope[a]	0.0024	–0.0031	0.688	0.528
Intercept[a]	0.001	–0.0006	0.032	–0.07
Correlation coefficient[a]	0.999	0.999	0.999	0.999
LOD / μg mL^{-1}	0.32	0.17	0.05	0.06
LOQ / μg mL^{-1}	1.07	0.58	0.19	0.24
RSD / %	1.2	1.0	1.1	1.1

[a]$Y = a + bc$, where c is concentration in μg mL^{-1} and Y is dA/dλ

TABLE II. The content of imidacloprid and 6-CNA in commercial formulations spiked with 6-CNA ($n = 6$)

Commercial formulation	Method of determination							
	Derivative spectrophotometry				HPLC–DAD			
	Imidacloprid		6-CNA		Imidacloprid		6-CNA	
	c / g L^{-1}	RSD / %	c / g L^{-1}	RSD / %	c / g L^{-1}	RSD / %	c / g L^{-1}	RSD / %
Confidor 200 SL	202.14	3.22	116.60	2.15	205.15	2.13	117.91	1.75
Macho 200 SL	196.68	2.54	115.81	3.12	194.30	1.40	115.80	2.85

CONCLUSIONS

A simple and rapid derivative spectrophotometric method, based on the zero-crossing approach, was developed for the simultaneous determination of imidacloprid and 6-CNA at pH 7.0. The first derivatives of the absorption spectra were used in the case of both compounds. Imidacloprid was determined at 249 nm, and 6-CNA at 236 nm. The method, tested by determining imidacloprid and 6-CNA in commercial formulations of imidacloprid, requires no sample clean-up, which saves time, money and the environment. Conventional spectrophotometry was successfully employed for the determination of imidacloprid in commercial formulations. The results of both the conventional and derivative spectrophotometric methods were in good agreement with the comparative HPLC–DAD procedure, and also with the composition declared by the manufacturer.

И З В О Д

БРЗО СПЕКТРОФОТОМЕТРИЈСКО ОДРЕЂИВАЊЕ ИМИДАКЛОПРИДА У ОДАБРАНИМ КОМЕРЦИЈАЛНИМ ПРЕПАРАТИМА У ПРИСУСТВУ 6-ХЛОРНИКОТИНСКЕ КИСЕЛИНЕ

VALÉRIA J. GUZSVÁNY[1], ZSIGMOND J. PAPP[1], САЊА Д. ЛАЗИЋ[2], FERENC F. GAÁL[1], ЛУКА Ј. БЈЕЛИЦА[1] и БИЉАНА Ф. АБРАМОВИЋ[1]

[1]*Департман за хемију, биохемију и заштиту животне средине, Природно–математички факултет, Универзитет у Новом Саду, Трг Д. Обрадовића 3, 21000 Нови Сад и* [2]*Пољопривредни факултет, Универзитет у Новом Саду, Трг Д. Обрадовића 8, 21000 Нови Сад*

Предложена је једноставна спектрофотометријска метода на бази првог извода за истовремено одређивање имидаклоприда и 6-хлорникотинске киселине (6-ХНК). Примењујући приступ нултог пресека имидаклоприд је одређиван у модел систему на 249 nm а 6-ХНК на 236 nm, са границама детекције од 0,32 и 0,17 μg mL^{-1}, респективно и релативном стандардном девијацијом мањом од 1,2 %. Предложена метода је примењена за одређивање имидаклоприда и 6-ХНК у комерцијалним препаратима. Конвенционална спектрофотометријска метода (на 270 nm) је такође примењена за одређивање садржаја имидаклоприда у истим комерцијалним препаратима. Резултати предложене спектрофотометријске методе су у доброј сагласности са резултатима добијеним методом течне хроматографије високе ефикасности.

(Примљено 15. октобра 2009)

REFERENCES

1. P. Jeschke, R. Nauen, *Pest Manag. Sci.* **64** (2008) 1084
2. A. Elbert, M. Haas, B. Springer, W. Thielert, R. Nauen, *Pest Manag. Sci.* **64** (2008) 1099
3. T. Iwasa, N. Motoyama, J. T. Ambrose, M. R. Roe, *Crop Prot.* **23** (2004) 371
4. B. Schäfer, *Chem. Unserer Zeit* **42** (2008) 408
5. A health farm for plants, http://www.research.bayer.com/edition_18/18_Stress_protection.pdfx (13 October 2009)
6. H. Obana, M. Okihashi, K. Akutsu, Y. Kitagawa, S. Hori, *J. Agric. Food Chem.* **50** (2002) 4464
7. A. Mandić, S. Lazić, S. Ökrész, F. Gaál, *J. Anal. Chem.* **12** (2005) 1134
8. S. Seccia, P. Fidente, D. Montesano, P. Morrica, *J. Chromatogr. A* **1214** (2008) 115
9. H. Obana, M. Okihashi, K. Akutsu, Y. Kitagawa, S. Hori, *J. Agric. Food Chem.* **51** (2003) 2501
10. S. Seccia, P. Fidente, D. Attard Barbini, P. Morrica, *Anal. Chim. Acta* **553** (2005) 21
11. V. Guzsvány, A. Madžgalj, P. Trebše, F. Gaál, M. Franko, *Environ. Chem. Lett.* **5** (2007) 203
12. E. Watanabe, H. Eun, K. Baba, T. Arao, Y. Ishii, S. Endo, M. Ueji, *J. Agric. Food Chem.* **52** (2004) 2756
13. E. Watanabe, H. Eun, K. Baba, T. Arao, Y. Ishii, S. Endo, M. Ueji, *Anal. Chim. Acta* **521** (2004) 45
14. J. L. Vilchez, M. C. Valencia, A. Navalón, B. Molinero-Morales, L. F. Capitán-Vallvey, *Anal. Chim. Acta* **439** (2001) 299
15. G. Quintás, S. Armenta, S. Garrigues, M. de la Guardia, *J. Braz. Chem. Soc.* **15** (2004) 307
16. A. Navalón, R. El-Khattabi, A. González-Casado, J. L. Vilchez, *Mikrochim. Acta* **130** (1999) 261

Available online at www.shd.org.rs/JSCS/

17. A. Guiberteau, T. Galeano, N. Mora, P. Parrilla, F. Salinas, *Talanta* **53** (2001) 943
18. V. Guzsvány, F. Gaál, L. Bjelica, S. Ökrész, *J. Serb. Chem. Soc.* **5** (2005) 735
19. V. Guzsvány, M. Kádár, Z. Papp, L. Bjelica, F. Gaál, K. Tóth, *Electroanal.* **20** (2008) 291
20. Z. Papp, I. Švancara, V. Guzsvány, K. Vytřas, F. Gaál, *Microchim. Acta* **166** (2009) 169
21. A. Segura Carretero, C. Cruces-Blanco, S. Pérez Durán, A. Fernandez Gutiérrez, *J. Chromatogr. A* **1003** (2003) 189
22. A. Garrido Frenich, F. J. Egea González, J. L. Martínez Vidal, P. Parrilla, M. Mateu Sánchez, *J. Chromatogr. A* **869** (2000) 497
23. M. Martínez Galera, A. Garrido Frenich, J. L. Martínez Vidal, P. Parrila Vázquez, *J. Chromatogr. A* **799** (1998) 149
24. N. R. de Erenchun, Z. G. de Balugera, M. A. Goicolea, R. J. Barrio, *Anal Chim Acta* **349** (1997) 199.
25. T. Pérez-Ruiz, C. Martínez-Lozano, V. Tomás, J. Martín, *J. Chromatogr. A* **1026** (2004) 57
26. S. Totti, M. Fernández, S. Ghini, Y. Picó, F. Fini, J. Mañes, S. Girotti, *Talanta* **69** (2006) 724
27. M. D. Gil García, M. Martinez Galera, R. Santiago Valverde, A. Galanti, S. Girotti, *J. Chromatogr. A* **1147** (2007) 17
28. F. J. Uroz, F. J. Arrebola, F. J. Egea-González, J. L. Martínez-Vidal, *Analyst* **126** (2001) 1355
29. F. S. Rojas, C. B. Ojeda, *Anal. Chim. Acta* **635** (2009) 22
30. C. B. Ojeda, F. S. Rojas, *Anal. Chim. Acta* **518** (2004) 1
31. V. Guzsvány, F. Gaál, S. Lazić, Z. Papp, in *Proceedings of the 43rd Meeting of the Serbian Chemical Society*, Belgrade, Serbia, (2005), p. 94
32. B. F. Abramović, V. B. Anderluh, F. F. Gaál, D. V. Šojić, *J. Serb. Chem. Soc.* **72** (2007) 809
33. J. L. M. Vidal, M. D. G. Garcia, M. M. Galera, A. G. Frenich, *Anal. Lett.* **30** (1997) 2409
34. I. Baranowska, C. Pieszko, *Chem. Anal. (Warsaw)* **45** (2000) 583
35. I. Baranowska, C. Pieszko, *Anal. Lett.* **35** (2002) 473
36. T.-L. Kuo, D.-L. Lin, R. H. Liu, F. Moriya, Y. Hashimoto, *Forensic Sci. Int.* **121** (2001) 134
37. A. G. Frenich, M. M. Galera, J. L. M. Vidal, P. P. Vazquez, M. D. G. Garcia, *Anal. Lett.* **30** (1997) 341
38. G. V. Popović, L. B. Pfendt, V. M. Stefanović, *J. Serb. Chem. Soc.* **65** (2000) 457.

Sensitive voltammetric detection of yeast RNA based on its interaction with Victoria Blue B

WEILI ZHANG[1], XUELIANG NIU[1], NA ZHAO[2] and WEI SUN[2*]

[1]Department of Basic Medicine, Shandong Wanjie Medical College, Zibo 25521 and [2]College of Chemistry and Molecular Engineering, Qingdao University of Science and Technology, Qingdao 266042, P. R. China

Abstract: Voltammetric studies of the interaction of yeast RNA (y-RNA) with Victoria Blue B (VBB) are described in this paper. Furthermore, a linear sweep voltammetric method for the detection of y-RNA was established. The reaction conditions, such as acidity and amount of buffer solution, the concentration of VBB, the reaction time and temperature, *etc*., were carefully investigated by second order derivative linear sweep voltammetry. Under the optimal conditions, the reduction peak current of VBB at –0.75 V decreased greatly after the addition of y-RNA to the solution without any shift of the reduction peak potential. Based on the decrease of the peak current, a new quantitative method for the determination of y-RNA was developed. The effects of co-existing substances on the determination were carefully investigated and three synthetic samples were determined with satisfactory results. The stoichiometry of the VBB–y-RNA complex was calculated by linear sweep voltammetry and the interaction mechanism is discussed.

Keywords: interaction; linear sweep voltammetry; Victoria Blue B; yeast RNA.

INTRODUCTION

Nucleic acids (NAs) are very important for their specific functions in life science. The determination of the content of NAs is very useful in mutation detection and clinical diagnostics. Hitherto, many methods have been proposed for the determination of NAs, including UV–Vis spectrophotometry,[1–3] fluorescence,[4] the light-scattering technique,[5,6] *etc*. However, spectrophotometric methods are limited by their low sensitivity, while fluorometric methods often suffer from inherent interference from proteins and other compounds present in biological samples. Recently, the light-scattering technique was extensively studied and applied to the determination of deoxyribonucleic acid (DNA).[7,8] Compared with

---

Available online at www.shd.org.rs/JSCS/

these analytical methods, electrochemical methods have some advantages, such as cheaper and smaller devices, a wider linear range and a lower detection limit. Electrochemical methods have been widely used to study the interaction of NAs in solution with molecules such as metal chelates,[9] dyes[10] and drugs.[11] Most of these studies were, however, focused on investigations with DNA because of its importance in relation to replication and transcription, mutation of genes, action mechanisms of some DNA-related diseases and DNA-targeted drugs, specific sequence gene detection, *etc*. Otherwise, to the best of our knowledge, reports concerning interactions with ribonucleic acid (RNA) are seldom. RNA also plays important roles in the process of transcription and some gene information is concerned with RNA. Proteins can also take advantage of conformational polymerphism in the RNA backbone. Thus, it is also important to study the electrochemical behavior of RNA. Palecek investigated the voltammetric behavior of RNA on hanging mercury working electrodes using cyclic voltammetry[12] and differential pulse voltammetry.[13] The results indicated that, in a weakly alkaline electrolyte, RNA produced a cathodic peak at –1.36 V (*vs*. SCE). The interaction of some metal chelates, such as rhodium(III) phenanthroline,[14,15] ruthenium(II) polypyridine,[16,17] lead(II),[18] *etc*., with RNA have been reported for recognition or hydrolysis reactions. Sun *et al*. investigated the interaction of pyronine B with RNA by an electrochemical method and further applied it to the quantitative detection of RNA.[19] Zhang *et al.* studied the interaction of a ciprofloxacin–copper complex with RNA by linear sweep voltammetry and established a new approach for RNA determination.[20] Jia *et al*. developed a method for detecting RNA by the resonance light scattering quenching technique.[21]

In this work, the electrochemical behavior of Victoria Blue B (VBB) in the absence and presence of yeast RNA (y-RNA) was examined. VBB is a cationic dye, the structure of which is shown in Fig. 1. It is a commonly used as a cheaper price indicator. In pH 3.5 Britton–Robinson (B–R) buffer solution, VBB has a sensitive linear sweep voltammetric reduction peak at a potential of –0.75 V (*vs*. SCE) and the addition of y-RNA into a VBB solution resulted in changes of the reduction peak current, which could be further used for the detection of y-RNA.
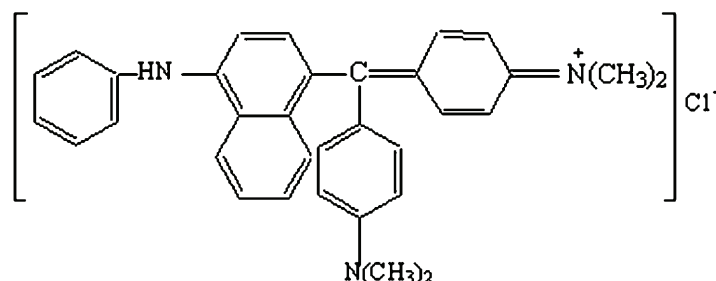
Fig. 1. The molecular structure of Victoria Blue B.

The optimal conditions for the interaction were selected. Under the optimal conditions, the binding number and the binding constant were calculated from the electrochemical data.

EXPERIMENTAL

Apparatus

All the electrochemical experiments were performed using a JP model 303 polarographic analyzer (Chengdu Apparatus Factory, China) with the traditional three-electrode system using a dropping mercury electrode (DME) as the working electrode, a platinum wire counter electrode and a saturated calomel reference electrode (SCE). All the potentials given in this paper are related to the SCE. A Cary 50 probe UV–Vis spectrophotometer (Varian Company, Australia) was used to record the UV–Vis absorption spectra. A pHS-25 acidimeter (Shanghai Leici Instrument Factory, China) was used for measuring the pH of the solutions. All the experiments were performed at 25 ± 2 °C, except when otherwise stated.

Reagents

Stock solutions of yeast RNA (y-RNA, Tianjin Damao Chemical Reagent Company, China) and fish sperm DNA (fs-DNA, Beijing Jingke Biochemical Reagent Company, China) (1.0 g L^{-1}) were prepared by dissolving them in doubly distilled water. The 1.0×10^{-3} mol L^{-1} solution of Victoria Blue B (VBB, Tianjin Kermel Chemical Reagent Company, China) was obtained by dissolving 0.0506 g VBB into 100 mL water. A Britton–Robinson (B–R) buffer solution (0.20 mol L^{-1}) was used to control the acidity of the interaction system. All other reagents were of analytical reagent grade and doubly distilled water was used throughout this study.

Procedure

Solutions of VBB (0.40 mL, 1.0×10^{-3} mol L^{-1}), pH 3.5 B–R buffer (2.5 mL) and an appropriate amount of y-RNA (or samples) were mixed in a 10 mL volumetric flask, diluted to the mark and mixed thoroughly. After reacting at room temperature for 15 min, the second order derivative linear sweep voltammetric curve was recorded in the potential range from -0.3 V to -1.0 V. The peak current of VBB reduction at a potential of -0.75 V (*vs.* SCE) was recorded as the blank response (Ip_0'') and the peak current of the VBB–y-RNA mixture was recorded as Ip''. The difference of the peak current ($\Delta Ip'' = Ip_0'' - Ip''$) was used for quantitative analysis.

RESULTS AND DISCUSSION

Absorption spectra

The UV–Vis absorption spectra of VBB in the absence and presence of different amounts of y-RNA are shown in Fig. 2. In pH 3.5 B–R buffer solution and in the scanning range from 350 to 800 nm, VBB had an absorption peak maximum at 612 nm (curve 1) and y-RNA had no absorption (curve 4). When y-RNA was mixed with VBB, the absorbance of VBB at 612 nm decreased (curves 2 and 3), with an isobestic point appearing at 646 nm. The more the y-RNA was added, the greater was the absorbance decrease, which indicates that a binding reaction between VBB and y-RNA had occurred in the mixture solution and a new biosupramolecular complex was formed under these experimental conditions.
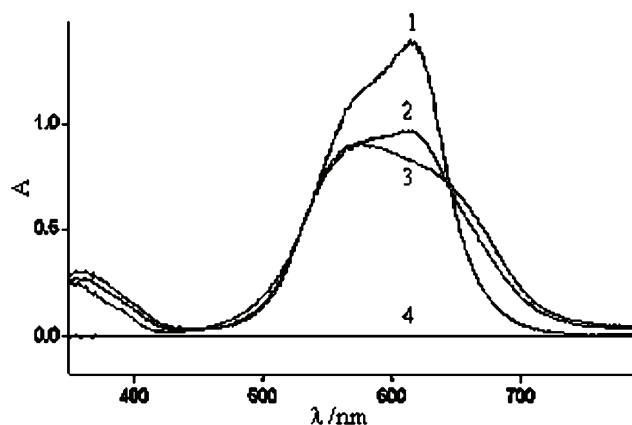
Fig. 2. UV–Vis Absorption spectra of the interaction of VBB with y-RNA. Reaction conditions: 1) pH 3.5 B–R buffer + 4.0×10^{-5} mol L^{-1} VBB; 2) and 3) pH 3.5 B–R buffer + 10.0 and 50.0 mg L^{-1} y-RNA, respectively; 4) pH 3.5 B–R buffer + 20.0 mg L^{-1} y-RNA.

Linear sweep voltammograms

Second order derivative linear sweep voltammetry can give a peak shape curve with high sensitivity; hence it was employed in this study. The second order derivative linear sweep voltammograms of VBB with different amounts of y-RNA are shown in Fig. 3. It can be seen that the B–R buffer did not have any electrochemical response (curve 1) and VBB had a sensitive second order derivative linear sweep voltammetric reduction peak at –0.75 V (*vs*. SCE) (curve 2), which was due to the electrochemical reduction of VBB on the mercury electrode, while y-RNA showed no electrochemical response in this potential range. After the addition of y-RNA into the VBB solution, the reduction peak current at the potential of –0.75 V decreased gradually with increasing y-RNA concentration (curves 3 and 4). The phenomena indicated that an interaction occurred in the mixture solution, which resulted in a decrease of free concentration of VBB
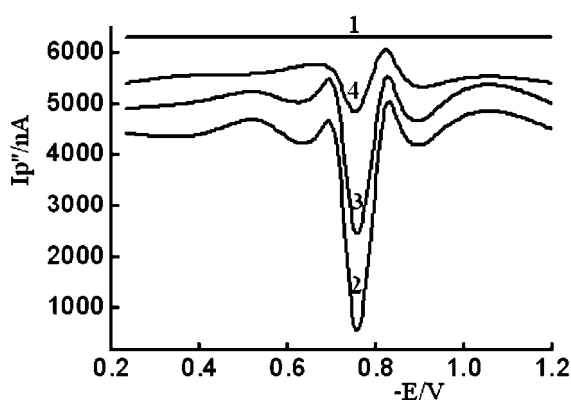
Fig. 3. Second order derivative linear sweep voltammograms of the interaction of VBB with y-RNA. Reaction conditions: 1) pH 3.5 B–R buffer; 2) pH 3.5 B–R buffer + 4.0×10^{-5} mol L^{-1} VBB; 3) and 4) pH 3.5 B–R buffer + 4.0×10^{-5} mol L^{-1} VBB + + 10.0 and 20.0 mg L^{-1} y-RNA, respectively.

Available online at www.shd.org.rs/JSCS/

in the solution and a decrease of the reduction peak current. Since the isoelectric point (pI) of y-RNA is in the range of 2.0 to 2.8 and the value of the pK_a of VBB is 8.25, in the selected pH 3.5 buffer solution, the phosphate in the backbone of y-RNA was highly negatively charged, while the VBB molecules were positively charged. Thus a strong electrostatic attraction reaction between VBB and y-RNA occurred in the solution to form a supramolecular complex. Based on the decrease in the peak current, a new voltammetric method for the quantification of NAs was further established.

Optimization of experimental conditions

The influence of pH on the difference of peak currents was examined in the pH range from 1.5 to 6.0 and the results are shown in Fig. 4, from which it can be seen that the ΔIp value reached its maximum at pH 3.5, hence this pH value was employed in the following experiments. Additionally, the experiments indicated that the response to the VBB–y-RNA reaction was larger in B–R buffer solution than in other buffers, such as NH_3–NH_4Cl, HOAc–NaOAc, *etc*. Hence, a B–R buffer solution of pH 3.5 was selected as being optimal. The effect of the concentration of the B–R buffer solution on the peak current difference was also studied in the range from 0.010 to 0.20 mol L^{-1} and the results showed that the ΔIp″ value reached a maximum when the concentration of the B–R buffer solution was 0.05 mol L^{-1}.
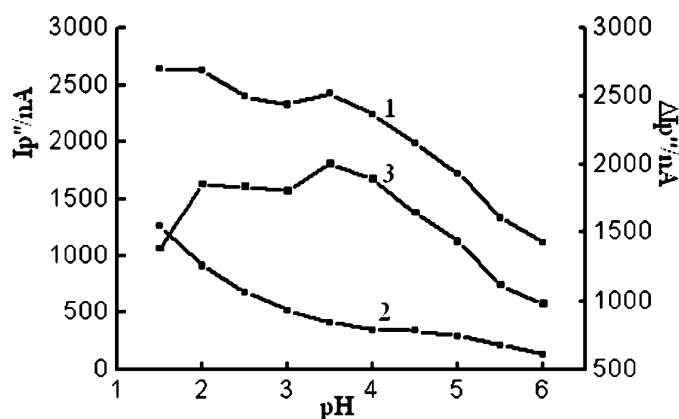
Fig. 4. The influence of buffer pH on the peak current (1 and 2) and the difference of peak currents (3). Reaction conditions: c(VBB) = 4.0×10^{-5} mol L^{-1}; 1) c(y-RNA) = 0; 2) c(y-RNA)= 20.0 mg L^{-1}; 3) ΔIp″ = Ip1″ − Ip2″.

The influence of the VBB concentration on the difference in the reduction peak current was measured using 20.0 mg L^{-1} y-RNA. As shown in Fig. 5, the ΔIp″ value increased with increasing VBB concentration and then decreased gra-

dually. The maximal value of $\Delta Ip''$ was obtained at a concentration of VBB of 4.0×10^{-5} mol L^{-1}; hence a 4.0×10^{-5} mol L^{-1} concentration of VBB was selected for use. Since the y-RNA concentration was fixed at 20.0 mg L^{-1}, when the VBB concentration was smaller than 4.0×10^{-5} mol L^{-1}, the interaction of VBB with y-RNA did not reach equilibrium, hence the value of $\Delta Ip''$ value increased gradually. When the VBB concentration was more than 4.0×10^{-5} mol L^{-1}, the reaction reached to the equilibrium and all the y-RNA was bound to VBB; hence any further increase of the VBB concentration in the reaction solution increased the concentration of free VBB in the reaction solution and then the $\Delta Ip''$ value decreased gradually.
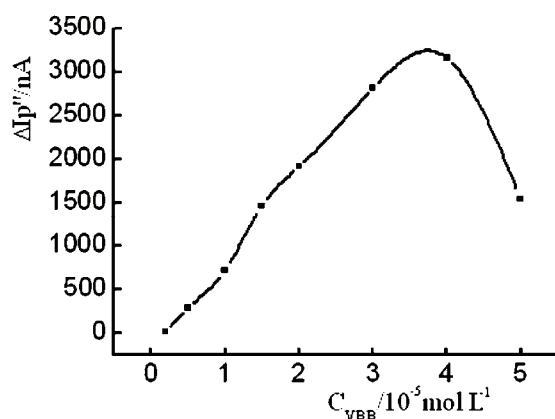
Fig. 5. The influence of the VBB concentration on the difference of peak currents ($\Delta Ip''$). Reaction conditions: 20.0 mg L^{-1} y-RNA and different concentrations of VBB in pH 3.5 B–R buffer solution.

The binding reaction occurred rapidly after y-RNA was mixed with VBB. The $\Delta Ip''$ value reached its maximum within 15 min and remained constant for at least 2 h. Therefore, this system gave ample time to measure the reduction current of a large number of real samples. In the reaction temperature range from 10 to 40 °C, no great differences were observed for the determination. When reaction temperature was more than 40 °C, y-RNA may be denatured. Hence, a temperature of 25 °C was used throughout in the following procedure.

The instrumental conditions of the polarographic analyzer, such as the scan rate and the dropping mercury standing time (lifetime of the mercury drop) were also selected. With increasing scan rate, the peak current increased, which is in accordance with the Ilkovic equation. The maximal $\Delta Ip''$ value was obtained at a scan rate as 900 mV s^{-1}, hence this scan rate was selected. The reduction peak current also increased with increasing standing time of the dropping mercury. However, when the dropping mercury standing time was more than 13 s, the mercury drop fell down naturally. Hence, a 12-second standing time of the dropping mercury was selected.

Generally speaking, biosamples are often diluted with NaCl solution to keep the bioactivity and biomicroenvironment of the target. Hence, the influence of ionic strength was also investigated by the addition of 1.0 mol L^{-1} NaCl to the mixture. As shown in Fig. 6, the peak current decreased greatly with increasing ionic strength, which was due to a decrease of the electrostatic force between the VBB anion and y-RNA. With increasing ionic strength, the shielding effect of the charges on the y-RNA was unbeneficial to the formation of the VBB–y-RNA complex.
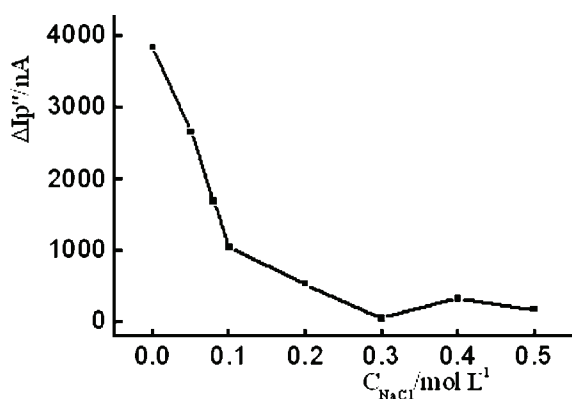
Fig. 6. The influence of ionic strength on the difference of peak currents ($\Delta Ip''$). Reaction conditions: 4.0×10^{-5} mol L^{-1} VBB + 20.0 mg L^{-1} y-RNA in pH 3.5 B–R buffer solution.

Interferences

The interferences of some co-existing substances, such as amino acids, metal ions, glucose, *etc*., on the determination of y-RNA were studied and the experimental results are shown in Table I. As can be seen, most of the investigated substances could be tolerated at higher concentrations without interference.

TABLE I. Tolerance to co-existing substances on the determination of 20.0 mg L^{-1} y-RNA in pH 3.5 B–R buffer solution with a VBB concentration of 4.0×10^{-5} mol L^{-1}

Coexisting substance	Concentration mg L^{-1}	Relative error %	Coexisting substance	Concentration μmol L^{-1}	Relative error %
L-Serine	0.5	4.99	Cu^{2+}	0.5	–4.98
L-Tyrosine	0.5	–3.17	Mn^{2+}	0.5	–0.29
L-Valine	0.5	2.08	Ca^{2+}	0.5	–0.06
L-Arginine	0.5	–2.28	Sn^{2+}	0.5	0.61
L-Leucine	0.5	1.25	Zn^{2+}	0.5	–3.19
L-Glutamine	0.5	–1.42	Mg^{2+}	0.5	–2.72
Glycine	0.5	–3.19	Co^{2+}	0.5	–2.36
Citric acid	0.5	2.92	Urea	0.5 mg L^{-1}	1.01
6-Amino caproic	0.5	12.02	Glucose	0.5 mg L^{-1}	–2.46

Calibration curves

Under the optimal conditions, calibration curves for the determination of NAs were constructed. As shown in Table II, the differences of the reduction peak current in the absence and presence of the two examined NAs were proportional to the concentration of the NA with a good linear relationship. The detection limit was calculated according to the equation of $LOD = KS_0/S$, where K is a constant related to the confidence level. According to the suggestion of the IUPAC, the value of K is 3 at the 99 % confidence level. S_0 is the standard deviation of ten blank-solution measurements (no added y-RNA) and S is the slope of the calibration graph. The relative standard deviation (*RSD*) for 11 parallel determinations of 20.0 mg L^{-1} y-RNA was 1.98 %.

TABLE II. Analytical parameters for the determination of different nucleic acids in pH 3.5 B–R buffer solution with a VBB concentration of 4.0×10^{-5} mol L^{-1}

NAs	Linear range mg L^{-1}	Standard regression equation	Detection limits (3σ), mg L^{-1}	Regression coefficient (γ)
y-RNA	6.0–20.0	$\Delta Ip'' = 190.08c - 889.72$	1.34	0.993
fs-DNA	6.0–16.0	$\Delta Ip'' = 287.68c - 1509.00$	0.57	0.991

Sample determinations

Artificial y-RNA samples containing metal ions and amino acids, *etc.*, were determined and the results are listed in Table III. It can be seen that y-RNA in the artificial samples could be determined with satisfactory results and the recoveries were in the range of 99.67–100.80 %, which indicates that this method is practical and reliable.

TABLE III. Results of the determination of y-RNA in synthetic samples ($n = 5$) in pH 3.5 B–R buffer solution with a VBB concentration of 4.0×10^{-5} mol L^{-1}

Sample	Coexisting substance[a]	Added mg L^{-1}	Found mg L^{-1}	*RSD* %	Recovery %
1	Glycine, citric acid, Zn^{2+}, Mn^{2+}	10.00	10.08	1.67	100.80
2	L-Arginine, urea, Ca^{2+}, Mg^{2+}	15.00	14.97	0.89	99.67
3	L-Valine, L-glutamine, Cu^{2+}, Co^{2+}	20.00	20.08	0.76	100.40

[a]Concentration of coexisting substances: 0.50 μmol L^{-1}

Stoichiometry of the VBB–y-RNA complex

In the selected pH 3.5 buffer solution, the VBB molecules were positively charged, while deprotonation of the phosphate groups resulted in negative charges on the y-RNA chains. Hence, the interaction of VBB with y-RNA was caused by electrostatic attraction. The stoichiometry of the VBB–y-RNA complex was calculated from the voltammetric data. According to a proposed method,[22,23] it was assumed that only a single complex of y-RNA–mVBB was formed when

VBB interacted with y-RNA. The binding number (m) and the equilibrium constant (β_s) of the binding reaction can be deduced as follows:

$$\text{y-RNA} + m\text{VBB} \leftrightarrow \text{y-RNA–}m\text{VBB} \tag{1}$$

The equilibrium constant is deduced as follows:

$$\beta_s = \frac{[\text{y-RNA–}m\text{VBB}]}{[\text{y-RNA}][\text{VBB}]^m} \tag{2}$$

as:

$$\Delta I_{max} = kc_{\text{y-RNA}} \tag{3}$$
$$\Delta I = k[\text{y-RNA–}m\text{VBB}] \tag{4}$$
$$[\text{y-RNA}] + [\text{y-RNA–}m\text{VBB}] = c_{\text{y-RNA}} \tag{5}$$

Therefore:

$$\Delta I_{max} - \Delta I = k(c_{\text{y-RNA}} - [\text{y-RNA–}m\text{VBB}]) = k[\text{y-RNA}] \tag{6}$$

Introducing Eqs. (2), (4) and (6) gives:

$$\log [\Delta I/(\Delta I_{max} - \Delta I)] = \log \beta_s + m \log [\text{VBB}] \tag{7}$$

where ΔI is the difference between the peak current of the sample and blank, ΔI_{max} corresponds the maximum value of difference of peak currents, $c_{\text{y-RNA}}$, [y-RNA–mVBB] and [y-RNA] correspond to the total, bound and free concentrations of y-RNA in the solution, respectively.

From Eq. (7), the relationship of log ($\Delta I/(\Delta I_{max} - \Delta I)$) with log [VBB] was calculated and a linear regression equation was obtained as:

$$\log (\Delta I/(\Delta I_{max} - \Delta I)) = 2.48\log [\text{VBB}] + 11.97 \quad (n = 6, \gamma = 0.992)$$

From the intercept and the slope, the values $m = 2.5$ and $\beta_s = 9.33 \times 10^{11}$ were deduced, which indicated that a stable 2:5 complex of 2y-RNA–5VBB was formed under the selected conditions.

CONCLUSIONS

The linear sweep voltammetric method was shown to be a useful method for bioanalysis with the advantages of a low detection limit, wide dynamic range and instrumental simplicity with moderate costs. Since the electrode reaction occurred at the electrode/solution interface, it can be applied to small amounts of samples. Based on the decrease of the reduction peak current of VBB after the addition of y-RNA under the selected conditions, a new voltammetric method for the determination of y-RNA was developed. The method is sensitive, reproducible and not affected by commonly co-existing substances. The stoichiometry of the VBB–y-RNA complex was calculated from the voltammetric data.

И З В О Д

ОСЕТЉИВА ВОЛТАМЕТРИЈСКА ДЕТЕКЦИЈА РНК КВАСЦА БАЗИРАНА
НА ИНТЕРАКЦИЈИ СА ВИКТОРИЈАПЛАВИМ Б

WEILI ZHANG[1], XUELIANG NIU[1], NA ZHAO[2] и WEI SUN[2]

[1]*Department of Basic Medicine, Shandong Wanjie Medical College, Zibo 255213 и* [2]*College of Chemistry and Molecular Engineering, Qingdao University of Science and Technology, Qingdao 266042, P. R. China*

У раду је описана волтаметријска анализа интеракције РНК квасца (РНКк) са викторијаплавим Б као и метода линеарне промене потенцијала за детекцију РНКк. Реакциони услови, као што су киселост, количина пуфера, концентрација викторијаплавог Б, реакционо време и температура, испитивани су диферцијалном линеарном променом потенцијала другог реда. Под оптималним условима, струјни врх редукције викторијаплавог Б на –0,75 V смањује се нагло по додатку РНКк у раствор, без промене потенцијала струјног врха. Метода за одређивање РНКк је базирана на смањењу струјног врха. Испитан је ефекат утицаја споредних компоненти на одређивање РНКк и три синтетичка узорка су успешно анализирана. Стрехиометријски састав комплекса викторијаплаво Б–РНКк је израчунат на основу волтаметријских података, а механизам интеракција дискутован је у раду.

(Примљено 7. јануара, ревидирано 25. маја 2009)

REFERENCES

1. C. Wilms, J. W. Noah, D. Zhong, P. Wollenzien, *RNA* **3** (1997) 602
2. S. C. Weatherly, I. V. Yang, P. A. Armistead, H. H. Thorp, *J. Phys. Chem. B* **107** (2003) 372
3. W. Chen, N. J. Turro, D. A. Tomalia, *Langmuir* **16** (2000) 5
4. Q. E. Cao, Y. K. Zhao, Y. Y. Xu, C. Z. Li, Z. D. Hu, Q. H. Xu, *Anal. Biochem.* **277** (2000) 214
5. F. Gao, L. Zhang, G. R. Bian, L. Wang, *Spectrochim. Acta A* **60** (2004) 2505
6. W. J. Zhang, H. P. Xu, S. Q. Wu, *Analyst* **126** (2001) 513
7. R. T. Liu, J. H. Yang, X. Wu, T. Hu, *Anal. Chim. Acta* **448** (2001) 85
8. Y. F. Li, C. Z. Huang, M. Li, *Anal. Chim. Acta* **452** (2002) 285
9. K. Jiao, Q. X. Wang, W. Sun, F. F. Jian, *J. Inorg. Biochem.* **99** (2005) 1369
10. S. F. Wang, T. Z. Peng, C. F. Yang, *Electroanalysis* **14** (2002) 1648
11. A. Radi, M. A. El Ries, S. Kandil, *Anal. Chim. Acta* **495** (2003) 61
12. M. Fojta, C. Teijeiro, E. Paleek, *Bioelectrochem. Bioenerg.* **34** (1994) 69
13. E. Paleek, M. Fojta, *Anal. Chem.* **66** (1994) 1566
14. P. J. Cater, C. C. Cheng, H. H. Thorp, *J. Am. Chem. Soc.* **120** (1998) 632
15. C. S. Chwo, J. K. Barton, *Biochemistry* **31** (1992) 5423
16. A. C. Lim, J. K. Barton, *Biochemistry* **37** (1998) 9138
17. H. Xu, H. Deng, H. Y. Hu, J. Z. Liu, H. Chao, J. Liu, L. N. Ji, *Chem. J. Chin. Univ.* **24** (2003) 25
18. M. Lindell, P. Romby, E. G. Wagner, *RNA* **8** (2002) 534
19. W. Sun, J. Y. You, Q. X. Wang, K. Jiao, *Chem. Anal.* **51** (2006) 477
20. N. Zhang, X. L. Zhang, Y. F. Zhao, *Talanta* **62** (2004) 1041
21. Z. Jia, J. H. Yang, X. Wu, C. X. Sun, S. F. Liu, F. Wang, Z. S. Zhao, *Spectrochim. Acta A* **64** (2006) 555
22. N. Q. Li, J. Min, *Chin. J. Anal. Chem.* **17** (1989) 346
23. W. Sun, J. Y. You, X. Hu, K. Jiao, *Anal. Sci.* **22** (2006) 691.

Available online at www.shd.org.rs/JSCS/

Geochemistry of Fe^{3+} in the hydrothermal dickite from Jedlina Zdroj (Lower Silesia, Poland)

PAVLE I. PREMOVIĆ[1*], JUSTYNA CIESIELCZUK[2], BRATISLAV Ž. TODOROVIĆ[3], DRAGAN M. DJORDJEVIĆ[1] and NENAD S. KRSTIĆ[1]

[1]*Laboratory for Geochemistry, Cosmochemistry and Astrochemistry, University of Niš, P.O. Box 224, 18000 Niš, Serbia,* [2]*Department of General Geology, Faculty of Earth Sciences, University of Silesia, Sosnowiec, Poland and* [3]*Laboratory for General Chemistry, Faculty of Technology, University of Niš, P.O. Box 79, 16000 Leskovac, Serbia*

Abstract: Geochemical analysis for Fe was made on a representative sample of dickite-rich hydrothermal clay from Jedlina Zdroj. The mineralogy of the sample is comparatively simple, dickite being the principal component (>95 wt. % of the total sample), with lesser amounts of goethite and barite. Geochemical fractionation and inductively coupled plasma–optical emission spectrometry indicated that most of the Fe (*ca.* 97 wt. % of the total metal) resides in the dickite. Electron spin resonance showed that some of the Fe in the dickite structure is in the form of Fe^{3+}. A substantial proportion of these ions (as well as Fe) in the dickite matrix were probably contained in the original hydrothermal dickite-forming solution. From the geochemistry of Fe^{3+}, it was deduced that the oxidation potential (*Eh*) and pH of the solution during the formation of dickite from the Jedlina Zdroj were approximately 0.45–0.95 V (highly oxygenated) and 0–4 (highly acidic), respectively.

Keywords: kaolinite; dickite; iron.

INTRODUCTION

The kaolinite group of minerals includes kaolinite, dickite, nacrite and halloysite. Kaolinite minerals are widespread in crustal rocks, particularly where there hydrothermal acid waters flow existed.[1] Hydrothermal dickites were mainly formed *in situ* through alteration of source minerals (mainly potassium-rich feldspars and other Al-rich silicates) by hydrothermal acid waters.[2,3] In Lower Silesia, hydrothermal dickite has been recognized for a long time and was named "pholerite" by researchers (*e.g.*, Kowalski and Lipiarski).[4] The Polish literature concerning hydrothermal dickite in Lower Silesia is, however, relatively scarce and this type of clay minerals is generally considered rare.[4,5] This report is a part

---

Available online at www.shd.org.rs/JSCS/

of a larger study that attempts to evaluate the nature and origin of hydrothermal dickite in volcanic rocks recovered from Lower Silesia.

In recent years, considerable attention has been given to the genesis of dickite in sedimentary conditions. However, its origin and genesis is still a matter of debate. Dickite is generally considered to be a relatively high-temperature polytype, although many other occurrences have been reported in hydrothermal and diagenetic environments, indicating that the genetic conditions are less restrictive than were initially envisaged.

Geochemical studies indicate that iron occurs in natural aquatic environments in two oxidation states, Fe(III) and Fe(II). In low (suboxic/anoxic) *Eh* natural environments, the main aqueous Fe(II) species are Fe^{2+} and $Fe(OH)^+$. In oxygenated (aerated) natural waters, Fe is predicted to occur in the +3 oxidation state, primarily as highly soluble and mobile ions. These ions have a strong tendency to interact with the surface of Al and other metal hydrous oxides and are thus capable of becoming specifically bound within colloidal clay particles.

Physicochemical conditions during the formation of non-hydrothermal kaolinites are usually deduced from field data as well as experimental/thermodynamic data. The stability of these mineral is often expressed in plots using pH and ion activities. The hydrothermal kaolinites/dickites are not frequently studied and knowledge of the physicochemical conditions necessary for their formation is still obscure.

One way to obtain an objective evaluation of the nature of a solution during the formation (precipitation) of hydrothermal dickite (or kaolinite) is to examine components that undoubtedly were introduced into its lattice by this solution. Such a component is, for certain, Fe^{3+}. On the other hand, chemical conversions of Fe^{3+} into Fe^{2+} in natural aquatic environments are characterized almost entirely by the pH and oxidation reduction potential (*Eh*) of the environment. These two parameters also have a strong influence on the mobility and complexation of Fe^{3+}. Thus, Fe^{3+} is a sensitive geochemical indicator of the geochemistry of dickite-forming waters and it may provide clues to the origin of hydrothermal clay deposits of the past. These facts led us to study Fe^{3+} in a well-ordered dickite, a hydrothermal mineral enriched with Fe, in a dickite-rich sample from Jedlina Zdroj. In addition, selective leaching procedures were used to establish geochemical associations and specific mineralogical residences for Fe and Fe^{3+} in this clay. As far as we are aware, this is the first time that this approach has been employed to describe the physicochemical conditions of formation of any clay mineral.

EXPERIMENTAL

Sample location and description

Jedlina Zdroj is a town situated in Lower Silesia (southwestern Poland) in the region of Walbrzych, the Sudetes Basin. The geographical location of the Jedlina Basin is shown in Fig. 1.

Fig. 1. Geographical location of Jedlina Zdroj and Nowa Ruda.

The blue-green dickite-rich clay at Jedlina Zdroj occurs mainly as veins of hydrothermal origin within volcanic (rhyolitic) rocks. This clay occurs also as small white nodules in late Paleozoic volcanic rocks.[5] A set of 11 samples were collected from the outcrop site at Jedlina Zdroj, in which dickite-rich veins are abundant; dickite is primarily associated with dark-grey kaolinitic shales, Fig. 2. Sub-samples were hand picked for analysis in order to minimize the inclusion of impurities. The present detailed study of dickite was performed on one of these

Fig. 2. Example of blue-green dickite filling the veins within black shales/slates from Jedlina Zdroj. Sample size: *ca*. 12×11 cm.

Available online at www.shd.org.rs/JSCS/

subsamples (hereafter JDS), which contained predominantly dickite. Powdered samples for analyses were obtained by scraping the dickite-rich clay surface with a razor blade.

Dickite-rich clay is also found throughout the abandoned coal mine Piast near the town of Nowa Ruda (about 20 km from Jedlina Zdroj, Fig. 1). According to Kowalski and Lipiarski,[4] dickite from Jedlina Zdroj and Nowa Ruda may have originated in hydrothermal solutions genetically related to the magmatism of the Late Carboniferous.

Analytical methods

Chemical analysis. Chemical analyses were realized using standard methods for silica and alumina, and colormetric methods for Fe and Ti.

Inductively coupled plasma–optical emission spectroscopy (ICP–OES) analysis. The Fe contents of the various fractions of JDS (see below) were analyzed by a Spectroflame ICP––OES instrument using Ar as the plasma gas.

X-Ray diffraction (XRD) analysis. XRD Patterns were obtained with a Philips PW 1729 vertical goniometer using CoKα radiation (35 kV, 30 mA). Powder diffractograms were acquired in the 3–90° 2θ range, with 7–20 s counting per 0.04° 2θ step. The samples were prepared using the back-loading procedure according to Moore and Reynolds,[6] which provides significant disorientation of the clay layers.

Fourier transform infrared (FTIR) spectrometry. FTIR Spectra were recorded in the absorbance mode using a BOMEM Michelson Series MB FTIR spectrometer set to give undeformed spectra. The resolution was 4 cm^{-1} in the 400–4000 cm^{-1} analyzed range. The spectra were obtained at room temperature from KBr pressed pellets prepared by mixing 1.5 mg of a dickite fraction (see below) sample with 150 mg of KBr.

Scanning electron microscopy (SEM)/energy-dispersive spectrometry (EDS). The morphology and the semi-quantitative chemical analyses of polished thin sections of JDS-s were performed by scanning electron microscopy (SEM; Philips XL 30 ESEM/TMP scanning microscope) coupled to an energy-dispersive spectrometer (EDAX type Sapphire). The analytical conditions were as follows: accelerating voltage 15 or 25 kV, probe current 60 nA, working distance 25 mm and counting time 100 s. The individual parameters are printed on the microphotographs: acceleration of electron beam, magnification, type of detector: SE (secondary electrons), CEN (BSE-backscattered electrons). The samples were coated with gold.

Electron spin resonance (ESR) spectrometry. The ESR measurements were performed on finely-ground powders of the dickite samples that were transferred to an ESR quartz tube. The spectra were recorded on a Bruker ESP 300E spectrometer at X-band (9.4 GHz) using standard 100 kHz field modulation. The spectra were recorded at room temperature. Additional experimental parameters were as follows: 100 mW microwave power and 1 mT modulation amplitude. The ESR spectra were recorded in the 0 to 6 mT magnetic field range.

Analysis and fractionation

The fractionation procedure was similar to that used by Premović.[7] The flow chart in Fig. 3 outlines the major steps in preparing the four fractions of JDS.

Thus, powdered rock (1 g) was treated (room temperature, 12 h) with acetate buffer (acetic acid/sodium acetate, 1 M, pH 5.0) to remove most of the carbonates. The soluble material constitutes the carbonate fraction. Carbonate removal was checked by FTIR/EDS analyses.

The insoluble residue (I) was demineralized further by repeated treatment with cold HCl (6 M). This acid solution removed mostly metal oxides, including Fe oxides. The soluble part constitutes the cold HCl-fraction.
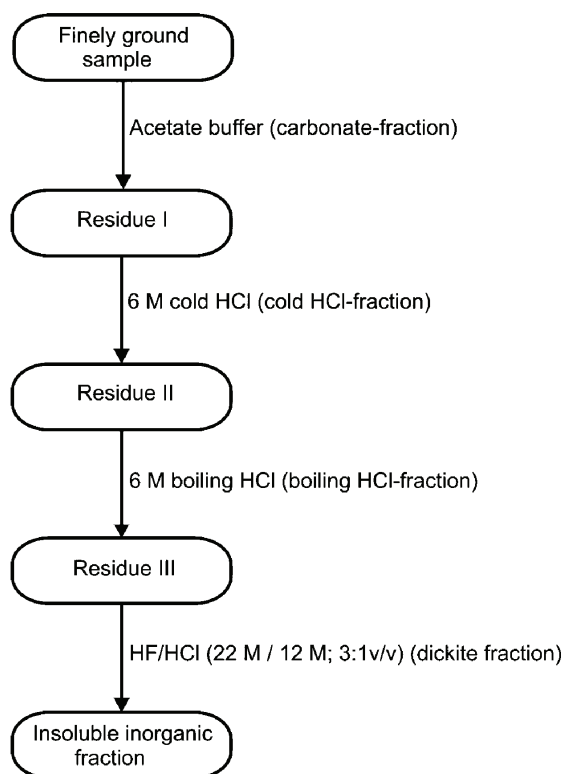
Fig. 3. Flow chart of the fractionation procedure.

The insoluble residue (II) was demineralized with boiling HCl (6 M, 80 °C, 12 h). This treatment removed most of the soluble silicates. The soluble part constitutes the boiling HCl--fraction.

The insoluble residue (III) was demineralized with boiling hydrofluoric acid HF/HCl (22 and 12 M, 3:1 v/v, respectively, 80 °C, 12 h). This acid mixture removes SiO_2 and Al_2O_3. The removal of SiO_2 and Al_2O_3 was checked by FTIR/EDS analyses. The soluble part constitutes the dickite fraction or phase.

The residue from (III) is the acid insoluble fraction.

RESULTS

Chemical and ICP–OES analyses

The acetate buffer/HCl demineralization steps removed only 9 wt. % of JDS. The mass loss was due to the total dissolution of carbonates (acetate buffer: 2 wt. %), the dissolution of metal oxides, including Fe-oxides (cold-HC1: 5 wt. %) and the destruction of some silicate minerals (boiling HCl: 2 wt. %), Table I. SiO_2 and Al_2O_3, the dominant constituents of JDS, seem to have been unaffected by the demineralization steps. Geochemical analysis also indicated that more than 91.5 wt. % of the dickite fraction was removed by the HF/HCl step. Chemical

analysis showed that the major components were 43.3 wt. % SiO_2, 40.0 wt. % Al_2O_3, 1.5. wt % TiO_2 and 1.0 wt. % Fe_2O_3.

The distribution of Fe among the four components of JDS is given in Table I, which shows that Fe was relatively abundant (2130 ppm) in JDS and that about 97 wt. % of this metal was associated with the dickite phase. A survey of the literature showed that the total Fe content in hydrothermal dickites was about 1 wt. %.

TABLE I. Geochemical distribution of Fe (ppm) from selective leaching experiments of JDS

Fraction	Sediment (±5 wt. %)	Fe
Acetate buffer	2.0	≤1[a]
Cold-HCl	5.0	3750
Boiling-HCl	2.0	5200
Dickite	91.5	1900
Insoluble residue	0.0	–
Total sample[b]	100.5	2130

[a]Detection limit of the ICP–OES employed; [b]the total Fe content obtained by summation of the Fe concentrations determined in the fractions by ICP–OES

FTIR Analyses

An accurate distinction between kaolinite and dickite can be achieved employing FTIR spectroscopy, by assessing the position and relative intensity of the OH-stretching bands in the 3600–3700 cm^{-1} region of an IR spectrum.[8] The FTIR spectrum of the dickite fraction of JDS, which is characteristic for dickite, is shown in Fig. 4a and, for comparison, the FTIR spectrum of a KGa-l reference sample is given in Fig. 4b. The KGa-l sample exhibited a strong absorption at 3697 cm^{-1}, a band of medium-strong intensity at 3620 cm^{-1} and two relatively weak absorptions at 3669 and 3652 cm^{-1}. On the other hand, the dickite sample showed a strong absorption at 3621 cm^{-1} and two medium-strong absorption bands at 3704 and 3654 cm^{-1}.

XRD Analyses

The XRD pattern of powdered JDS is shown in Fig. 5. The bulk samples showed dickite as the predominant mineral.

SEM/EDS Examination

The SEM results showed that the dickite phase of JDS had the morphology of well-formed, uniform aggregates of dickite particles (Fig. 6). EDS Analyses showed that this mineral mainly consists of O, Al and Si (Fig. 7a); minor amounts of K, Fe and Ti were also detected. In addition, the presence of minor amounts of goethite (Fig. 7b) and barite (Fig. 7c) was evidenced in JDS by the combined use of SEM/semi-quantitative chemical analysis of EDS. Apparently, dickite and goethite, (α-(FeO(OH)), precipitated simultaneously in JDS.
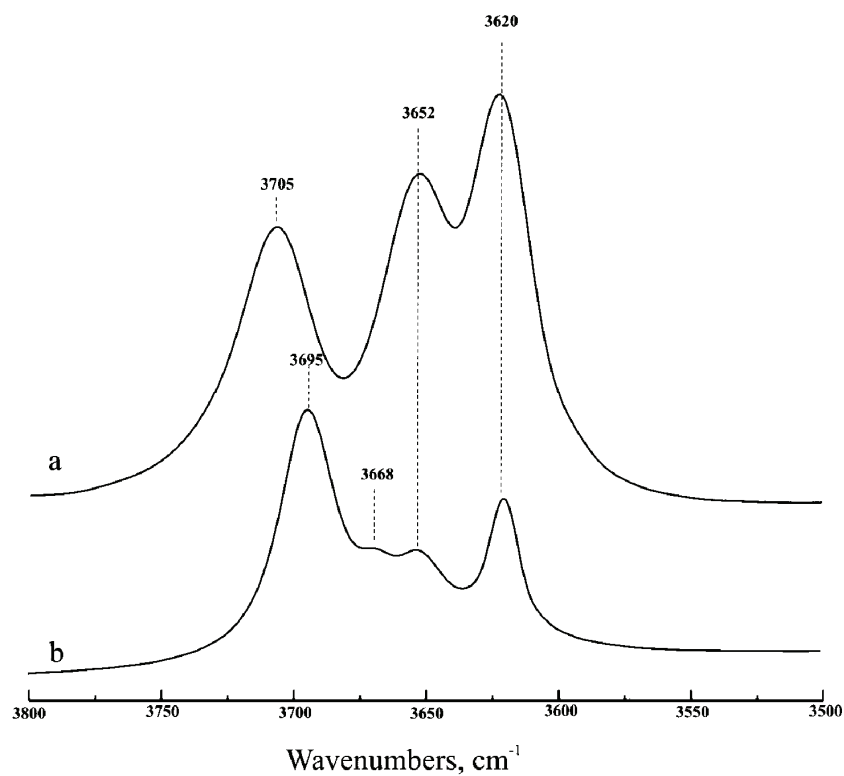
Fig. 4. FTIR Spectra in the OH stretching vibrations region of a) the dickite fraction of JDS Zdroj and b) KGa-l (a reference kaolinite).
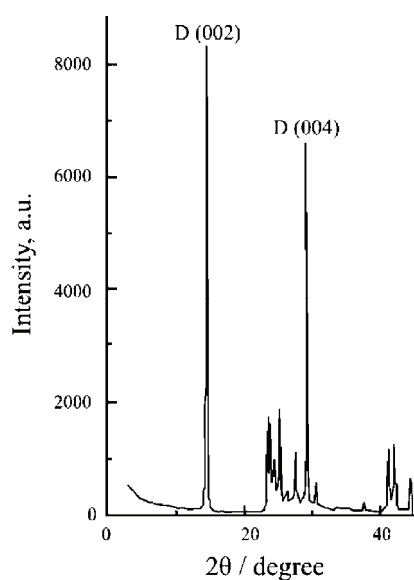
Fig. 5. X-Ray diffraction pattern of JDS. Diagnostic peaks of dickite are marked with D.
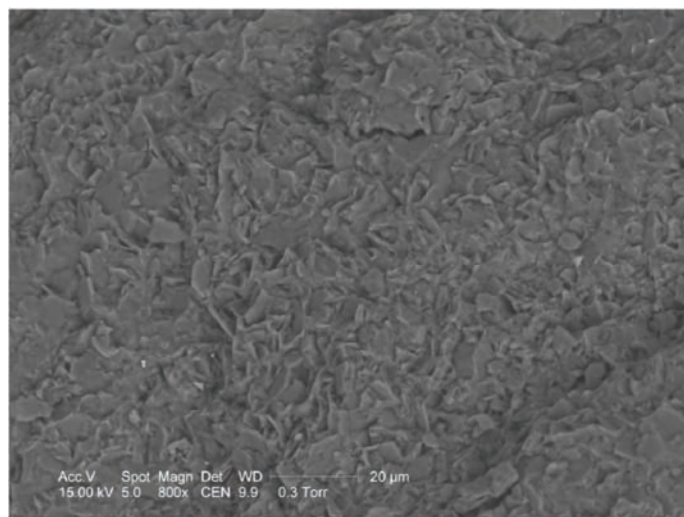
Fig. 6. Scanning electron micrographs of bulk JDS.

ESR Analyses

Untreated JDS showed only a complex ESR signal around $g = 4$ and a sharp isotropic ESR signal around $g \approx 2$, superimposed on a broader one (Fig. 8). The high *g*-pattern of JDS was often found for isolated Fe^{3+} in the structure of well--ordered kaolinites (*e.g*., KGa-1), substituting for Al^{3+} in the octahedral sheets.[9] The Fe^{3+} signals of JDS remained after chemical treatment with cold/boiling HCl, but they disappeared after treatment with HF/HCl solution. This means that Fe^{3+} are probably within the structure of the host dickite. The sharp ESR signal at around $g \approx 2$ is characteristic for a relatively stable paramagnetic defect within the structure of dickite.

DISCUSSION

The oxygenated dickite-forming solution

Kraynov and Ryzhenko,[10] who made a thorough study of the *Eh*/pH values in many geochemical water types, reported that the acidity of hydrothermal acid waters (in areas of contemporary magmatism) is within the pH range of *ca*. 0–4 and the *Eh* values vary from 0.6–0.9 V. The field of these waters in Fig. 9 is presented by the shaded area.

The fact that *ca*. 97 wt. % of the Fe of JDS (Table l) resides within the dickite structure indicates that some of the Fe in the dickite-forming hydrothermal solution was in a dissolved form. It is suggested that most of this metal was introduced into the dickite by this solution already enriched in Fe. This process occurred during mineral formation but not after afterwards.
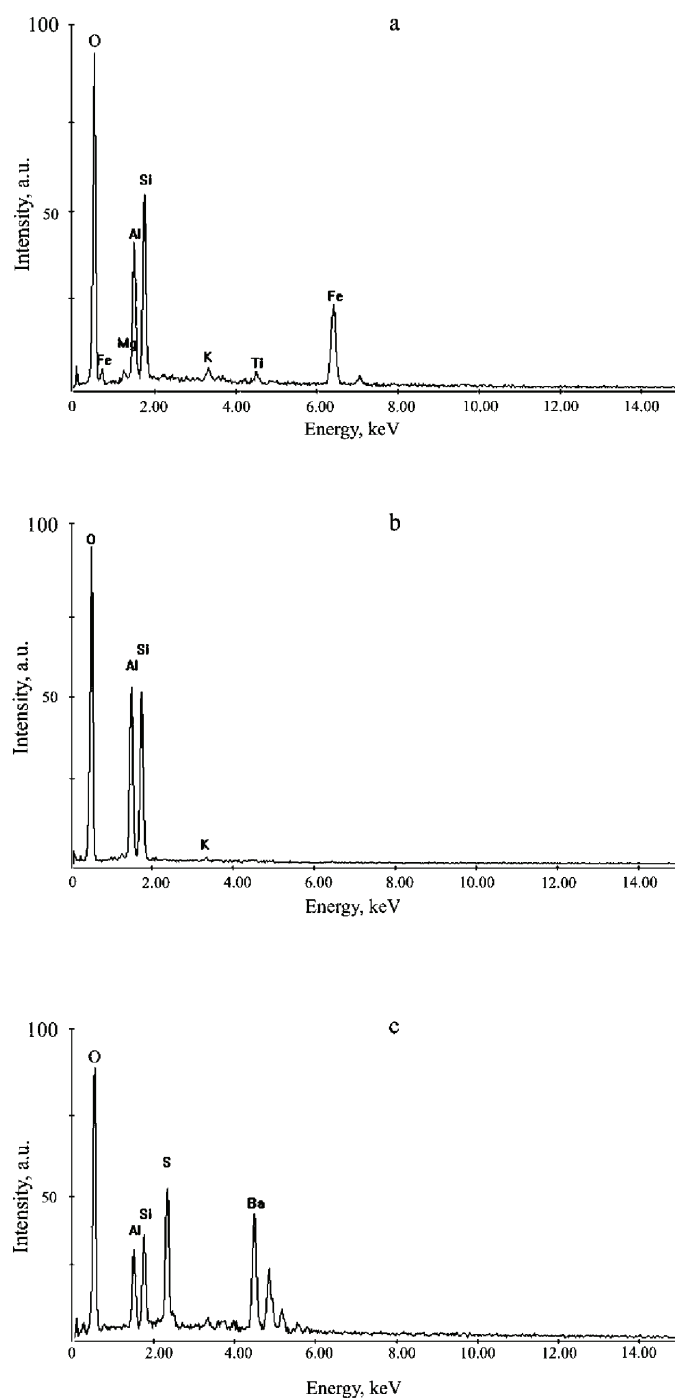
Fig. 7. EDS Analyses of the (a) dickite, (b) goethite and (c) barite in JDS.
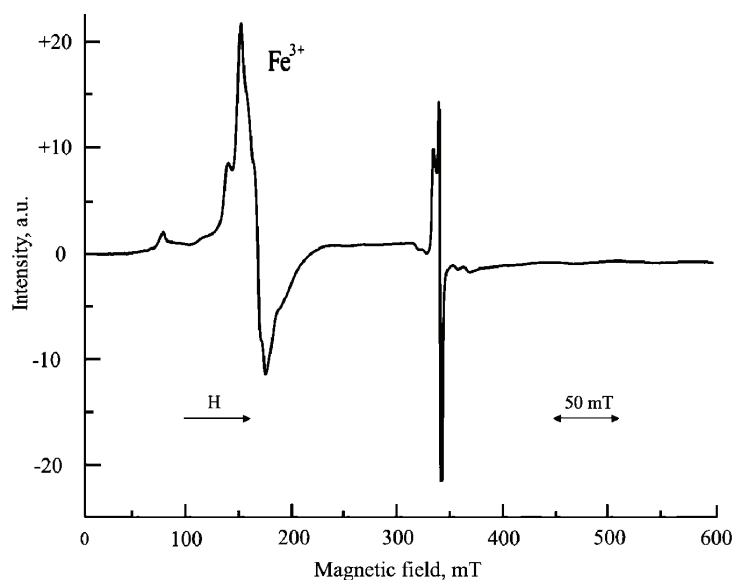
Fig. 8. The ESR spectrum of untreated JDS with Fe^{3+} within the dickite structure.
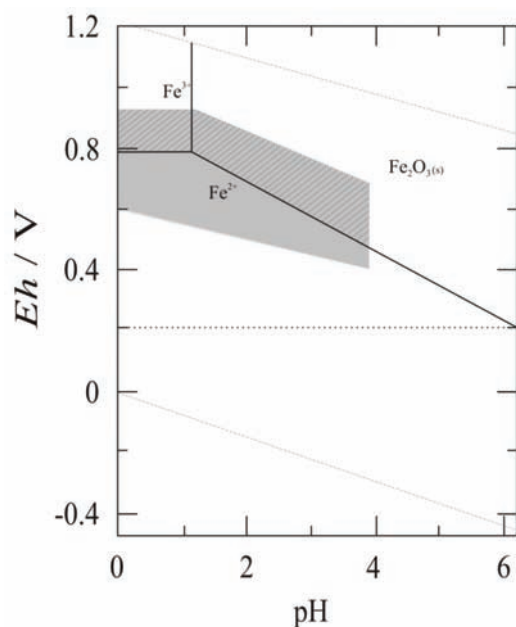
Fig. 9. *Eh*–pH diagrams for Fe^{3+} at 300 K and l atm of the forming solution (enriched with Fe^{3+}) of the dickite from Jedlina Zdroj. The assumed total Fe concentration was 200 ppm. The shaded area represents the *Eh*/pH region of hydrothermal waters defined by Kraynov and Ryzenko.[10] The probable physicochemical conditions of the dickite from Jedlina Zdroj are represented by the dashed area.

The ESR investigation showed that a high amount of the Fe^{3+} are incorporated into the structure of dickite. This indicates that these ions were present in relatively high concentrations in the precipitating solution at the time when this mineral was formed. It is also reasonable to suggest that this solution was oxy-

genated. Indeed, under anoxic conditions, Fe would precipitate mainly as pyrite (FeS_2), as both Fe^{2+} and Fe^{3+} are unstable with respect to pyrite in anoxic aquatic environments.[11]

The presence of authigenic goethite associated with JDS (Fig. 7b) is consistent with its formation occurring under highly oxygenated conditions, as goethite occurs only in a natural aqueous milieu under these conditions, with an *Eh* value above 0.15 V.[12] Note that formation of goethite and other Fe-hydroxides becomes predominant at pH > 3.[11]

Source of Fe

In general, all hydrothermal waters are brines and Fe is commonly present at levels of up to a few tens or hundreds ppm. The source(s) of this metal in a hydrothermal water can rarely, if ever, be identified with certainty.[13] Waters within a shallow-water hydrothermal system (such as Jedlina Zdroj) may be derived from any one or combination of the following sources: meteoric and juvenile (connate and magmatic) waters (*e.g*., Nicholson[14]). On-land hydrothermal systems derive most of their waters from meteoric sources along with possible magmatic contributions (*e.g*., Giggenbach[15]). A survey of the literature showed the magmatic waters usually contain very high concentrations of dissolved Fe (>1000 ppm). In contrast, meteoric waters are usually Fe-poor (about 10 ppm or so). Thus, it is speculated that the dickite-forming hydrothermal solution at Jedlina Zdroj was probably generated by the mixing of ascending magmatic Fe-rich waters and oxygenated Fe-poor meteoric water.

Eh–pH diagram

Employing the FactSage thermochemical software/Fact compound databases, stability diagrams of Fe^{3+} for physicochemical conditions close to natural hydrothermal conditions as defined by Kraynov and Ryzhenko[10] were constructed, Fig. 9. For the sake of simplicity, only a part of the diagram is shown. A total Fe concentration of 200 ppm was assumed in this construction. The critical boundary between the stability fields of Fe^{3+} is not significantly affected by modifying this value even 10-fold in either direction.

It is apparent from Fig. 9 that the Fe^{3+} is only thermodynamically stable under oxic conditions (*Eh* from 0.45 to 0.95 V) and at low pH values (0–4); accordingly, the relatively high concentration of Fe^{3+} within the dickite from Jedlina Zdroj is only consistent with a highly acidic (pH 0–4) and oxygenated (*Eh ca*. 0.45–0.95 V) dickite-forming solution. The above *Eh*–pH diagram was calculated for atmospheric pressure and a temperature of 25 °C. A thermochemical calculation indicated that no significant variations in the thermodynamic parameters on the scale of the diagram are to be expected up to a pressure of 10 bar. This is because pressure affects only slightly the chemistry of both ionic spe-

cies and solids of Fe within the O–H geochemical system. A similar calculation also showed that in a dickite-forming solution with temperatures reaching up to *ca*. 150 °C, the vertical line which represents the boundary between Fe^{3+} and Fe_2O_3 would be shifted only slightly.

Of course, the *Eh*–pH diagram presented in Fig. 9 it is not an accurate representation of the dickite-forming solution and it undoubtedly is highly variable in its approach to ideal. Yet, because it represents a quantitative estimate based on the available thermodynamic data, it should be a helpful tool, if used within its limitations.

CONCLUSIONS

Examination of a representative dickite-rich sample from Jedlina Zdroj by X-ray diffraction, scanning electron microscopy, energy dispersive X-ray and Fourier transform infrared analyses showed that dickite predominates with associated minor quantities of goethite and barite. Geochemical analysis showed a relatively high concentration of dissolved Fe which was present in the precipitating solution at the time when this hydrothermal mineral was formed. The abundant presence of Fe^{3+} (detected by ESR spectroscopy) within the dickite structure and the associated authigenic goethite indicates that this solution was highly oxygenated with an oxidation potential *Eh* and pH of *ca*. 0.45–0.95 V and 0–4, respectively.

ИЗВОД

ГЕОХЕМИЈА Fe У ХИДРОТЕРМАЛНОМ ДИКИТУ ИЗ ЈЕДЛИНЕ ЗДРОЈ (ДОЊА ШЛЕЗИЈА, ПОЉСКА)

ПАВЛЕ И. ПРЕМОВИЋ[1], JUSTYNA CIESIELCZUK[2], БРАТИСЛАВ Ж. ТОДОРОВИЋ[3], ДРАГАН М. ЂОРЂЕВИЋ[1] и НЕНАД С. КРСТИЋ[1]

[1]Лабораторија за геохемију, космохемију и астрохемију, Природно−математички факултет, Универзитет у Нишу, п. пр. 224, 18000 Ниш, [2]Department of General Geology, Faculty of Earth Sciences, University of Silesia, Sosnowiec, Poland и [3]Лабораторија за општу хемију, Технолошки факултет, Универзитет у Нишу, п. пр. 79, 16000 Лесковац, Србија

Урађена је геохемијска анализа Fe на репрезентативном узорку хидротермалне глине богате дикитом са локације Једлина Здрој. Минералогија узорка је веома једноставна. Дикит је основна компонента (>95 % од целокупног узорка), са мањим количинама гетита и барита. Геохемијска фракцинација и индуктивно спрегнута плазма–оптичко емисиона спектрометрија показују да је највећи део Fe (око 97 % од присутног метала) уграђен у структуру дикита. Електронспинска резонанца показује да се део Fe у структури дикита налази у облику Fe^{3+}. Значајан део Fe^{3+} (као и Fe) у дикитној структури се, вероватно, налази у првобитном хидротермалном раствору из кога се формирао дикит. На основу геохемије Fe^{3+} закљу-

чено је да су оксидациони потенцијал (*Eh*) и pH раствора за време формирања хидротермалног дикита са локације Једлина Здрој у опсегу 0,45–0,95 V (изразито оксидациони) и 0–4 (изразито кисело).

REFERENCES

1. G. Izquierdo, V. M. Arellano, A. Aragón, E. Portugal, I. Martinez, in *Proceedings of the World Geothermal Congress*, (2000), Kyushu – Tohoku, Japan, (2000), p. 1301
2. H. H. Murray, W. Bundy, C. Harvey, *Kaolin genesis and utilization*, The Clay Minerals Society, Special Publication 1, Clothbound, 1993
3. N. Malengreau, J.-P. Muller, G. Calas, *Clays Clay Miner.* **42** (1994) 137
4. W. M. Kowalski, I. Lipiarski, *Geol. T.* **78** (1973) 7
5. K. Lydka, *Arch. Mineral.* **26** (1966) 501
6. D. M. Moore, R. C. Reynolds Jr., in *X-ray Diffraction and the Identification and Analysis of Clay Minerals*, D. M. Moore Jr., R. C. Reynolds, Eds., Oxford University Press, Oxford and New York, 1989, p. 179
7. P. I. Premović, *Geochim. Cosmochim. Acta* **48** (1984) 873
8. J. D. Russell, in *Infrared methods*, M. J. Wilson, Ed., Blackie, Glasgow, 1987, p. 133
9. J. M. Gaite, P. Ermakoff , J. P. Muller, *Phys. Chem. Minerals* **20** (1993) 242
10. S. R. Kraynov, B. N. Ryzhenko, *Geochem. Int.* **29** (1992) 1
11. R. M. Garrels, C. L. Christ, *Solutions, Minerals and Equilibria*, Harper and Row, New York, 1965, p. 453
12. W. C. Krumbein, R. M. Garrels, *J. Geol.* **60** (1952) 1
13. *Geochemistry of Hydrothermal Ore Deposits*, 3rd ed., H. L. Barnes, Ed., Wiley, 1997
14. K. Nicholson, *Geothermal Fluids*, Springer-Verlag, Heidelberg, 1992, p. 266
15. W. F. Giggenbach, *Econ.Geol.* **87**(1992) 1927.

Contents of Volume 74

Available online at www.shd.org.rs/JSCS/

Available online at www.shd.org.rs/JSCS/

Available online at www.shd.org.rs/JSCS/

Available online at www.shd.org.rs/JSCS/

Available online at www.shd.org.rs/JSCS/

Available online at www.shd.org.rs/JSCS/

Available online at www.shd.org.rs/JSCS/

Available online at www.shd.org.rs/JSCS/

Available online at www.shd.org.rs/JSCS/

Subject index

Available online at www.shd.org.rs/JSCS/

Author index

Available online at www.shd.org.rs/JSCS/

End of Volume 74.